

https://dspace.org/

A design study of a scale model bearingless helicopter rotor system using composite materials

Cohen, Gary, M

1991

http://hdl.handle.net/10539/22844

Cohen, Gary M (1991) A design study of a scale model bearingless helicopter rotor system using composite materials, University of Witwatersrand, Johannesburg, <http://hdl.handle.net/10539/22844>

Downloaded from a DSpace repository. https://dspace.org/

A Design Study of a Scale Model Bearingless Helicopter Rotor System using Composite Materials

Gary M. Cohen

30 - January - 1991

A thesis submitted to the Faculty of Engineering, University of the Witwatersrand, Johannesburg, in fulfilment of the requirements for the degree of Master of Science in Engineering.

Abstract

The use of advanced composite materials in helicopter rotor systems offers opportunities for improvements in aerodynamic geometry, performance, weight, damage tolerance, maintenance and operating costs. Technical aspects of the design and analysis, and the practical aspects of the manufacture of a composite rotor system are discussed herein. The rotor system was compared to an existing conventional teetering rotor system, in order to establish the viability of the new composite rotor system.

This rotor system reduced the number of components by 55% and the manufacturing time by half, due to the simplicity of the design and lay up procedure, thus making the system economically more viable. The mass was predicted to within 1% of that acheived in practice and gave a mass advantage of 50.5% over the conventional rotor. Static tests identified the failure modes and stress concentration points, while the comparative hover tests showed the system to have ± 20% less drag. The composite feathering bearing limited the feathering of the blades and increased the control power necessary to pitch the blades, thus increasing the pitch link loads.

It was concluded, that for this application, the advantages of using advanced composite materials out weigh the dissadvantages, thus making for more efficient and cheaper helicopters.

Declaration

I declare that this dissertation is my own, unaided work. It is being submitted for the Degree of Master of Science in Engineering in the University of the Witwatersrand, Johannesburg. It has not been submitted before for any degree or examination in any other University.

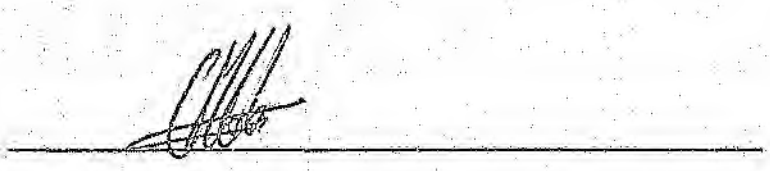

Gary M Cohen

7th day of March 1991

Table of Contents

1 INTRODUCTION 1

Overview of some Existing Designs 5

Teetering Rotor Systems 6

Articulated Rotor Systems 7

Cantilevered Rotor Systems 9

Hybrid and Experimental System 11

Aspects to be Covered 13

Limitations of the Investigation 16

Hardware Limitations 16

Computer Limitations 17

2 Literature Overview 18

Helicopter Rotor Aerodynamics 18

Structural Loads and Rotor Dynamics 24

Composite Rotor Applications 29

Composite Materials 32

Composite Joints. 33

3 Design Conceptualization and Rationale 37

Rotor System Concept 38

Rotor System Geometry 45

Flexbeam 48

Hub Center 49

Pitch Case 50

Pitch Link 51

Flexbeam / Blade root / Pitch case Attachment 52

Blade 54

4 Loads and Structural Analysis 56

Analytical Rotor Model 56

Design Iteration Procedure 64
Design Flight Conditions 66
Structural Analysis 67
Design Loads 67
Material Properties 68
Section Properties 70
Rotor Blade Analysis 72
Blade Root Analysis 74
Finite Element Methods Analysis 78
Dynamic Analysis 91
5 Manufacturing Development 93
Tooling Development 93
Flexbeam 93
Blade Core Shaper 94
Blade Mould 96
Fabrication Sequence 99
Flexbeam Rotor System 99
Rotor System Balancing 103
Static Balance 103
Blade Tracking 103
6 Rotor System Evaluation 106
Manufacturing Process 106
System Mass 108
Static Component Testing 110
Testing Procedure 110
Flexbeam System Results 115
Conventional System Results 119
Rotor Hover Tests 121
Test Procedure 121
Hover Test Results 122
Windtunnel Flight Tests 125

Flight Test Procedure 125
Windtunnel Test Results 125
Flow Visualization 126
Summary of the Advantages and Disadvantages of the Bearingless Rotor System Concept 128
7 Conclusions and Recommendations 129
8 References 131
A CARSANProgram 135
B Estimation of Section Properties 175
C Flight Conditions 179
D Finite Element Method Results 189
E Aerodynamic Data for NACA 632-01x Series Aerofoil . 233
F Computer Codes 237
G Dynamic Analysis Results 241
H Sample Data from Flight Tests 253
I Calibration Equipment 263

List of Figures

Figure 1:Leonardo's Airscrew 2
Figure 2: Basic Rotorhead Configurations 5
Figure 3: Teetering Type Hub 6
Figure 4: Hughes 500D 8
Figure 5: Sikorsky S-58 8
Figure 6: Sikorsky S-76 8
Figure 7: Bell 412 9
Figure 8: Locheed AH-56 9
Figure 9: MBB BO-105 10
Figure 10: Westland Lynx 10
Figure 11: Aerospatiale SA-365N Dauphin 2 10
Figure 12: Bell AH-1G 11
Figure 13: Bell 222 11
Figure 14: Robinson R22 12
Figure 15: Boeing-MBB Experimental Rotor Head 12
Figure 16: Design System Philosophy 15
Figure 17: Blade Element Theory 19
Figure 18: Finite Element Dynamic Model of Structure 26
Figure 19: Collective Mode (out-of-plane) 27
Figure 20: Cyclic Mode (out-of-plane) 28
Figure 21: Composite Laminate 32
Figure 22: Modes of Failure for Composite Bolted Joints 34
Figure 23: Selection of Lay-up Pattern for Composites 35
Figure 24: Continuous Hub and Blade Spar 38
Figure 25: Mechanical Bolt Connection 39
Figure 26: 'Coke Bottle' Root Retention 40
Figure 27: 'Wraparound' Root Retention 40
Figure 28: Wedge - Bond Root Concept 41

Figure 29: Rotor System Concept 44
Figure 30: Variation of Power with Change in Chord 46
Figure 31: Variation of Power with Radius 47
Figure 32: Flexbeam 48
Figure 33: Hub Center 49
Figure 34: Comparison Between Adhesive Shear Stresses 52
Figure 35: Exploded Stacking Sequence of Bond Area 53
Figure 36: Rotor Blade Cross - Section 54
Figure 37: Aerodynamic Blade Force System 57
Figure 38: Flexible Blade Force System 62
Figure 39: Design Iteration Process 65
Figure 40: Spanwise Structural Moment 67
Figure 41: Spanwise Structural Moment (Hover) 68
Figure 42: Spanwise Mass Distribution 70
Figure 43: Spanwise Stiffness Distribution 71
Figure 44: Chordwise Stiffness Distribution 71
Figure 45: Torsional Stiffness Distribution 72
Figure 46: Load Directions 73
Figure 47: Blade Geometry 74
Figure 48: Schematic of Blade Root Area 75
Figure 49: Theoretical Bond Strengths [15] 76
Figure 50: Loads at the Root Joint 77
Figure 51: Bond Area Geometry 78
Figure 52: Schematic of FEM Model 79
Figure 53: Root Lay-up Sequence 80
Figure 54: FEM Stress Results 81
Figure 55: FEM Stress Results 82
Figure 56: FEM Stress Results 83
Figure 57: FEM Stress Results 84
Figure 58: FEM Stress Results 85
Figure 59: FEM Stress Results 86
Figure 60: FEM Stress Results 87

Figure 61: FEM Stress Results 88
Figure 62: Bonded Joint Failure Mode 89
Figure 63: Natural Frequencies (Resonance Plot) 91
Figure 64: Flexbeam Mould 94
Figure 65: Core Shaping Mandrel 95
Figure 66: Rotor Blade Mould Plugs 96
Figure 67: Root End Mould Plug 97
Figure 68: Vacuum Bag Lay-up 98
Figure 69: Pitch Case Mould 98
Figure 70: Glassfibre Flexbeam Mould 99
Figure 71: Blade Fabrication Sequence 100
Figure 72: Blade Balancing (Static) 103
Figure 73: Blades Out of Track 105
Figure 74: Blades Correctly Tracked 105
Figure 75: Comparative Blade Costs [36] 107
Figure 76: Flexbeam Static Test 1 112
Figure 77: Flexbeam Static Test 2 113
Figure 78: Static Test of Conventional Blade 114
Figure 79:Failure Mode 116
Figure 80: Bond Stresses 116
Figure 81: Spanwise Cross-Section through Blade Root Area . . 116
Figure 82: Point Load Failure of Flexbeam 117
Figure 83: Anelastic Stress-Strain Behaviour [2] 120
Figure 84: Comparative Hover Test Results 122

List of Tables

Table 1: Rotor Geometric Parameters 47
Table 2: Flight Condition 66
Table 3: Design Loads 67
Table 4: Composite Material Properties 69
Table 5: 312L Adehesive Properties 69
Table 6: Tsai-Hill Values for Spar Layers 73
Table 7: Results of Mass Measurement 108
Table 8: Test Rig Error Bands 121

Notation

B — Tip loss factor

C_{d0} — Section profile drag coefficient

C_l — Section lift coefficient

E — Young's modulus for adherend (longitudinal) (N/m^2)

k — Eccentricity factor

l — Overlap (bond length) (m)

M_a — Aerodynamic moment (Nm)

M_s — Structural moment (Nm)

M_{ZV} — Vertical inertia matrix

P — Applied load on joint per unit width (N/m)

r — Blade element radius (m)

S — Shear loading (MPa)

t — Thickness of adherend (m)

T — Temperature (K)

u — non-Dimensional resultant velocity at blade element

x — non-Dimensional blade element radius

X — Longitudinal loading

Y — Transverse loading

Z_m — Deflection matrix

α — Coefficient of thermal expansion (/K)

β — Flapping angle (deg.)

$\ddot{\beta}$ — Flapping acceleration

β_0 — Precone angle (deg.)

β_h — Angle of flexible blade at hinge

η — Thickness of adhesive layer (m)

γ_e — Elastic adhesive shear strain

γ_p — Plastic adhesive shear strain

γ' — Mass constant of blade

ν — Section inflow

v_0 — Average inflow

ψ — Azimuth angle (deg.)

Φ — Inflow angle (deg.)

σ — Normal stress (MPa)

τ — Torsional Stress (MPa)

τ_{av} — Average adhesive shear stress (N/m^2)

τ_p — Plastic adhesive shear stress (N/m^2)

Ω — Angular velocity (rad/sec)

ω — Loading frequency

Subscripts

i,o — inner and outer adherends of joint

1,2 — longitudinal and transverse directions

Chapter 1

INTRODUCTION

'Although human subtlety makes a variety of inventions ... it will never devise an invention more beautiful, more simple or more direct than does nature, because in her inventions nothing is lacking and nothing is superfluous'

- Leonardo da Vinci.

The helicopter was one of the first visions man had of manned flight. In 1490 Leonardo da Vinci designed a machine of wood and starched linen, powered by a spring mechanism which he called a helical screw. But vertical flight was only achieved some 400 years later with very limited success. On 29 September 1907 the Breguet-Richet Gyroplane became the first rotary wing aircraft to lift itself from the ground. However, it was unstable and had to be steadied in the air by four men with poles. 1919 saw the Spaniard Juan de la Cierva deal with the problems of stability, control and torque reaction with his autogyro. His work led to the development of flap and lag hinges which are key features of modern rotor systems. Igor Sikorsky on 14 September 1939 tried to persuade the totally

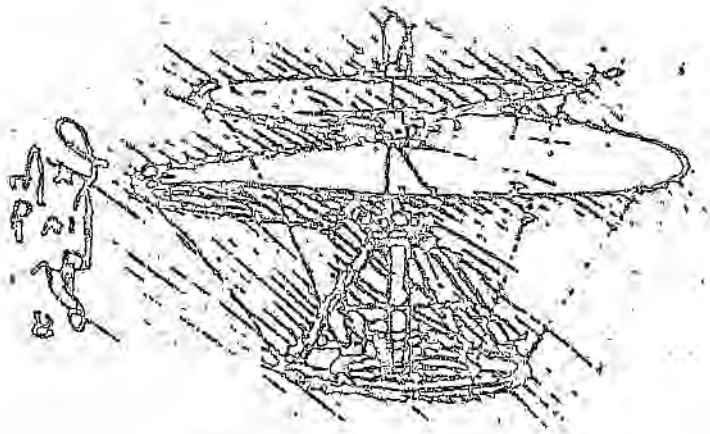

Figure 1: Leonardo's Airscrew

untamed VS-300, having a single main rotor and an anti-torque tail rotor, to obey pilot commands. Only after the second world war was progress achieved in helicopter development. Progress was slow with many problems in propulsion, aerodynamics and control to overcome. The last 20 years has seen a dramatic increase in the capability of the helicopter with no sign that the rate of progress will decrease.

Recently, with the development of strong, lightweight advanced composite materials, the design and capability of the helicopter is being completely revolutionized. These materials can be used to improve the performance, efficiency and maintainability of the helicopter making it an extremely versatile aircraft.

The design methodology to use these materials for an advanced rotor system concept makes up the subject matter of this dissertation.

More specifically, the research carried out here is the development of the design and manufacturing techniques to use advanced composite materials, namely Carbon fibre reinforced plastics (CFRP) and Glass fibre reinforced plastics (GFRP) in helicopter rotor systems. Thus ideally we would like to create a rotor system where ' *... nothing is lacking and nothing is superfluous.*'.

The research program is part of a larger program to increase the local level of technology and understanding in the field of helicopters. The global objective being to develop rotor systems that have low weight, low drag, low cost, long life, low maintenance, low part count, free from dynamic problems and adequate control power. It is evident from current design trends that there is a swing towards composite materials in the aerospace field in order to reach these global objectives. The change from conventional materials to composite materials is gaining momentum, with helicopter rotor blades being an integral part of this swing. Several existing helicopters, including the Boeing CH-47, Westland Lynx and the Aerospatiale Puma, have already been refitted with composite rotor blades creating immediate advantages for the helicopter and manufacturer. Such advantages are:

- good profile accuracy can be maintained,
- it is relatively easy to use complicated aerofoil sections, blade planforms and to include blade twist,
- the fatigue life of the blade is extended,
- 'Fail safe' or soft failure mode ie. early detectable signs of failure appear and
- high level of survivability from impact damage.

The main objective of this dissertation is to develop a bearingless helicopter rotor system concept, taking full advantage of advanced composite materials. The development of this rotor concept involves design, manufacturing and the evaluation of its overall performance as compared with an existing type rotor system. These objectives were accomplished by using a scale model of the rotor concept. Although the quantitative results from the evaluation cannot be extrapolated to a full scale helicopter directly, the operation and measurement of success of the rotor system concept will still be valid. Historically, scale models have been used to verify conceptual designs as far back as 1754, when Mikhail Lomonosov demonstrated a spring- powered helicopter model. More recently, Arthur Young developed a two bladed rotor, using a gyro stabilizer bar on a free flight model, which was controlled by an umbilical cord between the control box and the model helicopter. The success of this concept led to building the Bell

model 47 helicopter by Lawrence Bell in 1946. Thus, throughout history the use of models for development work is widely accepted in the engineering industry.

The secondary objectives, which are spinoffs of the project as a whole, are:

- to develop the analytical tools needed for the design process,
- to develop the manufacturing techniques,
- to develop a design philosophy in order to reach the desired goals effectively and efficiently and
- to develop a full understanding of the helicopter flight environment, and the processes for the creation of a successful product.

This research was carried out at the University of the Witwatersrand under the supervision of Professor Alan Nurick. My co-worker for the project was Larry Sheiman, whose work has been referenced in this document.

1.1 Overview of some Existing Designs

As shown in figure 2, rotor system designs can be broken down into three major categories namely:

- Articulated rotor hub restraints
- Teetering hub restraints
- 'Rigid' or Cantilevered hub restraints

the hub restraint being the major differentiating feature of a rotor system.

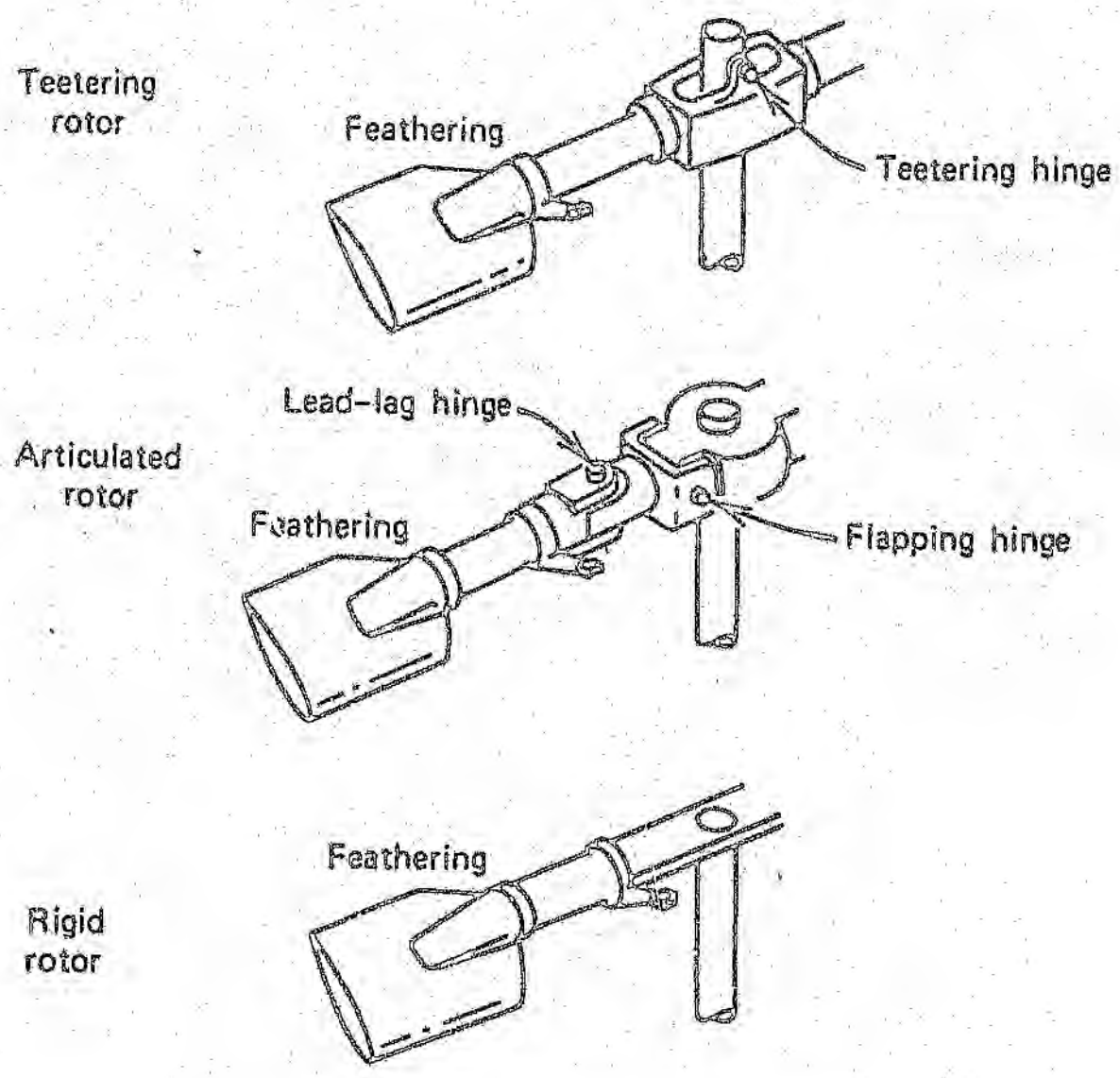

Figure 2: Basic Rotorhead Configurations

1.1.1 Teetering Rotor Systems

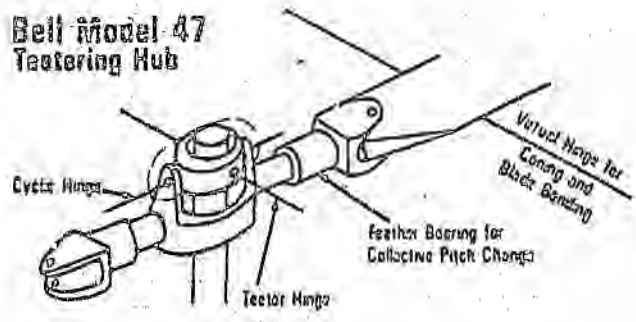

Figure 3: Teetering Type Hub

This system is possibly one of the oldest and simplest types of rotor systems. Briefly, the system can be described as having two rotor blades connected rigidly to the rotor hub, which in turn is connected to the rotor shaft by means of a pinned joint, called the teeter hinge. The teeter hinge allows the blades to 'seesaw' or teeter on the shaft, but not to flap independently. The feathering is achieved by means of mechanical bearings or as in the case of the Bell 206 Jet Ranger a tension-torsion wire pack strap. Lead-lag hinges on a teeter system are unnecessary for the following reasons:

- They are not needed to relieve chordwise stresses in the blade which are generated by the in-plane motion of the system. The in-plane motion is a result of the flapping or in this case the teetering motion of the system. As the system teeters the rising blade's center of gravity (CG) moves closer to the center of rotation, as does the sinking blade's CG. Because of this motion the blades accelerate conserving the momentum. As both blades accelerate at the same time the only restraint is that of the engine inertia which is softened by the torsional flexibility of the drive system. This restraint is soft enough so that the chordwise bending moment can be handled with moderate stiffening of the blade root.

- The second reason for not using lead-lag hinges on a two bladed rotor system is that the rotor system would be susceptible to unstable ground resonance for a wide range of rotor speeds, if such hinges were present.

The rotor system is simple with relatively few components, making it easy to manufacture and keeping the drag on the system relatively low. The system is, however, inherently limited to two blades which does result in a 2-per-revolution bounce in translational flight, since the majority of the lift is produced by the blades over the nose and tail of the helicopter.

The main disadvantage of the rotor system is the fatigue life of the bearings. The life of mechanical bearings and wire pack straps are very limited due to the dynamic environment in which they operate. For example, the wire pack strap on the Bell 206 Jet Ranger has to be replaced every 2000 hrs, which is a complicated and costly task. Mechanical bearings are limited by the load which they can handle, thus they cannot be used in rotors where high centrifugal operating loads are expected. The wire pack strap is not limited by high centrifugal loads but does require a relatively stronger control system compared to that of the mechanical bearing type.

1.1.2 Articulated Rotor Systems

Articulated rotor systems are widely used today especially in rotor systems where there are more than two rotor blades present. Each blade is independently connected to the hub, allowing them to flap individually. The rotor system is characterized by offset flapping hinges, lagging hinges and lead-lag dampers. The Lead- lag hinges are necessary for articulated rotor designs as the rotor blades are not necessarily accelerating in the chordwise plane simultaneously, thus the blades resist the motion of each other,increasing the chordwise stresses. The lead-lag hinges alleviate the chordwise bending stresses. Lead-lag dampers are generally used to take the rotor through ground resonance safely, while the rotor is being spun up on starting of the helicopter. Feathering of the blades is also achieved by some type of bearing. A few examples of fully articulated rotor designs are shown below:

- The Sikorsky S-58 [figure 5] has a pin jointed flap hinge, a pin jointed lead-lag hinge and mechanical thrust bearings for the blade feathering.

- In the Hughes 500D [figure 4] the flap hinge and feathering bearing are replaced by a flexible wire pack strap. This strap has a virtual flapping hinge due to it's flexibility and the feathering is accomplished by the twisting motion of the strap.
- Elastomeric bearings are used for the feathering, flapping and lead-lag motions of the rotor blade in the Sikorsky S-76 helicopter.[figure 6]

These systems generally have a high part count, are bulky and as such have a higher drag than that of other rotor systems. As with the teetering system, the hinges and bearings are limiting factors in the rotor's design, thus experiencing similar fatigue problems. High maintenance costs are generally associated with this type of rotor system, as they are relatively more complicated than other types of existing rotor systems.

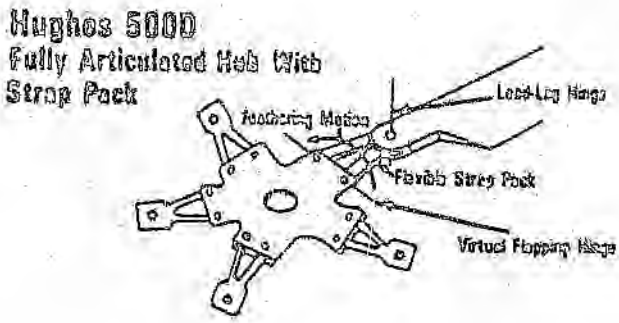

Figure 4: Hughes 500D

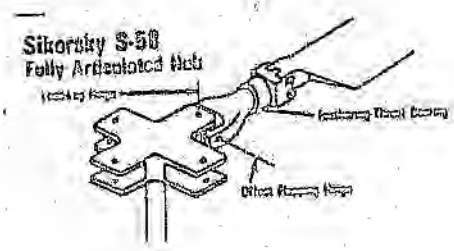

Figure 5: Sikorsky S-58

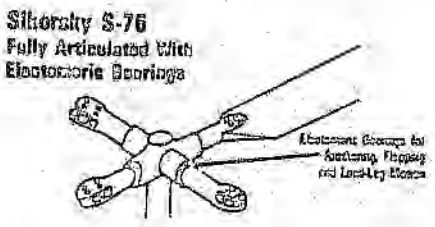

Figure 6: Sikorsky S-76

1.1.3 Cantilevered Rotor Systems

Cantilevered systems, often erroneously referred to as 'rigid rotor systems', do not have physical hinges but emulate hinges by virtue of their flexibility. The point on the hub or blade root around which the blade flaps or lags in thus known as a virtual hinge. Cantilevered rotor blades are coupled either to a flexible hub or they have a flexible root end which behaves much the same as an articulated rotor system. As with the previous rotor systems, the feathering bearing is retained using either mechanical thrust bearings, wire packs, straps or elastomeric bearings. Some examples of cantilevered rotor systems are shown below:

- The Bell 412 [figure 7] has a soft-in-plane hub with virtual flapping hinges, lead-lag hinges, with accompanying elastomeric lead-lag dampers, and feathering bearings.
- The lead-lag hinge does not exist in the stiff-in-plane hub of the Lockheed AH-56 [figure 8] helicopter. This design has a virtual flapping hinge and a door-hinge type feathering bearing.
- The MBB BO-105 [figure 9], Westland Lynx [figure 10] and the Aerospatiale SA-365N Dauphine 2 [figure 11] all have virtual flapping and lagging hinges. The feathering is handled by tension-torsion straps, with the latter helicopter having elastomeric bearings and dampers.

These cantilevered rotor systems have a low part count and can have a relatively smaller hub thickness thus having a lower aerodynamic drag. They are, however, still plagued by some of the problems of the previous types of rotor systems, such

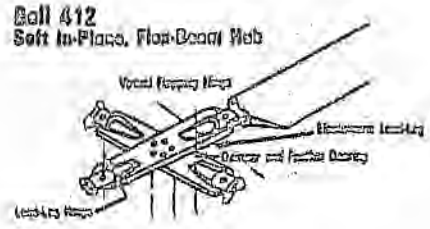

Figure 7: Bell 412

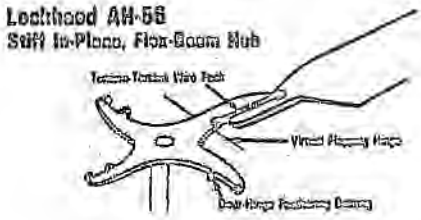

Figure 8: Locheed AH-56

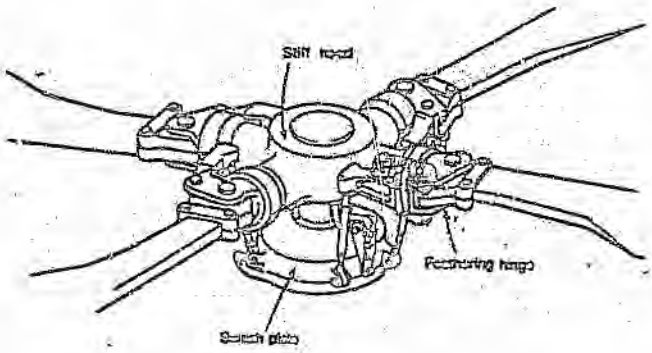

Figure 9: MBB BO-105

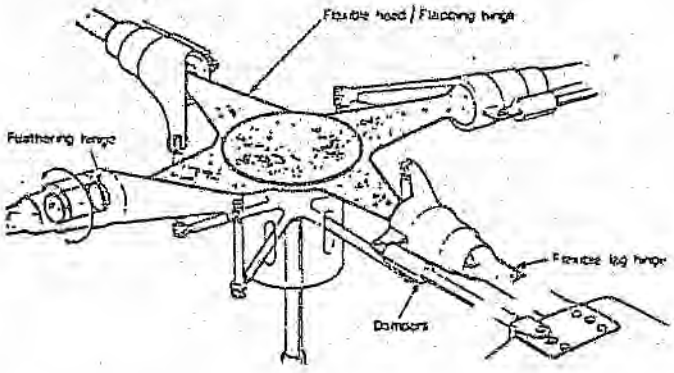

Figure 10: Westland Lynx

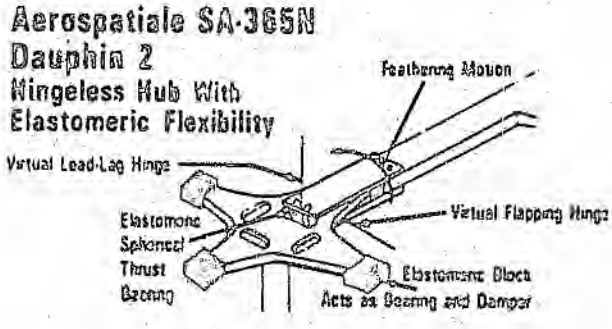

Figure 11: Aerospatiale SA-365N Dauphin 2

as high control loads and fatigue, and thus have similar maintenance costs associated with them.

1.1.4 Hybrid and Experimental System

A few hybrid rotor systems, which attempt to combine some of the best features of the previously discussed rotor system types, exist on some modern helicopters

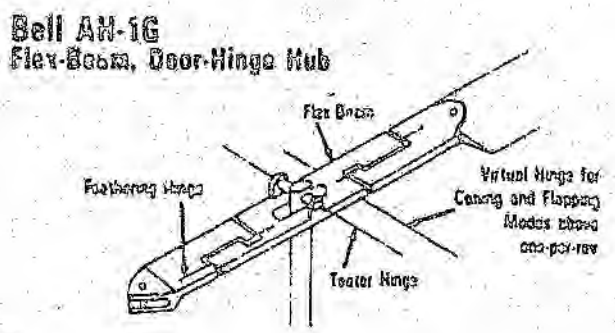

Figure 12: Bell AH-1G

today. Examples of hybrid rotor systems are shown below:

- The Bell AH-1G [figure 12] is a flexbeam, door-hinge hub with a teeter hinge. The flexbeam allows the system to cone while the teeter hinge allows it to flap.
- The Bell 222 [figure 13] has a flexbeam, teetering hub with a hub spring and an elastomeric feathering bearing.

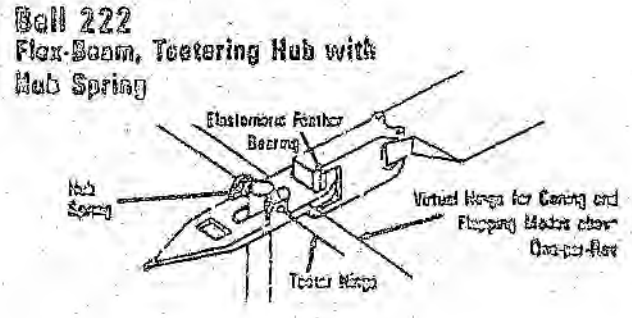

Figure 13: Bell 222

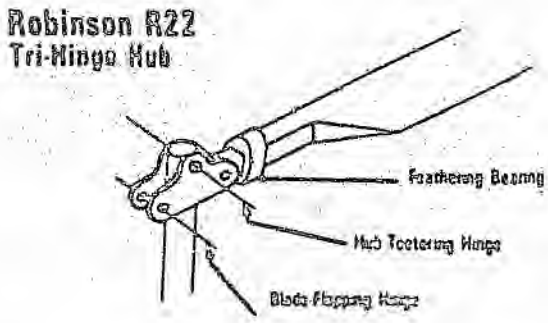

Figure 14: Robinson R22

- The Robinson R22 [figure 14] is a combination of an articulated system and a teetering system. It has a teeter hinge, offset flap hinges, mechanical thrust bearings, for feathering, and no lead-lag hinges.

An experimental hingeless and bearingless rotor system has been designed by Boeing Vertol and has been fitted to a MBB BO-105 helicopter[figure 15]. The system has a dual beam, made from composite materials and it relies on its flexibility to flap, lead-lag and twist thus eliminating the need for any bearings or dampers. This rotor system concept is the closest design to the ideal goals of an efficient helicopter rotor system.

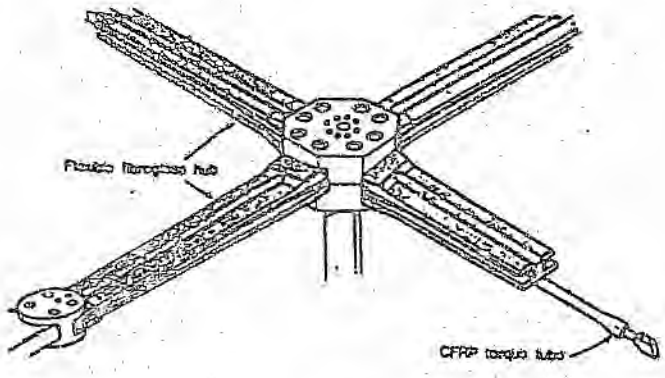

Figure 15: Boeing-MBB Experimental Rotor Head

1.2 Aspects to be Covered

This design study considers the design, analysis, manufacturing and evaluation of a helicopter rotor system concept. For this purpose a scale model of the concept was used. This model was scaled to the identical size of existing conventional teetering rotor which was designed by my co-worker Larry Sheiman and myself, for the commissioning of a translational flight rotor test facility. Although the design, analysis and manufacturing of the conventional teetering rotor is not considered in this report, it is however, mentioned here for comparative purposes. These comparisons are discussed in the evaluation of the rotor system's performance, manufacture and cost pertaining to the scale rotor models only.

The rotor system discussed here is a hybrid concept of a teetering system and the latest experimental rotor systems. Basically, this rotor has a teeter hinge with a flexbeam hub, made from advanced composite materials. The flexbeam emulates the flap hinge and the feathering bearing by virtue of the fact that the flexbeam can bend and twist, resulting in a completely bearingless rotor system.

The design of this rotor concept considers one area in particular for a more comprehensive analysis, this being the root section of the rotor blade. This area is a critical area on the blade as all the loads generated by the rotor blades are transmitted through the root to the hub. The rotor blade root area generally consists of a mechanical or bonded joint, thus having stress concentration effects and high stress levels associated with it. Thus the careful design of the root, using orthotropic materials, is vital to ensure the safety of operation of the complete rotor system.

The design of the rotor concept followed a design philosophy which can be best demonstrated by fig 16. This philosophy is divided into 4 major sections namely:

Conceptualization

- the definition of the rotor concept, its basic sizing considering the objectives and the imposed limitations.

Design development

- the determination of flight loads, aerodynamic performance, structural and dynamic load analysis, design refinement and the final analysis of the rotor.

Manufacturing development

- the design and development of the tooling needed for the fabrication of the rotor components and the development of the fabrication sequences and processes necessary to produce the final product.

Testing and Qualification

- the static laboratory testing and dynamic windtunnel flight testing of the rotor system on instrumented test equipment for the qualification of the rotor design.

The design iterations that were done to reach the final rotor system's configuration are not shown here, only the final rotor system design and it's analysis is shown.

During the design and analysis phase a significant amount of time was spent on the development of computer software for the purposes of load prediction and rotor analysis. The prediction capability of the software includes aerodynamic performance, airloads, structural bending loads, natural frequency and mode shape determination. The theory, mathematical models and solution methods for the computer codes are discussed in little detail in this report, however, a detailed presentation can be found in Cohen and Sheiman [8,APPENDIX A]. Additional software utilized for the calculation of blade section properties and Classical Lamination Theory analysis were also developed.

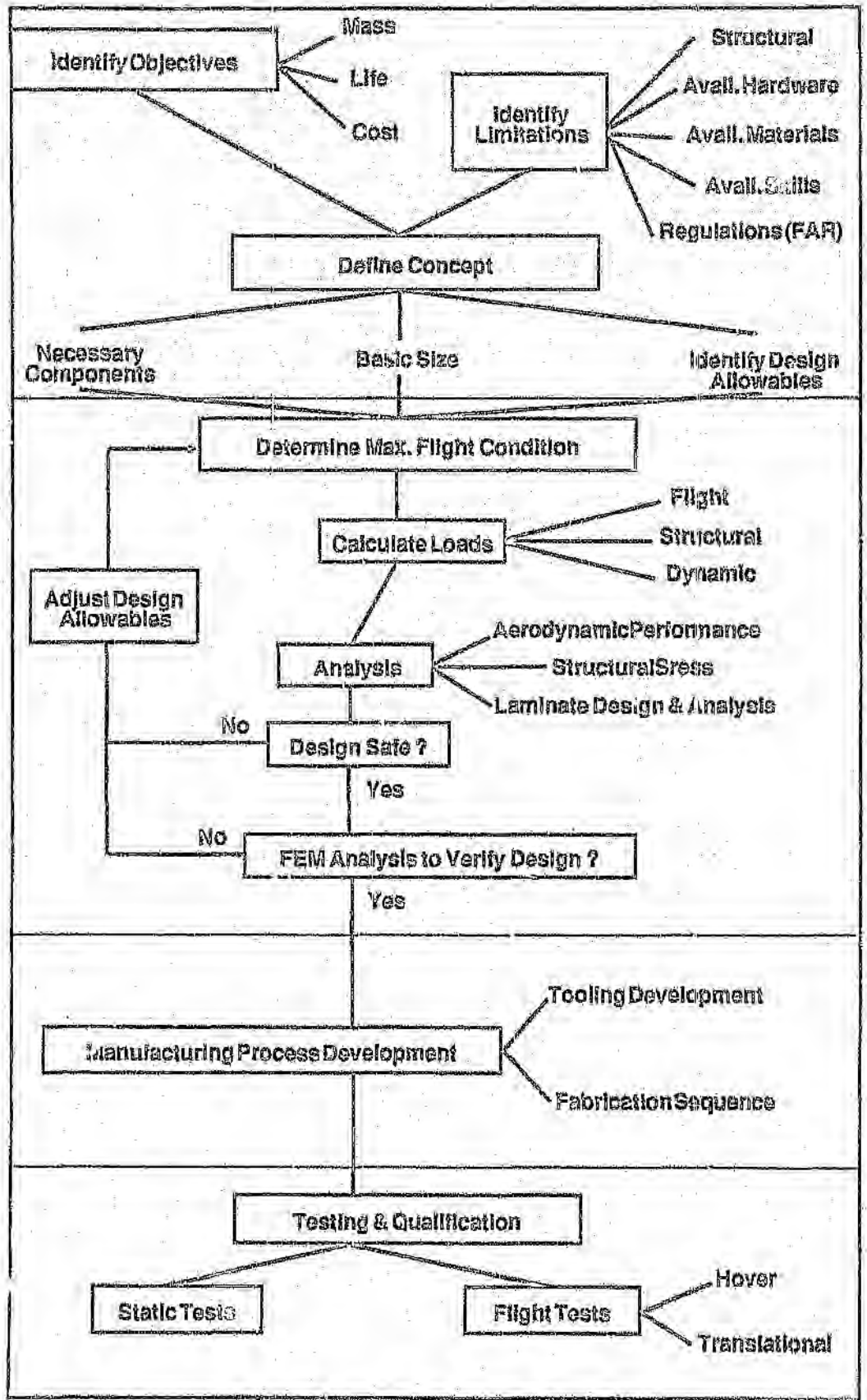

Figure 16: Design System Philosophy

1.3 Limitations of the Investigation

Initially, the objective of the program was to replace the current rotor system on Robinson R22 light commercial helicopters with a new rotor system manufactured from advanced composite materials. The project was being done in conjunction with a number of different people and organizations, placing a large number of restrictions on the development of this rotor system. The groups, not wishing to alter the performance or the aerodynamic characteristics of the Robinson to any great degree, retained certain features for the new rotor design. Some of these features being:

- the retention of the rotor blade aerofoil section which is given as a NACA 63$_2$-015 series,
- the retention of the rotor blade geometry and
- the blade root had to fit in with a composite rotor blade which had already been designed.

However, the project suffered some problems making it impossible to install such a rotor system on the Robinson helicopter. The rotor system was then scaled down and redesigned so as to be tested on a translational flight test facility, which was being developed. The aerofoil section from the Robinson helicopter rotor blade was retained in an attempt to construct a functional scale model of the rotor system which was to be placed on the Robinson R22 helicopter.

1.3.1 Hardware Limitations

The rotor system was designed to fit onto the translational flight test facility. This facility is portable and was designed to fit in the university's 1.5m x 1.5m low speed windtunnel. The windtunnel, in its present state, can deliver a maximum air velocity of 27 m/s at the test section, while the rotor test rig has a maximum power output of 4 kW within the speed range of 15rev/min to 3000rev/min. Parameters that can be measured by the rig are:

- thrust (-1500 to 1500 N ± 5.0N),
- torque (-25 to 25 Nm ± 0.1Nm),

- flapping angle (-15 to 15 deg. ± 0.3 deg.),
- control angles including collective (0 to 28 deg. ± 1.0 deg.) and cyclic (-7 to 7 deg. ± 1.0 deg. for both lateral and longitudinal cyclic),
- rotor shaft inclination (-80 to 80 deg. ± 0.3 deg.),
- rotor shaft speed (15 to 3000 rev/min ± 2.0rev/min) and
- strain measurements from the rotor blade surfaces.

The test rig and the windtunnel thus put limitations on the geometry of the rotor system.

Other hardware limitations on the design of the rotor were:

- the availability of materials and their associated costs,
- the available manufacturing skills and machines to manufacture some of the more complicated components,
- the size of the autoclave which was available at the university for use in the manufacture of components using composite materials.

1.3.2 Computer Limitations

The limitations caused by the use of computers only effect two areas of the project, namely the design-analysis and the testing phases. The acquisition of software for the analysis of rotor systems, which is currently being used elsewhere, was not possible and was thus developed as part of the project.

The only computers that were available for use were IBM type PC- AT workstations. The inherent memory and operating speed limitations of these workstations placed severe restrictions on the analytical software and data acquisition software.

Chapter 2

Literature Overview

2.1 Helicopter Rotor Aerodynamics

The most elemen. .y analysis of rotary wing aerodynamics is momentum theory. This considers the momentum balance of the fluid upstream and downstream of the rotor. This analysis, accounting for the entire rotor disk, can be used effectively for performance calculations, however, it does not give spanwise blade loads. The analysis thus makes no contribution toward the structural design of the rotor blades and as such will not be considered. Nikolsky[32] presented a method using blade element theory, as does Johnson[20], which is used to find the section aerodynamic forces. In the theory it is assumed that a blade section acts as a two dimensional aerofoil for which the influence of the rotor wake consists entirely of an induced velocity at the section. The two-dimensionality of the blade section in the theory also requires that the aspect ratio be high, which is generally the case for helicopter rotor blades. Thus two-dimensional aerofoil characteristics can be used to calculate the section loads in terms of the blade motion and aerodynamic environment of that section. Blade element theory is, however, dependent on the induced velocity which can

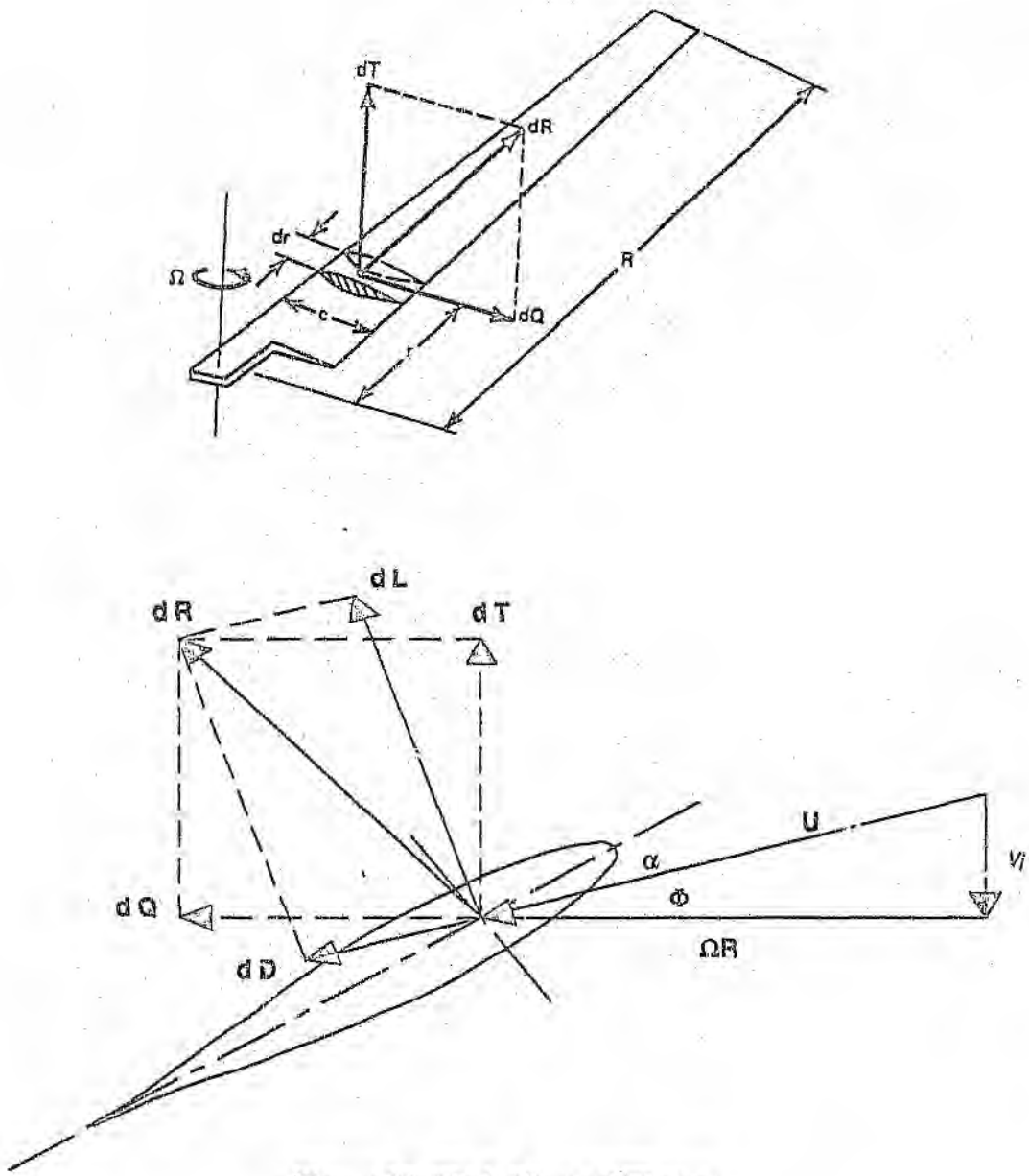

Figure 17: Blade Element Theory

be obtained by various means such as momentum theory, vortex theory and/or non- uniform free wake inflow calculations.

Associated with blade element theory are a number of assumptions which limit the accuracy of the analysis. Some such limiting assumptions are:

- Lifting line theory which is a fundamental assumption of rotor aerodynamics but is not valid in the vicinity of the blade tip. The rotor tip loss significantly influences both the performance and the blade flapping motion, thus necessitating the use of tip loss factors in the analysis.

- Tip stall of the retreating blade is neglected, which may only be valid at high forward speeds.

- Compressibility effects of the advancing blade are neglected. This assumption is invalid as the major portion of the blade producing the lift is generally operating at high Mach numbers.

- The section lift curve slope is considered linear.

- All the harmonics of motion above the second are small and thus have been neglected. This simplifies the analysis but does effect the load and dynamic analysis. An investigation done by Ludi[26] indicates that in a stalled condition the higher harmonics can become almost as large numerically and are as important as the lower harmonics.

- The trailing edge of each element in the reverse flow region is considered to be the leading edge, thus disregarding the effects of stall is a questionable assumption.

- Uniform inflow may be satisfactory for performance calculations at high speeds, but leads to significant errors in the calculation of the blade flap motion.

- The blades are considered to be infinitely stiff, which is reasonable for an aerodynamic analysis but cannot be assumed for the structural load and dynamic analysis of a rotor blade.

- A small angle assumption is used for all angles except the azimuth angle. This assumption is only valid for angles less than 15 degrees, which may not always be the case. For example the flapping angle can exceed 20 degrees.

Similar methods are presented in a number of publications such as Stepniewsky[39], Saunders[37], Layton[24] and Wheatley[46] who used the method for autogiros. For accurate quantitative results for the analysis/design of a rotor blade, the above model is too limiting. Thus most of the assumptions made should be eliminated so as to consider a thorough analysis of the helicopter rotor in forward flight.

A more theoretical approach for determining the performance of a rotor in forward flight is presented in Bailey[3]. All the rotor parameters, such as flapping, thrust and torque are represented as simple functions of the inflow velocity, tip speed ratio and the blade pitch. However, this method seriously underestimates the drag coefficients and it also does not account for the compressibility effects, thus the approach becomes optimistic.

A set of theoretical rotor performance charts for both hover and forward flight is presented by Tanner[43]. The charts are calculated using numerical techniques which include stall, compressibility effects and disregards the small angle assumptions. The charts cover linear twists of -8, -4, 0 degrees, advance ratios from 0.25 to 1.4 and advancing blade tip Mach numbers of 0.7, 0.8, 0.85 and 0.9. These charts do allow for a reasonably accurate rotor performance prediction, but the spanwise loading is not given in the charts, making this method useless for the design of the rotor blade and structure.

Equations and procedures, based on blade element theory, are presented by Gessow[13] for numerical analysis of lifting rotors, using computers. The equations are general and can account for stall and compressibility, hinge offsets, reverse flow performance and other limiting assumptions usually associated with the conventional analytical solutions. The model can contend with variable geometry, variable aerofoil sections, variable flight conditions including pitch, roll maneouvers and transient blade motion caused by control input changes. The general equations are solved using numerical techniques thus allowing any number of harmonics of blade motion and blade loading to be extracted. This model is thus very attractive for the analysis of a rotor system. Gessow & Crim[12] expanded this model to include 'seesaw' or teetering rotor systems, where the integro-differential equations motion for the rotor system include the effect of both blades on each other, as they are coupled together at the teeter hinge. A further in depth look at this model and the derivation of the equations shall be discussed later.

Although the numerical techniques eliminate many of the restrictive assumptions and simplifications of the conventional rotor analysis, some assumptions still remain. One of the more important assumptions, which is inherent in most theoretical rotor analyses, is the use of steady, two-dimensional aerofoil characteristics for evaluating section forces and moments. Comparisons of theory to data that have been made thus far do show good agreement. Also the use of experimental aerofoil data does improve the accuracy of the analytical model.

A further restriction on the method is the inflow model that is used to determine the air velocities and inflow. As has been mentioned, a uniform inflow model may be acceptable for performance calculations, however, it produces significant errors in the calculation of the blade flap motion, which is the basis of the analysis. A first harmonic model for induced velocity considering the linear variation of inflow with radius and azimuth, in translational flight, is suggested in Johnson[20].

This model uses a mean induced velocity which, may be obtained from momentum theory or any other method, and first harmonic terms, which are functions of inflow and tip speed ratio. The mean induced velocity term can be calculated from an inflow model presented by Nikolsky[32] which is based on a previous model by Nikolsky & Seckel[32]. A vortex model for translational flight was not used as it yields similar results to those obtained using momentum theory and it would increase the complexity of analysis with no real gain [10]. Goldstein's Modified Vortex Theory, presented in Nikolsky[32], was used for the hover flight analysis as it includes the tip losses and provides far better results than does momentum theory, thus justifying its use.

Further assumptions that were made are those of blade rigidity, which is reasonable except for aeroelastic and dynamic analysis, and neglecting the radial velocity component along the blade, which would probably be significant only at high tip speed ratios wherein they might influence the profile drag and stall pattern of the rotor.

Aerodynamic models using vortex lattice methods, prescribed and free wake inflow, the solution of the Navier Stokes equations and external flow to increase the accuracy of the load prediction were superficially investigated but not considered for this application. The increase of accuracy for the load prediction did not warrant the increase in complexity. In addition design safety factors were used on the predicted loads thus allowing for inaccuracies in the calculations.

2.2 Structural Loads and Rotor Dynamics

Numerous methods are available for calculating the uncoupled spanwise bending moments of rotor blades in steady unaccelerated flight. One method involves the tabular solution of the differential blade deformation equation [22]. The moments are linear functions of several independent rotor parameters and can be computed by transfer function, superposition techniques. The blade flapwise equation of motion is integrated numerically giving the transfer coefficients which relate the independent rotor parameters to the moment harmonics. Charts of the transfer coefficients are provided giving qualitatively accurate results of the flapwise bending moments. These tabular procedures are very lengthy, particularly when numerous loading conditions and rotor speeds are being investigated, which is characteristic of the design iteration process.

Other methods for calculating structural loads require the calculation of mode shapes and natural frequencies of the blade. Such a method that requires the bending mode shapes is that which is presented in Johnson[20]. This method equates the moment due to the aerodynamic, inertial and centrifugal forces to the structural moment due to the curvature of the blade, resulting in a partial differential equation. The boundary conditions needed for the solution of this equation are that the moment and shear force be zero at the blade tip while the inboard boundary conditions are dependent on the hub constraints ie. a cantilevered hub restraint has zero displacement and zero slope at the root. The equation is solved by the method of separation of variables, giving a series of mode shapes describing the spanwise deformation. The bending moment can now be obtained from the corresponding mode shapes or from the blade curvature. Similar methods have been documented by Tse, Morse and Hinkle[44], Blankenship and Harvey[5], Mil'et_al[30] and many others. However, these methods are very laborious and must usually be repeated for each rotor speed and flight condition to account for the full rotor envelope.

A method for calculating bending moments without preliminary mode shape or natural frequency calculations is presented by Mayo[28]. This method is adaptable to cantilevered, teetering and articulated rotor hub restraints. The differential equation for the blade bending moment is composed of matrix expressions for the centrifugal and vertical inertia, damping loads and aerodynamic loads. The effect of structural damping, which has generally been omitted in other methods, is included in this formulation. The boundary constraints at the hub are, as mentioned, dependent on the type of hub used. The equations are derived for articulated and cantilevered hub restraints, however, for the solution of the teetering hub restraint to be accomplished, the even harmonic loadings, as applied to a cantilevered constraint, and the odd harmonic loadings, as applied to a hinged constraint, must be considered [28].

This method is a finite element method in which each term of the moment equation is represented in matrix form from where the solution can be found by normal matrix manipulations. The method and the formulation of the method into a computer code will be discussed later. The validation of this method for teetering rotors was done by Mayo[29], where the measured structural bending moments were compared to the calculated results. The method is also capable of calculating the blade deflections, natural frequencies and mode shapes, however, the natural frequencies and mode shapes are difficult to find due to the slow convergence of this formulation.

The dynamic analysis of the rotor system is done during the design phase in order to establish the resonant frequencies of the system, and to ensure that they do not coincide with the operating frequencies of the rotor system. The natural frequencies of the rotor blades can be calculated by the methods outlined above, however, they are complex and laborious. Simpler methods for the evaluation of natural frequencies are available. Some of these methods are presented in Tse, Morse, and Hinkle[44]. The Rayleigh method is a simple technique applied to discrete systems. This method is generally only used to calculate the fundamental natural frequency since the dynamic mode shapes have to be assumed.

The first mode shape for this method can, however, be calculated from the static deflection [44]. Another method is the Holtzer method which is a semidefinite method. This method is essentially a systematic tabulation of the frequency equation of the system. It assumes a frequency with a solution being reached when the assumed frequency satisfies the boundary constraints of the system. The transfer matrix and Myklestad- Prohl method are finite element methods for continuous systems using a Holtze type approach. A continuous system is approximated by an equivalent discrete system of springs and lumped masses, where the spring of each element is determined by the structural properties of that element. This type of method thus allows complex systems to be modelled.

Another method for the dynamic analysis is the Holzer-Myklestad approach

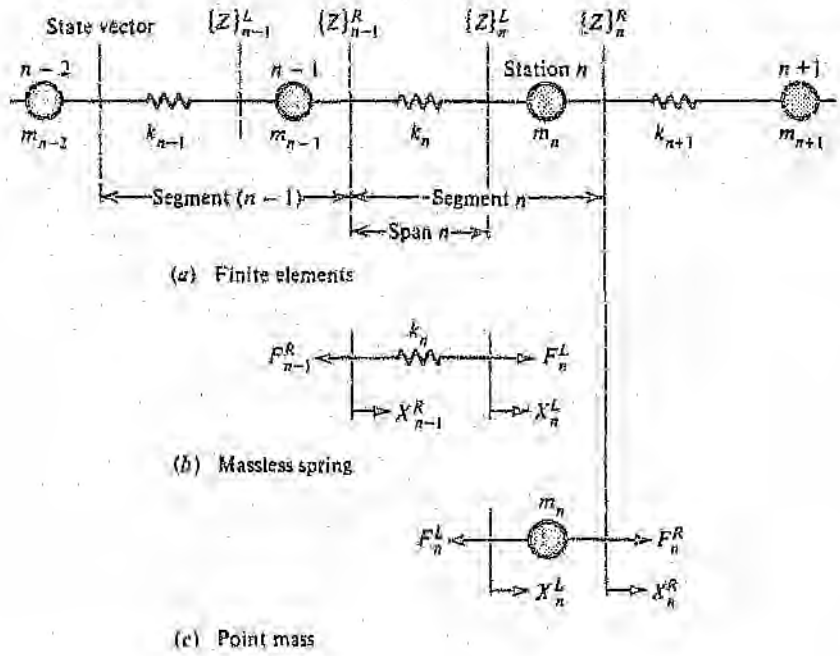

Figure 18: Finite Element Dynamic Model of Structure

adapted for rotating beams [45]. The method is based on a finite element approach, as discussed above, with the rotor blade being modelled as a lumped mass system with elastic coupling. Rotary inertia, blade geometric pitch and

vertical inertia are among the five degrees of freedom at each mass station. Blade properties at the discrete spanwise elements and the various hub configurations are also catered for. In this analysis different sets of boundary conditions are used, depending on the hub restraints. The resulting modal characteristics due to the boundary conditions are designated as collective, cyclic and scissors modes. The collective mode is characterized by symmetric out-of-plane and antisymmetric in- plane deflections of the opposing pair of blades, whereas the cyclic mode has symmetric in-plane and antisymmetric out-of-plane deflections about the center of rotation.

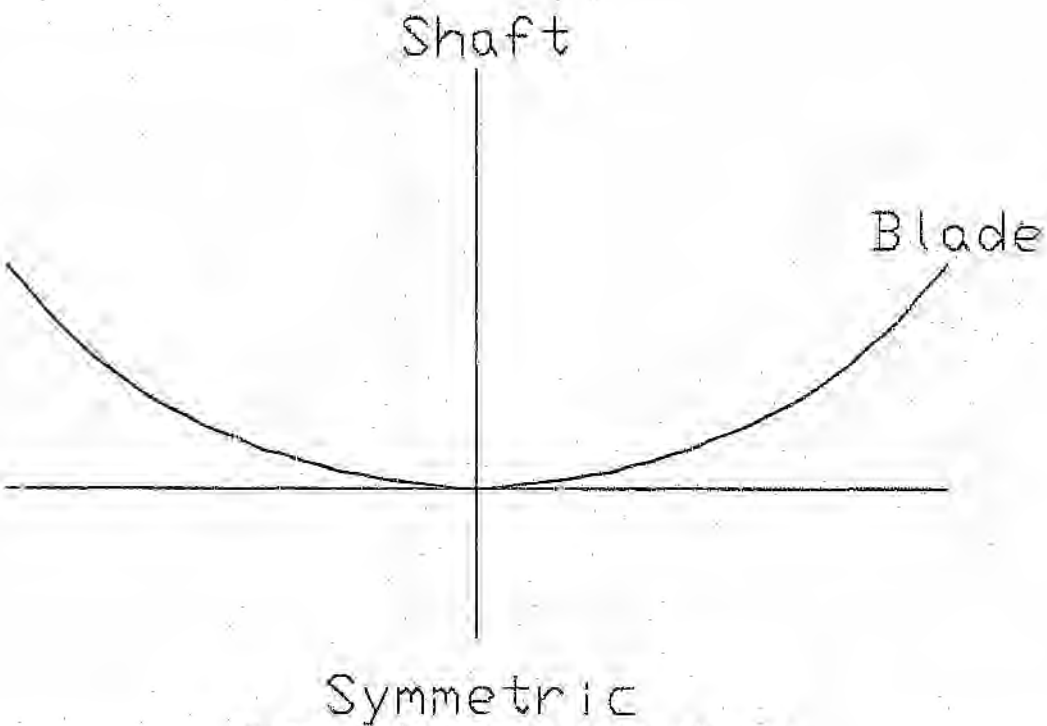

Figure 19: Collective Mode (out-of-plane)

For the scissors mode, the in-plane and out-of-plane boundary conditions at the center line represent clamping of the blades to an immovable hub. This method has been formulated in a computer code by Weller and Mineck[45] which makes it extremely versatile and easy to use. The output of this program gives resonance plots and mode shape data completing the dynamic analysis of the rotor system. The objective of this dynamic analysis is to ensure that all the harmonics of the

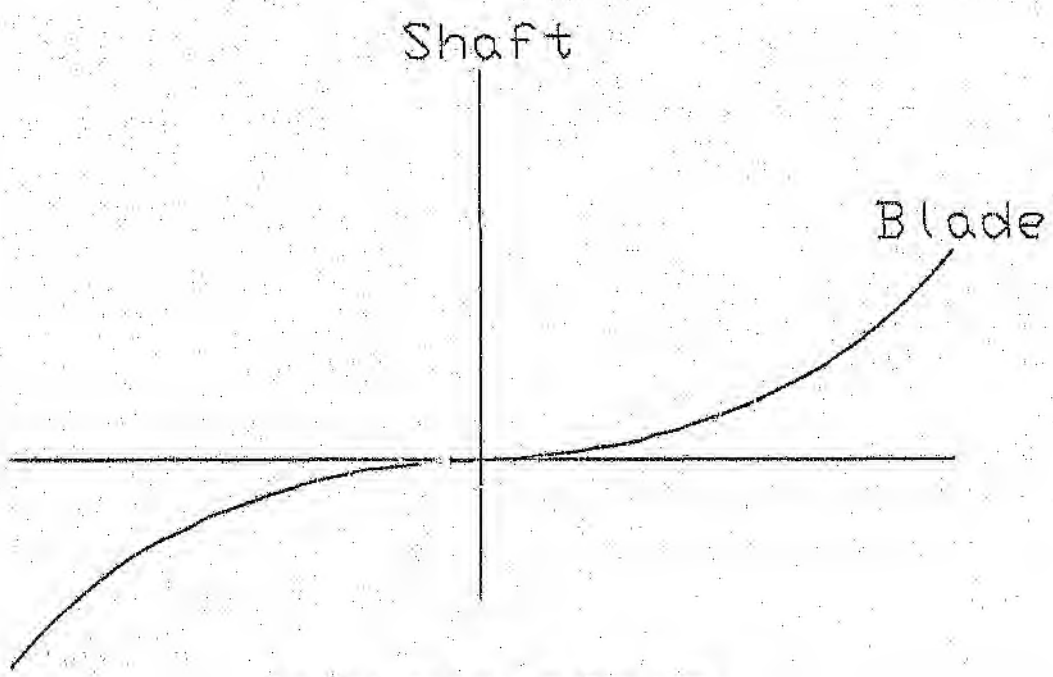

Figure 20: Cyclic Mode (out-of-plane)

rotor system are not excited by the operating frequencies, Mil'et_al[30] suggests that only the first eight harmonics are necessary for the analysis in order to minimize the computing time while still retaining the necessary accuracy.

2.3 Composite Rotor Applications

The application of composite materials to helicopters has been well documented by Foye & Shipley[10] and Rotor & Wing magazine[35]. These publications document the evolution of composite material applications since their emergence in the 1940's. The following discussion on the application of composite materials to helicopter rotors is based, among others, on the content of these two publications.

Composite materials had their start in the early 1940's with the introduction of fiberglass and polyester. This material saw applications in radomes, fairings and rocket launch tubes. The first application of composites to helicopters occured in the Sikorsky R-6, which had the floor coverings manufactured from fiberglass reinforced plastic. The 1950's saw the first composite structures on helicopters. The YH-32 helicopter, developed by Piasecki Aircraft, had a primary fuselage structure made from a metal truss covered with glassfiber skins. This helicopter showed that composites could be used without weight penalty and that the potential existed for lowering the structural weight and costs. The late '50's were also marked by the appearance of graphite and boron fiber materials, although they were not used on helicopters at that time.

In the 1960's inroads were made in applying composites to rotor blades. A study conducted by Bell in 1966 concluded *'... there were no major benefits in applying composites to helicopters except in the rotor blade area.'* Kaman Aerospace and Boeing helicopters developed composite main rotor blades, which eventually led to the composite advanced geometry blade program for the CH-47 main rotor. Sikorsky also began with composite rotor blades and by 1968 had flown a boron composite tail rotor on the S-61. By the end of the decade, dozens of components had been built out of advanced composites, but these materials made no substantial production inroads.

In the 1970's, new helicopter programs in both the US and Europe began to make extensive use of composites, especially in primary structures such as fuselages and rotor hubs. Aerospatiale was a leader in the development of a composite rotor hub, which was designated the Starflex. In the Starflex hub the mechanical hinges were replaced with flexible composites, which reduced the part count on the hub from 377 to 70 and made the Starflex cheaper to produce and easier to maintain. In recent years, every major helicopter manufacturer has developed or is developing a composite rotor system.

Currently, two major composite helicopter programs exist, namely: the Advanced Composite Airframe Program (ACAP) in the United States and the British Experimental Rotor Program (BERP) in Europe. In addition Boeing is funding its own composite program for the all composite Model 360. It is also involved with MBB in the development of an all composite hingeless and bearingless rotor system, which is currently being tested on a MBB-105.

The development of composite rotor blades and hubs is directed towards: [38]

- Improved performance and lift capability of the rotor for a given size and weight.
- Reducing the size required for a rotor system to achieve a specific performance or lift capability.
- Reducing the weight for a given size of rotor system.
- Improving the rotor system's safety, maintainability and reliability.
- Reducing the projected cost of ownership by virtue of a longer fatigue life and less required maintenance [36].

The materials and the design concepts required to fully exploit their advantages have the capability to achieve an unsurpassed level of fail safety and damage tolerance without sacrificing the cost objectives [38].

Manufacturing techniques for composite rotor blades generally follow the same pattern. The blades are manufactured in two halves, the upper surface half and

the lower surface half. The blade halves are assembled in their respective tool halves, the tooling moulds then being placed on top of each other closing the mould, giving the completed blade section. Such methods of construction are used by Boeing Vertol [38], Sikorsky Aircraft [36], Hughes Helicopters [42], Westland Helicopters and Aerospatiale. These manufacturing methods were adopted and are discussed in more detail, including the adaptions needed for the design and manufacturing limitations, further on in this report.

2.4 Composite Materials

The analysis of composite laminates using classical lamination theory (CLT) is well documented in Jones[21]. This theory considers the macromechanical behaviour of a laminate. The laminate is made up of a number of unidirectional lamina, which are oriented to provide the best strength and stiffness in the required directions. The theory is based on a thin plate analysis with a number of assumptions being made. These assumptions being:

- A perfect bond exists between each layer in the laminate.
- The behavior of the laminate is linear elastic.
- The plate thickness is small compared to the length and width of the laminate.
- There is a linear variation of strain with stress.
- Each layer is in a state of plane stress.
- Transverse strains are assumed zero.

These assumptions do limit the use of CLT to regions of the structure away from free edges, load introduction points and boundary constraints. This, however, does not limit the usefulness of CLT.

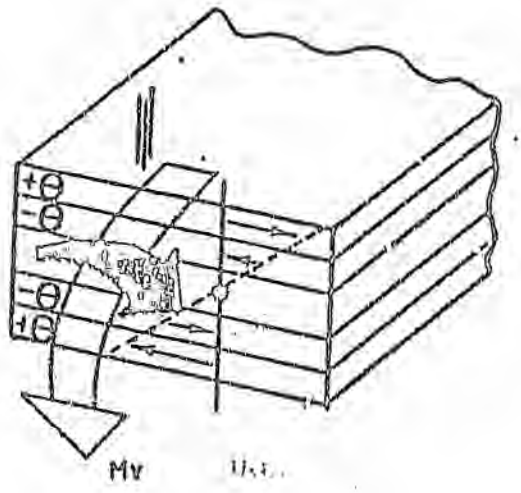

Figure 21: Composite Laminate

The failure of composite laminates can be predicted by means of a number of failure criteria theories, the most common of which are:

- Maximum stress theory which states that if any of the stresses in the principal material axes exceeds the corresponding allowable stress, failure will occur.
- Maximum strain theory which states that failure will occur if any strains in the principle axes exceed the corresponding allowable strains.
- Tsai-Hill theory which takes into account the interaction between the various stresses and strength.

The Tsai-Hill theory is the most conservative of the three mentioned above. Simply stated, failure occurs when the LHS of the following equation is greater than or equal to 1.

$$\frac{\sigma_1^2}{x^2} - \frac{\sigma_1 \sigma_2}{x^2} + \frac{\sigma_2^2}{y^2} + \frac{\tau_{12}^2}{S^2} \geq 1 \qquad (1)$$

The CLT analysis method using the Tsai-Hill failure criteria was adopted and formulated into a computer code and is described by Sheiman[49].

2.4.1 Composite Joints.

Often, the full strength and stiffness characteristics of the laminate cannot be transferred through a joint without a significant weight penalty. Thus the fastening of composite materials is critical to its successful use [21].

The first type of joint to be considered is the bolted joint. This type of joint introduces holes into the composite laminate considerably weakening the composite. The failure modes of mechanically fastened composites are tension, shear, bearing, cleavage and pullout, as shown if figure 22.

Unlike metals, the failure mechanisms are complex and varied and depend on many factors such as fibre type, orientation, surface treatment and matrix, etc [27]. Methods of minimizing the failure of a bolted joint are to use metal inserts

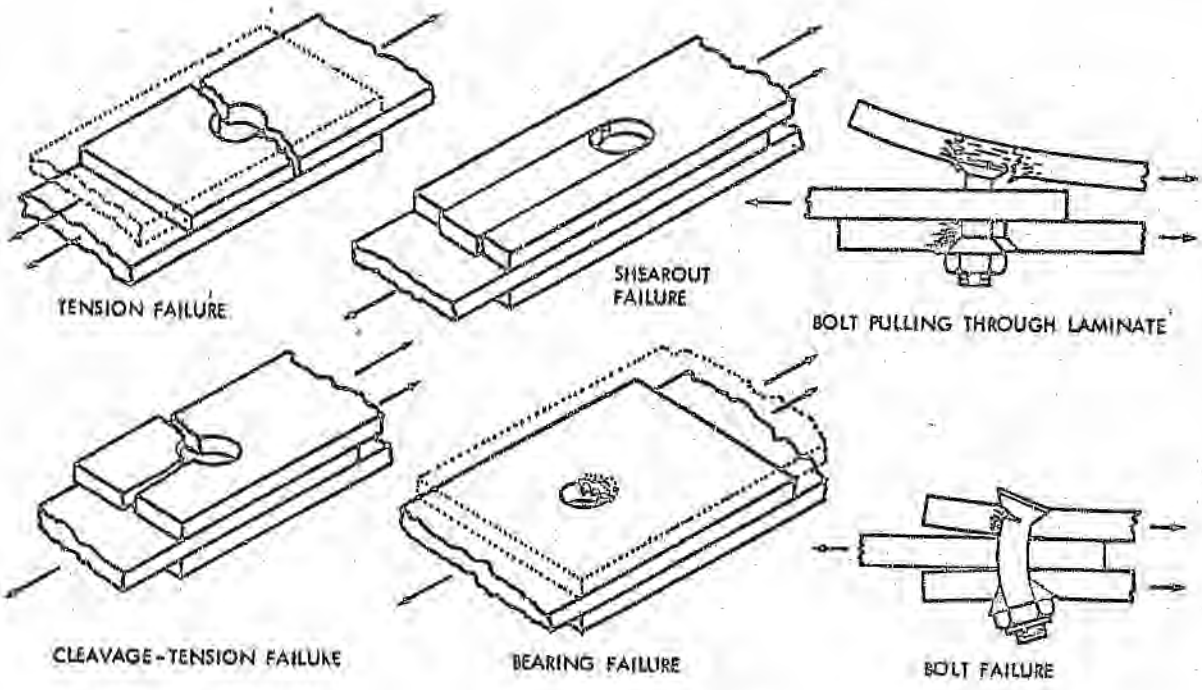

Figure 22: Modes of Failure for Composite Bolted Joints

[21] or to use quasi- isotropic laminates [27] (see figure 23). An empirical analysis used in the design of bolted connections in composites is presented in Matthews[27]. The approach of this method is to identify which factors must be accounted for and which can be neglected for any particular material, based on the material's known behavior.

A bonded joint is another type of joint that can be used to fasten composite laminates. There are many configurations of bonded joints, namely double lap, single lap, scarf and stepped lap joints. Methods for analyzing bonded joints in composites are presented in Hart-Smith[15]. These solutions are largely closed form analytical results, employing iterative solutions for the more complicated joint configurations. The method covers tensile, compressive and in-plane shear load conditions. In addition to the usual geometric variables, adhesive plasticity, adherend stiffness imbalance and adherend thermal mismatch are considered. The adhesive plasticity increases the joint failure strength dramatically above

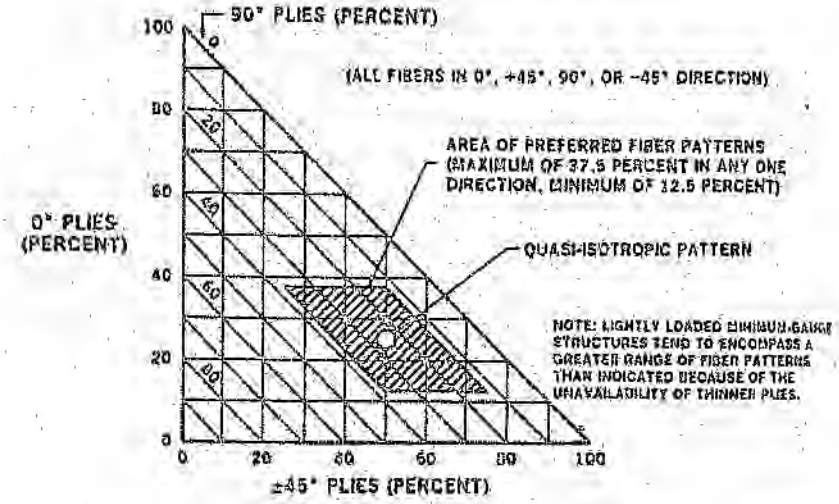

Figure 23: Selection of Lay-up Pattern for Composites

the predictions of the purely elastic analysis as the maximum lap joint strengths are shown to be defined by the adhesive strain energy in shear. The dissimilarity in the adherends reduces the joint strength. Three types of failure modes are prevalent in bonded joints. Firstly, the failure will occur outside the joint, which is particularly dominant in single lap joints. Secondly, the ultimate adhesive shear strain may be exceeded. Thirdly is the peel stresses induced at the end of the joint may exceed the interlaminar tension strength of the laminate, resulting in a splitting failure of the laminate. This latter failure is particular to thick section lap joints, but can be virtually eliminated by simple geometric modifications. The complete mathematical analysis for double lap joints is published in Hart-Smith[14]. The analytical form of the analysis was used in the design of the joint for the rotor system.

Further methods for the design and analysis of joints include theoretical solutions using finite element stress methods. These methods are presented in Matthews[27] for both mechanical and bonded joints. An additional finite element method analysis for the design of mechanically fastened joints is presented in Chang,Scott and Springer[7] using the Yamada-Sun failure criterion. These finite element methods are, however, complicated and the results

gained from this type of analysis over the classical analysis do not warrant the complication for the conceptual design process of this rotor system.

Chapter 3

Design Conceptualization and Rationale

'All parts of a helicopter are of equal importance but main rotors are more equal than others' [34]. It is for this reason that special care be taken in selecting the parameters for the design of the rotor in order to reap the greatest benefit. The goals of the parameter selection for the rotor are to ensure the best possible hover performance, best forward flight performance, lowest cost, lowest weight, etc. Some of these goals, however, complicate the design and conceptualization process as they are mutually contradictory in nature. Satisfying these contradictions, using a compromised solution within the limitations placed on the design, make up the definition and basic size of this new rotor system concept. The discussion of these compromises in order to reach the final concept constitute the content of this chapter.

3.1 Rotor System Concept

The current trend in helicopter rotor system technology is toward hingeless and bearingless rotor concepts. The best example of a hingeless rotor concept is the Starflex system, developed by Aerospatiale. This system has been fitted to the Dauphine and Astar/Twin Star families of helicopters. An example of a completely hingeless and bearingless rotor concept is under development at Boeing Vertol. This rotor system has been installed on a MBB BO-105 and is the closest yet to achieving those desired goals for the ideal rotor system. These rotor concepts have only been made possible by the recent onrush of composite materials research and development and application of this material to primary flight structures. These current trends in the helicopter industry were thus used as a starting point for the concept development of this new rotor system.

As there was a two blade limitation on the rotor system it was decided initially, to make a single unit, continuous system. Thus the two rotor blades and the hub would consist of one component, avoiding the need for any joints in the system. Referring to figure 24, the spar of the rotor blades would act as a flexbeam near the blade root. An aluminum center piece would then attach the whole rotor system to the shaft of the helicopter. A teeter hinge connection to the shaft was selected so as not to pass any out-of-plane bending moments into the shaft. However, this system does have a complicated fabrication process, as the

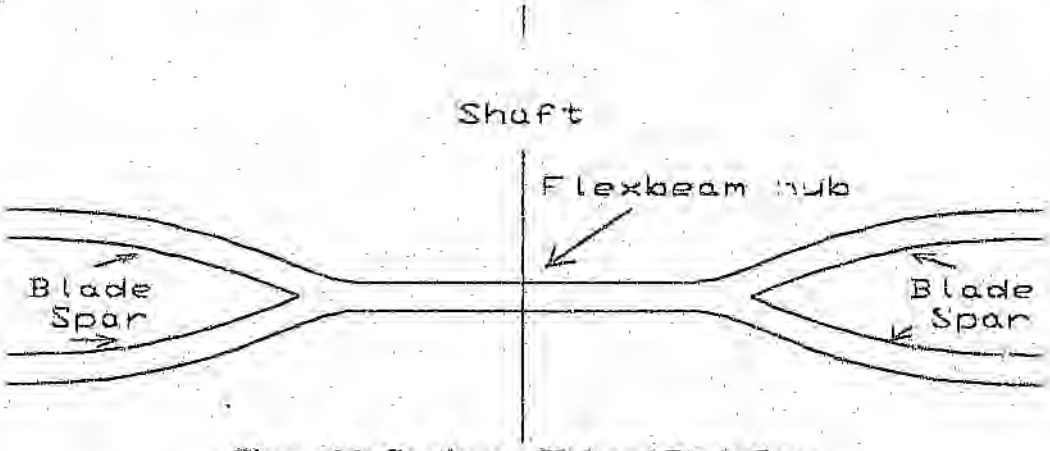

Figure 24: Continuous Hub and Blade Spar

spar/hub would have to be prefabricated and then inserted into the moulds during the fabrication of the complete rotor system. This type of system also requires a large autoclave for the curing of the complete rotor system, which was unavailable. Another disadvantage of a one piece rotor is that if one blade or both blades get damaged for any reason, the whole system including the hub has to be replaced, which can be a costly exercise.

The rotor system thus had to be in two parts for it to be manufactured. Initially,

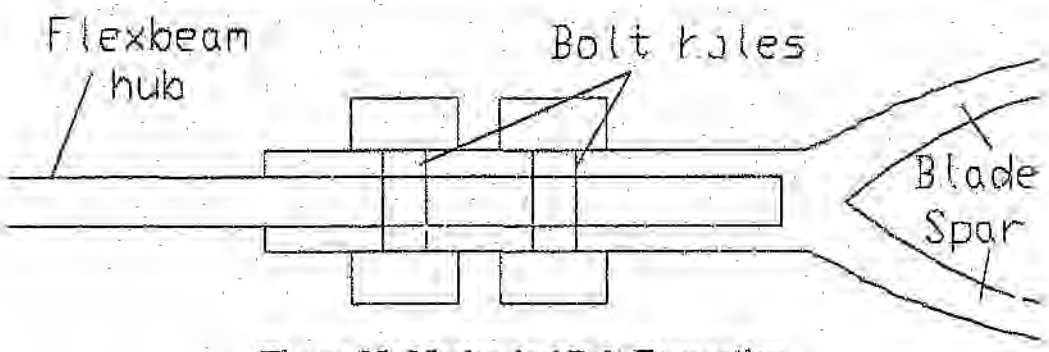

Figure 25: Mechanical Bolt Connection

the blades were to be separated from the flexbeam rotor hub. This meant that there would be a mechanical connection between the hub and the blade,as shown in figure 25. For this type of bolted connection in the blade root, two root retention systems were explored, these being:

- The 'coke bottle' type construction as shown in figure 26. This type of construction has the retention holes drilled into the laminate after the fabrication of the blades. Metal bushings and washers are then bonded into these holes. The bushings are used to relieve bearing stresses which can easily start cracks propagating into the laminate, as the fibres around the holes have been damaged. However, with the soft failure modes of fibreglass, this damage does not pose a threat when stress levels are low, and the crack growth is properly monitored.

- The 'wraparound' type construction as shown in figure 27. This retention concept has unidirectional fibres wrapped around the connection points. The fibres are thus not damaged in any way, providing a failsafe and damage tolerant system. This retention system has been verified to be significantly lighter than the 'coke bottle' type construction [38]. However, the fabrication of this

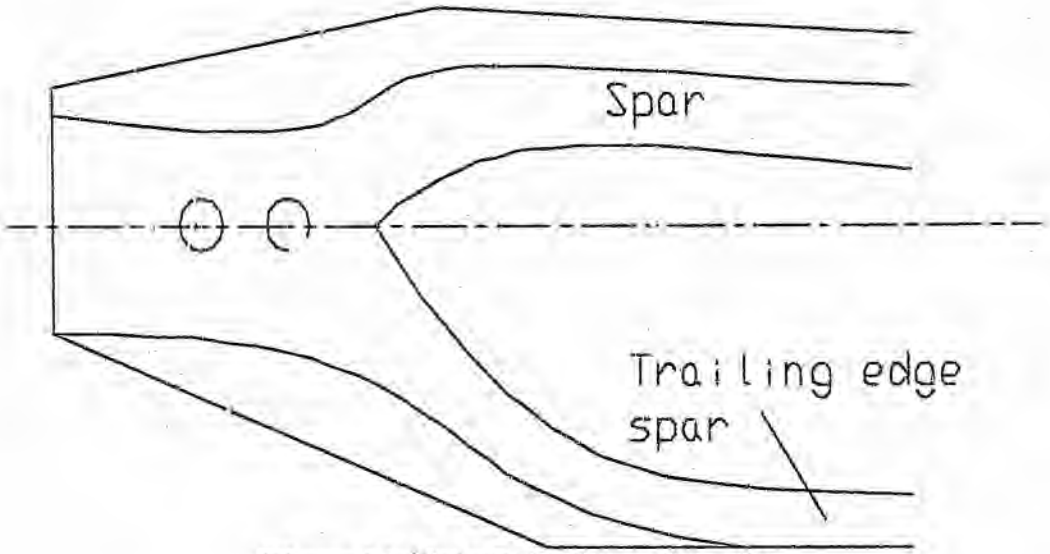

Figure 26: 'Coke Bottle' Root Retention

type of root retentic is more complicated than that
of the 'coke bottle
Thus the 'wraparound' root rete. favoured for the design.

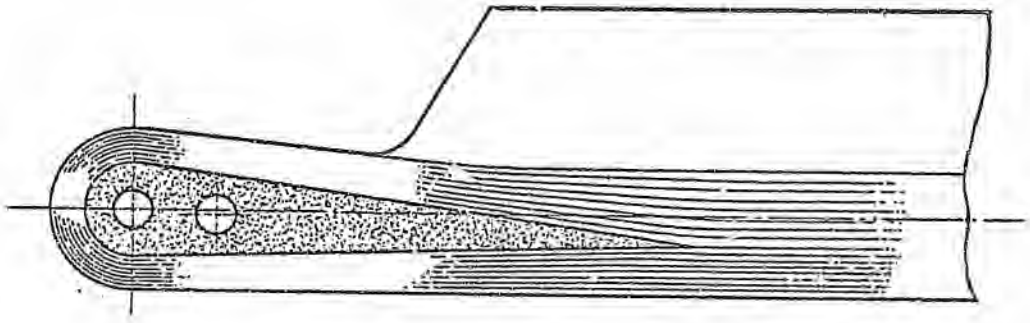

Figure 27: 'Wraparound' Root Retention

A problem now arose with the connection on the hub end of the joint. The flexbeam hub was to be fabricated using a carbon fibre preimpregnated material, because of the material's low moduli in the transverse and shear directions, thus

allowing it to twist readily. Although the specific strength and stiffness properties for carbon are excellent, the static and fatigue failure modes with their associated crack propagation properties are too rapid and severe causing catastrophic failure. Thus inserting holes into the flexbeam laminate would provide crack initiators for a catastrophic failure, making the system unsafe. To reduce the crack propagation rate and improve the damage tolerance of the carbon, fiberglass can be combined with the carbon. The fiberglass impedes the crack growth, thus giving the carbon a softer failure mode. However, this would severely impair the operation of the flexbeam, limiting its twisting and flexing capability.

Thus the use of pure carbon fibre in the flexbeam ruled out the possibility of a mechanical bolted connection. The solution of this problem finally led to the concept that was adopted. The problem was solved by splitting the flexbeam hub in two and bonding each half of the hub into the root of each blade, thus making the hub part of the rotor blade. The flexbeam hub is then connected to the hub center piece by means of a wedge type connection. The inboard section of the flexbeam hub has the carbon fibre material wrapped around a wedge shaped core, thus not damaging the fibres in the flexbeam. The hub center piece has two components which bolt together holding the flexbeam wedge in place. The outboard end of the flexbeam is bonded onto the spar of the blade with an adhesive, thus making the manufacture of the blade simpler and safe, as no holes

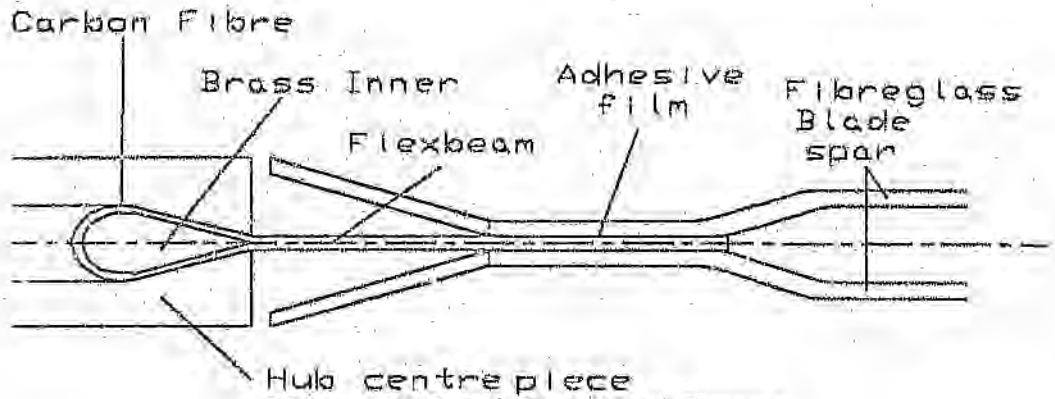

Figure 28: Wedge - Bond Root Concept

have to be cut into the blade root or the flexbeam. This concept can best be seen in figure 28.

Another factor that has a large influence on the conceptual design of the rotor system is the root cut-out area. The component in this area of the rotor that has the largest effect on the root cut-out is the flexbeam hub. In order for this flexbeam to operate effectively as a flap hinge and have sufficient strength to carry the centrifugal loads, it has to have a high aspect ratio (ie. be relatively long as compared to the width and thickness). This would suggest, that in order to accommodate the flexbeam, a large root cut-out is necessary. Aerodynamically, the only benefit gained from a large root cut- out would be to minimize drag on the retreating blade in a translational flight condition. However, a small root cut-out offers benefits for both hover and translational flight. The streamlining of the components close to the center of rotation to create a small root cut-out, reduces the drag in hover and on the advancing blade for forward flight, thus allowing for a more efficient power to weight ratio. The disadvantage of the small root cut-out is that the aerofoil in the reverse flow region of the rotor disc acts as a shovel scooping the air and creating high drag and down force on the blade.

This undesirable effect of a small root cut-out on the retreating blade can be compensated for by untwisting the blade near the root. This reduces the angle of attack in the reverse flow region, thus reducing its drag effect, while not adversely affecting the advancing side. It was thus decided to enclose the flexbeam in a faring so as to minimize the aerodynamic effects of the root cut-out, while maintaining the length of the flexbeam.

A secondary use of the faring is to input the feather controls into the rotor blade, allowing control of the rotor system. The faring can thus also be referred to as a pitch case. However, controlling the blade pitch using the pitch case causes a secondary out-of-plane bending of the blade at the blade root. These bending moments can be minimized by using an elastomeric bearing that is stiff with

respect to radial loading, but soft in torsion and in-plane shear. The bearing is bonded into the pitch case at the feathering axis of the rotor blade, which is at the center of the flexbeam. The elastomeric bearing, which is generally called a 'snubber', is compressed at all times so as to prevent it from debonding due to the relative motions between the flexbeam and the pitch case.

The resulting definition of the rotor concept shape is best represented below in figure 29. This rotor system design was frozen at this point, thus taking this definition to be the final conceptual design. A detail description of the components in the design concept follows.

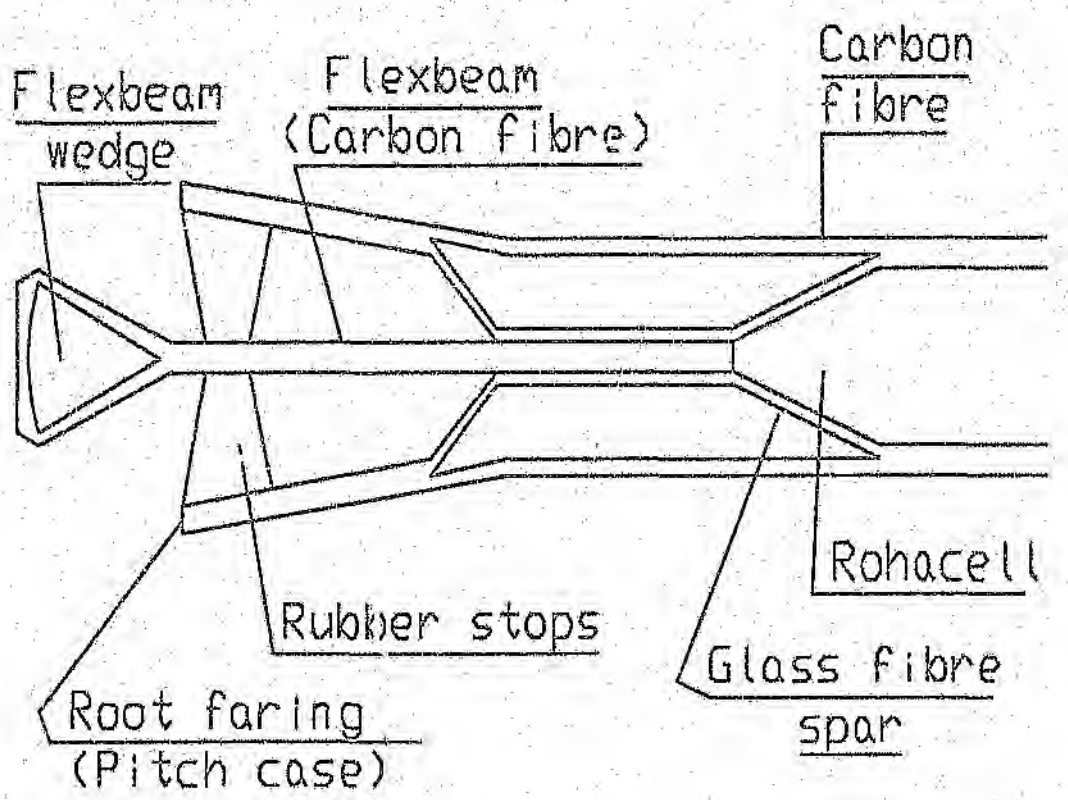

Figure 29: Rotor System Concept

3.2 Rotor System Geometry

The basic geometry of the rotor system was defined by optimizing its aerodynamic performance. Within the given objectives and limitations, the design allowable parameters were altered in order to obtain the optimum aerodynamic performance. The parametric study was done with the aid of the aerodynamic performance module of the design/analysis computer program (to be discussed later). Parameters that were kept constant in the iterative procedure are listed below:

- The aerofoil section was retained as a NACA 6 series 63_2-015. This is a symmetrical aerofoil with 15% thickness and a Cl range of +/- 1.4. The complete set of lift and drag data can be found in [APPENDIX E].
- The number of blades was kept at 2.
- The rotor blade twist was kept at 0 degrees as the machining capability for a twisted blade geometry was not available, ie. The only machine available to manufacture the blade pattern was a MAHO 3 axis CNC machine which can only work in two axes, while keeping the third constant.

The geometric design allowable parameters, with their associated limitations, used in the basic sizing of the rotor system design are listed below:

- The main rotor diameter, which cannot be larger the 1.5m as this will clash with the test section of the windtunnel into which the test rig is to be placed. A rotor diameter of this size will in any event be operating inside the boundary layer of the wind tunnel as well as in ground effect. Ideally, for a minimal air flow interference, the wind tunnel test section walls should be at least three rotor diameters away from the rotor disc edge. [11].
- The chord of the rotor blade which can be of any size. However, the aspect ratio of the blade should be kept to within reasonable limits, preferabley high for the theory to be valid.
- The root cut-out radius, which will be kept to a minimum for the reasons discussed previously.
- The precone angle, which is optimized to keep the operating out-of-plane bending moment to a minimum.

To assist with the sizing of the rotor system, a parametric study, based on a thrust capacity for the rotor of 350N (size of thrust load to be discussed later), was

carried out to determine the effects of the chord and radius on the power consumption. Two flight conditions were considered, these being translational flight at the windtunnel speed of 100km/h, and hover. The results showing the effects of chord with the radius kept constant and the effect of radius at constant chord are shown in figure 30 and figure 31, respectively. The design possibility that arose out of the parameter study that was considered most viable is that shown in table 1 below. These figures thus define the geometry of the rotor system concept.

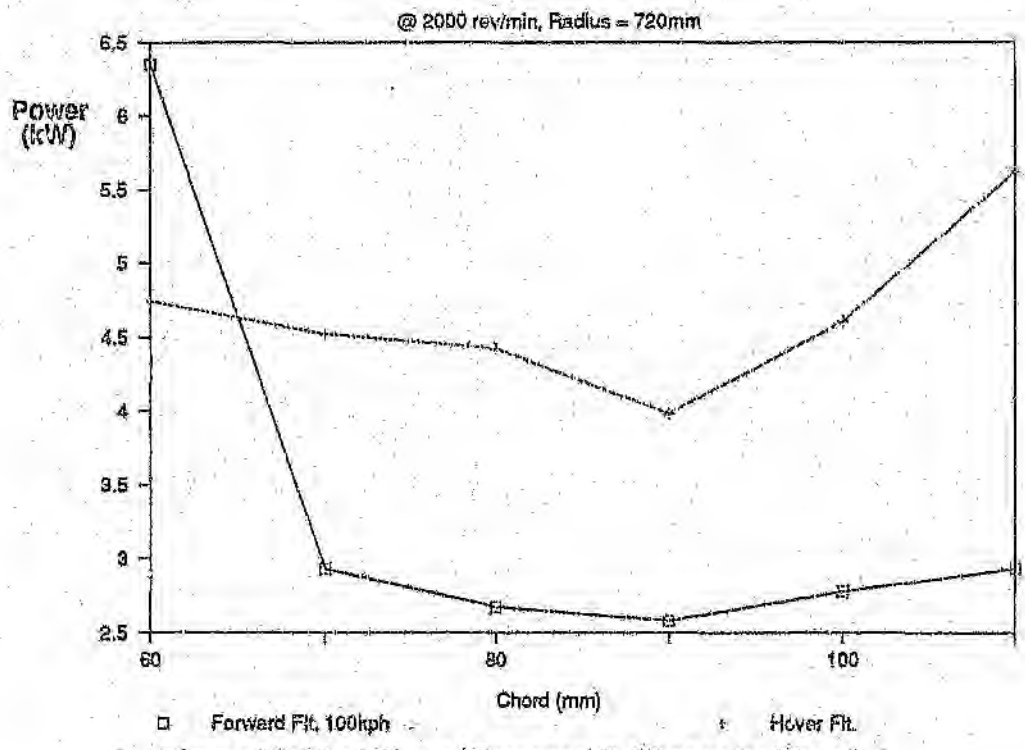

Figure 30: Variation of Power with Change in Chord

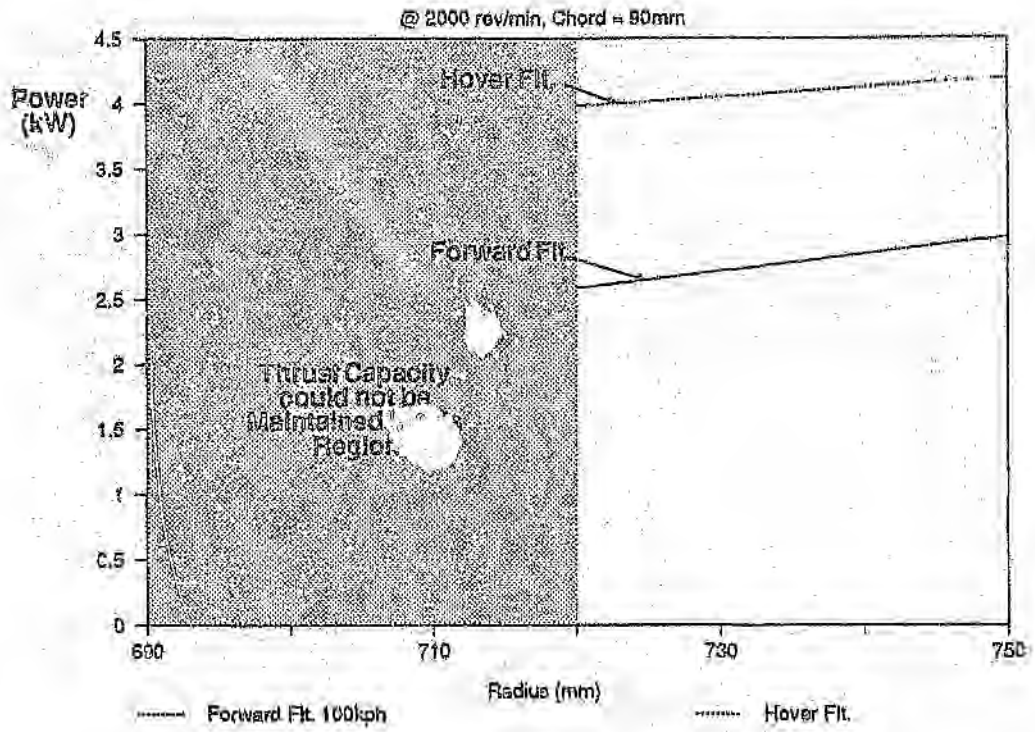

Figure 31: V .on of Power with Radius

Table 1: Rotor Geometric Parameters

Number of Blades	2
Rotor Radius	720 mm
Root Cut-out	0 mm
Blade Twist	0 deg.
Blade Chord	90 mm
Rotor Precone Angle	3 deg.
Aerofoil Section	NACA 63_2-015

3.3 Flexbeam

The flexbeam is the primary structural component that connects the two rotor blade assemblies to the central rotor hub. The flexbeam carries all the loads and transfers them into the central hub, where they are balanced with the opposing blade or transferred into the rotor shaft.

The flexbeam, shown in figure 32, is 167mm in length with a 15.23mm wedge length. The wedge has been optimized, based on stress levels, to give an optimum included wedge angle of 20 degrees. The wedge core was machined from brass with the flexbeam laminate wrapped around it. The flexbeam is formed as a flat rectangular beam which is untwisted. It is inserted into the blade giving a 0 deg. blade setting angle. The flexbeam laminate is built up of unidirectional Vicotex 913C T-300 carbon/epoxy preimpregnated material with a $(0/0/0/0/0/0/90/0/90)_s$ fibre orientation. This material was chosen because of its low shear modulus and high tensile strength. The fibre orientation is mainly 0 degrees giving it a capacity to carry large centrifugal loads, while maintaining a low torsional stiffness. The 90 degree layers aid the interlaminar shear transfer and provide transverse strength for the in-plane loads. The details of the flexbeam and its design can be found in Sheiman[49].

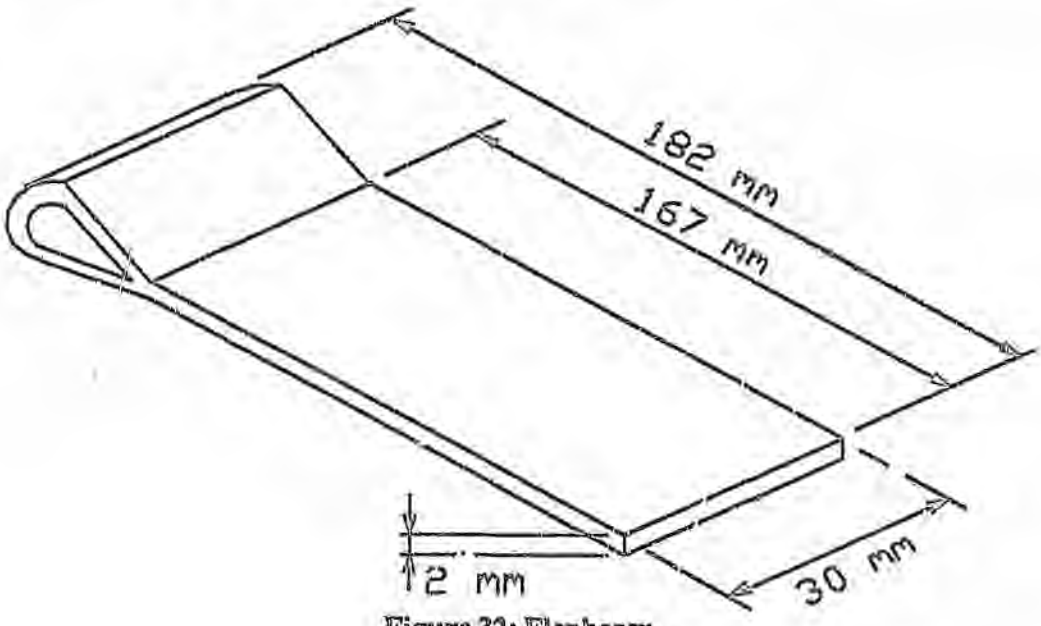

Figure 32: Flexbeam

3.4 Hub Center

The center piece of the hub, shown in figure 33, consists of an upper and a lower hub plate which hold the flexbeams in place. The upper hub plate is machined from mild steel with center lugs for connection to the drive shaft. The lower hub plate has a large hole through its center which fits over the shaft thus allowing the system to teeter to a maximum value of 25 degrees. The two hub plates are joined together by six anchor bolts, thus preventing the flexbeams from pulling out. Elastomeric pads have been inserted to provide a soft mount between the hub plates and flexbeam thus minimizing the compressive stresses on the flexbeam. These elastomeric pads also prevent frictional erosion and maintain a preload on the flexbeam so as to prevent it from slipping within the hub plates. The hub plates are designed to be strong enough to carry the centrifugal loads of each blade, the out-of-plane bending moments due to flapping, and the Coriolis induced in-plane bending moments. These Coriolis forces can, however, be greatly reduced by *'underslinging'* the rotor. The wedge section of the flexbeam is fitted into the hub with a small clearance fit. A 20mm edge constraint allows the torque reaction from the drive system to be transmitted to the blades and is also acts as a constraint for the in-plane blade loads. The detailed design of this component is not shown in this report but can be found in Sheiman[49].

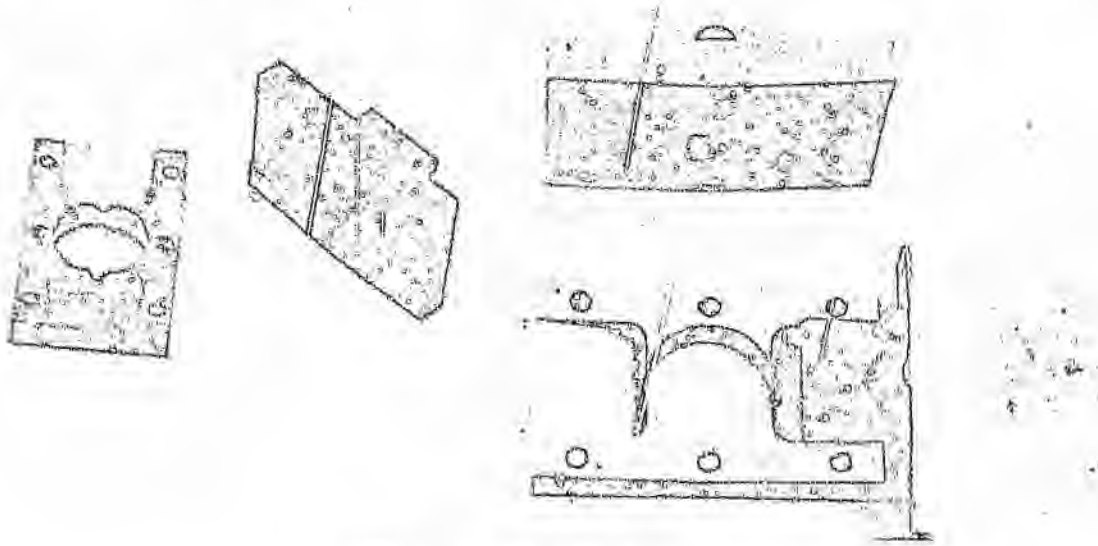

Figure 33: Hub Center

3.5 Pitch Case

The pitch case or root faring, shown in figure 29, is fabricated from unidirectional Vicotex 913C T- 300 carbon fibre laid at +/- 45 degree laminate angles and M9 R-Glass laid at 0 degrees. Inboard of the blade root, the pitch case enlarges to give sufficient clearance so that the flexbeam can twist and flap. The pitch case [figure 29] tapers in the spanwise direction to reduce the flapwise stiffness but without sacrificing the torsional rigidity. The inboard trailing edge of the pitch case is strengthened with the R-glass to provide support for the pitch horn.

A steel pitch horn, to which the pitch link attaches, is bolted to the strengthened trailing edge of the pitch case. The spanwise location of the pitch link connection defines the δ_3 angle, which is the pitch-flap coupling ratio. For the current design the pitch link connection is at the center of rotation giving a 0 degree δ_3 angle thus no pitch-flap coupling.

The pitch case is fabricated at the same time and in the same mould as the main rotor blade, thus making it part of the rotor blade structure. The outboard section of the pitch case retained the same aerofoil section as the rotor blade while the inboard section of the pitch case has its chord length increased to 135mm. The snubbers are bonded onto the inner surface of the pitch case at the feathering axis, as has been discussed previously.

3.6 Pitch Link

The pitch link is attached to the pitch horn with a pitch-flap coupling of 0 degrees ($\delta_3 = 0$). Since the pitch link is connected to the trailing edge of the blade, the pitch link loads are tensile for any positive blade setting angle. The diameter of the pitch links can be relatively small due to the fact that the flexbeam has a tendency to return the blade to a zero pitch angle thus maintaining a tensile load on the pitch links. However, buckling of the pitch link should be considered as a possibility as cyclic compressive loads may be experienced in this dynamic environment.

3.7 Flexbeam / Blade root / Pitch case Attachment

The root end of the blade is a critical structural area for the load transfer. It is here that the torsional bending moments are transferred from the blade to the pitch case, and where the flapwise, chordwise bending moments and the remaining centrifugal force of the blade is dumped into the flexbeam.

A bonded joint was selected for its structural efficiency and because it eliminates the induced stress concentration inherent in the mechanical fastening of composite structures (stress concentration factors for glass/epoxy of 4 and 9 for graphite/epoxy [21]) .

The prefabricated flexbeam is bonded onto the spar of the blade using a ductile thin film adhesive. A ductile adhesive was used against that of a brittle adhesive [figure 34], because of its more uniformly distributed load carrying capacity and softer failure mode. The shear stress levels have no sharp changes as is the case with the brittle adhesive. A high bond to adherend strength ratio was selected to ensure that the failure mode is the failure of the adherend outside the joint and not the shear failure of the adhesive joint itself (adherends are the components that are to be bonded together by the adhesive).

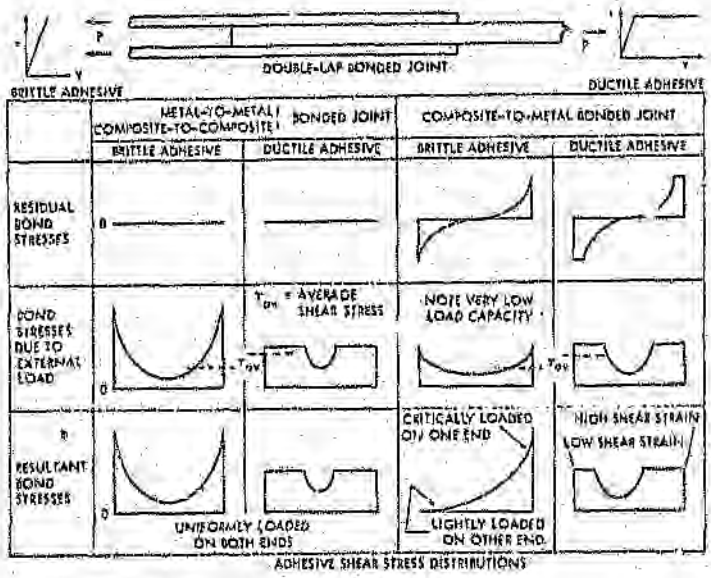

Figure 34: Comparison Between Adhesive Shear Stresses

The stacking sequence of the blade root connection area is shown in figure 35. The spar of the blade is brought in towards the center of the blade cross-section where it is then bonded onto the flexbeam. Inboard of the bonded joint, the spar returns to the surface of the blade cross-section and is then carried into the pitch case to provide additional strength. Mould pressure at the bond area is created by inserting the blade core material between the spar and blade surface, this also maaintains the blade profile at this point.

The position at which the flexbeam is bonded into the root of the blade is such that the torsional axis of the flexbeam coincides with the pitch axis of the blad which is at 25% blade chord. This is done to avoid any pitch-lag coupling of the rotor system.

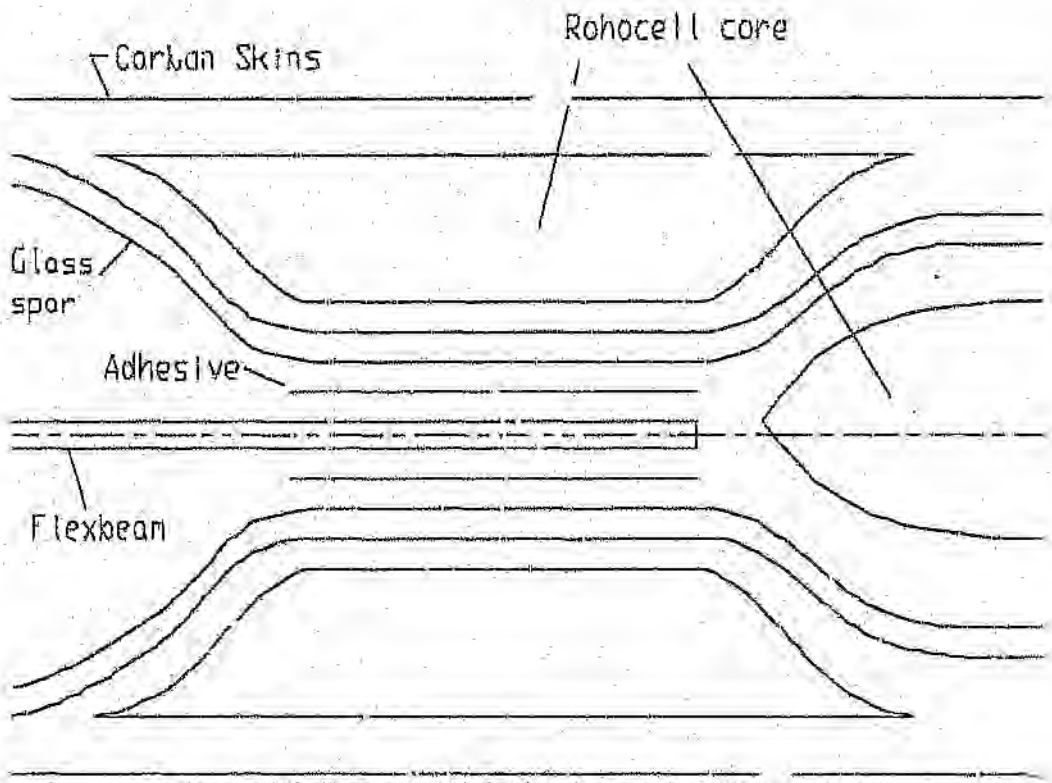

Figure 35: Exploded Stacking Sequence of Bond Area

3.8 Blade

The primary materials used in the construction of the blade structure [figure 36], are: (the specific materials used were those that were available and met the requirements)

- The skin of the rotor blade is used to provide torsional rigidity. In order to keep the mass to a minimum and maintain the torsional strength, a high tensile carbon fibre was considered. These requirements would be met by using 2 layers of carbon at +/- 45deg. laminate angles. The carbon that was available for use was Vicotex 913C T-300 carbon fibre.

- The material selected for the design of the spar was Fibreglass. The reasons for using this material is that it has a soft failure mode with slow crack propagation rate and a high damage tolerance, giving it an inherent fail safe quality. The environment of the rotor blade is dynamic with high alternating loads, thus requiring a material that has good fatigue properties. Fibreglass possesses 2.5 times the fatigue strain capability of steel and 3.3 times the capability of aluminium [38], thus making it a good material for a hostile fatigue environment. Unidirectional M9 R-Glass glass fibre, which has the same cure cycle as the carbon fibre, was available and used for the construction of the blade spar and trailing edge. The spar and trailing edge lamination angles are 0 deg. only, with the zero degree angle being in the spanwise direction. The spar carries all the out-of-plane and centrifugal loads and transfers the in- plane loads to the flexbeam, while the material in the trailing edge is used for dynamic tuning and to provide chordwise stiffness.

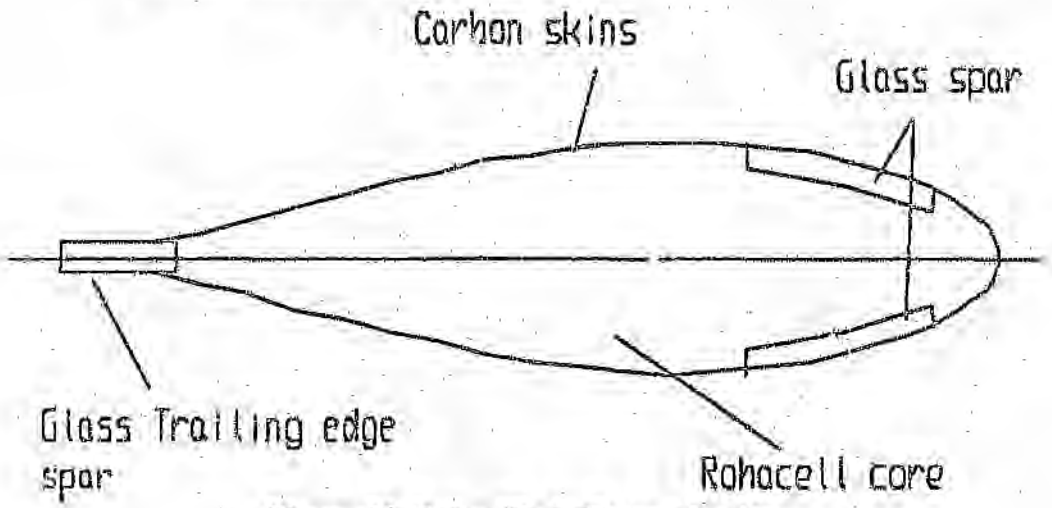

Figure 36: Rotor Blade Cross - Section

- Rohacell foam was available and used for the core of the blade section. The core serves to maintain (i) mould pressure during the curing process, (ii) a consistent blade profile and (iii) to control the shear deformation as a result of the torsional loads on the blade.

- Redux 312L thin film adhesive which met the ductile bonding requirements in the root, was available and is also used to bond the core and the skins of the blade together, making for a torsionally stiff blade section.

Outboard of the blade root section the blade has a constant profile, a cross section of which is shown if figure 36. The blade is laid up in two halves with the respective cores being bonded together when the mould is closed.

The blade has not been designed with any erosion strip to provide leading edge protection in the high wear region of the blade. It can, however, be added if it is found to be necessary for this particular design.

Chapter 4

Loads and Structural Analysis

This chapter is concerned with the prediction of the design loads, the structural analysis of the rotor system and the analysis of the critical bond area of the blade root.

4.1 Analytical Rotor Model

The rotor model developed for the prediction of loads and performance and the analysis of the rotor system concept has three sub-sections, namely:

- A rigid aerodynamic model used for the performance prediction, parametric study and airload prediction.
- An elastic structural model used for the prediction of blade bending moments.
- A fully coupled elastic dynamic model used for the determination of mode shapes and rotor blade natural frequencies.

The equations presented are used for the computing of the characteristics of a rotor system. These characteristics include thrust, drag, power, flap motion, airloads, control angles, structural loads, natural frequencies and blade mode shapes. The equations are general and can account for stall, compressibility

effects, hinge offsets, precone, multiple aerofoils, variable geometry and other factors normally omitted from the conventional analytical treatments.

The flight regimes in which this rotor model is valid are hover flight and full translational flight, including pitch and roll manoeuvres. The assumptions and limitations of this model are:

- The blades are considered to be rigid for the aerodynamic sub-model.
- The aerodynamic characteristics are limited by the use of statically determined, two dimensional aerofoil data.
- The inflow model for translational flight is a first harmonic model and is limited to use in the region of advance ratios from 0.175 to 0.5.
- The structural prediction sub-model is limited to calculating out-of-plane bending moments.

The integro-differential equations of motion are derived by resolving moments of the forces acting on an element of the blade, about the flapping hinge. Considering figure 37, the resulting moment balance is given by

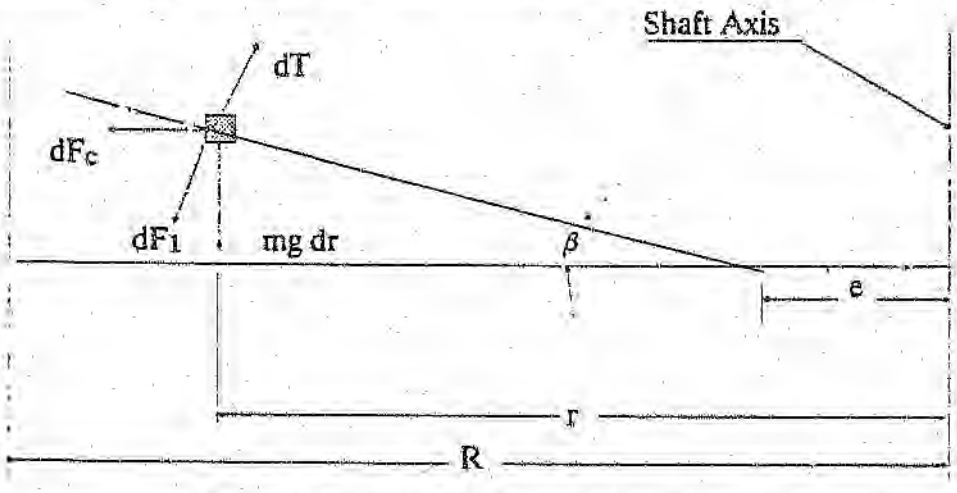

Figure 37: Aerodynamic Blade Force System

$$M_T - M_C - M_I - M_W = 0 \qquad (2)$$

where

M_T = Thrust Moment

$$M_T = \int_{r_c}^{BR} \frac{1}{2} \rho U^2 c \left(r - e \right) C_l \, Cos \, \Phi \, dr + \int_{r_o}^{R} \frac{1}{2} \rho U^2 c \left(r - e \right) C_{do} \, Sin \, \Phi \, dr \tag{3}$$

M_C = Centrifugal Moment

$$M_C = \int_e^R m \, \Omega^2 \left(r - e \right) \left[e + \left(r - e \right) Cos \, \beta \right] Sin \, \beta \, dr \tag{4}$$

M_I = Inertia Moment

$$M_I = \int_e^R m \, \ddot{\beta} \left(r - e \right)^2 dr \tag{5}$$

M_W = Weight Moment = $M_W' \, Cos \, \beta$

$$M_W = \int_e^R m \, g \left(r - e \right) Cos \, \beta \, dr \tag{6}$$

These equations are non-dimensionalised by defining

$$x = \frac{r}{R}, \xi = \frac{e}{R}, u = \frac{U}{\Omega R}$$

and substituting for

$$\dot{\beta} = \Omega \frac{d\beta}{d\varphi} = \Omega \beta'$$

$$\ddot{\beta} = \Omega \frac{d^2 \beta}{d\varphi \, dt} = \Omega^2 \frac{d^2 \beta}{d\varphi^2} = \Omega^2 \beta''$$

$$I_H = \int_e^R m\left(r - e\right)^2 dr$$

Thus resulting in the general flapping motion equation

$$\frac{1}{2}\gamma\left[\int_{x_c}^{B} u^2\left(x - \xi\right) C_l \cos\Phi\, dx + \int_{x_c}^{1} u^2\left(x - \xi\right) C_{d_o} \sin\Phi\, dx\right]$$

$$- \sin\beta\left(\cos\beta + \frac{eM_W'}{gI_h}\right) - \overset{=}{\beta} - \frac{M_W' \cos\beta}{\Omega^2 I_h} = 0 \qquad (7)$$

where

$$\gamma = \frac{\rho c R^4}{I_h} \qquad (8)$$

The section angle of attack needed for the determination of the lift and drag coefficients C_l and C_d is calculated from

$$\alpha_r = \theta_0 + \theta_1 x - A_1 \cos\varphi - B_1 \sin\varphi + \Phi \qquad (9)$$

The elemental, non-dimensional resultant velocity and inflow angle needed for the solution of the above equations, are given by

$$u = \left[U_p^2 + U_T^2\right]^{\frac{1}{2}} \qquad (10)$$

$$\Phi = \text{ArcTan}\,\frac{U_p}{U_T} \qquad (11)$$

where

$$U_p = \lambda Cos\beta - \left(x - \xi \right) \overline{\beta} - \mu Sin\beta Cos\varphi + \frac{q}{\Omega} x Cos\varphi + \frac{p}{\Omega} x Sin\varphi \quad (12)$$

$$U_T = \xi + \left(x - \xi \right) Cos\beta - \mu Sin\varphi \quad (13)$$

These velocity equations depend on the inflow ratio λ which is computed from an inflow model. Two inflow models have been used in this formulation, namely:

- Goldstein's Modified vortex theory hover inflow model. This theory considers the wake to be a rigid helicoidal surface of infinite length and of finite radius, moving parallel to its axis with a uniform velocity. The derivation of the equations used in this model are described in detail in Nikolsky[32], the result of which is

$$\nu = \frac{\sigma_x C_l U}{8 x Tan\Phi \kappa} \quad (14)$$

This equation is solved using a numerical algorithm which is shown in [APPENDIX A] and Nikolsky[32].

- The translational flight inflow model is described in Nikolsky[32] and is shown below, expressed in terms of λ

$$t_1 \lambda^2 + \left(\frac{2 C_T}{a \sigma} \right) t_2 \lambda + \left(\frac{2 C_T}{a \sigma} \right)^2 t_7 + t_{22} \frac{\delta}{a} + \frac{2 C_Q}{a \sigma} = 0 \quad (15)$$

where the coefficients t_1, t_2, t_7 & t_{22} are given in the reference. The constant inflow is then modified by

$$\nu = \nu_o \left(1 + \kappa_x r Cos\varphi + \kappa_y r Sin\varphi \right) \quad (16)$$

where

$$\kappa_x = \frac{4}{3}\left[\left(1 - 1.8\mu^2\right)\left[1 + \left(\frac{\lambda}{\mu}\right)^2\right]^{\frac{1}{2}} - \frac{\lambda}{\mu}\right]$$

$$\kappa_y = -2\mu$$

to give a linear model varying with radius and azimuth.

The Integro-differential equation of motion for the teetering constraint is derived in an analogous manner. The difference being that the moments are resolved about the teeter hinge with the effect of both blades being taken into account. The resulting equation is given as

$$\frac{1}{2}\gamma\left[\left(\int_{x_c}^{B} u^2 x C_l \cos\Phi\, dx + \int_{x_c}^{1} u^2 x C_{d_o} \sin\Phi\, dx\right)_{\varphi} -$$

$$\left(\int_{x_c}^{B} u^2 x C_l \cos\Phi\, dx + \int_{x_c}^{1} u^2 x C_{d_o} \sin\Phi\, dx\right)_{\varphi+\pi}\right] -$$

$$\left(2\sin\beta\cos\beta + 2\ddot{\beta}\right)_{\varphi} - \beta_o = 0 \qquad (17)$$

where

β_o = Precone Angle

The complete solution to the Integro-differential equations, for a particular flight condition,is achieved by using a 4th order Runga Kutta numerical scheme with the aid of a computer. The details concerning the formulation of the solving algorithm and verification of the computer codes and solutions is given in [APPENDIX A].

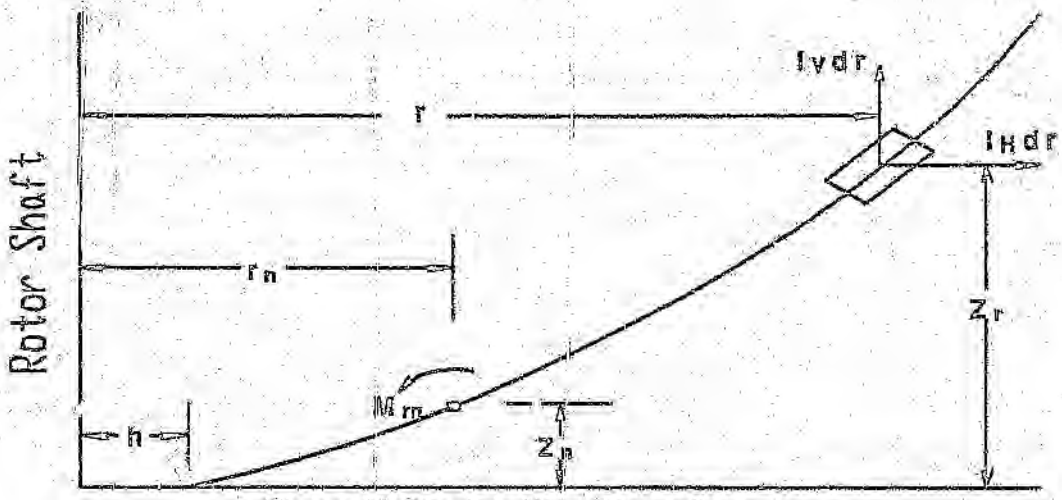

Figure 38: Flexible Blade Force System

In order to calculate the structural bending moments, flexibility has to be introduced into the rotor model. A method using a separate flexible model, dependent on the aerodynamics, was adopted. The general equation governing this flexible model is shown below and the detail derivation is presented in Mayo[28].

Consider the forces acting on an element of the blade under a particular flight condition. From figure 38 it is seen that the bending moment M_m at any station r_n due to the loads acting on the blade is given by

$$M_m = \int_{r_n}^{R} l_V \left(r - r_n \right) dr - \int_{r_n}^{R} l_H \left(z - z_n \right) dr \qquad (18)$$

This equation can be rewritten to a matrix equivalent form

$$\{M\} = [r]\{l_V\} - \Omega^2 [F]\{Z\} \qquad (19)$$

where

[r] and [F] are integrating matrices incorporating vertical and horizontal loads and integrating values, respectively.

The matrix form of the moment equation lends itself to a numerical solution algorithm which is easily programmable. The details concerning the method of solution and the computer solution algorithm are described in detail in [APPENDIX A].

The final model needed to complete the analysis of the rotor system, is the dynamic model. The model used is completely independent of the previous two models discussed, and its function is to calculate the mode shapes and natural frequencies of the rotor blades. The model is based on the Holzer-Myklestad approach adapted for rotating beams. The model exists as a computer software program supplied by NASA Cosmic software. The codes have been fully documented, including the equations and the techniques for solution [45]. This computer code was used, without modification, for the analysis of the rotor system, as it was completely validated by the above mentioned authors of the documentation.

In later sections of this dissertation only the results from the above mentioned rotor models are presented. The use and operation of the computer codes do not form part of this dissertation and as such will not be discussed.

4.2 Design Iteration Procedure

The design iteration process followed the steps shown in figure 39 below, until an acceptable solution was reached:

- The external rotor blade geometry was adopted considering the results of the geometric parameter study.
- Flight conditions, to be defined later, were calculated for the rotor geometry.
- The results of the flight conditions are compared to the required performance.
- Mass and stiffness distributions were estimated thus giving the structural loads on the rotor blade.
- The structure was then analyzed for failure with the blade properties being adjusted until the structure was safe. A safety factor of 2 was used due to the uncertainty of the manufacturing quality.
- Once the rotor system was fully defined all the properties were calculated and the system analyzed, with the bond area being analyzed using Finite Element Methods.

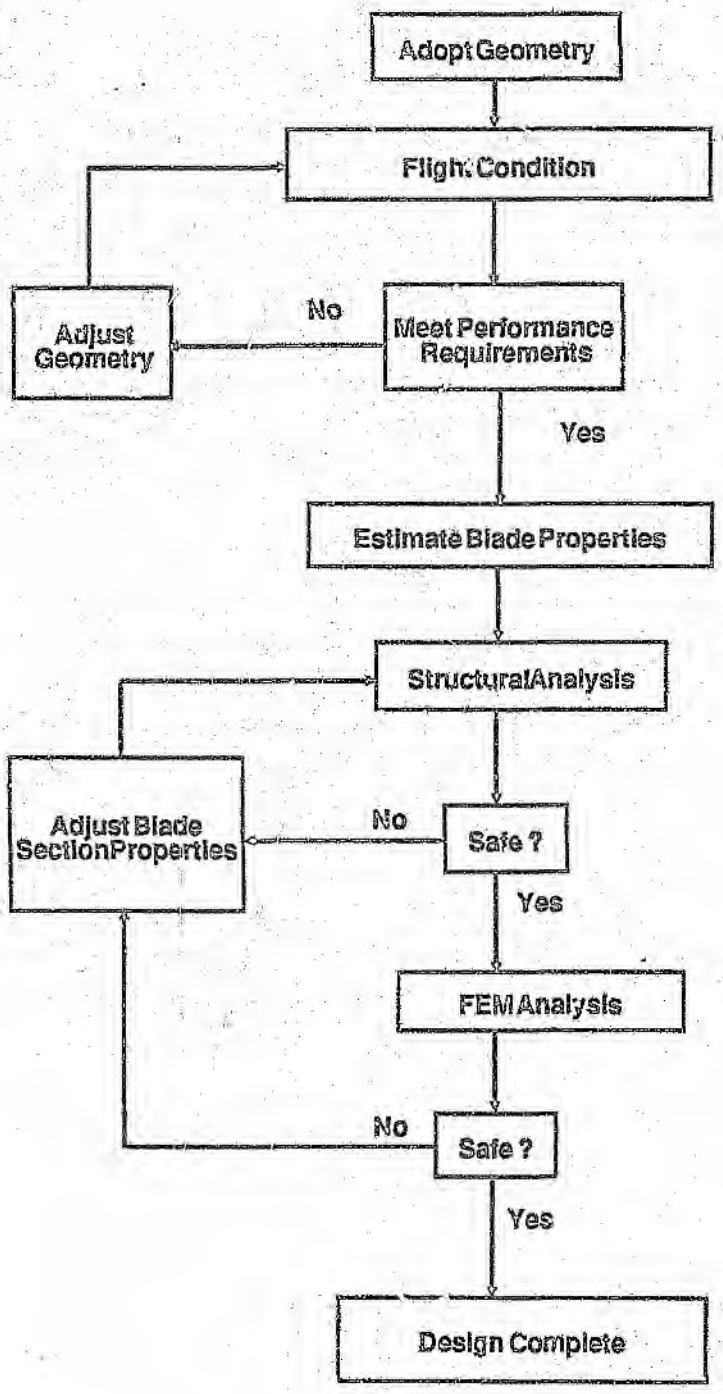

Figure 39: Design Iteration Process

4.3 Design Flight Conditions

The flight conditions used for design purposes are as a result of the geometric parameter study mentioned earlier, and the test facility limitations. The parameter study in the hover condition showed that with an installed power of 4kW a maximum lift capability of ± 350N was obtainable. This lift capacity was thus used as a performance requirement for the translational flight conditions.

The resulting flight conditions [Table 2], which were considered for the calculation of flight loads and structural loads are:

- Maximum level flight speed, including windtunnel limits.
- Hover at maximum installed power.

Table 2: Flight Condition

	Forward Flight	Hover Flight
Rotor Speed	2000 rev/min	2000 rev/min
Forward Speed	100 km/h	0 km/h
All up Mass	35 kg	35 kg
Collective Pitch	8 deg.	10.5 deg.
Lateral Cyclic	0.746 deg.	0 deg.
Longitudinal Cyclic	-3.597 deg.	0 deg.
Helicopter Pitch Vel.	0 m/s	0 m/s
Helicopter Roll Vel.	0 m/s	0 m/s
Air Density	1.2 kg/m^3	1.2 kg/m^3
Air Temperature	15 °C	15 °C

Both conditions were at the calculated maximum lift capacity of the rotor.

4.4 Structural Analysis

4.4.1 Design Loads

Table 3 shows the design loads for the maximum level speed flight condition, as derived with the aid of the computer code in [APPENDIX A]. Figure 40 shows the out-of-plane spanwise structural bending moment of the rotor system for this flight condition. The out-of-plane structural bending moment for the hover condition, shown in figure 41, was minimized by altering the precone angle on the hub. This bending moment is thus much smaller than that for the forward flight condition and as such has not been considered in the structural analysis.

Table 3: Design Loads

Max. Out-of-Plane Bending Moment	30 Nm
Max. Out-of-Plane Shear Force	22.8 N
Max In-Plane Bending Moment	4.5 Nm
Max In-Plane Shear Force	3.2 N
Centrifugal Force	2988 N

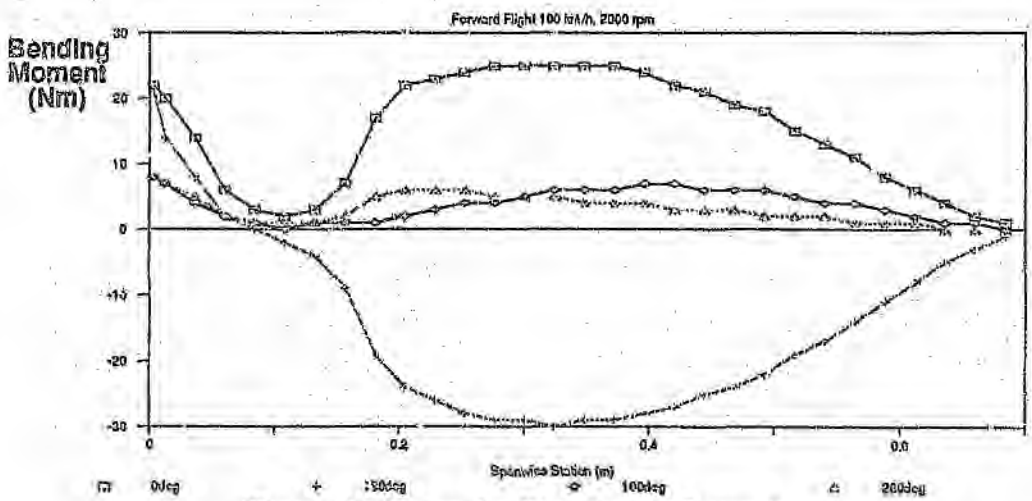

Figure 40: Spanwise Structural Moment

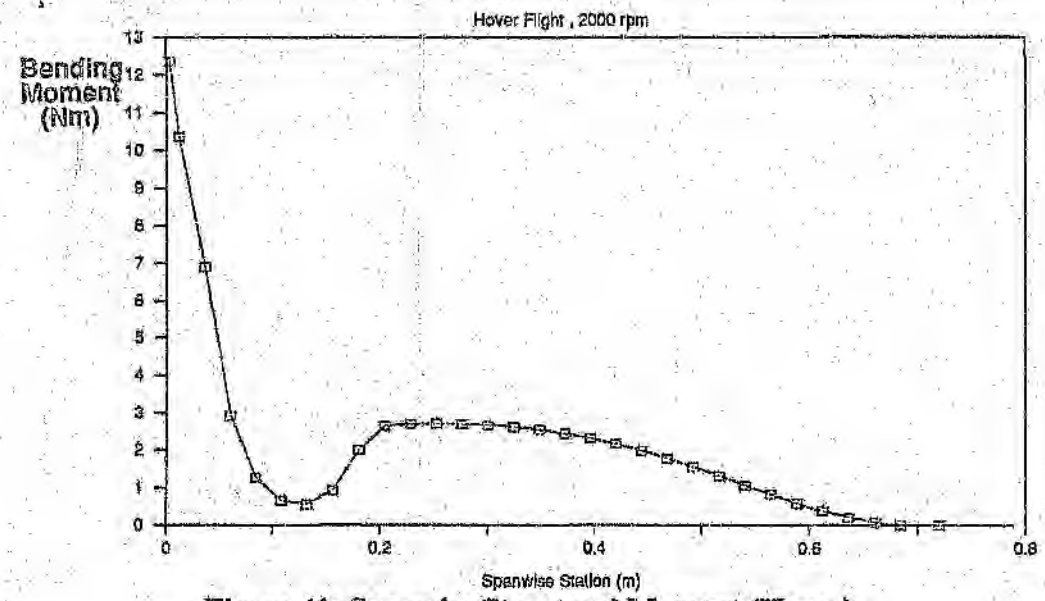

Figure 41: Spanwise Structural Moment (Hover)

4.4.2 Material Properties

The mechanical properties of the two primary composite materials used in the design and manufacture of the rotor blade are shown in table 4. These materials are Vicotex 913C T-300 unidirectional carbon fibre and M9 R-Glass unidirectional glass fibre. Additional materials used were Redux 312L thin film adhesive,shown in table 5, and the Rohacell core material. It was assumed that the Rohacell has no structural strength and thus plays no part in restraining the loads imposed on the rotor.

Table 4: Composite Material Properties

	Glass Fibre	Carbon Fibre
E_1	51 GPa	150 GPa
E_2	15 GPa	9.5 GPa
G_{12}	6 GPa	4.5 GPa
ν_{12}	0.3	0.263
X_t	1550 MPa	1990 MPa
Y_t	74 MPa	60 MPa
X_c	864 MPa	1200 MPa
Y_c	156 MPa	155 MPa
S	86 MPa	70 MPa
t	0.6 mm	0.125 mm

Table 5: 312L Adehesive Properties

τ_p	41.4 MPa
η	0.13 mm
$\frac{\gamma_p}{\gamma_e}$	20
$\eta\left(\frac{1}{2}\gamma_e + \gamma_p\right)$	0.259 mm
E_c	3.45 GPa
$\sigma_{c_{max}}$	69 MPa

4.4.3 Section Properties

The section properties for each element of the rotor blade were calculated using the method presented in chapter A3 in Bruhn[6]. The method was formulated into a computer code [APPENDIX F] and was then used for the determination of every blade element's section properties. This method gives the section area, the area of the material and the second moments of area for each blade element [APPENDIX B].

The total mass of each blade is calculated as 672.9g, being distributed spanwise as shown in figure 42. Th CG position, as a result of the mass distribution, was calculated to be 255mm from the center of rotation.

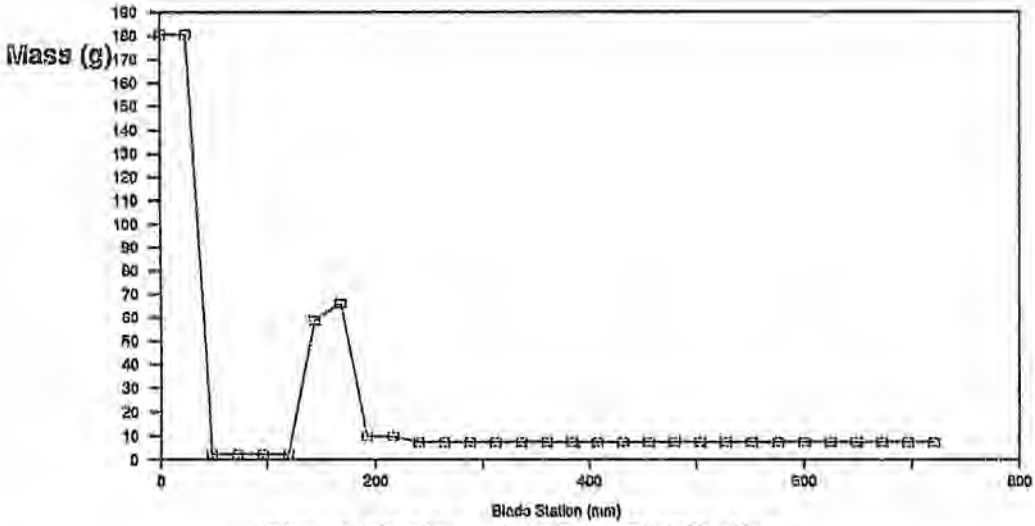

Figure 42: Spanwise Mass Distribution

The apparent material constants, for the specific laminate layup of the blade elements [APPENDIX B], were calculated using classical lamination theory as described in Jones[21]. The blade stiffness properties were derived using the section properties and the apparent material constants for each element. The spanwise, chordwise and torsional stiffness distributions of the rotor blade are

shown in figure 43 t[illegible]ough figure 45 respectively, with the numerical results shown in [APPENDIX B].

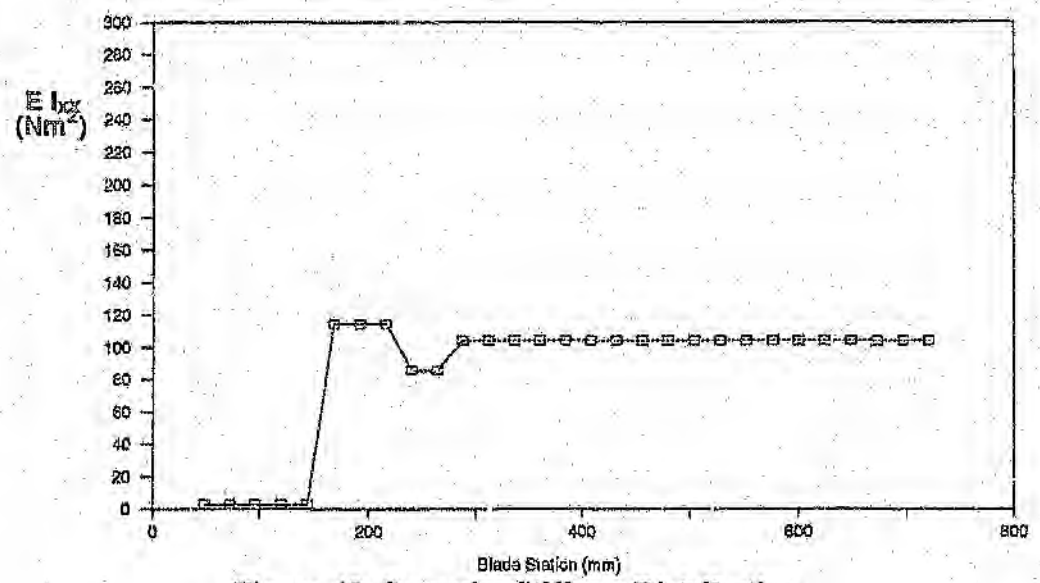

Figure 43: Spanwise Stiffness Distribution

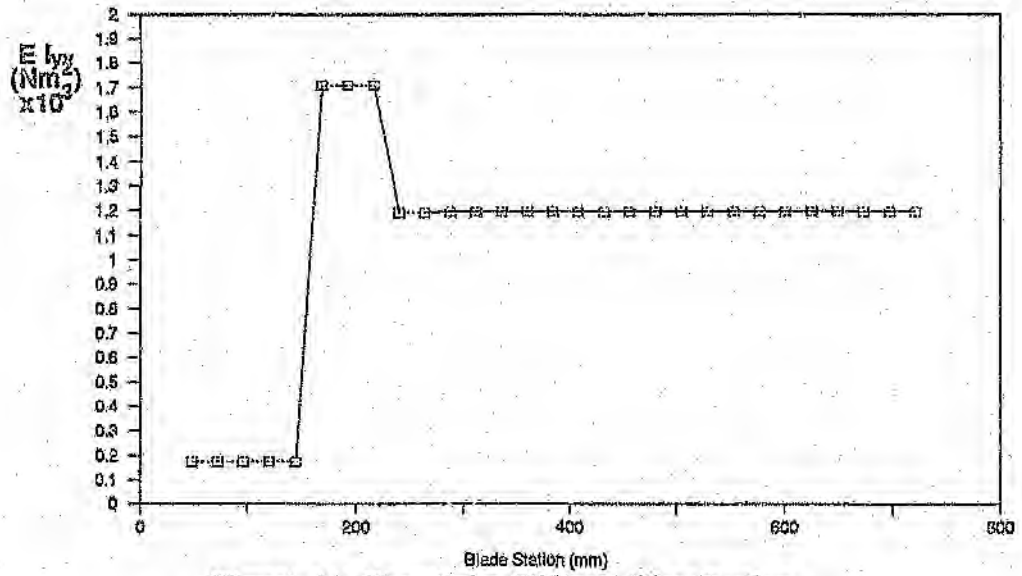

Figure 44: Chordwise Stiffness Distribution

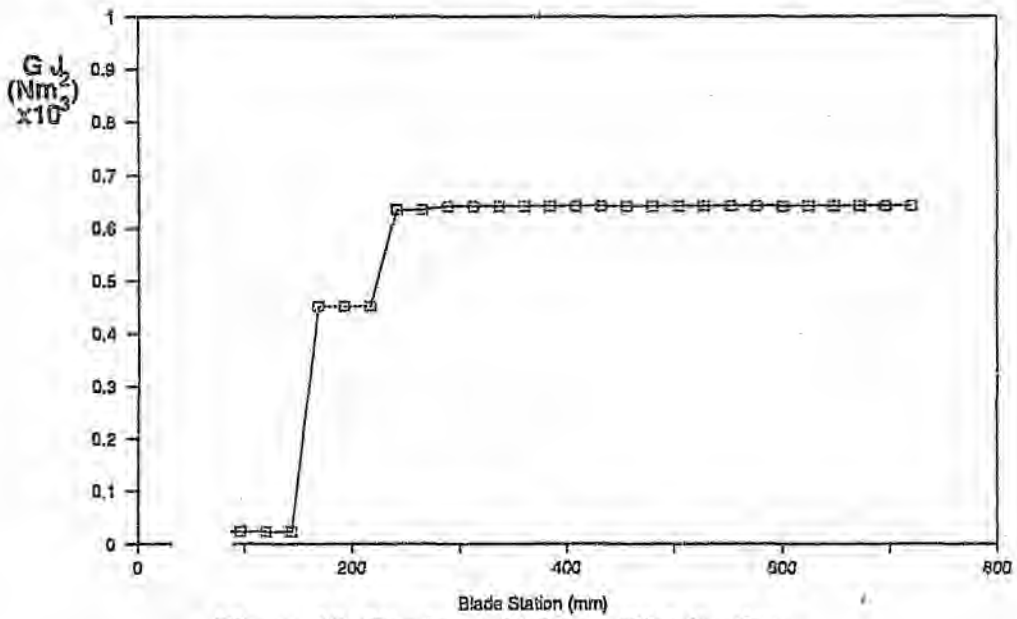

Figure 45: Torsional Stiffness Distribution

4.4.4 Rotor Blade Analysis

The structural stress analysis of the blade was done at a spanwise station of 321mm from the center of rotation, this being a critical point of maximum loading. The magnitude and direction of these loads, at this point on the blade, are given in table 3 and figure 46, respectively.

The spar of the rotor blade was considered to be the major load carrying structure in the blade section, with the skin and core of the blade providing only torsional rigidity.

Classical lamination theory, which was formulated into a computer code [see [49] for source listing], was used with the above loading case to carry out the design/analysis of the blade spar. The Tsai-Hill failure criteria was applied in the iteration to determine the number of layers and the layer orientations required for the spar laminate to be safe.

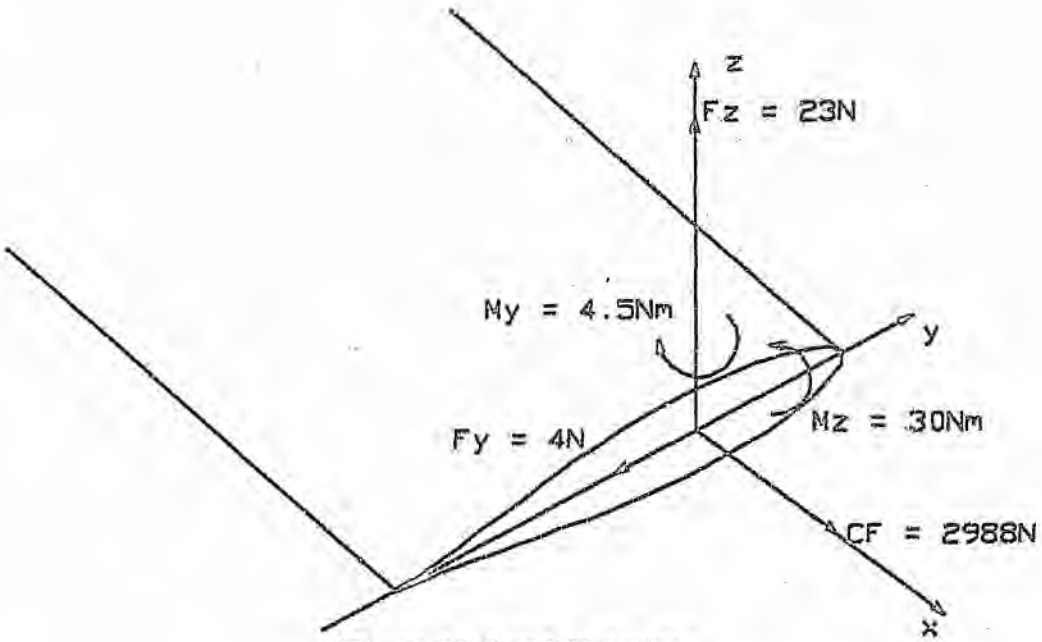

Figure 46: Load Directions

The final results of this iteration showed that 4 layers, all oriented at 0 degrees spanwise, would be sufficient to carry the given load case. The specific Tsai-Hill values for each layer are shown in table 6, below. The outer layer of the laminate shows a Tsai-Hill value of 1.099, indicating a failure. It was, however, accepted considering that:

Table 6: Tsai-Hill Values for Spar Layers

Layer	Tsai-HillValue
1	0.693
2	0.002
3	0.296
4	1.099

- Tsai-Hill is a conservative failure criteria, involving a compound failure mode, and
- that an additional layer in the laminate would increase the mass of the blade, thereby increasing the centrifugal load, thus giving higher Tsai-Hill failure values than those indicated. This conclusion was reached during the iterative design process.

The resulting geometry of the spar in the blade section, is given in figure 47.

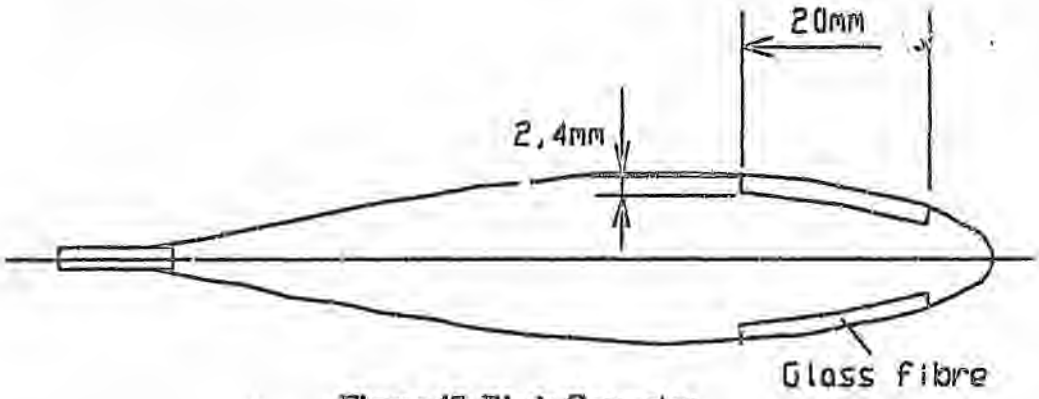

Figure 47: Blade Geometry

4.4.5 Blade Root Analysis

The blade root area is considered to be a critical area as it is the connection point between the rotor blade, flexbeam and the pitch case [see figure 48].The pitch case forms part of the main blade with the blade spar being carried through the pitch case, providing additional strength and a load path for the pitch control loads. The flexbeam, however, is an independent component which has to be bonded onto the blade spar during the manufacture of the blade. Two different analytical methods were used to design and effectively analyze this bonded joint. The first method, which was used primarily for the design of the bonded joint, is a classical method presented by Hart-Smith[15]. The second method, to be discussed later, is a finite element model analysis of the blade root area.

The bond between the flexbeam and the blade spar is an unbalanced double lap joint, since the materials on either side of the joint differ. The inner adherend of the joint, being the flexbeam, has a thickness of 2mm, thus figure 49 indicates

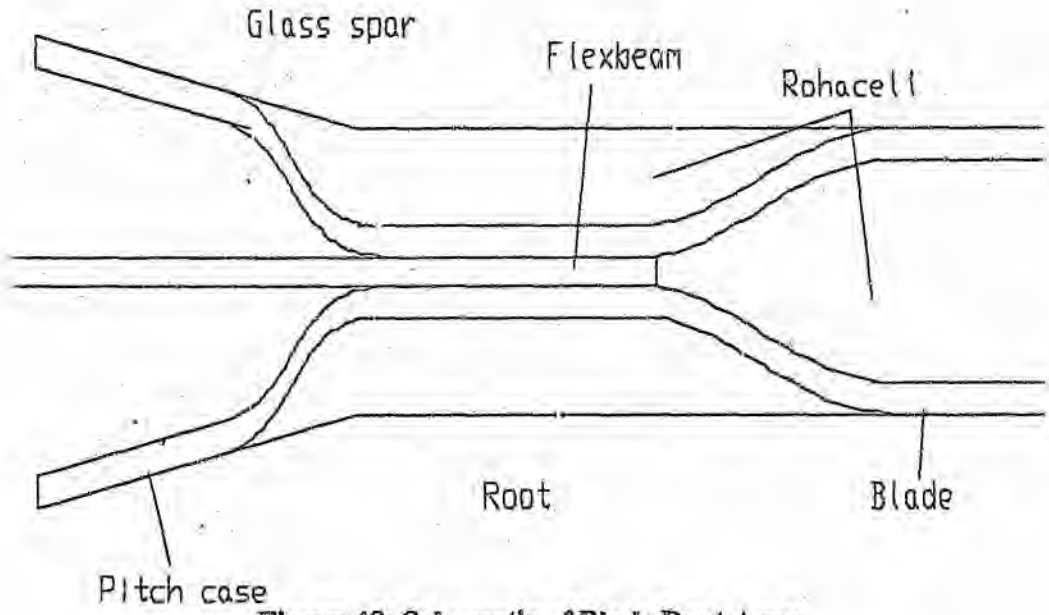

Figure 48: Schematic of Blade Root Area

that the failure of the joint would be in the adherend. The critical end of the joint, however, is not readily identifiable thus the maximum possible bond shear strength will be given by the lesser resultant value of equations 20 and 21. The material properties and the adhesive properties needed for the solution of these equations are those shown previously.

$$P_i = 2\tau_{av} l = \left(\alpha_o - \alpha_i\right)\Delta T E_{it_i} + \left[2k\tau_p\eta\left(\gamma_e + \gamma_p\right)2E_{it_i}\left[1 + \left(\frac{E_{it_i}}{2E_{o^t o}}\right)\right]\right]^{\frac{1}{2}} \quad (20\ [15])$$

$$P_o = 2\tau_{av} l = \left(\alpha_i - \alpha_o\right)\Delta T 2E_{ot_o} + \left[2k\tau_p\eta\left(\gamma_e + \gamma_p\right)4E_{ot_o}\left[1 + \left(\frac{2E_{ot_o}}{E_{it_i}}\right)\right]\right]^{\frac{1}{2}} \quad (21\ [15])$$

$$\Delta T = T_{operating} - T_{stressfree}$$

$$k = \frac{\left(\frac{1}{2}\gamma_e + \gamma_p\right)}{\left(\gamma_e + \gamma_p\right)}$$

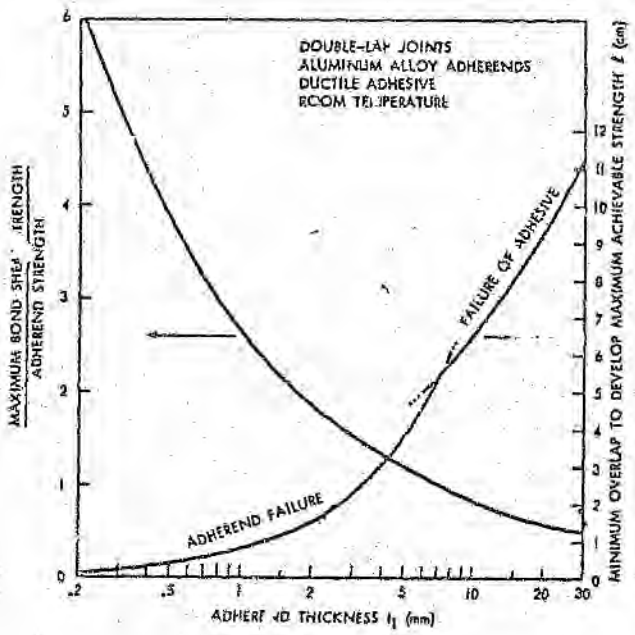

Figure 49: Theoretical Bond Strengths [15]

The results of equations 20 and 21 respectively, show the inner adherend to have a maximum bond shear strength per unit width of

$$P_i = 127.52 \times 10^6 \text{ N/m}$$

and the outer adherend a shear strength per unit width of

$$P_o = 4.793 \times 10^6 \text{ N/m}$$

thus making the outer adherend the critical end of the joint. The minimum necessary overlap to realize the full shear strength of the bond is given by equation 22, giving a overlap length of

$$l_{practicaldesign} = \frac{P}{2\tau_p} + \frac{2}{\left[\frac{\tau_p}{\eta\gamma_e}\left(\frac{1}{E_0 t_0} + \frac{2}{E_i t_i}\right)\right]^{\frac{1}{2}}} \qquad (22\ [15])$$

$l_{practical\ design}$ = 66.11 mm.

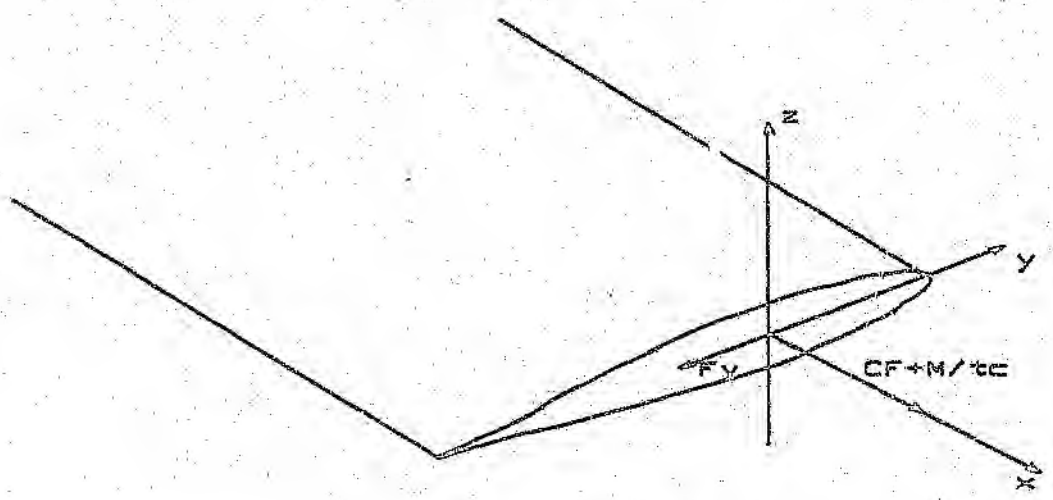

$$P = \left[F_y^2 + \left(CF + \frac{M}{t_c}\right)^2\right]^{\frac{1}{2}}$$

Figure 50: Loads at the Root Joint

The predicted loading case on the joint [figure 50] gives a total value of

$$F_{shear} = 9461.8\ N$$

including the safety factor of 2. This gives a shear loading per unit width of

$$P = 473.1 \times 10^3 \text{ N/m}$$

which constitutes 10% of the maximum shear strength of the bond. Although this is a small percentage of the shear strength, there was a large degree of uncertainty in the bonding process due to the fact that the bond is inside the blade thus reducing the control over the manufacturing process. For this reason the maximum bond shear strength was retained, thus defining the bond geometry as shown below in figure 51.

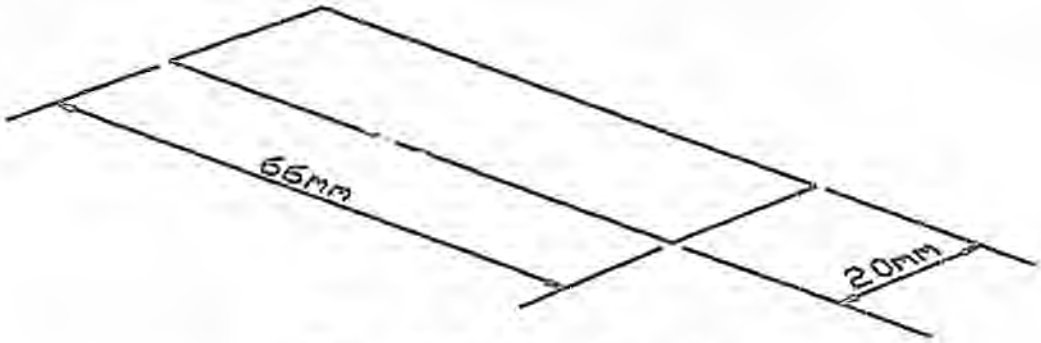

Figure 51: Bond Area Geometry

4.4.6 Finite Element Methods Analysis

The finite element investigation was carried out to determine the stresses and stress concentrations of the bonded joint under the combined loading case of loads and moments presented earlier. The model [see figure 52] used for this investigation includes the flexbeam, blade root including the bonded joint and a short section of the blade spar. A larger model encompassing the entire blade could not be analyzed due to the limitations of the available computer hardware. The analytical solver used was the E .R.C NISA286 FEM analysis computer package. The elements available in the program library and the solution methods are similar to those described in Zienkiewicz[48] and Livesley[25]. The selection of an element for use in the model is critical in that poor modelling and poor element selection can lead to erroneous results.

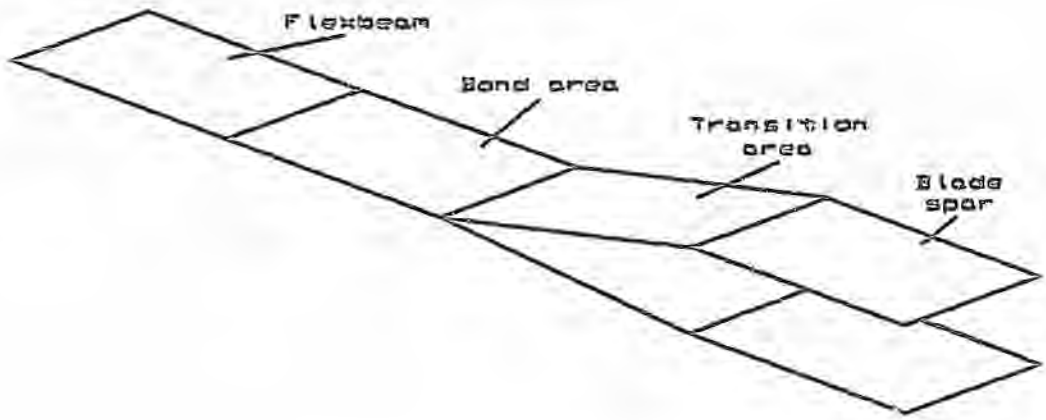

Figure 52: Schematic of FEM Model

An anisotropic, composite 8 noded, quadrilateral element was used to model the critical areas of the rotor blade. This element may have curved sides, exhibit good convergence properties and superior accuracy, thus making it better able to cope with a pure bending state. The accuracy of this element is maintained by keeping the sides straight with the midside node located in the middle of the side and the element in a parallelogram form. This however, does not guarantee accuracy as the aspect ratio of the element is important. As a general rule the aspect ratio of the elements should not exceed 7 where displacements are of primary interest or 3 where stress is of primary interest. An equivalent system of forces is used and St.Venant's principle is invoked to justify the substitution of one system of forces for another. The local effects of the equivalent force system should be ignored as they do not represent the actual force system, but the effect far away from the load inputs is representative of the real system.

The model is completed by restraining the wedge section of the flexbeam for all six degrees of freedom and applying the loading at the blade spar. The lamination sequence of each element in the model is as follows:

- The flexbeam sequence is the same as the CLT analysis done on the flexbeam and also corresponds to the FEM analysis done on the pure flexbeam by Sheiman[49].
- The blade root lamination sequence includes the blade spar sequence, the bondline and the flexbeam sequence [figure 53].
- The blade spar lamination sequence is the same as that used in the CLT analysis of the blade shown previously.

0^0 (G)lass	layer 1
0^0 (C)arbon	2
90^0 C	3
0^0 C	4
90^0 C	5
90^0 C	6
0^0 C	7
90^0 C	8
0^0 C	9
0^0 G	10

Figure 53: Root Lay-up Sequence

The numerical results of the FEM analysis can be found in [APPENDIX D], with some graphical results shown below in figure 54 through figure 61.

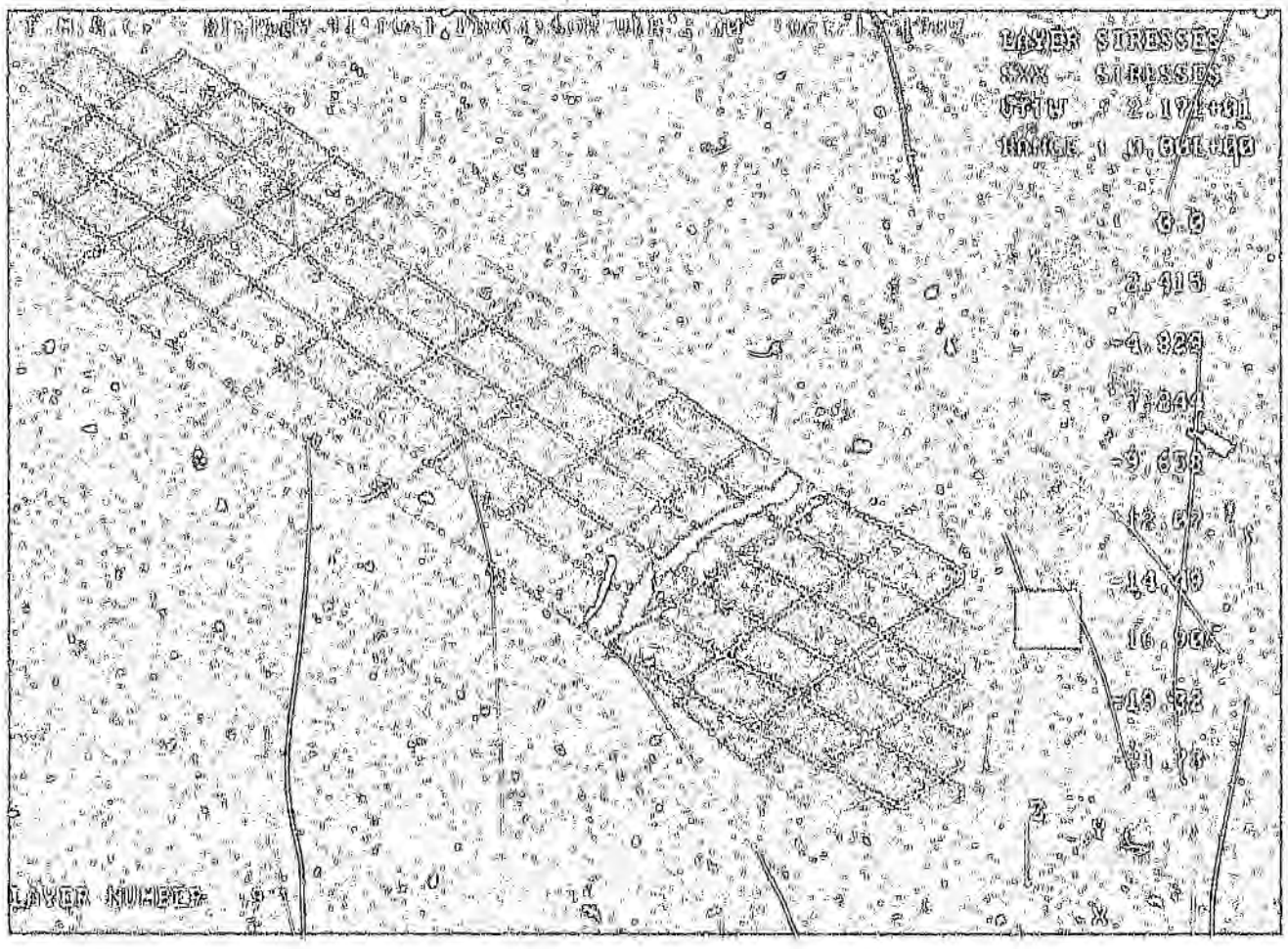

Figure 54: FEM Stress Results

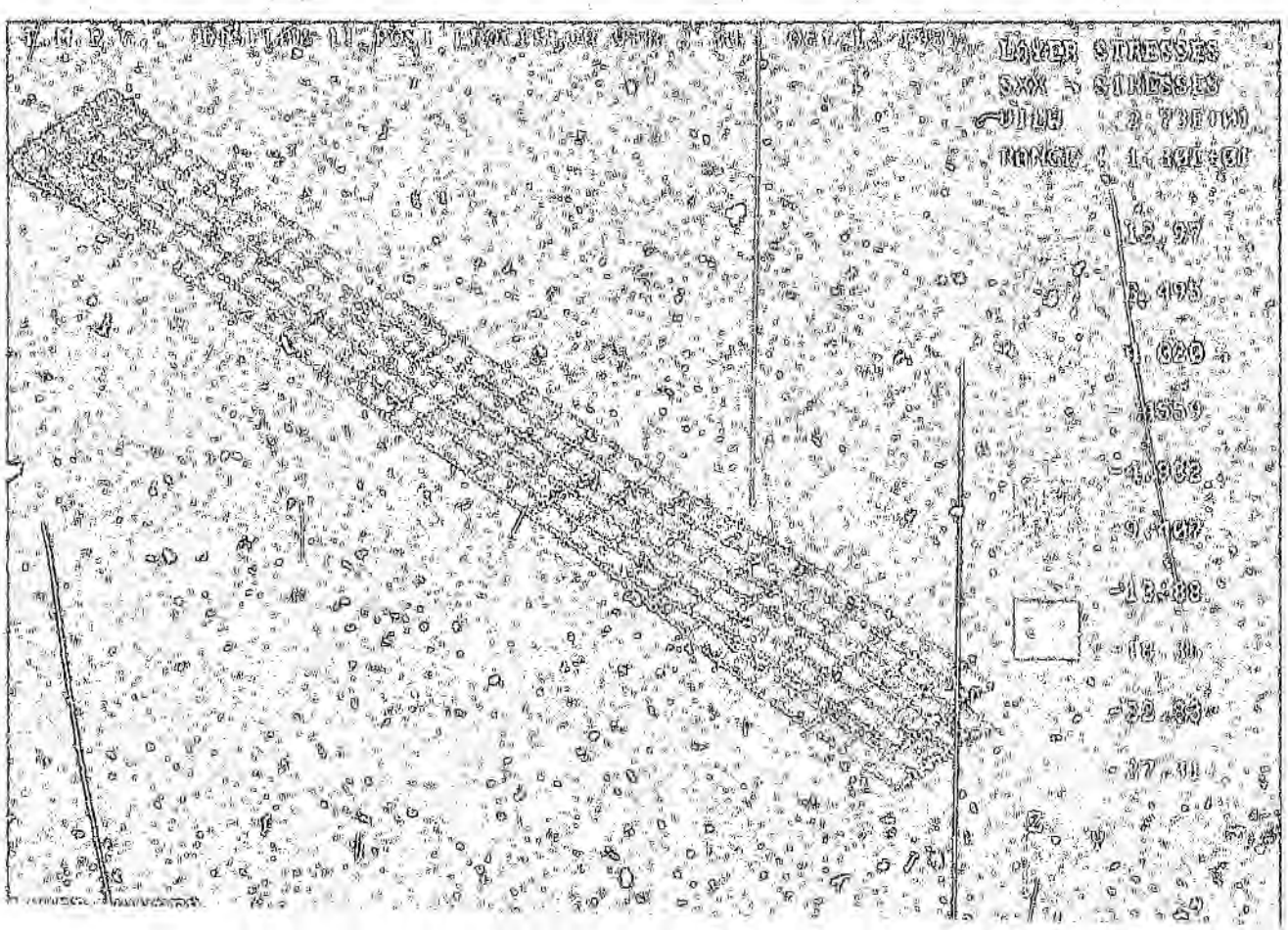

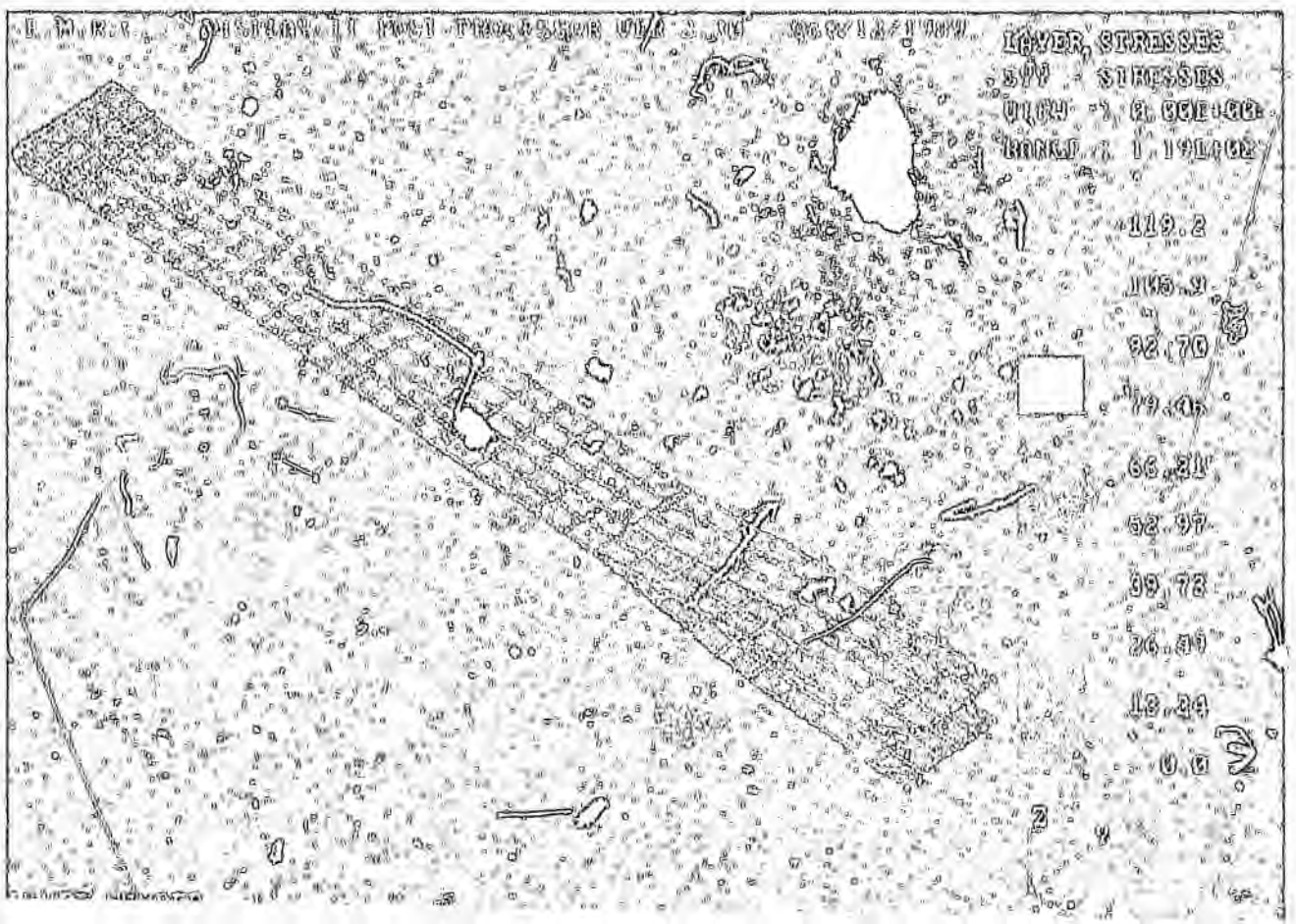
LAYER STRESSES
119.2
105.9
92.70
79.46
66.21
52.97
39.73
26.49
13.24
0.0

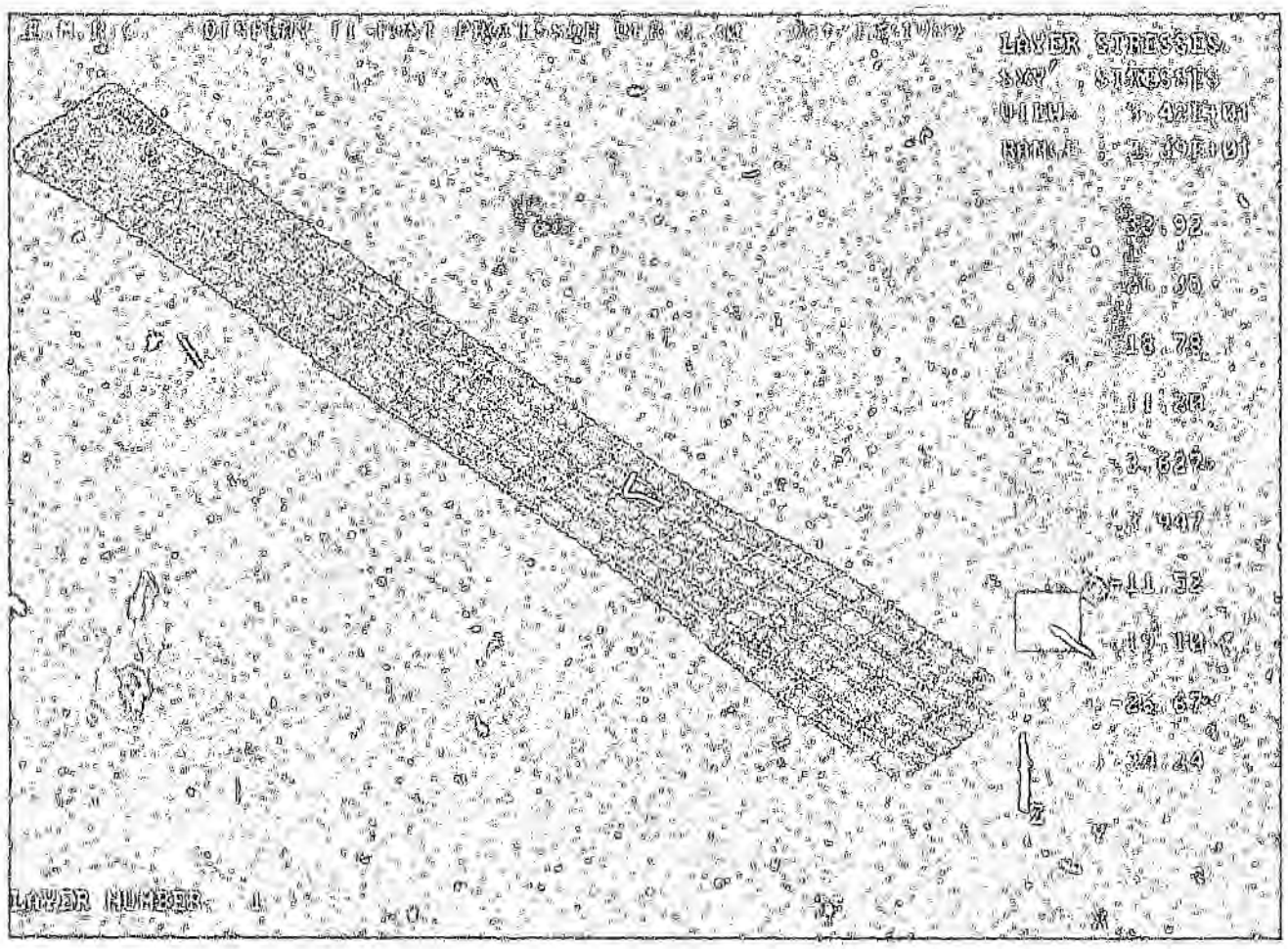

Figure 57: FEM Stress Results

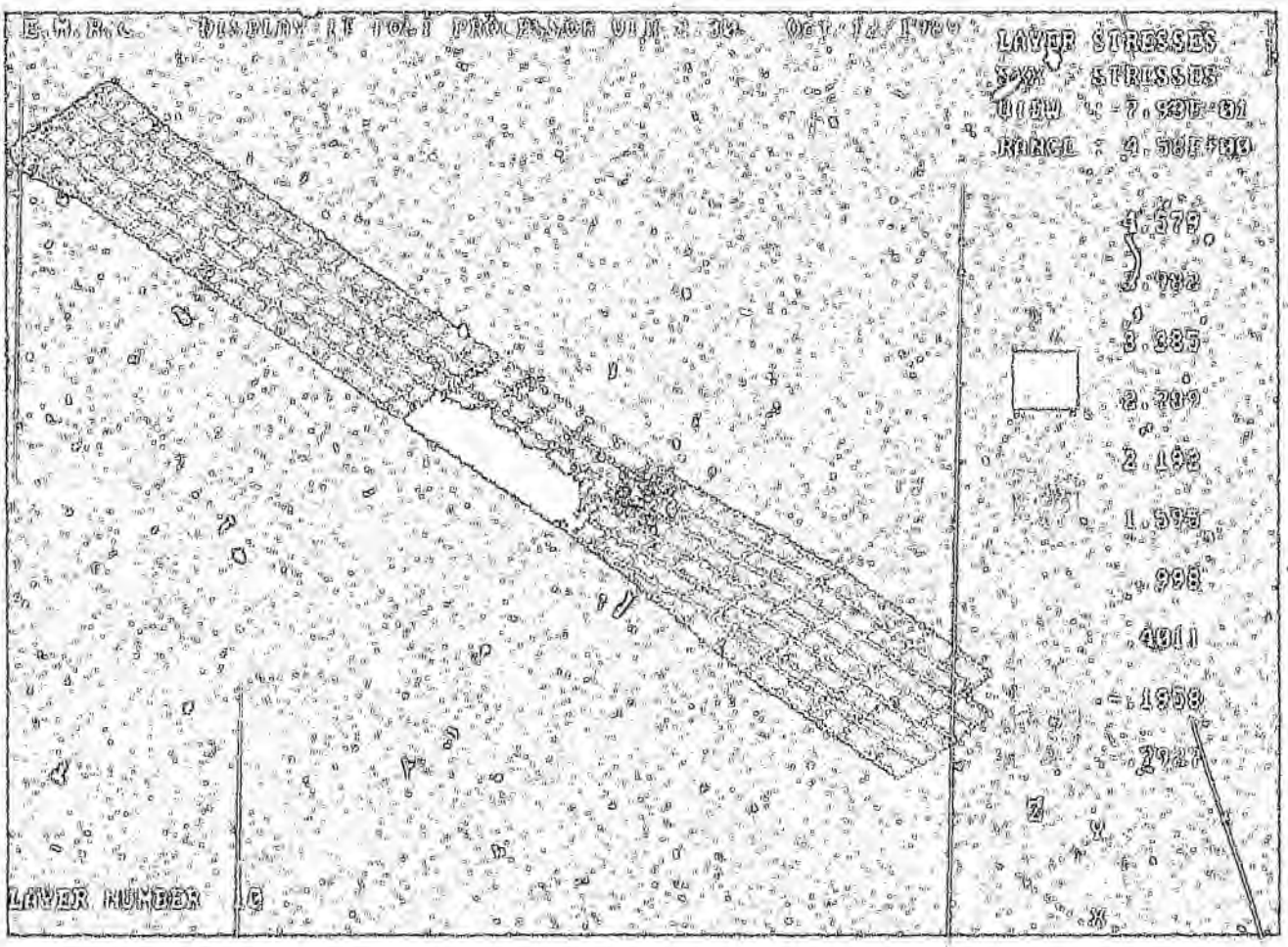

Figure 58: FEM Stress Results

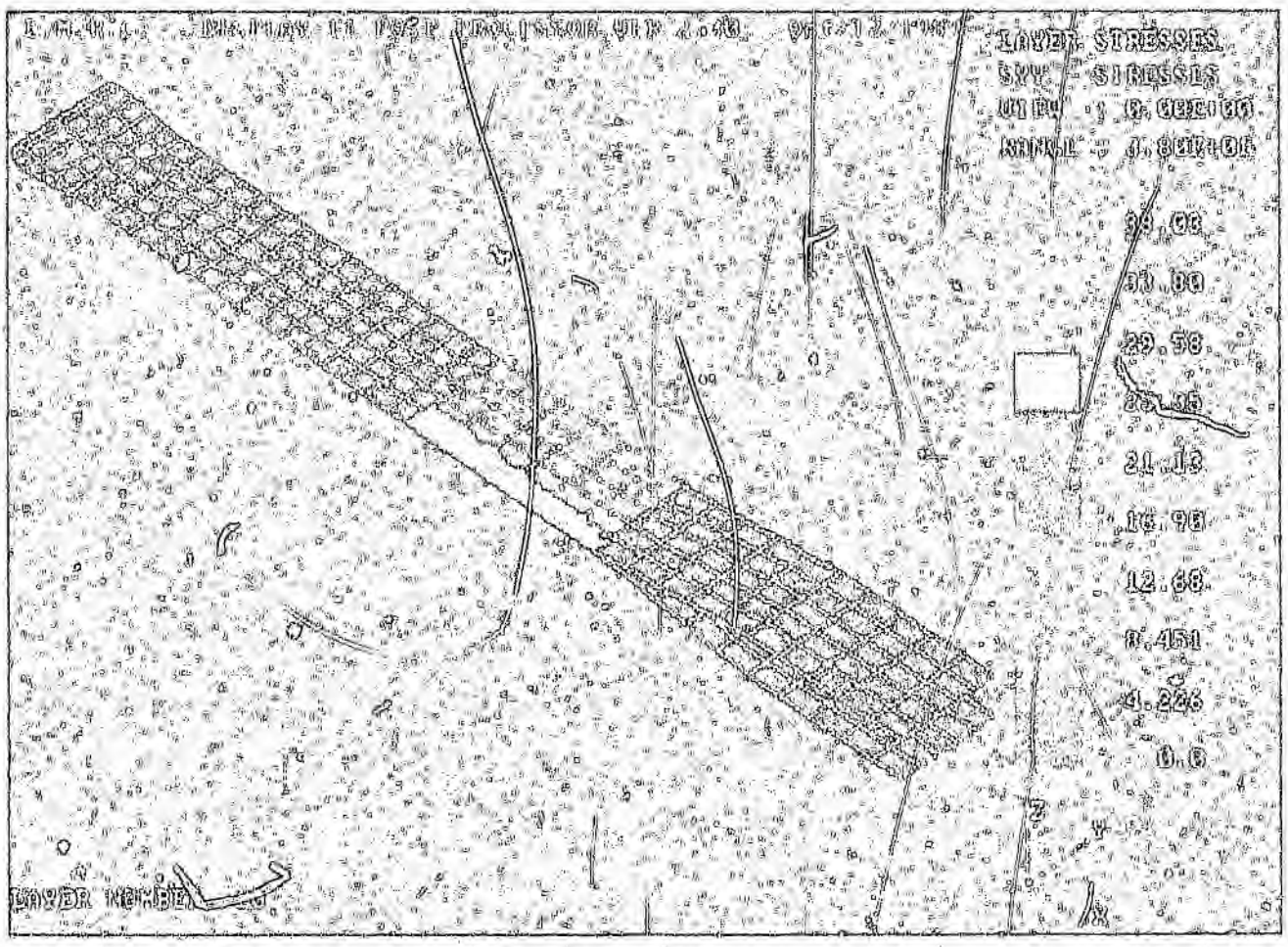

Figure 59: FEM Stress Results

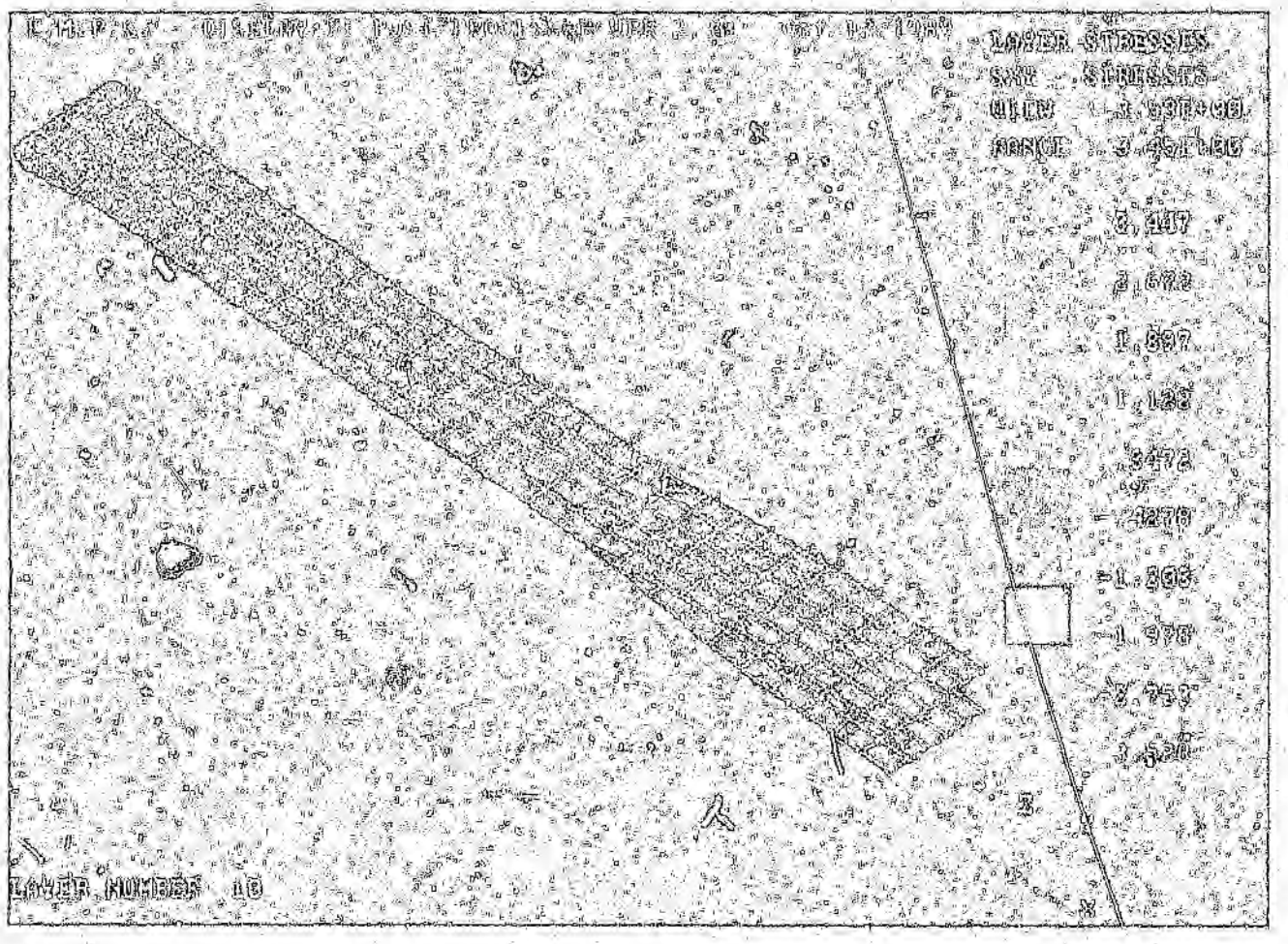

Figure 60: FEM Stress Results

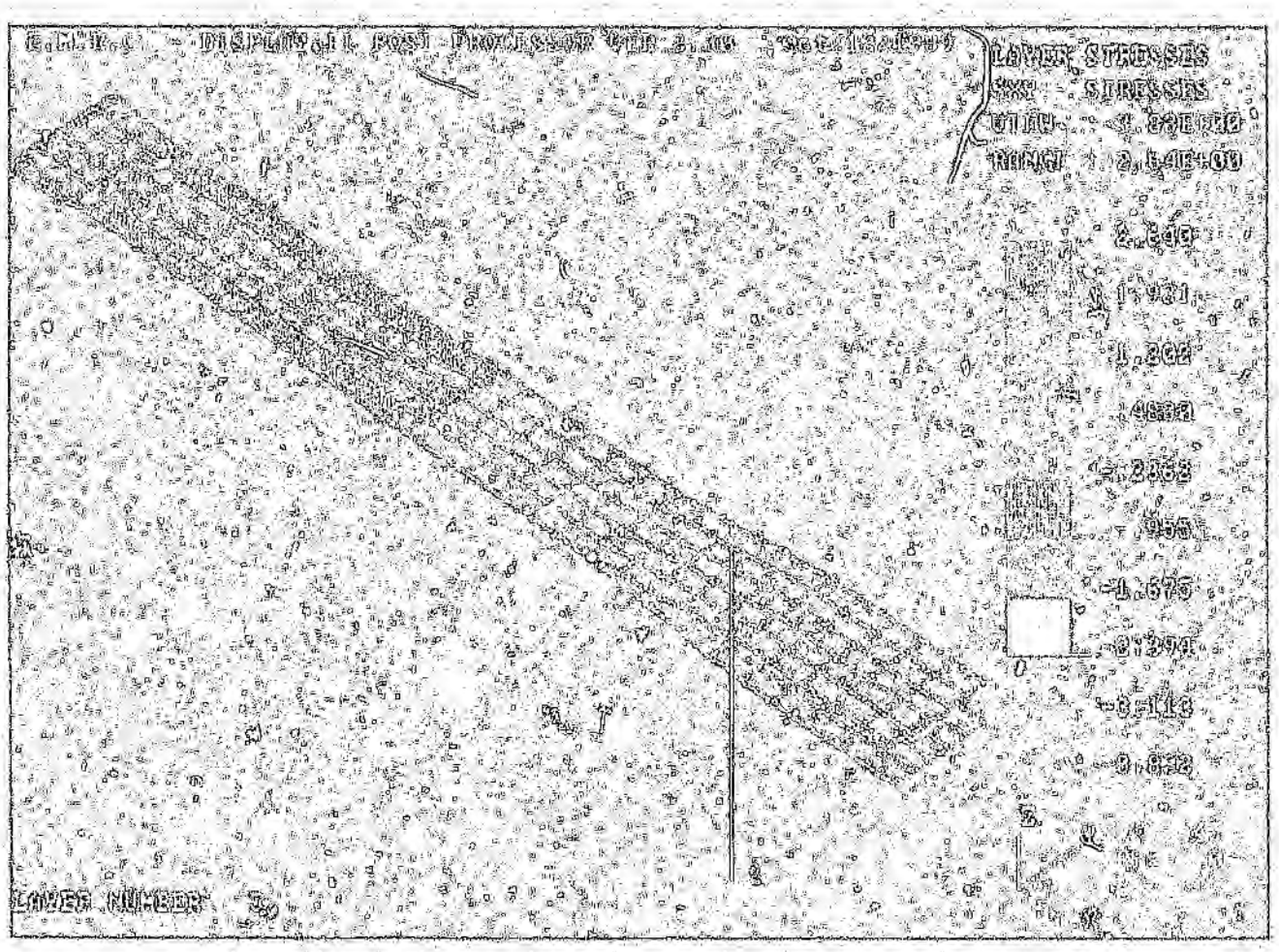

Figure 61: FEM Stress Results

Of particular interest is figure 54, which shows the inner adherend of the joint. This figure clearly shows a stress concentration point at the outboard edge of the joint, which is different to what would be expected. figure 62, [15], shows a characteristic failure mode of a double lap joint, where the inner adherend is torn apart in a peel stress failure situation. This type of failure, however, would only occur at the inboard edge of the joint. The FEM results would indicate that

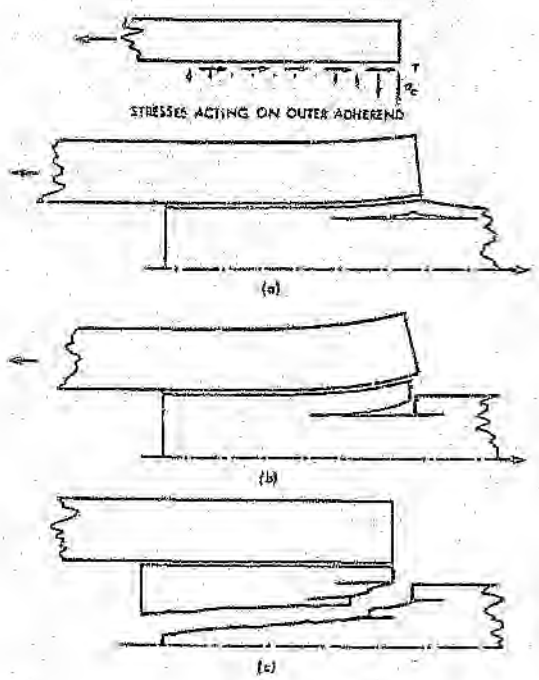

Figure 62: Bonded Joint Failure Mode

since the spar (outer adherend) separates to return to the blade surface, at the outboard edge of the joint, that an additional stress concentration point exists. Thus making this layer of the joint the most critical layer at which failure would most likely occur, with either point being the point at which the failure would be initiated.

Figures 55 through figures 59 show the stresses in the blade spar only. The stresses shown in the flexbeam can be ignored as it is not part of this layer. The high stress levels shown on the outboard end nodes of the spar can also be

ignored as this is where the loading was applied in the form of point loads at each of the nodes.

Layer 10, shown in figure 58 through figure 60, show the stresses in the outer or blade spar adherend of the joint.

All the stresses, indicated on the right hand side of the figures, are low compared to the ultimate failure stresses of the materials. The maximum stresses being calculated are in the transverse direction, to the laminate lay-up, of approximately 38MPa in magnitude. The FEM thus showed that the design was safe for the given loading conditions and it also provided insight into the areas of possible failure.

4.5 Dynamic Analysis

The dynamic analysis of the rotor system was done using the dynamic analysis code mentioned earlier.

The program requires the physical and mechanical properties of the rotor system as input data. These properties include the blade geometry, mass and stiffness distributions and section properties which were obtained from the above design definition and the materials.

The analysis was carried out at 8deg. collective, using 10 rotor speeds ranging from 500 rev/min to 2500 rev/min, covering the complete expected flight envelope of the test rig.

The results of the dynamic analysis are shown graphically below, in the form of a fan plot or resonance diagram. At the rig operating speed of 2000 rev/min the first chord frequency is at 0.65/rev which provides a good separation from the first flap frequency and the 2/rev Coriolis excitation. The figure shows that the

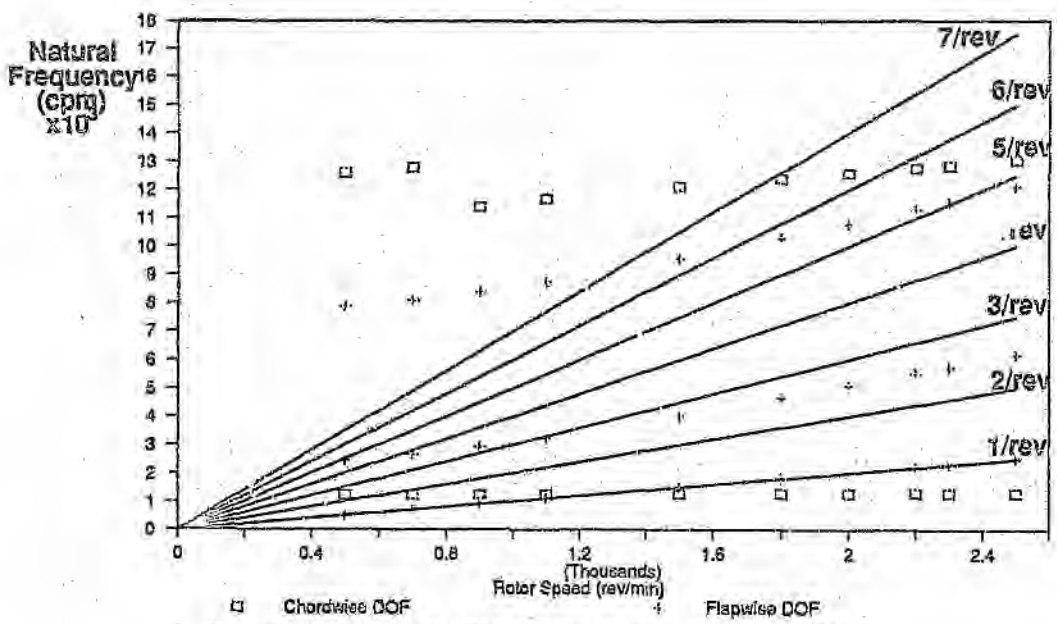

Figure 63: Natural Frequencies (Resonance Plot)

blade does pass though resonant modes while spinning up but at the operating speed all the modes are separated from resonance allowing the smooth operation of the system. The damping of this system is dependent only on the stiffnesses of the rotor system and the hub shear damping characteristics. No additional damping was necessary for the present rotor system.

The analysis of the design showed that the system was safe and could operate smoothly. The design was thus frozen at this point with no further refinement taking place.

Chapter 5

Manufacturing Development

The fabrication of the rotor system involved a wide range of state of the art composite manufacturing techniques. These included manual lay-up, vacuum bagging, internally pressurized split moulds, autoclave curing, disposable foam mandrels, steel and high temperature epoxy tooling. The manufacturing process includes the development of the tooling as well as the development of the fabrication sequence in order to obtain the completed product. Some of the techniques used were borne out of consultation with a company manufacturing rotor blades under licence, and from the experience of the composites facility at the university, while others were new experimental techniques.

5.1 Tooling Development

5.1.1 Flexbeam

The steel flexbeam mould [figure 64] was designed by Sheiman[49] and manufactured in the University's Mechanical Engineering workshop. The mould is a split mould which is pressurized by high tensile steel bolts, placed either side of the mould. The wedge cores, which are inserted into the flexbeam laminate,

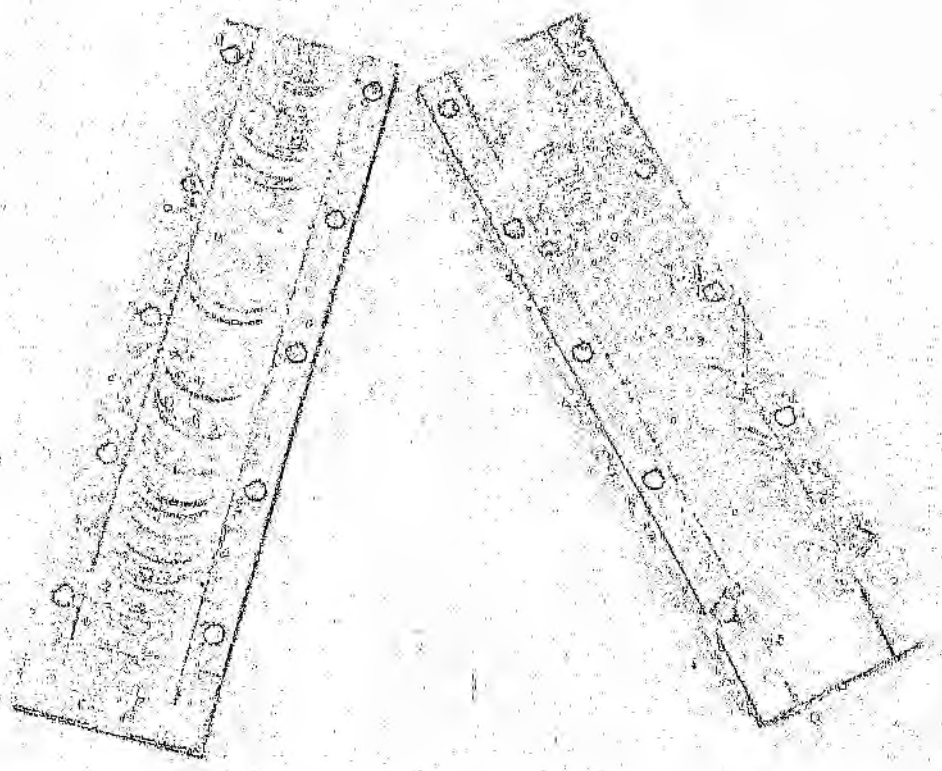

Figure 64: Flexbeam Mould

were also manufactured in the engineering workshop on a general purpose milling machine.

5.1.2 Blade Core Shaper

The Rohacell foam, used as the core material in the blade, is distributed in sheet form. It thus has to be shaped into the profile of the blade. The foam could be shaped by using a CNC type milling machine, but this was ruled out for the following reasons:

- The trailing edge of the core would be destroyed by the cutting tool on the milling machine, as the core material is very fragile.

- Thickening the core would require that it get worked down to its required dimensions after machining, thus increasing the labour and manufacturing time on the core.

The core was thus to be shaped using a rotary core shaping machine.

A mandrel [figure 65], was cut out of laminated wood on a profiling lathe. A positive of the blade profile was cut on the CNC machine and then placed on the lathe, where it was used to cut a negative profile into the mandrel. This allows the mandrel to cut out a positive core shape. The mandrel was then covered with a grit and coated with an epoxy resin, thus turning it into a *'grindingwheel'* which, once placed on the shaping machine, would produce the core.

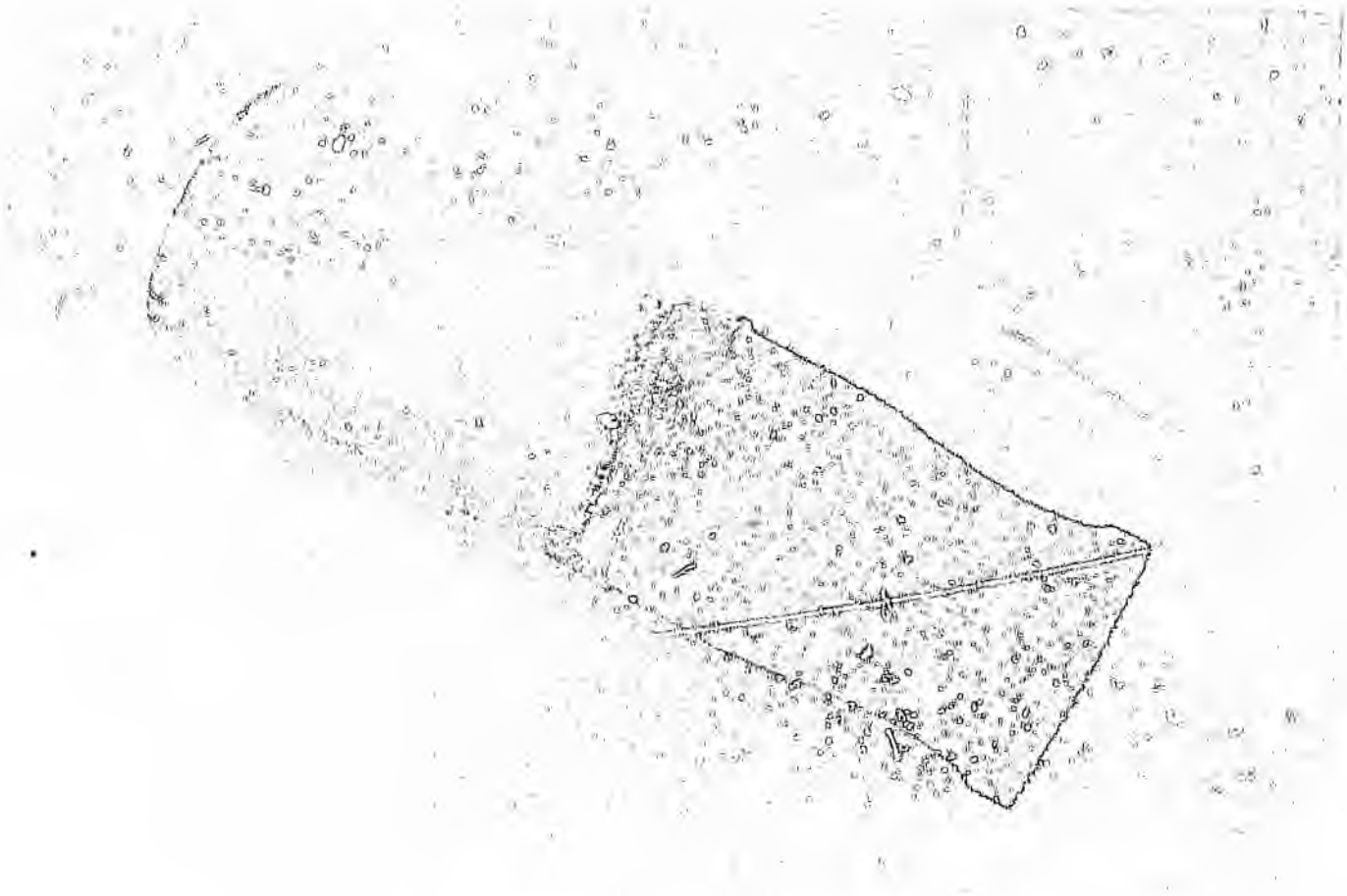

Figure 65: Core Shaping Mandrel

5.1.3 Blade Mould

The blade mould was designed to incorporate the moulding of the blade, pitch case and to allow the flexbeam to be bonded in. The mould is a split mould type, made from high temperature glassfibre/epoxy, preimpregnated tooling fabric.

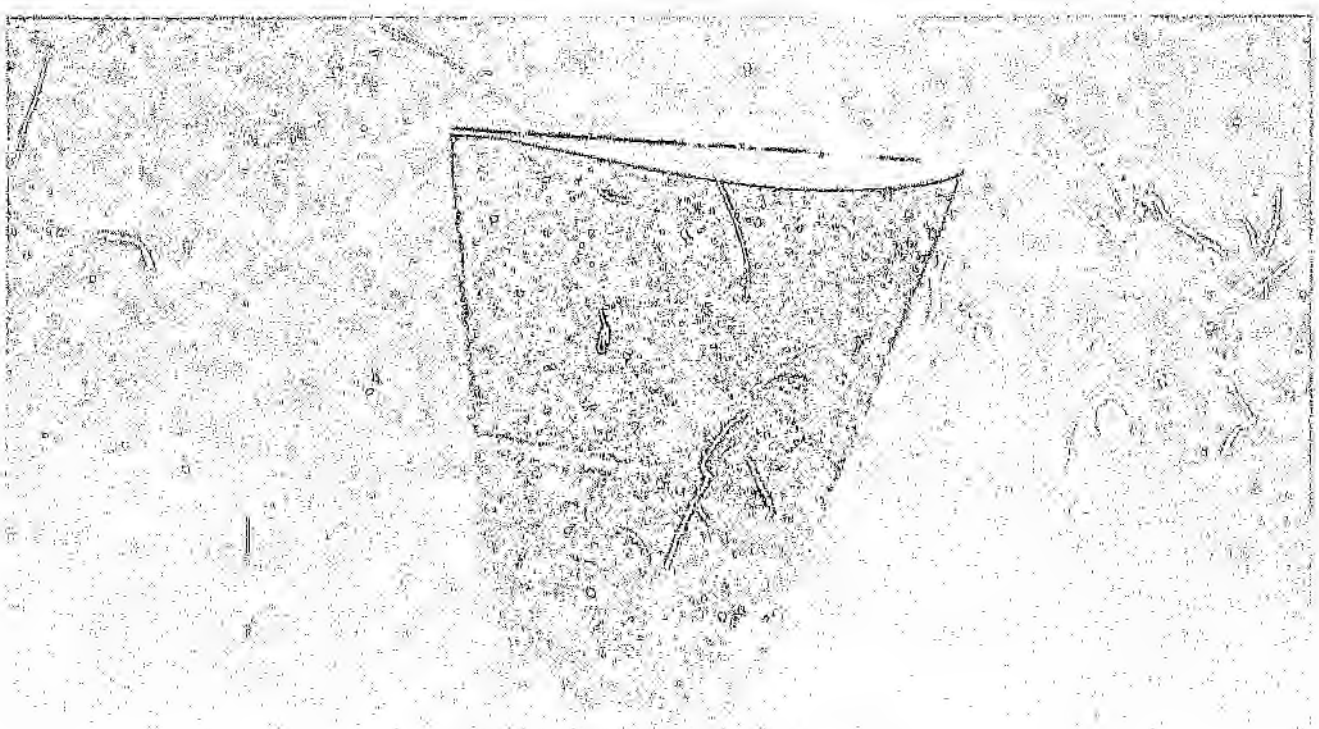

Figure 66: Rotor Blade Mould Plugs

The plugs used to manufacture the mould [figure 66], were machined on the 3 axis MAHO CNC milling machine. The material used for the plugs was aluminium. The machining was done by moving the cutting tool along the span and then incrementing the chord value. 300 coordinates were used along the 90mm chord to attain the smooth finish. The plug is made longer than the intended blade length so as to provide a run-out area in the mould. The root end for the flexbeam rotor system [figure 67], which includes the pitch case faring could not be manufactured with the CNC machine, as the machine does not have the ability to move in three planes simultaneously. The root plug was thus manufactured by hand using an epoxy moulding material.

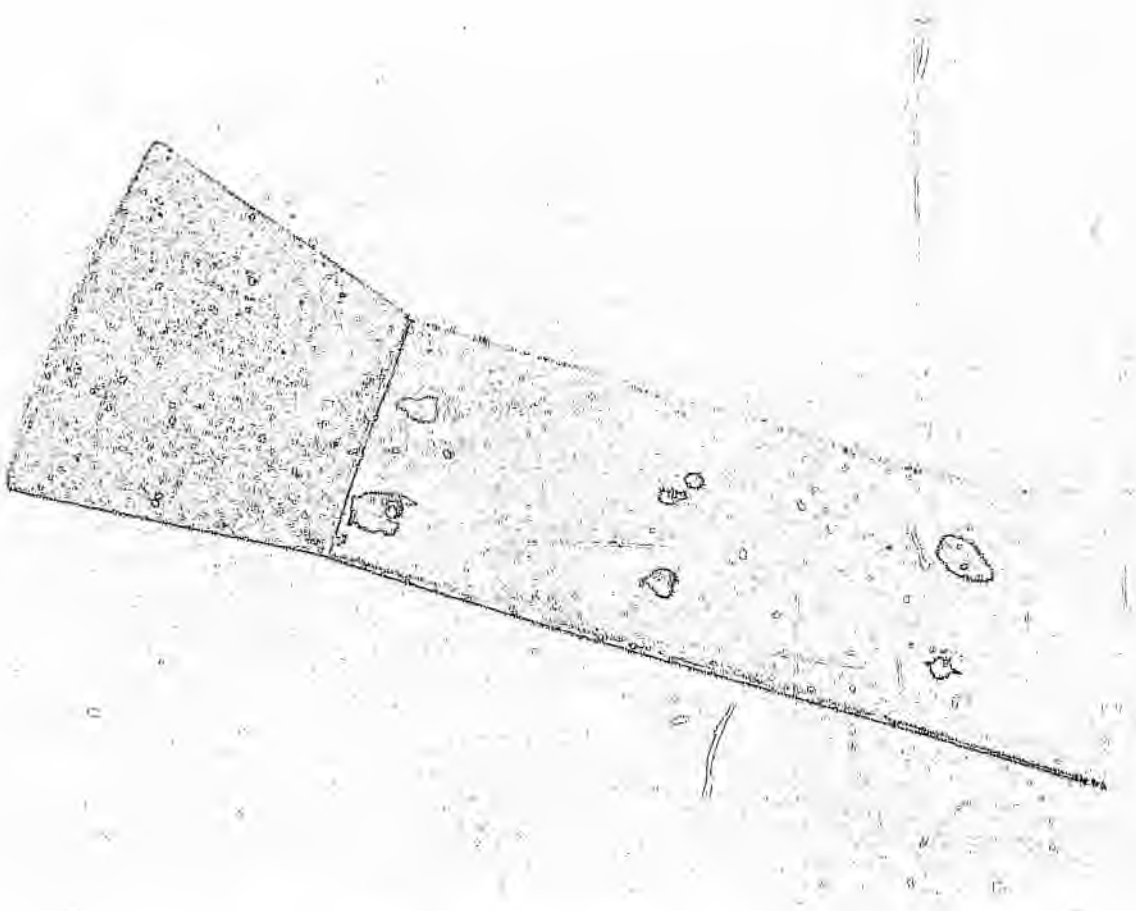

Figure 67: Root End Mould Plug

The manufacture of the moulds was as follows:

The plugs were bonded, using a thin film adhesive, to a flat plate and coated with a release agent. The tooling fabric was cut into square patches and laid-up over the plate and plugs. Eight layers of the tooling fabric were used to achieve the desired mould strength. The mould was then vacuum bagged [figure 68], and allowed to debulk (allowed to settle) for 12 hours. The mould was then placed into the autoclave and allowed to cure. The cure cycle for the tooling fabric was a cure at 150°C, at 4 MPa for a period of 6 hours. After cooling the mould was then removed from the plugs, cleaned up and then post cured at 120°C. The plugs were then removed from the plate and bolted together to represent the

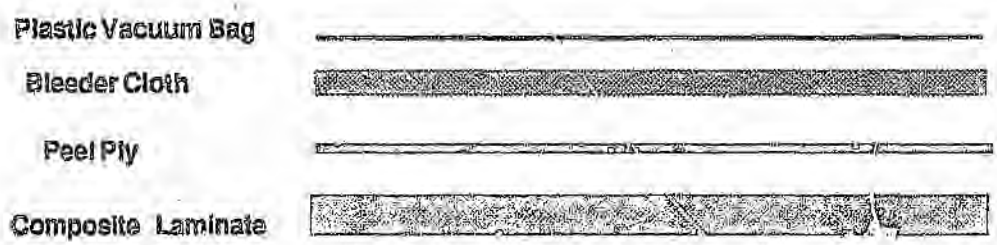

Figure 68: Vacuum Bag Lay-up

complete blade. The plug was then inserted into the mould so as to align the two halves of the mould relative to each other. Locating holes were then drilled into the edges of the mould laminate where locating pins would be inserted during the manufacture of the blade. Additional holes are drilled into the pitch case faring [figure 69] to allow the disposable expanding foam to be injected into the mould. A locating slot was machined into the root edge of the mould. This slot serves to locate the flexbeam in the mould and to control the position at which the flexbeam is bonded into the blade. A photograph of the mould is shown in figure 70.

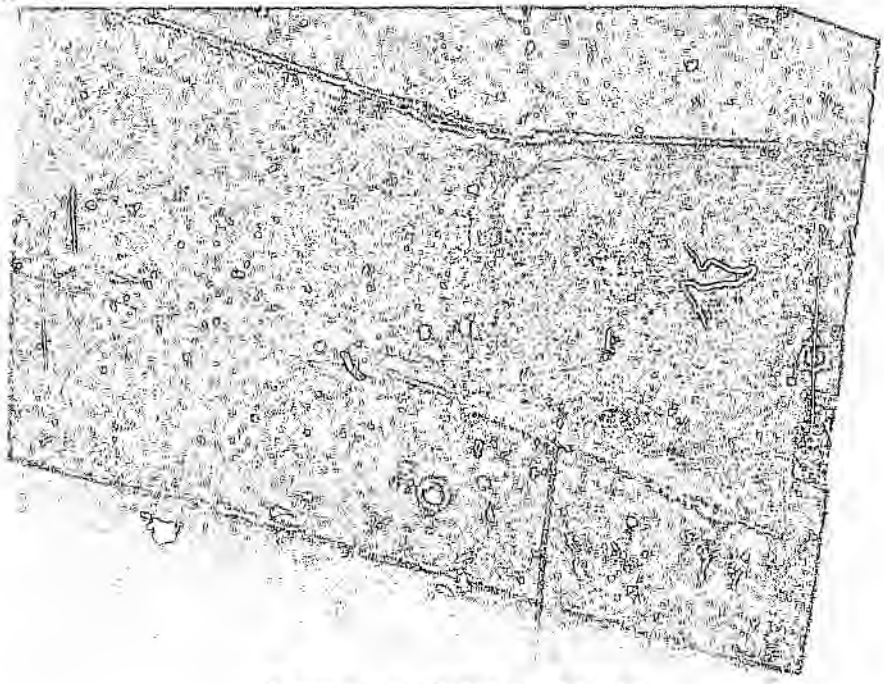

Figure 69: Pitch Case Mould

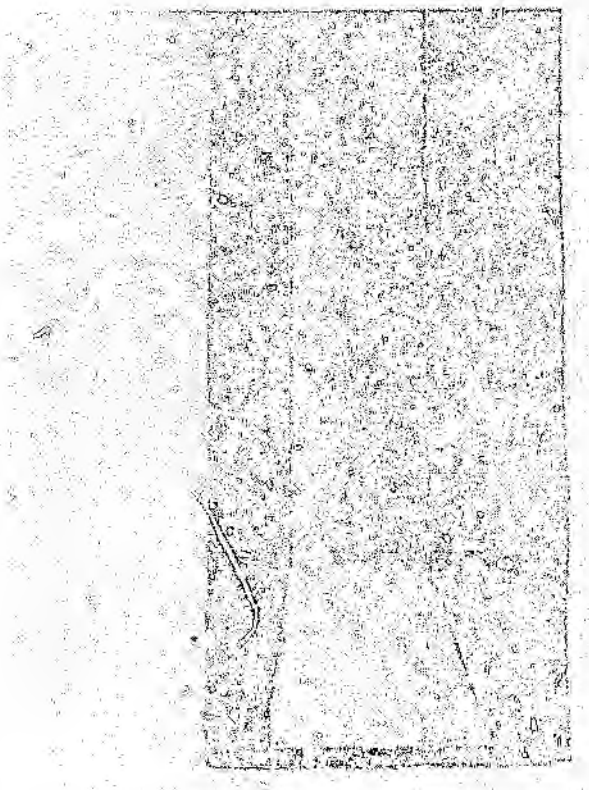

Figure 70: Glassfibre Flexbeam Mould

5.2 Fabrication Sequence

5.2.1 Flexbeam Rotor System

The fabrication sequence of the flexbeam rotor system is shown below in figure 71. Apart from the manufacture of the flexbeam, the blade is manufactured in a one shot process.

The flexbeam is laid-up in the one half of its mould according to the lamination sequence given in the design. The brass wedge is then inserted into the mould, with the laminate being wrapped around it. The mould is then closed and

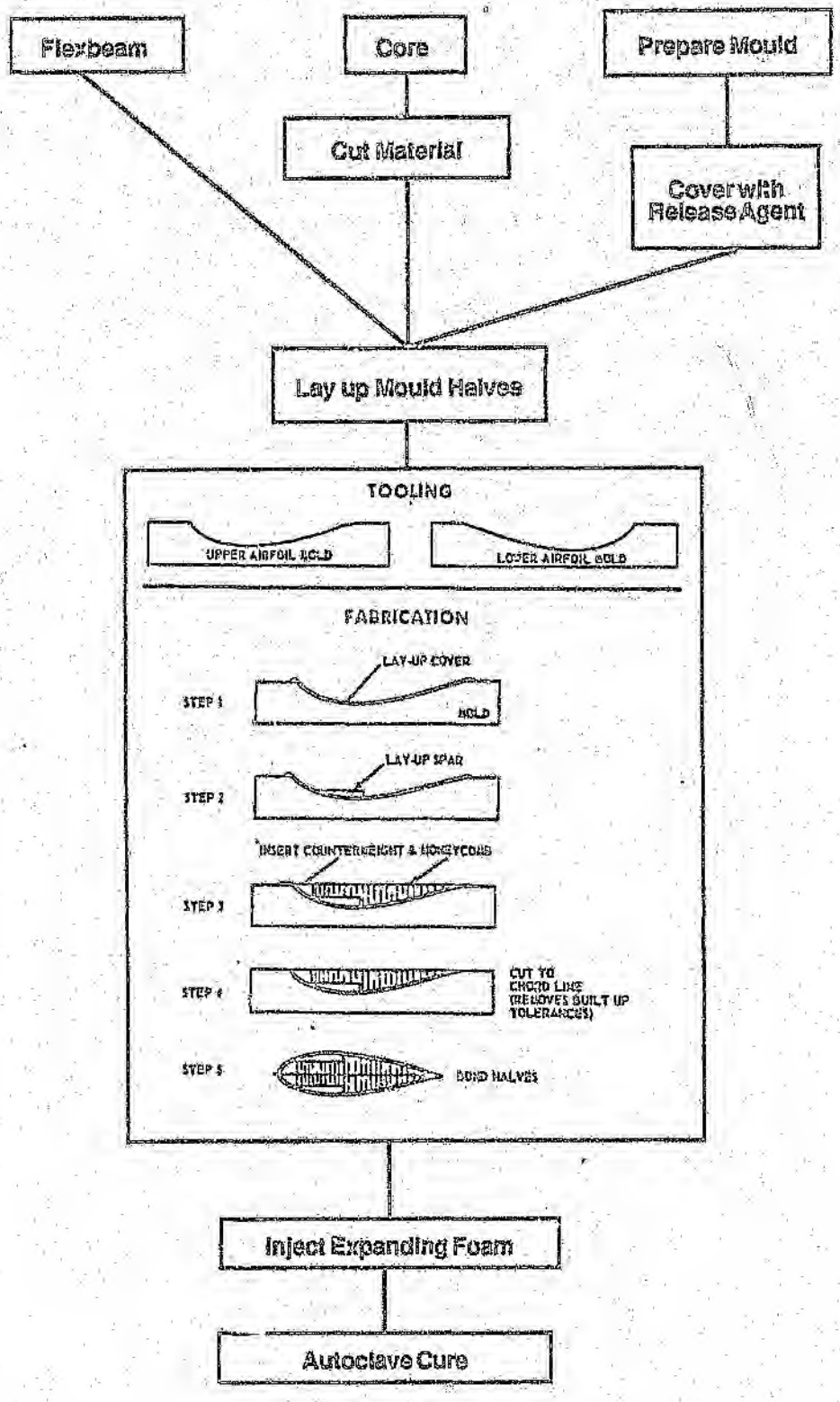

Figure 71: Blade Fabrication Sequence

pressurized, using the bolts. It is then inserted into the oven to cure. The cure cycle for the carbon used was 2 hours at 120°C. The details of the fabrication of the flexbeam are given by Sheiman[49].

The core for the blade is shaped using the core shaping machine and then cleaned up for use in the blade. The shaped core is slightly oversize so as to provide an internal mould pressure when the mould is closed and pressurized. The materials are cut to size and made ready for the lay-up procedure. The mould is cleaned and a release agent is applied to its inner surfaces. Once all the necessary equipment is ready, the lay-up procedure can continue.

The +/- 45 deg. skins are laid in the mould and are continued inboard into the pitch case faring. The +/-45 deg. layers of the faring are also inserted in the mould at this time. The thin film adhesive is then placed into the mould so as to bond the skins to the core. The inboard core material, used to provide pressure for the bonded joint area, is then inserted into the blade root area of the mould. The four 0 deg. layers of the spar are then laid up in a spanwise direction, at the 0.25 chord position. The core is then inserted into the mould. The thin film adhesive, for the bonding of the blade spar to the flexbeam, is then placed in position, with additional adhesive being placed on the core so as to bond the two halves of the core together. The flexbeam is then positioned on the spar adhesive, using the slot in the mould, allowing for the designed bond area.

The mould is then closed and located by inserting bolts into the locating holes on the edges of the mould. The mould is then pressurized by means of clamps which are placed around the edges of the mould. Expanding foam is then injected into the mould through the holes that have been provided. The foam serves to pressurize the pitch case so as to keep the materials in place and preserve it's shape. It also provides pressure for the preimpregnated material to cure satisfactorily. Once the expanding foam is cured the mould is placed into the autoclave, for a cure cycle of 120°C for two hours.

Once the cure cycle is complete the mould is allowed to cool to room temperature. The mould is then opened and the cured blade ejected. The blade is then cleaned up, removing the excess resin and the expanding foam from inside the pitch case. The blade is then cut to the correct length and spray painted to give a smooth finish.

5.3 Rotor System Balancing

5.3.1 Static Balance

The rotor system has to be balanced to minimize the eccentric loading on the rotor shaft. The static balancing of the rotors is done in the following manner:

- Each blade in the system has it's mass and CG position measured and recorded [see figure 72].
- The mass of each blade is then adjusted by adding mass or removing mass so as to get each blade in the set to the same mass.
- The position of the CG is adjusted by adding mass to or removing mass from positions on both blades so as to move the CG to the identical position on each blade.

The blades were balanced to within 0.01 grams of each other and the CG position to within 1 mm of each other.

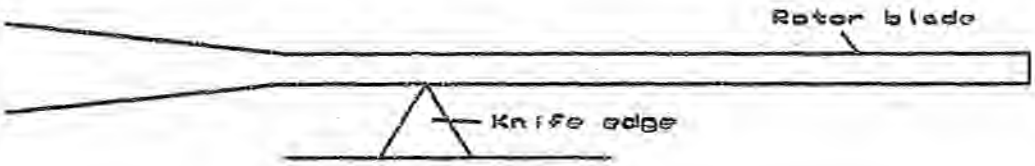

Figure 72: Blade Balancing (Static)

5.3.2 Blade Tracking

Blade tracking is the manner in which the blades follow each other, ie. the path taken by each blade. Out of track blades are blades that follow their own individual path around the azimuth and produce irritating vibrations which can affect the instruments on the test rig. Tracked blades follow the same path and lead to smooth operation. If every blade was made 100% identical, blade tracking would not be necessary, but since every blade is not identical, ie. aerofoil profile, mass distribution, stiffness distribution and hub installation may differ, the blades have to be tracked.

The blades are tracked in the 'lowing manor:

- Each rotor blade tip is marked with an identifying color marker.
- The rotor system is spun up with a flat pitch to the operating speed.
- A strobe light is pointed at the rotor system with its frequency adjusted to twice that of the operating frequency of the rotor system. This allows both blade paths to be seen 'simultaneously'.
- Each blade position is clearly identified [figure 73].
- The rotor system is then stopped and the pitch links are adjusted to reduce the angle on the upper blade and increase the angle on the lower blade.
- The procedure is repeated until the blades follow each other in the same flight path (figure 74].
- The tracking is then checked with an increased blade pitch setting angle.

An alternative method of tracking the blades is to attach trim tabs to the outboard trailing edge of each rotor blade. They adjust the lift on the blade to bring it into line with the other blade. Once the rotor system is balanced and tracked it is ready for operation.

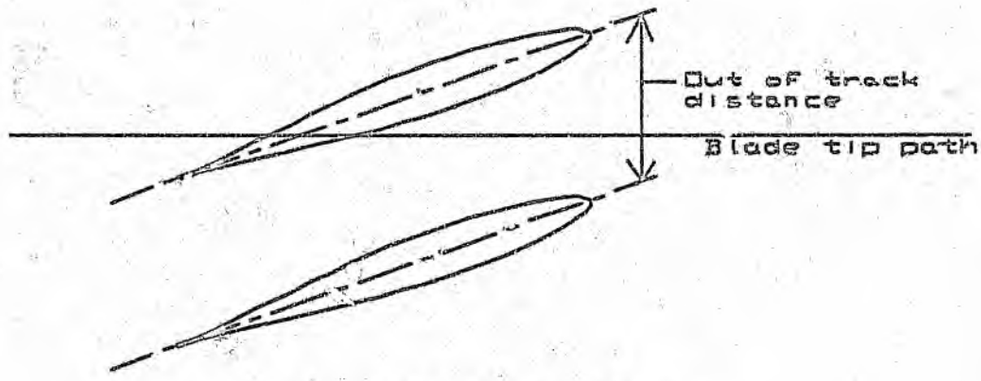

Figure 73: Blades Out of Track

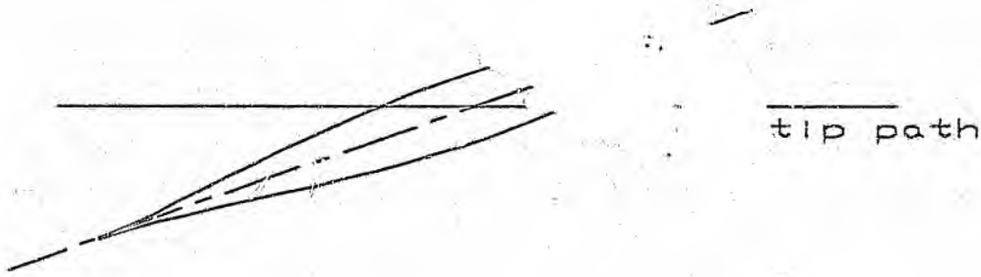

Figure 74: Blades Correctly Tracked

Chapter 6

Rotor System Evaluation

The new concept flexbeam rotor system was tested in a range of static tests and windtunnel flight tests. Comparisons were made with a conventional teetering rotor system so as to show some of the advantages and disadvantages of the new rotor system. The testing that concerns the flexbeam itself is presented by Sheiman[49] and is not discussed in detail here.

6.1 Manufacturing Process

During the manufacture of both the flexbeam rotor system and the conventional rotor system a few points worthy of discussion were noted. While these observations are purely qualitative they do provide insight into some of the advantages of this new concept rotor system that may not be readily apparent.

The manufacture of a rotor system plays an important role in its design and in the economics of the concept as a whole. Time is considered to be one of the more important aspects of the manufacturing phase of any project. Time spent on the manufacture can be minimized by simple, easy to assemble designs with low part count and low material usage. The latter aspect also influencing the cost

by making maximum use of the material with minimal scrappage. The time taken to manufacture the conventional rotor system was considerably larger relative to that of the flexbeam system. The reasons being:

- The conventional hub had a large number of components which had to be machined, some with a high degree of accuracy. Whereas the flexbeam hub only had one component to be machined, which has very low tolerances. This reason has the largest influence on the manufacturing time, reducing it by a significant amount.

- The composite material for the flexbeam system was easy to cut, with very little scrappage. Whereas the conventional system had a large amount of material with an intricate pattern to cut for the root region of the blade. This also led to a relatively large amount of material scrappage.

- The flexbeam concept lends itself to a quick and easy lay up while the conventional system, on the other hand, has an intricate lay up procedure near the root, increasing the lay up time.

- The curing procedure takes the same amount of time for either blade, however, the post cure finishing off of the blades is shorter for the flexbeam concept as no holes have to be drilled and no root connection erosion strips bonded on.

A comparative cost study done by Sikorsky Aircraft [36] between a metal blade and a composite blade [figure 75], indicates that economic benefit is gained from the production and ownership of a composite blade. As discussed above, the flexbeam composite hub concept shows that it can have a vast economic benefit

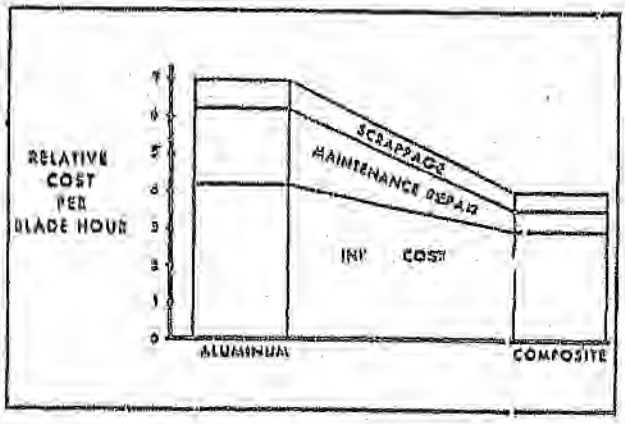

Figure 75: Comparative Blade Costs [36]

for production. It can also lend itself to an automated lay up procedure, reducing production time and cost. Thus the flexbeam concept as a whole, from a production point of view, has many advantages and goes a long way to decreasing the overall costs of a helicopter.

6.2 System Mass

The scale used for the mass measurement of both the flexbeam and conventional rotor systems has specifications as shown in [APPENDIX I].The results from these measurement tests are shown below in table 7.

Table 7: Results of Mass Measurement

Conventional Rotor System	2747.4 g
Flexbeam Rotor System	1359.3 g

As calculated previously, the predicted mass of the flexbeam rotor is given as

$$M_{flex} = 672.92 \text{ g/blade} = 1345.8 \text{ g (total)}$$

The error between the predicted value and the actual measured value is 1.0%. This shows that the analytical methods used to estimate the system mass correlate favorably with the actual measured results, thus verifying its use in the design process.

Comparing the masses of the two rotor systems shows that the mass of the flexbeam concept is less than half of that of the conventional system. Quantitatively this constitutes a weight saving of 50.5% on that of the conventional system. Such a weight saving cannot be directly extrapolated to a full scale rotor

system, however, industry has shown that weight savings can be gained by the use of composite materials, for example:

The company MBB found that a weight and cost reduction in the range of 20% can be achieved, when comparing the new composite bearingless tailrotors to the conventional tailrotor with the same thrust capacity [17]. Sikorsky and Bell, contracted for the Advanced Composite Airframe Program (ACAP), achieved a 24% weight saving through the use of composites for the helicopter. Westland Helicopters, as part of the British Experimental Rotor Program (BERP), developed composite rotor blades for the EH101. Apart from improving on performance, they weighed less than their metallic counterparts (Quantitative results on the mass or percentage weight saving of the composite blades is currently unavailable.) [35]. Thus a weight saving advantage on a full scale system could be expected.

The advantages of weight saving are numerous and are fundamental to the design of any helicopter. Immediate advantages would be an increase in the payload capacity of the helicopter or the decrease of the fuel consumption, due to the lower power requirement of the helicopter. All these advantages translate into a more economically efficient helicopter, thus passing an economic benefit to the owner of the helicopter.

6.3 Static Component Testing

Static tests were done on both the flexbeam blades and the conventional rotor system blades. The tests were carried out at the University of the Witwatersrand's Mechanical Engineering Laboratory and were aimed at verifying the design and manufacture of the blades and to create confidence in the use of the systems at the operating conditions.

6.3.1 Testing Procedure

The tests of the full size model blades were carried out on a JJ Lloyd tensile testing machine, which has a maximum tensile loading capacity of 20kN.

Aluminium wedge grips were manufactured to restrain the flexbeam wedge in the testing machine. Aluminium tabs were bonded to the blade tips, over the spar, to provide the other grip attachment point. The tabs are bonded on using Araldite adhesive, cured for one hour at 120°C. The tabs are necessary as the grips on the tensile testing machine tear the composite material making it impossible to grip the composite without any slippage. A pin attachment was manufactured to restrain the root end attachment point of the conventional rotor blade. This was done so as to test the bolt hole connection point, on th conventional blade, for a bearing, shear or tensile failure mode.

The method of testing for each of the blade types is described as follows:

- The flexbeam blade was loaded up to a tensile load of 6kN, which is approximately 1.5 times the operating load. The pitch case faring was then twisted such that the flexbeam would twist to its maximum twist allowed within the geometric constraints of the pitch case faring. The twist angle was not measured directly but, based on the geometry of the pitch case faring, could twist to a maximum of 18 degrees. The load on the blade was then increased slowly until destruction of the blade. Two blades were tested in this manner with the results being recorded graphically on a XY plotter [see figure 76 & figure 77].
- The conventional blade was loaded up slowly until the destruction of the blade. Only one blade was tested with the results being recorded graphically [see figure 78].

The testing machine and plotter were originally calibrated for a maximum load capacity of 8kN, however, this was found to be insufficient. They were then recalibrated to their full scale range of 20kN.

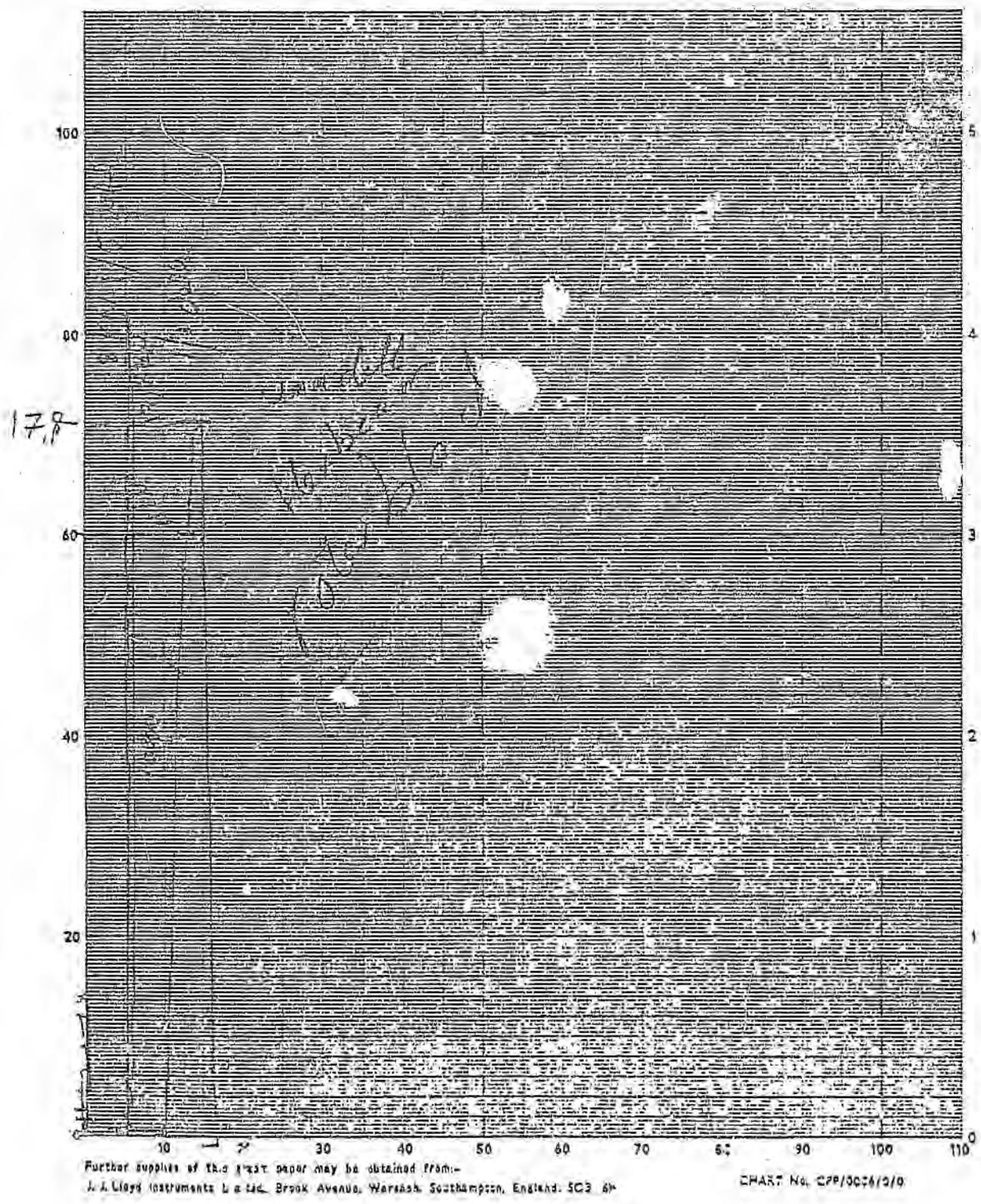

Figure 7: Flexbeam Static Test 1

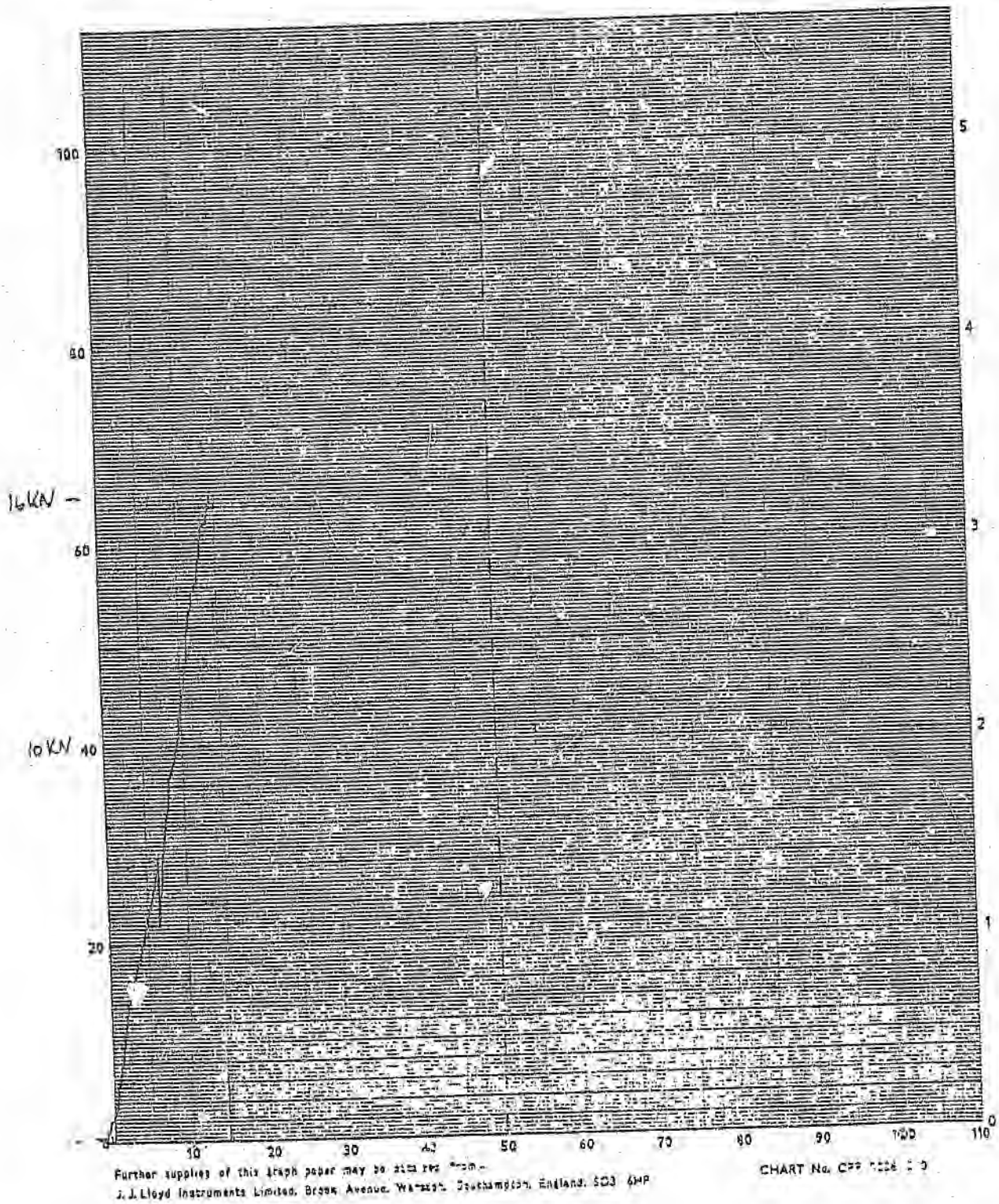

Figure 77: Flexbeam Static Test 2

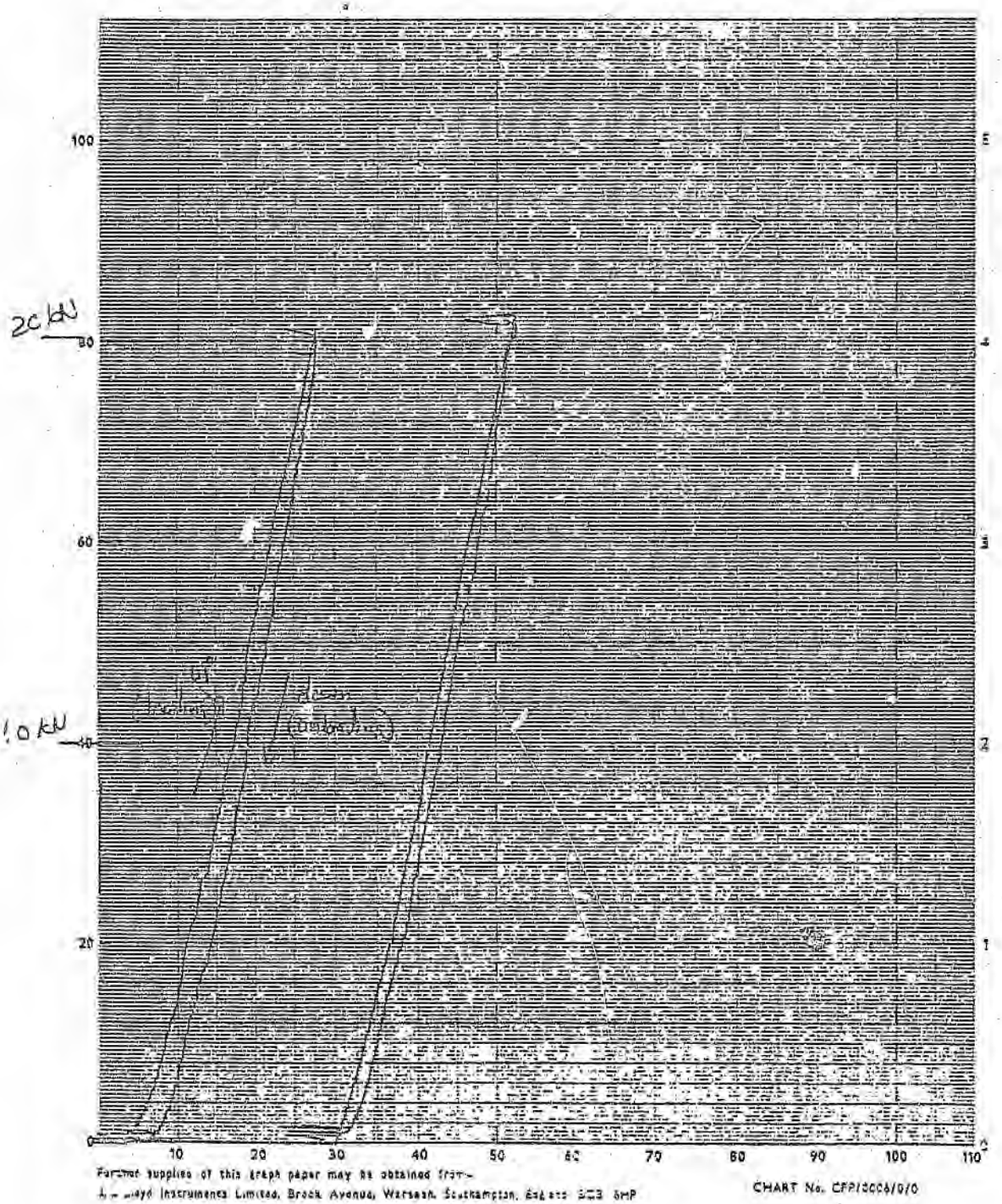

Figure 78: Static Test of Conventional Blade

6.3.2 Flexbeam System Results

Both flexbeam blades were tested to destruction with the first reaching a maximum tensile load of 17.8kN and the second blade, a maximum load of 16.3kN.

In both tests the initial failure is not clearly evident. On the first blade [figure 76] a kink in the loading curve can be seen at approximately 11.6kN which may constitute a first ply failure. Failures then occurred at intervals until there was an ultimate failure which occurred at 17.8kN. The failure at this point was determined by the inability of the blade to carry any further loading and the test was thus stopped. This type of failure constitutes a soft failure mode, which is a characteristic failure mode of glassfibre composite material. This failure also demonstrates the inherent fail safety of the design by using these materials.

The component that failed on this blade was not initially known. It was expected that failure would develop from a stress concentration point in or near the root area of the blade. The stress concentration points that exist are:

- The inboard section of the bonded joint, which has a characteristic peel stress failure mode [figure 79]. The bond peel stress distribution along the bond [figure 80] makes this a plausible area for failure to occur.
- The outboard section of the bonded joint has a stress concentration point which was identified by the FEM analysis of the bond in the root section.
- Another stress concentration point was that which could occur at the wedge of the flexbeam. At this point the flexbeam laminate is separated so as to be wrapped around the brass insert, from where it rejoins the laminate. This will thus induce a stress concentration point.



Figure 79:Failure Mode

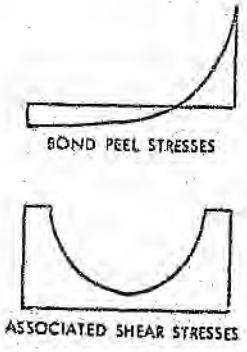

Figure 80: Bond Stresses



Figure 81: Spanwise Cross-Section through Blade Root Area

A spanwise cross-section was cut into the blade [figure 81] for inspection and to aid in determining the exact point of failure. Immediately apparent was a crack

45mm in length in the inboard section of the flexbeam starting from the wedge. On closer examination the crack was found to be a delamination between the 90 deg. and 0 deg. layers in the flexbeam. This failure could thus have been caused by the stress concentration point at the wedge with the peel stress of the bond contributing to this type of failure. It can be deduced that this point at the flexbeam wedge is the dominant point at which failure occurs in this design.

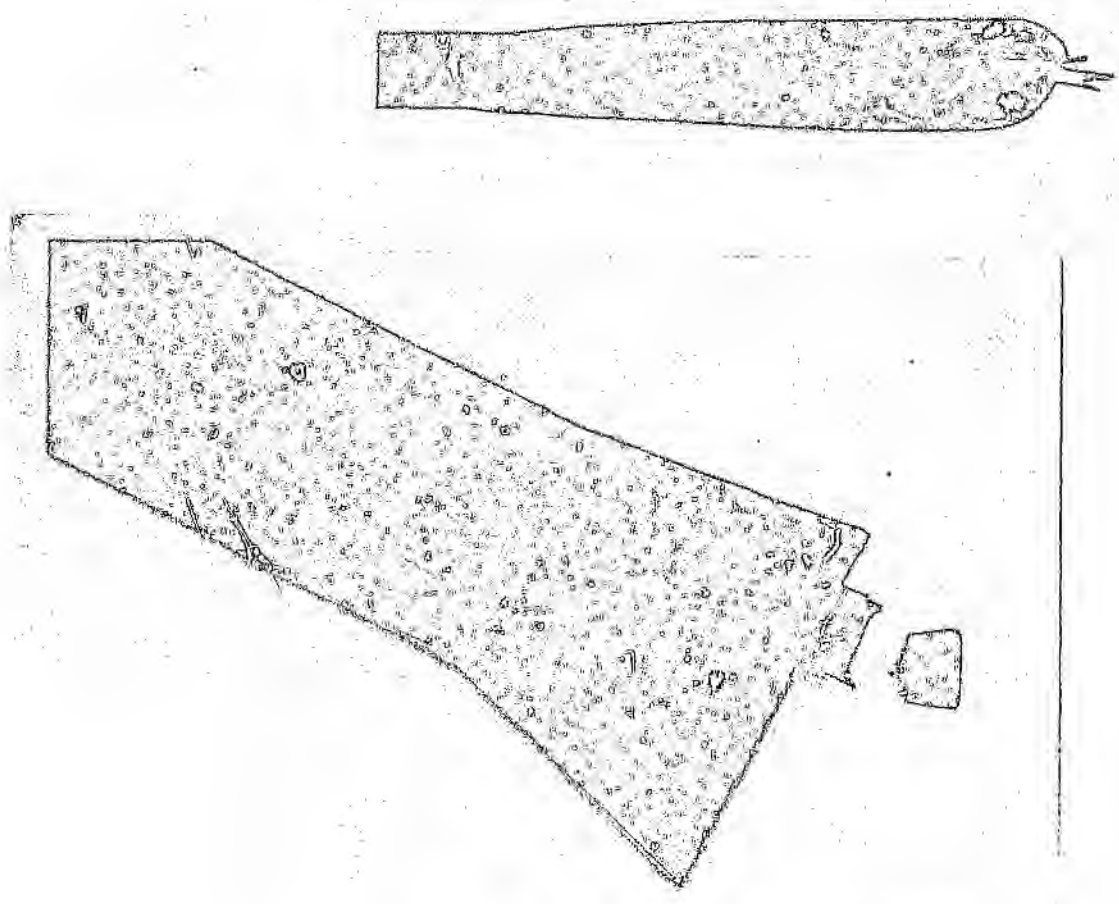

Figure 82: Point Load Failure of Flexbeam

The second blade [figure 77], did not show any signs of failure until a load of 15.5kN was reached at which point a kink in the loading curve can be seen. An unexpected catastrophic failure of the flexbeam occurred at a load of 16.3kN. However, this failure was not attributed to a stress concentration point in the

-sign, but rather to the influence of the machine grips. The aluminium wedge grips had been distorted in the previous test thus inducing a large compressive point load on the wedge surface, which eventually lead to the failure of the flexbeam. The line at which the failure occurred is clearly visible in figure 82, thus identifying the above reason to be the only cause of failure. This catastrophic failure is characteristic of carbon fibre thus being consistent with the argument, used in the design concept, for not drilling holes into the flexbeam laminate.

Inspection of the blade spar itself showed there to be no sign of failure. It can thus be deduced that the spar is not a critical part of this design concept.

The failure loads obtained in the static tests far exceed the required design centrifugal loads for the rotor which operates at 2000rev/min. This translates into a reserve safety factor of 4.2. This may constitute an over design, however, in the design a combination of both in-plane and out-of-plane loads were considered. The combination of these loads takes place in the following manner:

A positive bending moment on the blade increases the tensile load on the lower surface while putting the upper surface into compression. The centrifugal load, being tensile in nature, will increase the tensile load on the lower surface and decrease the compression load on the upper surface of the blade. Compressive stresses are undesirable as the strength then depends on the matrix properties, instead of the fibre properties. Thus a sufficiently high centrifugal load to eliminate the compressive stresses would be desirable. Thus, when considering this combined loading, the reserve safety factor would drop to ± 2.2. An optimum precone angle will also reduce the mean oscillating bending moment, thus maintaining a generally state of tension on both surfaces of the blade.

6.3.3 Conventional System Results

The results of the tests performed on the conventional teetering rotor blade have been included as they demonstrate some of the behaviour characteristics of mechanically bolted joints and the stress - strain relationships of glassfibre composite materials. Only one blade of the conventional rotor system was available for the static destructive tests. However, the capacity of the tensile testing machine was exceeded before there was any visible sign of failure.

During the testing, the blade was loaded up to the maximum capacity of the testing machine. The blade showed no sign of failure at this point, and continuing the test would have resulted in the permanent damage to the testing machine. Visual observation of the blade specimen under the 20kN load revealed that the bolt hole, which was also under test, had slight elongation, showing signs typical of a bearing failure. The blade was then unloaded and retested to check repeatability and to verify that the blade had not failed.

The results [see figure 78], although not revealing any failure, do have some interesting features. The slope of both curves are linear and are identical. This is characteristic of a composite material which behaves in a linear-elastic fashion until the first ply failure. This material thus does not yield before ultimate failure as do isotropic materials. Another feature of the results is that the unloading of the specimen did not follow the loading up of the specimen. There are two identifiable reasons for this hysteresis, namely:

- The first reason is that the composite material does not have an elastic stress-strain relationship but rather an anelastic stress-strain relationship. All solids are anelastic to a small extent, even in the regime where they are nominally elastic. The loading curve does not exactly follow the unloading curve, and energy is dissipated when the solid is cycled [2]. The figure below [figure 83] shows a typical stress-strain curve for glassfibre which exhibits anelastic stress-strain behavior. The anelastic behavior of this material would also account for the damping capacity of glassfibre to damp out noise and vibration.

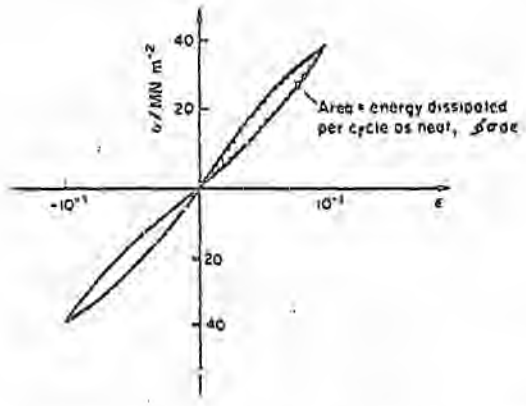

Figure 83: Anelastic Stress-Strain Behaviour [2]

- Secondly, the pin connection hole on the blade could have suffered a bearing failure. On closer inspection of the hole area, it was found that the material inboard of the hole had been compressed, leading to a slight elongation and a through thickness expansion of the compressed material around the hole. The hole was then measured with a vernier and it was found that it had elongated by 2% from its original diameter. This would explain the change in the hysteresis between the first and second test of the blade.

To lessen the chance of this type of bearing failure of the blades being used on the test rig, aluminum tabs were bonded onto the blade, over the hole, thus providing a clamping action. This clamping action provides a constraint against the Poisson's expansion normal to the plane of the laminate so that fibres acting transversely to the load will undergo a different mode of failure. The quasi-isotropic laminate used for the root section also reduced the possibility of a shear out or cleavage failure.

The conventional blade, with its high stress concentration hole, proved to be stronger than originally expected, thus increasing its confidence level so as to be used in the high speed dynamic rotor environment.

6.4 Rotor Hover Tests

Comparative hover tests were performed at the Mechanical Engineering Laboratory of the University of the Witwatersrand. The tests were to compare the drag of the flexbeam rotor system against that of the conventional teetering system.

6.4.1 Test Procedure

Both the conventional rotor system and the flexbeam rotor system were tested under the same conditions. The collective setting on the test rig was set at 8 degrees. On the flexbeam system the collective had to be locked in place as the control servos could not maintain the 8deg. collective setting. The rotor systems were tested in the speed range from 400rev/min to 1600rev/min. Four tests were done at each interval between the given speed range, and the results recorded.

All the instrumentation on the test rig was calibrated using the equipment shown in [APPENDIX I].

The errors in the test rig instrumentation are shown below in Table 8.

Table 8: Test Rig Error Bands

Thrust	± 5 *N*
Torque	± 0.1 *Nm*
Control Angles	± 1 deg.
Shaft Angle	± 0.3 deg.
Flapping Angle	± 0.3 deg.
Rotor Speed	± 2 *rev/min*

6.4.2 Hover Test Results

The results of the hover tests for both rotor systems were plotted and are shown together in figure 84.

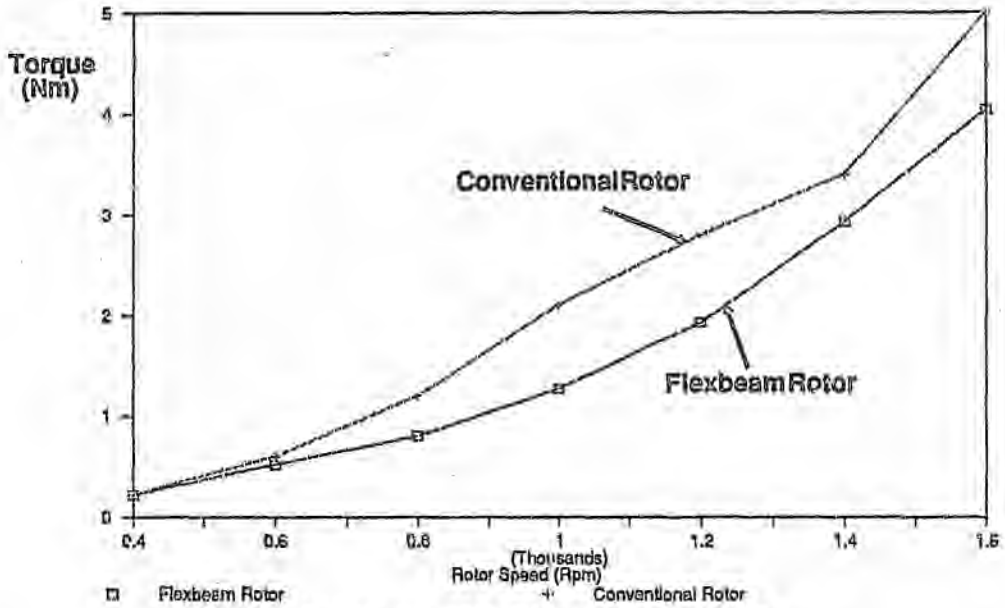

Figure 84: Comparative Hover Test Results

The results show the flexbeam rotor system to be more efficient in comparison to the conventional rotor system. Since the blade geometry, including the planform shape, radius, chord, and aerofoil section are common to both rotor systems, the discrepancy in the measured drag can only be attributed to the different hub and root configurations.

The main geometric features in the root area responsible for influencing the rotor drag are:

- The measured blade root cut-out, which is given as 150mm for the conventional system and 45mm for the flexbeam system, representing a 70% reduction in the root cut-out radius for the flexbeam system.

- The thickness of the structure in the root area of the rotor system. The measured thickness of the conventional system outboard of the shaft connection is a maximum of 50mm, while the thickness of the flexbeam system has a maximum value of 20.25mm, reflecting a 59.5% reduction.

Figure 84 shows that the flexbeam rotor system has lower torque thus absorbing less power than the conventional rotor system, especially at the higher rotor speeds. The apparent trend is that the difference in torque, between the rotor systems, increases with rotor speed, which is to be expected. It was noted that no difference was detected at or below 400rev/min.

However, the relatively large difference in the rotor torque, at high rotor speeds, may not be completely due to the differences in the hub geometry, but may be influenced by the limitations of the test rig's control system. The method of setting the collective on the two rotors was different. The reason for this was that the test rig collective servo was unable to twist the flexbeam to the required blade pitch angle. The blade pitch angle on the conventional system was controlled by the collective output of the test rig, to within ± 1deg. of the required angle. Whereas, the blade pitch angle on the flexbeam was locked in place and the angle measured with a clinometer to within 1 minute or 0.0166 deg. of the required angle. The effect of a one degree increase in the blade angle constitutes a 22.5% increase in the torque, as calculated with the aid of the computer program in [APPENDIX A]. (The computer program was validated and found to have an error of less than 5.67% in hover). The computer program was executed using 1600rev/min and an 8deg. collective angle, representing the test conditions. The program computed a torque of 5.375Nm which is only 7.5% above the measured value of 5Nm. Thus it may be concluded that the blade angle was close to the required 8degrees.

The results presented in figure 84 show that the difference in torque between the conventional system and the flexbeam system is 20% at 1600rev/min. Even though there is an uncertainty in the blade angle of the conventional system, the

flexbeam system did show an improvement in performance over the conventional system in the hover condition.

During the testing phase, some qualitative observations were made. These observations relate mainly to the natural frequency vibrations of the rotor system. When testing the flexbeam rotor system, it was noted that at approximately 1000rev/min the test rig experienced large vibrations. The results of the dynamic analysis [see figure 63] show that there is a 2/rev excitation near 1000rev/min mark. The 2/rev excitation is an in-plane excitation caused by the Coriolis forces. Since the rotor system is stiff in-plane these loads are transferred into the rotor shaft and drive system, causing the vibration of the test rig. Thus the observed vibration of the rig, at this rotor speed, does correlate with the predicted vibration modes of the design. The design point of the rotor system is 2000rev/min, where it was predicted that no n ·ral modes would be excited. When operating the test rig at this design point of 2000rev/min, no vibration was apparent, thus correlating with the results of the dynamic analysis.

The conventional rotor system did not vibrate, the reason being:

- the rotor blades were attached to hub by means of a pinned joint. This joint would act like a lagging hinge thus alleviating the in-plane loads, including the Coriolis loads and loads due to the imbalance of the chordwise CG. As a result of this hinge the loads are not transferred into the drive system, thus not inducing any forced vibration.

6.5 Windtunnel Flight Tests

Translational flight tests were conducted in the CSIR's 7m x 6m low speed windtunnel. The objective of these tests was to compare the performance of the two rotor systems, and to verify their performance against the analytical predictions.

6.5.1 Flight Test Procedure

Both the conventional rotor system and the flexbeam rotor system were tested with windtunnel speeds ranging from 5m/s to 19m/s and a constant rotor speed of 800rev/min. Higher rotor speeds could be used due to the lack of control power in the collective servo, thus making it impossible to pitch the blades. For the conventional rotor system the blades were pitched using the collective control servo on the test rig, while for the flexbeam system the collective pitch was set at an angle and then locked.

The shaft carriage of the rig was unlocked during the tests of the conventional system so that the system would *'flyfreely'* and find its own equilibrium or trim position.

The results of the tests were recorded using the rig's computer data acquisition system. Smoke was used for flow visualization tests with the results being recorded on 8mm format video tape. The smoke probe was traversed across the disk plane focusing on the tip areas.

6.5.2 Windtunnel Test Results

A sample of the unprocessed flight test data received from the test rig's data acquisition system is shown in [APPENDIX H]. After the analysis of all the data received in the windtunnel tests, it was found that no meaningful conclusions could be drawn from the data. Some of the reasons for the failure of the tests to produce any meaningful results were:

- The tests were used to commission the test rig as well as provide the performance data for the verification of the design concept, and analytical models. This was done as the windtunnel was only available for one day in which to set up and complete the testing.

- The test rig itself presented a few short comings, namely, the force transferred from the actuators to the blade pitch links was not sufficient to control the blades ie. the bearing loads and flexbeam loads were too great for the available control loads to overcome. There was also insufficient cyclic control at high wind tunnel speeds, thus not allowing adequate control for the rotor system.

- An insufficient number of tests were done, due to the limited time, thus not providing sufficient data for the construction of the performance curves of the rotor systems.

The University of the Witwatersrand's windtunnel could not be used as the rotor system and rig were too large for the test section, in terms that the rotor system would be operating inside the boundary layer of the tunnel walls and running in ground effect thus giving erroneous results. Thus with further upgrading of the rig and the use of a large enough windtunnel for a length of time, full validation tests can be done, proving the design concept for performance.

5.5.3 Flow Visualization

The flow visualization was completely qualitative showing the flow fields ahead, on and after the rotor disk plane. What could be seen from the video footage were the blade tip vortices, which were circulating from the lower surface to the top surface, and the circulating trailing vortex flow field. The lead-lag motion of the conventional system could also be clearly seen from the high speed video footage that was shot.

The flow visualization was done purely to provide insight into the physical flow field around the rotor system and to show the actual motion of the rotor blades in translational flight. The visualization of the flapping motion of the blades confirmed that the rotor blades flap up in the front and down at the back, which agrees with the flapping motion predicted by the aerodynamic design software

[APPENDIX A]. The video footage also showed that the lead - lag motions of the blade can be relatively large.

6.6 Summary of the Advantages and Disadvantages of the Bearingless Rotor System Concept

The advantages and disadvantages of this rotor system concept arise from the comparisons done between itself and the conventional teetering rotor. The major advantages of the rotor, as discussed previously, are those of weight, manufacturing cost and time saving and an increase in flight performance. These advantages generally affect the manufacturing and ownership costs and can lead to a more efficient rotor overall.

The rotor is, however, not without its short comings. A major disadvantage of the rotor system was the increase in control loads necessary to twist the flexbeam in order to pitch the blade. The rotor could not be controlled at all from the test rig's control system, thus making it necessary to lock the pitch on the blades before the testing began. The flexbeam has to be correctly tailored in order to minimize the force needed to twist the blade. It also has to be manufactured carefully so as to achieve a repeatable product and to maintain even control loads on both sides of head.

This highlights another major disadvantage inherent in the manufacture of any component using composite materials. This being the quality control of the product and the repeatability of manufacture. As a result of the current manufacturing techniques and the form of the raw composite materials, close tolerances are difficult to maintain which can lead to the rejection of many components, which can be costly.

Thus composite materials would only suite applications where the tolerances are low and strength in particular directions are required. The use of composite materials must be carefully considered in the design of any component to ensure that the component warrants being made from composites and that the advantages do out-weigh the disadvantages.

Chapter 7

Conclusions and Recommendations

A scale model bearingless rotor system, using composite materials, was designed, manufactured and tested. When comparing it to a conventional teetering rotor system of the same thrust capacity, the following conclusions were drawn:

- The rotor system has no moving parts with the number of components being reduced by 55%.
- As a result of the fewer components and the simplicity of the design and lay up, the manufacturing time was reduced, thus making the system economically more viable.
- The total mass of the rotor system was 1345.8g, which represents a 50.5% mass saving as compared to the conventional rotor system. The mass also represents a 1% error between the predicted and actual mass value, thus verifying the analytical methods used for mass prediction.
- The static tests showed the design to be fail safe by demonstrating the soft failure mode characteristics of glassfibre composite material. The tests also proved that the blades were capable of sustaining the expected operating loads while also verifying the analytical design methods.
- Comparative hover tests revealed that the rotor system has 20% less drag and thus absorbs less energy than the conventional rotor

system, thus improving the performance for the same thrust capacity.

- In relation to the conventional rotor system, the flexbeam rotor requires increased control power in order to pitch the blades.

- As a result of the design process, a number of tools for the analysis and design of rotor systems in general were developed.

Based on the findings of the design study, including the manufacturing and testing of systems, the following recommendations can be made:

- The further development of the computer codes for predicting the aerodynamics and performance, especially in the areas of inflow modeling, transitional flight and non-rigid aerodynamics, would enhance the capability of the program.

- The optimization of the flexbeam, its shape and structure, so as to improve its performance for twisting and flapping as well as reducing the control power necessary for pitching the blades.

- An indepth study into the failure modes of composite bonded and mechanical joints for both glassfibre and carbon fibre pre-impregnated materials.

- The upgrading of the translational flight test facility so to enable comprehensive studies of rotor systems and their environment for translational flight. This would also assist in the complete validation of the design/analysis tools that were developed for this project.

References

1 Abbot IH, Von Doenhoff AE, *Theory of Wing Sections*, Dover Publications, 1959.

2 Ashby MF, Jones DRH, *Engineering Materials*, Pergamon Press, 1980.

3 Bailey FJ, *A Simplified Theoretical Method of Determining the Characteristics of a Lifting Rotor in Forward Flight*, NACA Report 716.

4 Bielawa RL, Cheney MC, Novak RC, *Investigation of a Bearingless Helicopter Rotor Concept having a Composite Primary Structure*, NASA CR-2637, 1976.

5 Blankenship BL, Harvey KW, *A Digital Analysis for Helicopter Performance and Rotor Blade Bending Moments*, Bell Helicopter Company.

6 Bruhn EF, *Analysis and Design of Flight Vehicle Structures*, Purdue University.

7 Chang FK, Scott RA, Springer GS, *Failure of Composite Laminates Containing Pin Loaded Holes*, Journal of Composite Materials, Vol.18, 1984.

8 Cohen GM, Sheiman L, *Computer-Aided Rotor System Analysis*, Second South African Aeronautical Engineering Conference, CSIR, 1990.

9 *Federal Aviation Regulations*, Part 27, 1974.

10 Foye RL, Shipley JL, *Evolution of the Application of Composite Materials to Helicopters*, Journal of the American Helicopter Society, October, 1981.

11 Ganzer VM, Rae WH, *An Experimental Investigation of the Effect of Wind Tunnel Walls on the Aerodynamic Performance of a Helicopter*, NASA TN D-415, 1960.

12 Gessow A, Crim AD, *A Method for Studying the Transient Blade Flapping Behavior of Lifting Rotors at Extreme Operating Conditions*, NACA TN 3366.

13 Gessow A, *Equations and Procedures for Numerically Calculating the Aerodynamic Characteristics of Lifting Rotors*, NACA TN 3747.

14 Hart-Smith LJ, *Adhesive-Bonded Double-Lap Joints*, NASA CR-112235, 1973.

15 Hart-Smith LJ, *Analysis and Design of Advanced Composite Bonded Joints*, NASA CR-2218, 1974.

16 Heyson HH, *A Note on the Mean Value of Induced Velocity for a Helicopter Rotor*, NASA TN D-240, 1960.

17 Huber H, Frommlet H, Buchs W, *Development of a Bearingless Helicopter Tailrotor*, Vertica, Vol.15, 1981.

18 Hunt MS, *Investigation into the Use of Composite Materials for Rotorcraft Rotors*, CSIR Report 609, 1977.

19 Jacobs EN, Sherman A, *Airfoil Section Characteristics as Affected by Variations of the Reynolds Number*, NACA Report 586, 1937.

20 Johnson W, *Helicopter Theory*, Princeton University Press, 1980.

21 Jones RM, *Mechanics of Composite Materials*, McGraw- Hill.

22 Landgrebe AJ, *Simplified Procedures for Estimating Flapwise Bending Moments on Helicopter Rotor Blades*, NASA CR- 1440, 1969.

23 Landgrebe AJ, *Simplified Procedures for Estimating Flapwise Bending Moments on Helicopter Rotor Blades*, NASA CR- 1441, Part II - Tables, 1969.

24 Layton DM, *Helicopter Performance*, Matrix Publishers, 1984.

25 Livesley RK, *Finite Elements: and introduction for engineers*, Cambridge University Press, 1983.

26 Ludi LH, *Flight Investigation of the Effects of Retreating Blade Stall on Bending and Torsional Moments Encountered by a Helicopter Rotor Blade*, NACA TN 4254, 1958.

27 Matthews FL, *Joining Fibre-Reinforced Plastics*, Elsevier Applied Science, 1987.

28 Mayo AP, *Matrix Method for Obtaining Spanwise Moments and Deflections of Torsionally Rigid Rotor Blades with Arbitrary Loadings*, NACA TN 4304, 1958.

29 Mayo AP, *Comparison of Measured Flapwise Structural Bending Moments on a Teetering Rotor Blade with Results Calculated from the Measured Pressure Distribution*, NASA Memo 2- 28-59L, 1959.

30 Mil'et al ML, *Helicopters - Calculation and Design*, NASA TT F-494, Volume I, 1967.

31 Mil'et al ML, *Helicopters - Calculation and Design*, NASA TT F-519, Volume II, 1968.

32 Nikolsky AA, *Helicopter Analysis*, John-Wiley & Sons, 1951.

33 Parker I, *Westland Advances Rotor Blade Technology*, Flight International, 17 July 1982.

34 Prouty RW, *Helicopter Aerodynamics*, Rotor & Wing, 1985.

35 Rotor & Wing International, *Composites*, Special Advertising Section.

36 Salkind MJ, *The Twin Beam Composite Rotor Blade*, 29th Annual National Forum of the American Helicopter Society, 1973.

37 Saunders GH, *Dynamics of Helicopter Flight*, John- Wiley & Sons, 1975.

38 Scarpati T, Sandford R, Powell R, *The Heavy Lift Helicopter Rotor Blade*, Boeing Vertol Company,

39 Stepniewski WZ, Keys CN, *Rotary-Wing Aerodynamics*, Dover Publications, 1984.

40 Straub FK, Johnston RA, Head RE, Kelly HL, *Design and Development of a Dynamically Scaled Model AH-64 Main Rotor*, Vertica, Vol.19, 1985.

41 Taggart AWM, *Helicopter Air Power*, Aerospace, November 1988.

42 Taha S, Messinger RH, *Manufacturing Methods and Technology Program for a YAH-64 Composite Flexbeam Tail Rotor*, AVRADCOM AD-A134277, 1982.

43 Tanner WH, *Charts for Estimating Rotary Wing Performance in Hover and at High Forward Speeds*, NASA CR-114, 1964.

44 Tse FS, Morse IE, Hinkle RT, *Mechanical Vibrations - Theory and Applications*, Allyn & Bacon Inc, 1978.

45 Weller WH, Mineck RE, *An Improved Computational Procedure for determining Helicopter Rotor Blade Natural Modes*, NASA TM 78670, 1978.

46 Wheatley JB, *An Aerodynamic Analysis of the Autogiro Rotor with a Comparison between Calculated and Experimental Results*, NACA Report 487, 1934.

47 Velupillai D, *Rotorheads Today*, Flight International, 17 July 1982.

48 Zienkiewicz OC, *The Finite Element Method in Structural and Continuum Mechanics*, McGraw-Hill, 1977.

49 Sheiman L, *The Design, Development and Testing of a Carbon Fibre Composite Flexbeam Rotor Hub for a 1/5 Scale Teetering Rotor System*, MSc Thesis, Univ. of the Witwatersrand, 1990.

APPENDIX A

CARSAN Program

ABSTRACT

A computer code, suitable for use on a PC-AT type computer, has been developed to analyse single lifting rotor systems for aerodynamics, structural loads and dynamics. The program covers teetering, articulated and cantilevered rotor systems.

Aerodynamic performance in both hover and translational flight is presented based on a method by *Alfred Gessow and Almer D Crim*. The method has been improved to incorporate hover procedures, fully coupled blade flapping and lagging degrees of freedom and precone evaluation for teetering rotor systems. The code has been validated for hover and translational flight of the articulated rotor system type using flight test performance data for the Aerospatiale Puma SA 330 J. Hover performance was found to predict to within 6% being the worst case, and translational flight to within 14%.

The structural program is based on the method in NACA TN 4304 by *Alton P Mayo* and was validated using NASA MEMO 2-28-59L as no test flight data is available.

The code for the dynamic analysis program was taken from NASA TM 78670 by *William H Weller and Raymond F Mineck*, which is fully validated, and adapted to run on a PC-AT computer. The code has been metricated and integrated into the environment of the aerodynamic and structural modules of the program so as to run as a unit.

Table of Contents

1 INTRODUCTION 1 - 1

Program Scope 1 - 2

Program Limitations 1 - 3

Program Methodology 1 - 4

2 NOTATION 2 - 5

3 METHOD OF ANALYSIS 3 - 8

Solution of the Flapping Equations 3 - 8

Articulated Rotor Constraints 3 - 8

Teetering Rotor Constraints 3 - 10

Solution of the Blade Lagging Equations 3 - 11

Helicopter Inflow Models 3 - 13

Hover Inflow Model 3 - 13

Translational Flight Inflow Model 3 - 13

Structural Spanwise Blade Loading 3 - 15

Helicopter Rotor Blade Natural Modes 3 - 17

4 DESCRIPTION OF COMPUTER CODE 4 - 18

Computer Program Logic 4 - 18

General Program Description 4 - 20

Computer Requirements 4 - 20

Program Performance 4 - 20

Program Operation and Description 4 - 21

Description of Program Output 4 - 24

5 PROGRAM VALIDATION 5 - 29

Input Data Deck 5 - 29

Geometric Data 5 - 29

Aerofoil Library Data 5 - 30

Mass and Stiffness Data 5 - 30

Flight Condition Data 5 - 31

Environmental Data 5 - 31

Aerodynamic Module Validation 5 - 32

Hover Performance 5 - 32

Translational Flight 5 - 33

6 CONCLUSIONS 6 - 35

7 REFERENCES 7 - 36

8 APPENDIX A

9 APPENDIX B

10 APPENDIX C

INTRODUCTION

The numerical analysis of helicopter rotor systems for aerodynamic performance and airloads, in both hover and translational flight, is presented based on blade element theory. The problem of determining the aerodynamic environment, using this theory, involves calculating the forces and moments on a rotating three dimensional lifting surface from statically measured two dimensional aerofoil-section data. Further complications exist, not in an aerodynamic sense but in the geometric boundary conditions. To analyse single lifting rotor systems and to maintain a degree of generality, it is therefore necessary to include the rotor hub restraints for different rotor configurations. The code thus developed covers teetering, articulated and cantilevered boundary restraints. To integrate the aerodynamic environment with the physical structural loading necessitates the introduction of some flexibility into the rigid aerodynamic analysis in the various degrees of freedom. Although, articulated two degree of freedom coupled aerodynamic flap-lag code is presented, out-of-plane flexible structural characteristics have been coded to evaluate physical out-of-plane bending moments. Furthermore, a code for three degree of freedom coupled dynamics for the boundary constraints mentioned above, has been adapted to operate in the same environment as the aerodynamic and structural codes.

Analytical blade element theory is complicated by trying to incorporate boundary conditions specific to helicopter hub types. Furthermore, assumptions and simplifications have to be made in order to evaluate the flapping equations without having to resort to numerical marching methods. The need arose to define the six force and moment loads existing at any blade spanwise station, in order to design a rotor blade, hub and root sections.

1.1 Program Scope

The assumptions normally associated with blade element theory have been neglected. These assumptions are listed below:

- No small angle assumptions.
- Flap hinge geometry is included.
- Includes the aerofoil performance in the reverse flow region.
- Is adapted for input of coefficients of lift and drag for any range of mach numbers, thus including compressibility effects, as well as neglecting the assumption of constant lift curve slope and a mean profile drag coefficient. Stall and post stall effects are therefore included.
- Up to ten different aerofoil sections may be incorporated to analyse spanwise variations in blade profiles.
- The inflow model for hover is a modified vortex theory model which includes tip loss effects.
- Root cut-out and tip loss together with variable spanwise weight distributions can be analysed.
- The aerodynamic code can produce flapping harmonics to any desired level, however, it is only shown to the third harmonic for aerodynamic analysis, and to the eight harmonic for structural loading analysis.
- Helicopter pitch and roll manoeuvres as well as transient flapping motion for any arbitrary control input can be analysed.
- Includes pitch-flap coupling and for the articulated constraint flap-lag coupling.
- Temperature and altitude effects are included.

The program numerically computes the following rotor characteristics:

- Rotor thrust and torque.
- Induced and profile power.

- Flapping angles, velocities and accelerations.
- Lagging angles, velocities and accelerations.
- Angle of attack and mach number contours.
- Aerodynamic load, Cl and Cd spanwise and azimuthal variations.
- Aerodynamic load time histories.
- Rotor shaft angle relative to flight path.
- Maximum in and out -of-plane aerodynamic forces and moments, at any blade spanwise station.
- Structural spanwise bending moments at any blade station.
- Structural spanwise bending moment time histories.
- Natural frequencies and mode shapes coupled for the three degrees of freedom.
- Fan plots of the variation of natural frequency with rotor speeds.

1.2 Program Limitations

Induced velocity for translational flight is based on Drees [7], which is a first harmonic approach. This inflow model can only be used for advance ratios of $\mu = 0.175$ to $\mu = 0.5$, which limits the programs use to fully developed translational flight. The transition area between hover and translational flight cannot be analysed using this inflow model.

The rotor blades are assumed to be rigid for the aerodynamic analysis, and flexible for the structural and dynamic analysis.

The aerodynamic characteristics are limited to the use of statically determined, two dimensional aerofoil data.

1.3 Program Methodology

It is the purpose of this paper to present the equations, theory and computer codes necessary for numerically computing the aerodynamic, structural and dynamic characteristics of lifting rotors. Firstly, the general theory used in the analysis will be presented. This will be followed by a description of the computer program and finally, a sample case will be presented for the articulated hub type. This example will be for the Aerospatiale Puma SA 330 J, whose flight test performance data will be compared to the program analysis.

NOTATION

A_1, B_1 – lateral and longitudinal cyclic pitch respectively (deg.)

a_0 – constant term in blade flapping fourier series (deg.)

a – lift curve slope (/rad)

a_n – coefficients for Cos $n\psi$ in expression for β (deg.)

B – tip loss factor

b – number of blades per rotor

b_n – coefficients for Sin $n\psi$ in expression for β (deg.)

c – blade section chord at radial station x (m)

C_ζ – blade lag damping coefficient (kg s)

C_{d0} – section profile drag coefficient

C_F – centrifugal moment in lagging equation (Nm)

C_l – section lift coefficient

C_M – coriolis moment in blade lagging equation (Nm)

C_Q – drag coefficient

C_T – thrust coefficient

D_M – drag moment in lagging equation (Nm)

e – flapping hinge offset (m)

e_L – lagging hinge offset (m)

f_x – drag force in lagging equation (N)

g – gravitational acceleration (m/s^2)

I_h – mass moment of inertia of blade about the flapping hinge ($kg\ m^2$)

I_M – inertia moment in lagging equation (Nm)

K_ζ – lag spring constant (N/m)

M_C – centrifugal moment in flapping equation (Nm)

M_I – inertia moment in flapping equation (Nm)

M_T – thrust moment of blade about the flapping hinge (N m)

M_W – weight moment of blade about the flapping hinge (N m)

m	–	mass of blade element (kg)
P	–	shaft power (kW)
p	–	helicopter rolling velocity (rad/sec)
Q	–	shaft torque (N m)
q	–	helicopter pitching velocity (rad/sec)
R	–	blade tip radius measured from center of rotation (m)
r	–	blade element radius measured from center of rotation (m)
T	–	total thrust (N)
u	–	non-dimensional resultant velocity at blade element
U_P	–	non-dimensional component velocity parallel to shaft axis
U_T	–	non-dimensional component velocity perpendicular to the shaft axis
V	–	true airspeed of helicopter (km/h)
v	–	induced velocity at rotor (m/s)
x	–	non-dimensional blade element radius
α	–	angle between shaft axis and plane perpendicular to the flight path (deg.)
α_{CF}	–	angle between centrifugal force vector and axis system in blade lagging equation
α_r	–	element angle of attack (rad)
β	–	blade flapping angle (deg.)
$\dot{\beta}$	–	blade flapping velocity (rad/sec)
δ	–	average drag coefficient
γ'	–	mass constant of blade
θ_0	–	collective pitch at blade root (deg.)
θ_1	–	blade linear twist, negative for washout (deg.)
$\varkappa$	–	airscrew correction
λ	–	inflow ratio
μ	–	tip speed ratio
ω	–	blade loading frequency in spanwise structural dynamics
ξ	–	non-dimensional flap hinge dimension (e/R)

π — 3.14159265

ρ — mass density of air (kg/m^3)

σ — rotor solidity

ζ — blade lagging angle (deg.)

$\dot{\zeta}$ — blade lagging velocity (rad/sec)

Φ — inflow angle of resultant velocity (deg.)

ψ — blade azimuth angle measured counter clockwise from the downwind position (deg.)

Ω — rotor angular velocity (rpm)

METHOD OF ANALYSIS

3.1 Solution of the Flapping Equations

3.1.1 Articulated Rotor Constraints

The differential equation of the blade flapping motion is derived in the following manner with refernce to figures 3.1.1 and 3.1.2

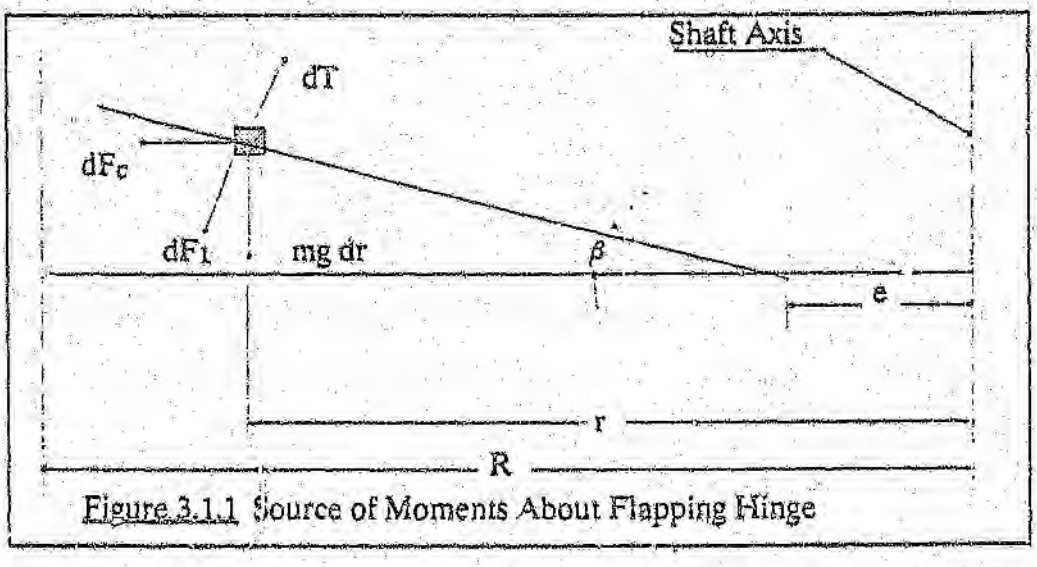

Figure 3.1.1 Source of Moments About Flapping Hinge

The origin of the various moments are shown in figure 3.1.1 and the resulting equation is

$$M_T - M_C - M_I - M_W = 0 \qquad 3.1.1.1$$

$$Mc = \int_e^R m\Omega^2 (r - e)\,[e + (r - e)\,Cos\beta\,]\,Sin\beta\,dr \qquad 3.1.1.2$$

$$\text{define } I_h = \int_e^R m(r - e)^2\,dr \qquad 3.1.1.3$$

$$\text{and } Mw = \dot{M}w\,Cos\beta = \int_e^R mg\,(r - e)\,Cos\beta\,dr \qquad 3.1.1.4$$

$$\text{thus } \dot{M}_C = \Omega^2 Sin\beta\ (I_h\ Cos\beta + \frac{e}{g} M\dot{W}) \qquad 3.1.1.5$$

$$M_I = \int_e^R m\ddot{\beta}\ (r - e)^2\, dr = \ddot{\beta} I_h \qquad 3.1.1.6$$

$$\text{now } \dot{\beta} = \Omega \frac{d\beta}{d\psi} = \Omega\bar{\beta} \qquad 3.1.1.7$$

$$\ddot{\beta} = \Omega \frac{d^2\beta}{d\psi\, dt} = \Omega^2 \frac{d^2\beta}{d\psi^2} = \Omega^2\bar{\beta} \qquad 3.1.1.8$$

Therefore equation 3.1.1.5 becomes M $\Omega^2\bar{\beta}$ 3.1.1.9

$$M_T = \int_{r_c}^{BR} \frac{1}{2}\rho\, U^2 c\,(r - e)\, C_l\, Cos\Phi\, dr + \int_{r_c}^{R} \frac{1}{2}\rho\, U^2 c\,(r - e)\, C_{d_0}\, Sin\Phi\, dr \qquad 3.1.1.10$$

$$\text{by defining } x = \frac{r}{R}\ ,\ \xi = \frac{e}{R}\ ,\ u = \frac{U}{\Omega R}$$

and substituting to non - dimensionalise gives

$$M_T = \frac{1}{2}\rho\, c\, \Omega^2 R^4 [\int_{x_c}^{B} u^2 (x - \xi)\, C_l\, Cos\Phi\, dx + \int_{x_c}^{\lambda} u^2 (x - \xi)\, C_{d_0}\, Sin\Phi\, dx] \qquad 3.1.1.11$$

The section non - dimensional resultant velocity u and the inflow angle Φ (see fig.3.1.2) may be found from the following equations:

$$u = \sqrt{U_P^2 + U_T^2} \qquad 3.1.1.12$$

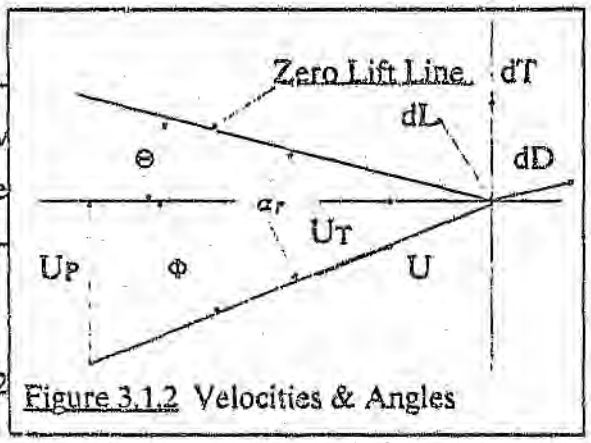

Figure 3.1.2 Velocities & Angles

$$U_P = \lambda\, Cos\beta - (x - \xi)\bar{\beta} - \mu Sin\beta\, Cos\psi + \frac{q}{\Omega} x\, Cos\psi + \frac{p}{\Omega} x\, Sin\psi \qquad 3.1.1.13$$

$$U_T = \xi + (x - \xi)\, Cos\beta + \mu\, Sin\psi \qquad 3.1.1.14$$

$$\Phi = arctan\, \frac{U_P}{U_T} \qquad 3.1.1.15$$

With section angle of attack

$$\alpha_r = \theta_0 + \theta_1 x - A_1\, Cos\psi - B_1\, Sin\psi + \Phi \qquad 3.1.1.16$$

substituting into 3.1.1.1 gives the articulated rotor flapping equation

$$\frac{1}{2}\gamma' \left[\int_{x_c}^{B} u^2 (x - \xi)\, C_l\, Cos\Phi\, dx + \int_{x_c}^{1} u^2 (x - \xi)\, C_{d_0}\, Sin\Phi\, dx\right] -$$

$$Sin\beta\, (Cos\beta + \frac{eM'W}{gI_h}) - \ddot{\beta} - \frac{M'W\, Cos\beta}{\Omega^2 I_h} = 0 \qquad 3.1.1.17$$

$$\text{where } \gamma' = \frac{\rho c R^4}{I_h}$$

3.1.2 Teetering Rotor Constraints

The differential equation of blade flapping motion for the teetering rotor system may be derived in the same way and including precone yields the following equation :

$$\frac{1}{2}\gamma' \left[\left(\int_{x_c}^{B} u^2 x\, C_l\, Cos\Phi\, dx + \int_{x_c}^{1} u^2 x\, C_{d_0}\, Sin\Phi\, dx \right)\psi -\right.$$

$$\left. \left(\int_{x_c}^{B} u^2 x\, C_l\, Cos\Phi\, dx + \int_{x_c}^{1} u^2 x\, C_{d_0}\, Sin\Phi\, dx \right)\psi + \pi \right] -$$

$$(2\, Sin\beta\, Cos\beta - 2\ddot{\beta})\psi - \beta_0 = 0 \qquad 3.1.2.1$$

where β_0 = *Precone angle*

3.2 Solution of the Blade Lagging Equations

The blade lagging equation is derived in the following manner with reference to fig 3.2.1.

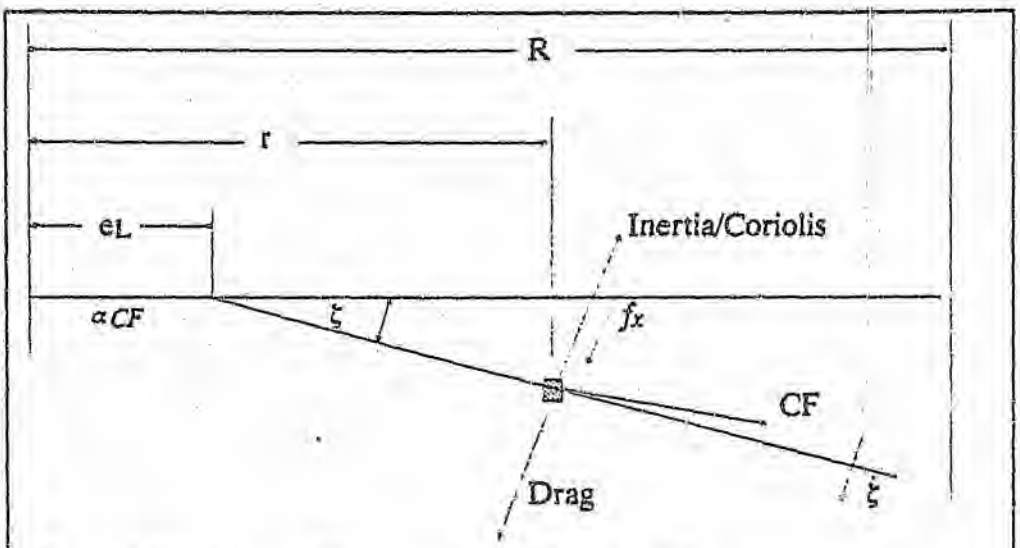

Figure 3.2.1 Source of Moments about Lagging Hinge

The inertia moment is given as

$$I_M = \int_{e_L}^{R} \frac{(r - e_L)^2 m}{Cos\zeta} \ddot{\zeta}\, dr \qquad 3.2.0.1$$

The coriolis moment is given as

$$C_M = \int_{e_L}^{R} \frac{2\,\Omega\,\dot{\beta}\,Sin\,\beta\,(r - e)\,m\,(r - e_L)}{Cos\,\zeta}\, dr \qquad 3.2.0.2$$

The drag moment is given as

$$D_M = \int_{e_L}^{R} \frac{f_x\,(r - e_L)}{Cos\,\zeta}\, dr \qquad 3.2.0.3$$

The centrifugal moment is given as

$$C_F = \int_{e_L}^{R} m\Omega^2 (r - e_L)\,\zeta\, dr \qquad 3.2.0.4$$

From fig 3.2.1, taking moments about the Lagging hinge in the clockwise direction and considering a spring and damper moment of $K_\zeta \zeta$ and $C_\zeta \dot{\zeta}$ respectively, gives a moment balance as

$$D_M - C_M - I_M - C_F - K_\zeta \zeta - C_\zeta \dot{\zeta} = 0 \qquad 3.2.0.5$$

The equations for both flapping and lagging were solved using a 4th order Runga - Kutta numerical routine.

3.3 Helicopter Inflow Models

3.3.1 Hover Inflow Model

The inflow model used for all the hover routines is the Goldstein's Modified Vortex Theory. In this theory the wake of the rotor is pictured as a rigid helicoidal surface of infinite length, but finite radius, moving parallel to its axis with a uniform velocity [ref 6]. The derivation of the equations used in the model are described in detail in the above mentioned reference, the result of which is shown as

$$v = \frac{\sigma_x C_l U}{8 x \, Tan \, \Phi \, \kappa} \qquad 3.3.1.1$$

The algorithm used to solve for the inflow numerically is listed as

- For each blade station calculate the rotor solidity given by

$$\sigma_x = \frac{B c}{\pi R x} \qquad 3.3.1.2$$

- Find blade setting angle for each element
- Assume an inflow angle
- Calculate C_l from equation 3.3.1.1 above
- Compare the calculated C_l with the aerofoil section C_l data. If the difference between the values is greater than 0.0001 the process is repeated.

3.3.2 Translational Flight Inflow Model

The translational flight inflow model is based upon the model described in [ref 6], where the inflow is expressed as a quadratic equation in λ as shown below.

$$t_1 \lambda^2 + \left(\frac{2 C_T}{a \sigma}\right) t_2 \lambda + \left(\frac{2 C_T}{a \sigma}\right)^2 t_7 + t_{22} \frac{\delta}{a} + \frac{2 C_Q}{a \sigma} = 0 \qquad 3.3.2.1$$

where the coefficients t_1, t_2, t_7 and t_{22} come from the given reference.

The non - dimensional inflow ratio is modified based on the equations given in [ref 7] and are shown below

$$K_x = \frac{4}{3}\left[(1 - 1.8\,\mu^2)\sqrt{1 + \left(\frac{\lambda}{\mu}\right)^2} - \frac{\lambda}{\mu}\right] \qquad 3.3.2.2$$

$$K_y = -2\,\mu \qquad 3.3.2.3$$

$$\text{thus } \nu = \nu_0\,(1 + K_x\, r\, Cos\,\psi + K_y\, r\, Sin\,\psi) \qquad 3.3.2.4$$

which is a first harmonic approach to translational flight inflow modelling.

3.4 Str. ctural Spanwise Blade Loading

The governing equation is derived from the following diagrams [ref 3].

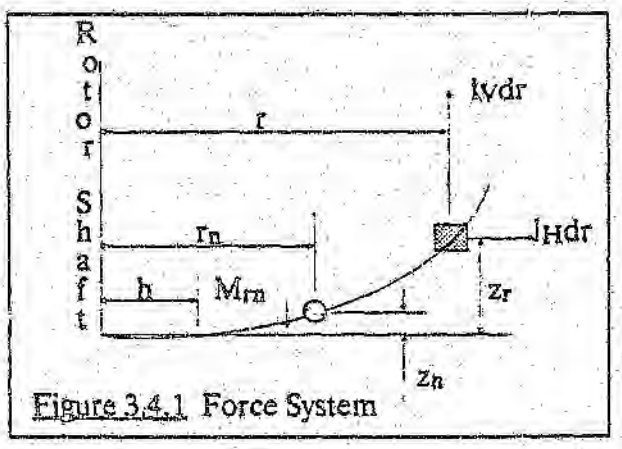

Figure 3.4.1 Force System

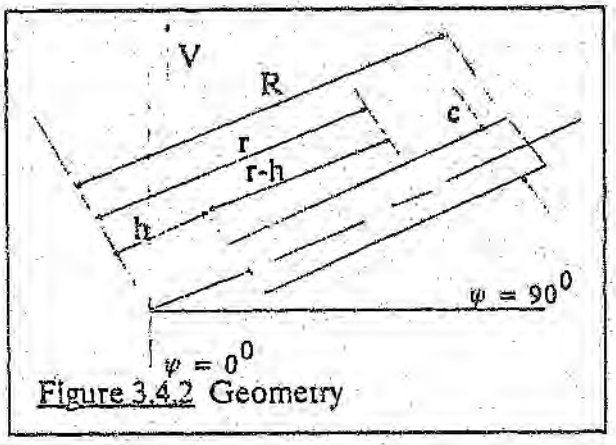

Figure 3.4.2 Geometry

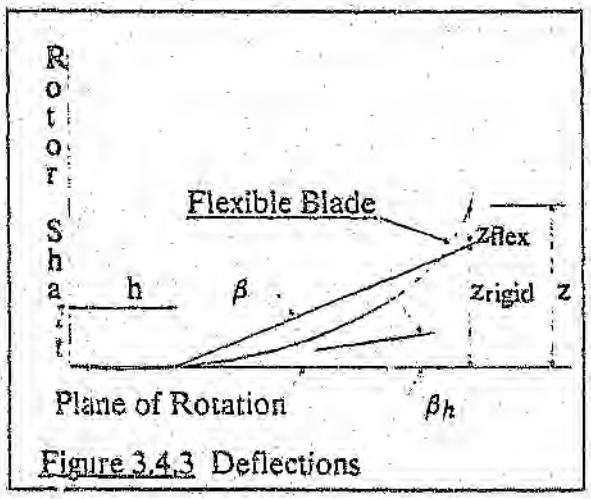

Figure 3.4.3 Deflections

The blade geometry, the forces acting on an infinitesimal element of the blade under translational flight conditions, and the resulting force system are shown in figures 3.4.1, 3.4.2 & 3.4.3. From these figures it is seen that the bending moment M_{rn} at any station r_n due to loads acting on the blade is given by

$$M_m = \int_{r_n}^{R} l_V (r - r_n)\, dr - \int_{r_n}^{R} l_H (z - z_n)\, dr \qquad 3.4.0.1$$

with reference to [ref 3] equation 3.4.0.1 can be written in matrix form as a general equation as follows

$$\left\{\begin{matrix}\{M_s\} \\ \beta_h\end{matrix}\right\} = [(1.0 + i\,g)\left[\begin{matrix}[1.0] & \{0\} \\ [0] & 0\end{matrix}\right] + \Omega^2 [F]\left[[Z_M] \mid \{r - h\}\right] -$$

$$\omega^2 [M_{zv}]\left[[Z_M] \mid \{r - h\}\right] - i\,\omega\,\Omega\,[r][A]\left[[Z_M] \mid \{r - h\}\right]]^{-1} \{M_a\} \qquad 3.4.0.2$$

$$\text{where } \{M_a\} = [r]\{L_a\}$$

with i being the complex $\sqrt{-1}$.

Equation 3.4.0.2 also applies to the hovering condition if the terms which pertain to the blade's vertical velocity and acceleration are omitted ie. $\omega = 0$ and $g = 0$.

If the blade root angle β_h is zero in equation 3.4.0.2 the result is the equation for the cantilevered blade in forward flight.

The analysis of a teetering blade considers using ev. nonic loading as applied to the cantilevered equation 3.4.0.2 and odd harmonic loadings to equation 3.4.0.2 itself.

3.5 Helicopter Rotor Blade Natural Modes

A computer code used for predicting the natural frequencies and mode shapes of helicopter rotor blades is presented in [ref 5]. The program is based on the Holzer-Myklestad approach adapted for rotating beams. The code considers fully three degree of freedom coupled blade spanwise, chordwise and torsional motion.

The equations, theory and method of solution are presented in the above reference. The code has been modified to operate on an IBM PC/AT type computer, and has been metricated to be incorporated into the environment of the aerodynamic and structural codes. The dynamic code has already been validated and this is shown in [ref 5].

DESCRIPTION OF COMPUTER CODE

4.1 Computer Program Logic

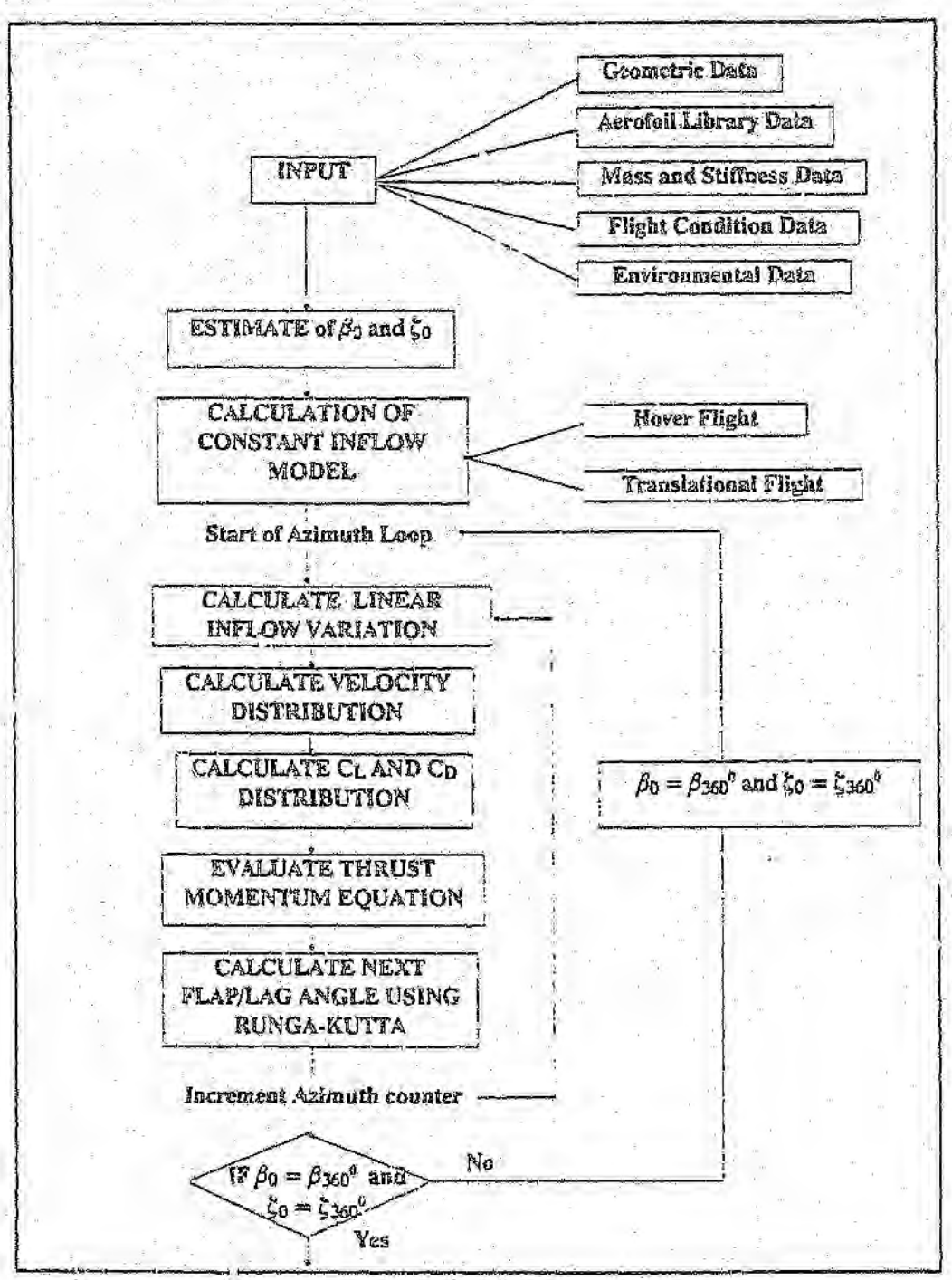

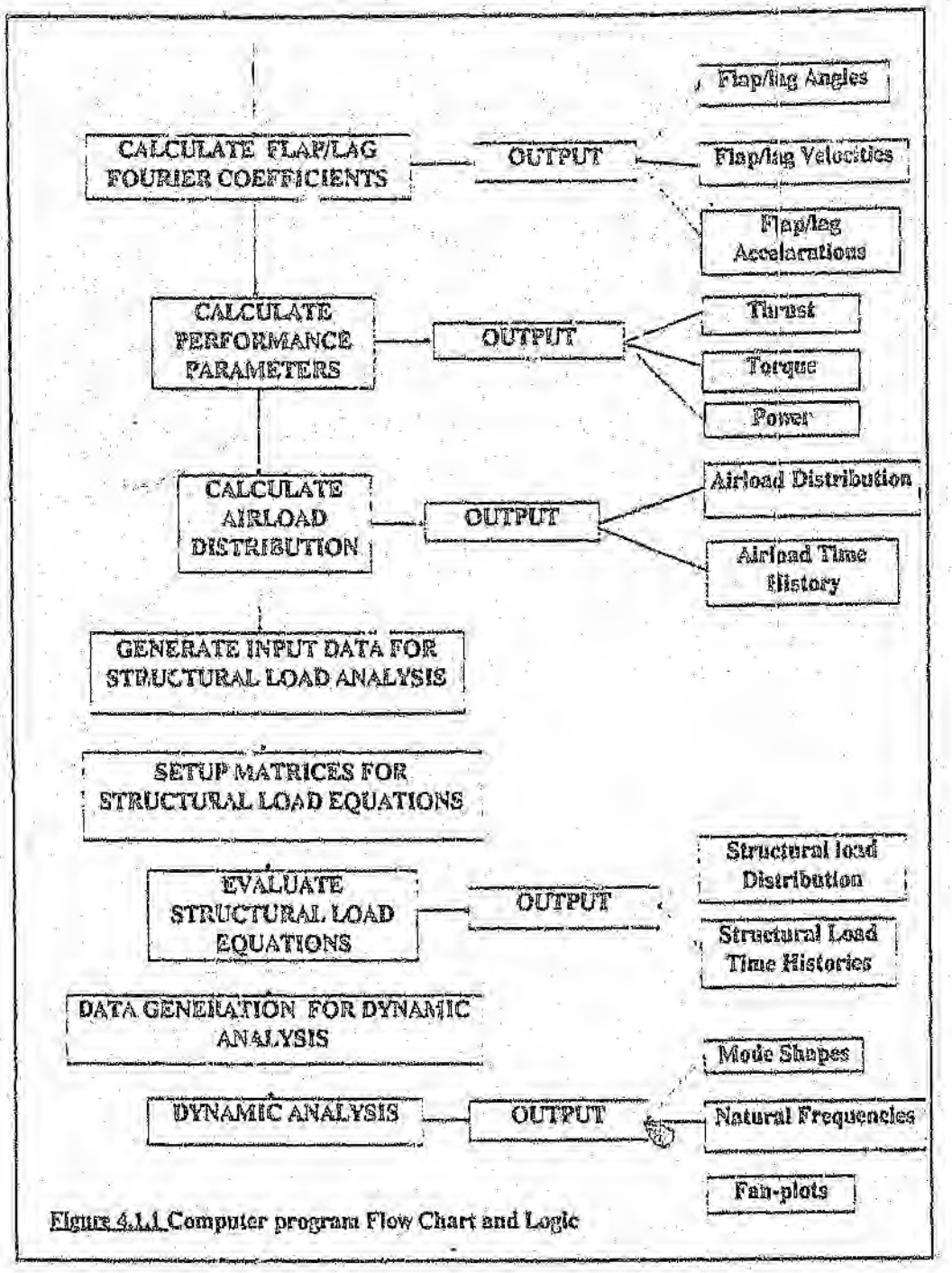

Figure 4.1.1 Computer program Flow Chart and Logic

4.2 General Program Description

4.2.1 Computer Requirements

The computer code has been written using a BASIC compiler (screen control, graphics and menu options), with MS-FORTRAN compiler for numerical method solving. All the execution codes are linked via a main menu code and must all reside on a hard disk. The core requirements for code storage is 2 MByte hard disk space with a further 4 MByte required for the program working area. The minimum requirements for realistic operating time is the IBM PC/AT 80286 processor with 80287 10/12 MHz co-processor running DOS version 3.0 or greater. A 40 MByte high speed (28 ms) hard disk and 2 MByte on board RAM are necessary. Graphical output may be acheived using Lotus 1-2-3, as all user output files are in a Lotus format. A PASCAL code to map angle of attack contours has been included which outputs a text file in HPGL format. For optimum usage all the computer codes must be resident in a configured 1.3 MByte RAM drive.

4.2.2 Program Performance

The following table represents the times for one iteration with 30 spanwise blade elements, 20 degree azimuth increments and 1,2 and 3 spanwise blade aerofoil profiles, respectively. This does not represent the most timeous case which is upto 10 aerofoil profiles for 30 spanwise blade elements and 10 degree azimuth increments.

Table 4.2.2.1 Program Time Performance

No of Profiles	No of Elements	Azimuth Increment	Time per Iteration (s)
1	30	20	105
2	30	20	113
3	30	20	124

These times were obtained with the configuration as described in section 4.2.1 above. The same operations performed on a 80386 DX processor and 80387 20 MHz co-processor yielded times approximately half those stated in the above table. The output presented in the validation section of this report used three aerofoil profiles with the corresponding time of 124 seconds per iteration. This represented a total time for all performance calculations of 3 hours.

4.2.3 Program Operation and Description

Figure 4.1.1 represents the logical flow of the program. Each subroutine represented in the flow chart is described below.

The main program controls the execution of each module, namely, the aerodynamic module, the structural module and the dynamic module for each rotor type root constraint. The aerodynamic module is first called, this module contains the data input as well as the aerodynamic analysis.

The input section of the program is subdivided into:

Geometric data — which consists of number of blades, blade radius, root cut-out radius, blade twist, blade chord, flap hinge offset, flap hinge spring, lag hinge offset, lag hinge spring and damper, pitch-flap coupling, blade weight moment and blade inertia.

Aerofoil Library data

which consists of section aerofoil lift and drag data (upto 10 mach numbers and 40 angles of attack), average drag coefficient and lift curve slope, aerofoil spanwise change selection (upto 10 different aerofoil profiles may be considered).

Mass & Stiffness Data — consists of blade element mass distribution and blade element stiffness distribution (EI_x, EI_y and torsional stiffness GJ).

Flight condition Data — consists of lateral and longitudinal cyclic coefficients, root collective pitch setting, rotor angular velocity, forward speed of helicopter, all-up weight, pitch and roll velocity and helicopter climb velocity.

Environmental Data — consists of air density and local air temperature.

An example of the input deck is shown in the validation section [section 5].

After all the input data has been retrieved and the rotor disk mesh has been defined (ie. number of blade elements and azimuth increments selected), the program requests an estimate of the blade flapping/lagging angles and velocities to start the solution of the differential equations. Depending on the flight condition chosen, either the hover or translational flight inflow model will be selected. If, however, the flight condition falls within the transition region, $\mu = 0.03$ and $\mu = 0.175$, the program execution will be halted as the inflow model does not cater for this flight regime. The hover inflow model is an iterative procedure following the algorithm in section 3.3.1. The velocity distribution along the blade span is then calculated using equation 3.1.1.12 through 3.1.1.15. The mach numbers for the blade elements are then calculated by dividing the total velocity (equation 3.1.1.12) by the local speed of sound in air. The section angle of attack is then calculated using equation 3.1.1.16. The local C_l and C_d values are then obtained from the aerofoil library data using the mach number and angle of attack along with two dimensional linear interpolation.

The thrust momentum equations (equations 3.1.1.17 or 3.1.2.1) are then evaluated at the current azimuth position. The integrals in these equations are solved using Simpson's numerical integration techniques. For this integration tech-

nique to be used there must be an even number of blade elements. A 4th order Runga-Kutta numerical technique is then used to solve the thrust momentum equation in order to obtain values of the flapping angle and velocity at the next azimuth position. This procedure is repeated around the entire rotor disk. The initial flap angle and velocity is then compared to the calculated flap angle and velocity at the zero azimuth. If the two values are equal (within a tolerance of 0.0001) then the calculated values from the thrust momentum equations are considered to be correct, else the procedure is repeated until a solution is found. In general, the method is stable for any size step increment (ie. from 2 to 30 elements, 10 to 20 degree azimuth steps) and converges to a solution within 5 iterations.

From the solution of the thrust momentum equations a full map of the rotor disk aerodynamic environment is generated. This includes spanwise lift curves and shear force, bending moment, centrifugal load maps, mach number map, Cl and Cd maps, angle of attack map (this map needs to be converted to a contour map format for meaningful understanding using the PASCAL code described in section 4.2.1), velocity distribution map and flapping angle (including flapping fourier coefficients), velocity and acceleration map. All this information is Lotus compatible and can be viewed and/or plotted using Lotus.

This information is then processed into a format acceptable to the structural module of the program. Upon entering the structural program the matrices needed to evaluate equation 3.4.0.2 are generated. Sectors of the azimuth may then be evaluated for structural bending load analysis (the user can define the start and end azimuth positions over which the analysis is to be performed). The processing time for this analysis is approximately 2.5 minutes and the output is in the form of structural load spanwise distributions and loading time histories.

The dynamic analysis requires additional input in the chordwise and torsional degrees of freedom. This is a stand alone program that has been integrated into the environment of the aerodynamic and structural modules with the controlling program acting as a pre-processor.

4.2.4 Description of Program Output

This program provides a large spectrum of output which may be displayed in any format required by the user. This includes tabulated data as well as graphical representations. The examples of the program output below are of a graphical form only and were derived using the PUMA SA330 J at its full speed rating, in level flight, with an all up weight of 8200kg at ISO sea level. Figure 4.2.4.1 shows the aforementioned helicopter rotor flapping motion. The figure shows the flapping angles which are direct outputs from the thrust momentum integral equation. From this third harmonic fourier coefficients are displayed as screen output after every convergent iteration. The third harmonic was chosen as an error of 0.1% was evaluated between the actual solution and the 3rd harmonic fourier series. It must be noted that the program uses upto the 8th harmonic for the structural load calculations. This was done because larger errors arise if only low order fourier harmonics are used for the aerodynamic loading [ref 11]. Transient blade flapping motion may be viewed in graphical form while the program is running.

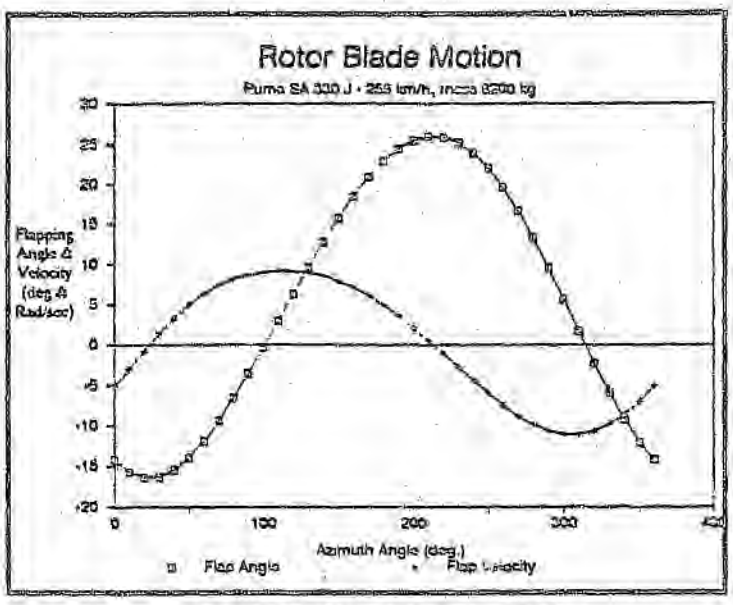

Figure 4.2.4.1 Blade Flapping Motion

The performance at any specific flight condition is output to screen and either a file or printer. It is in a tabular form as shown in figure 4.2.4.2. The performance contains the thrust, power and torque generated by the rotor system. The power and torque are indicated as negative values showing that the rotor is absorbing this power. In order to generate performance curves (eg. power vs. forward

speed), the program must be run with multiple flight conditions, and the data from these tables collected as shown in the validation (section 5).

AERODYNAMICS FOR ARTICULATED ROTOR SYSTEM

ROTOR PERFORMANCE

THE OVERALL ROTOR PERFORMANCE IS CALCULATED AS:

ROTOR THRUST =	82654.90 N
HELICOPTER SHAFT ANGLE =	+ 13.79 deg
ROTOR LIFT =	+ 80270.963 N
HELICOPTER WEIGHT =	80442.000 N
ROTOR TORQUE =	-44106.37 Nm
ROTOR INDUCED AND PROFILE POWER =	-1223.98 kW

(Figures are for the rotor system only)

Figure 4.2.4.2 Performance Output Data

The airload distribution is represented in figure 4.2.4.3. The program calculates the airload distribution for every azimuth position but the example only shows 4 azimuth positions. The figure clearly shows where blade spanwise aerofoil profile changes occur, namely at 5.215 and 6.786 m. Depending upon the number of spanwise blade elements chosen for the calculations, airload time histories may be plotted for each blade element. The time history for loads close to the root of the blade are shown in figure 4.2.4.4.

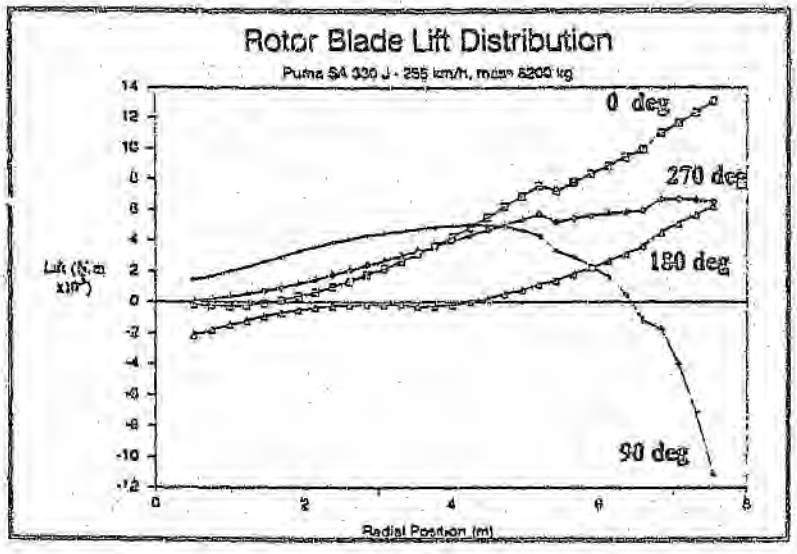

Figure 4.2.4.3 Blade Spanwise Airload Distribution

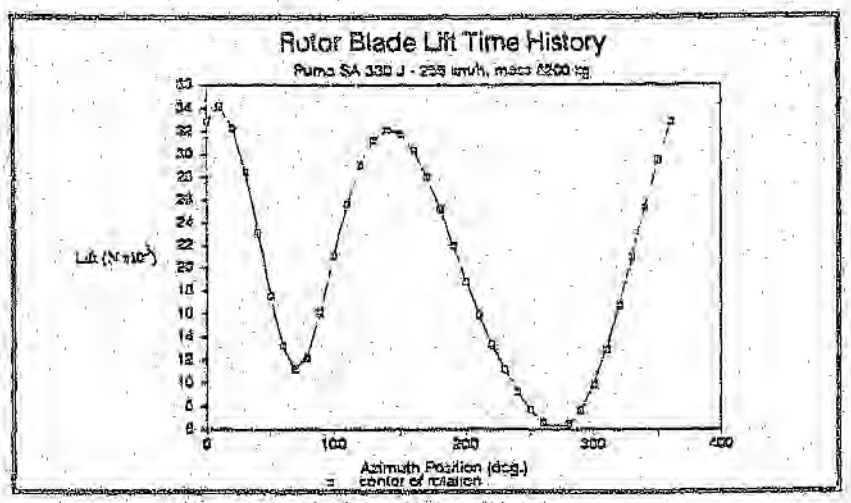

Figure 4.2.4.4 Airload Time History

Additional output that can be obtained from the aerodynamic module for a specific flight condition are angle of attack contour maps, C_l, C_d and mach number maps. The example in figure 4.2.4.5 is an angle of attack contour plot, the other maps are not shown. Contours may be user defined to any desired integer step, the plot shown in the example has a one degree step from -2^0 to $+14^0$ angle of attack. The lines are not automatically plotted between the points, but have to be manually inserted by hand. The ouput plot file is in HPGL format and can be plotted and scaled for any plotter capable of accepting this format. This plot is a useful design tool, as the designer can see the effects of various blade aerofoil spanwise sections and the

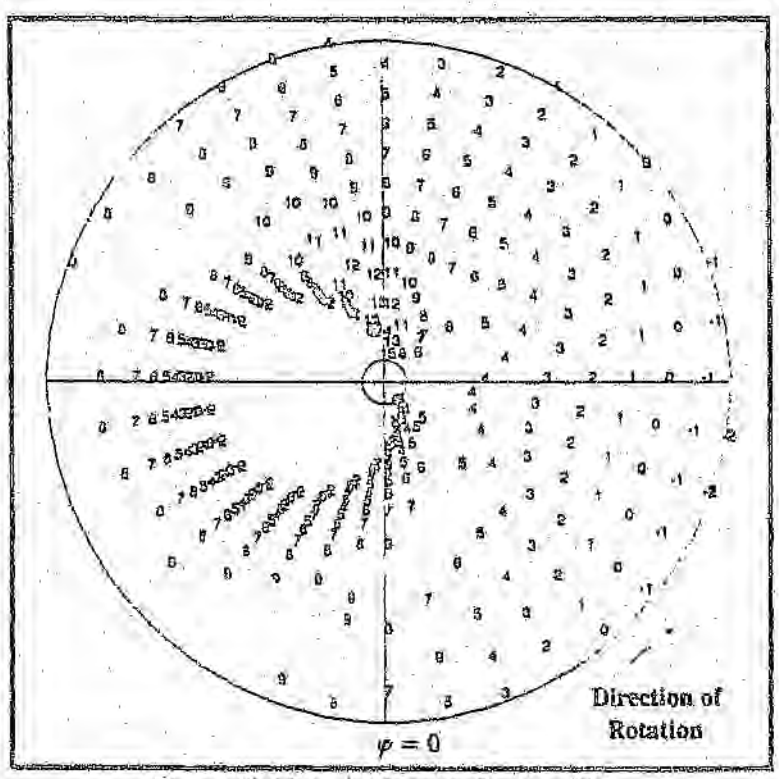

Figure 4.2.4.5 Angle of attack Contour Plot

effects of blade twist. This type of plot has not been successfully measured to date [ref 22], thus this ouput has not been validated.

The structural module of the program ouputs two data files namely, a structural load spanwise bending moment distribution and a structural load time history for every blade station. This module only processes with 30 spanwise blade elements, but will accomodate either 10^0 or 20^0 azimuth increments from the aerodynamic module. Figure 4.2.4.6 shows the bending moment spanwise distribution for the 0, 90, 180 and 270 degree azimuth positions. All azimuth positions have been calculated but the above mentioned ones have been displayed in this example. The mass and stiffness distributions used in this example are not realistic as they were unavailable for the Puma SA330 J. The structural bending mo-

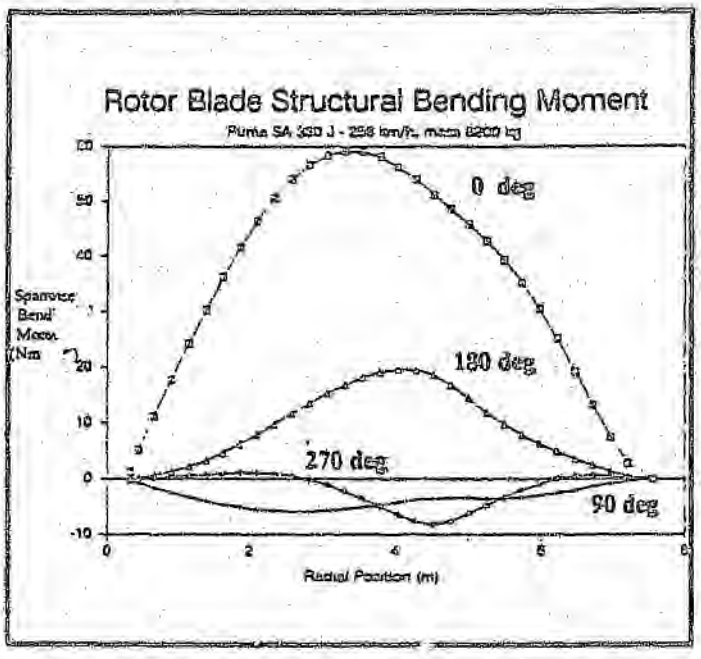

Figure 4.2.4.6 Structural Bending Moment Distribution

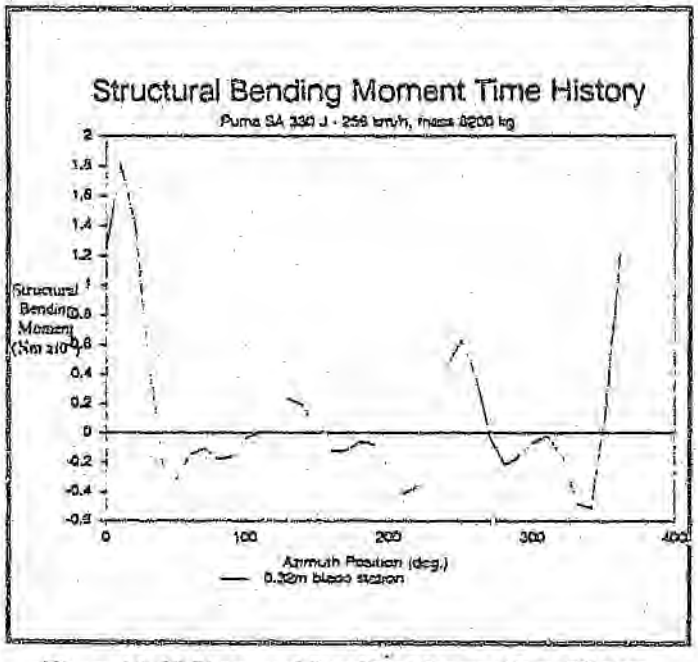

Figure 4.2.4.7 Structural Bending Moment Time History

ment data is arranged in a format such that time histories for each blade station may be graphically represented. An example of this is shown in figure 4.2.4.7.

The ouput from the dynamic code is the same as in reference 5. Examples of mode shapes and fan plots taken from this reference are shown below. The example of the Puma SA330 J could not be dynamically analysed as the information needed was unavailable.

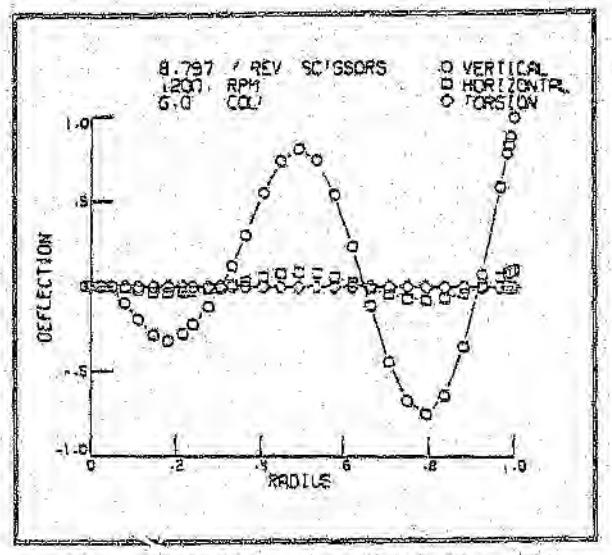

Figure 4.2.4.8 Illustration of Mode Shape Plot

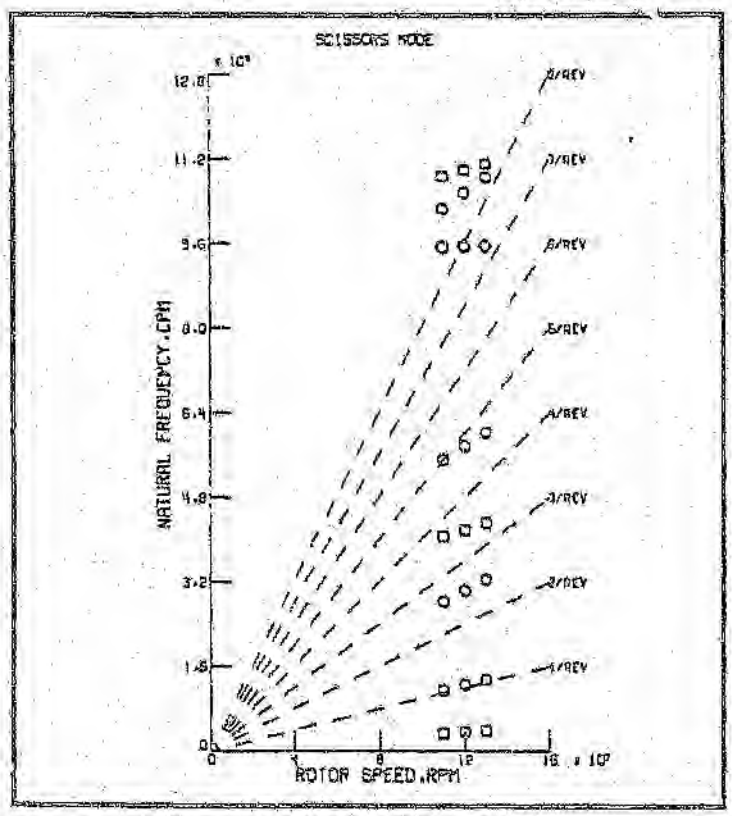

Figure 4.2.4.9 Illustration of Fan Plot

PROGRAM VALIDATION

5.1 Input Data Deck

The data used for the validation is for the Aerospatiale PUMA SA330 J helicopter. No structural blade data was available for the validation of the structural module, however the method used has been validated in reference 3.

5.1.1 Geometric Data

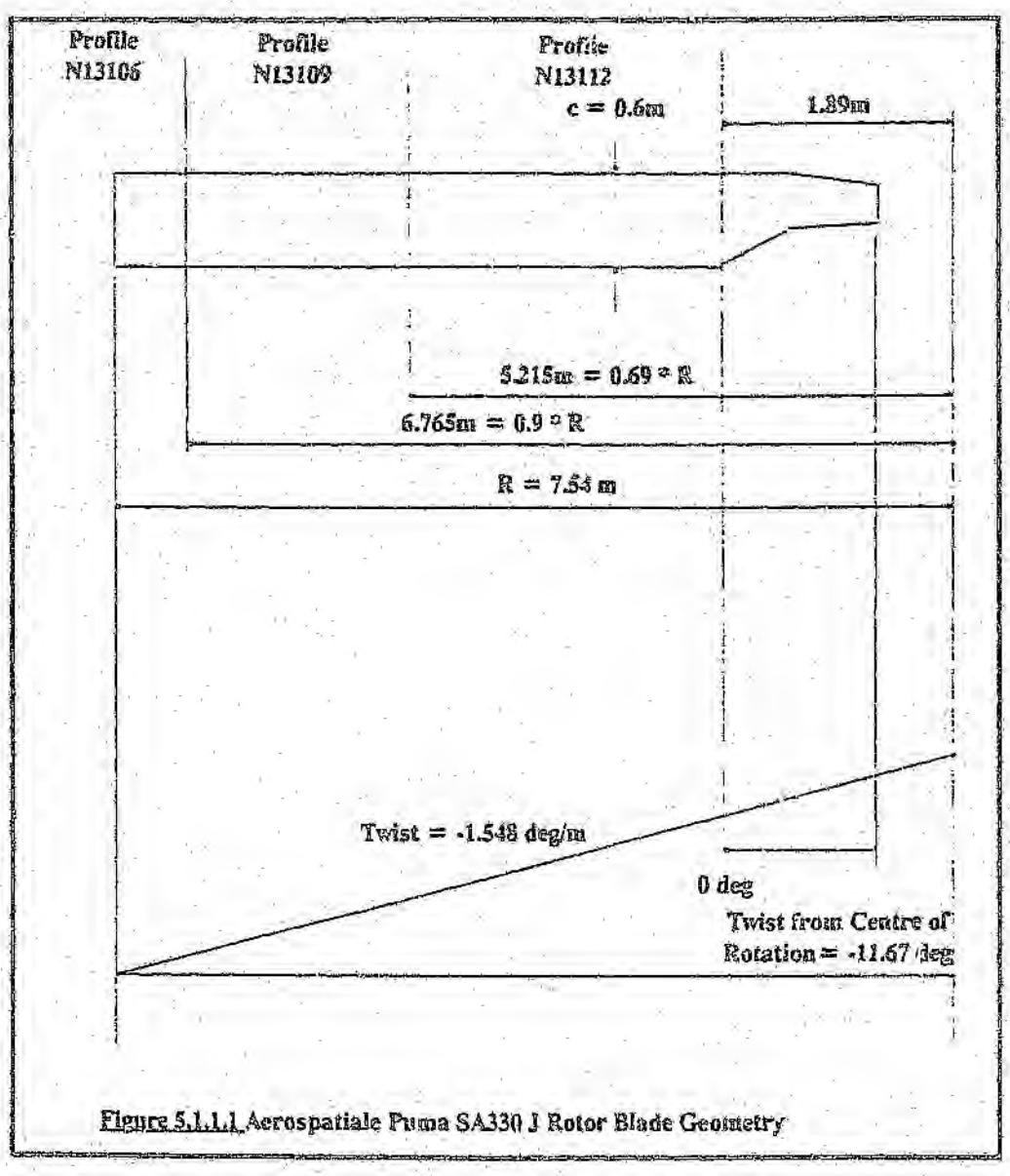

Figure 5.1.1.1 Aerospatiale Puma SA330 J Rotor Blade Geometry

Number of Blades	4
Blade Radius	7.54 meters
Root Cut-out Radius to Cuff	0.79 meters
Blade Chord	0.6 meters
Blade Twist from COR	-11.67 deg
Flap Hinge Offset	0.29 meters
Total Blade Mass	82.7 kg
Static Blade Weight Moment	277 kg m
Blade Mass Moment of Inertia	1321 kg m^2

Table 5.1.1.1 Aerospatiale Puma SA330 J Geometric Data

5.1.2 Aerofoil Library Data

The blades have three aerofoil section changes along their span as shown in figure 5.1.1.1. The two dimensional aerofoil section data for these profiles are shown in appendix B.

5.1.3 Mass and Stiffness Data

The blade total mass is shown in table 5.1.1.1, but the mass distribution data as well as stiffness data were unavailable, and are not needed for the validation (when validating the performance characteristics) of the aerodynamic module.

5.1.4 Flight Condition Data

Lateral Cyclic Coefficient	0 deg
Longitudinal Cyclic Coefficient	0 deg
Collective Pitch at blade cuff	14.9 .. 17.3 deg
Rotor Angular Velocity	265 rpm
Helicopter All-up Mass	6000 .. 9000 kg

Table 5.1.4.1 Hover Flight Conditions

Lateral Cyclic Coefficient	[illegible]
Longitudinal Cyclic Coefficient	[illegible]
Collective Pitch at blade cuff	14.0 .. 17.[illegible]
Rotor Angular Velocity	265 rpm
Helicopter All-up Mass	8200 kg
Forward Speed	0 .. 20, 111 .. 256 km/hr
Input Torque Setting	19000 .. 39000 Nm

Table 5.1.4.2 Translational Flight Conditions

5.1.5 Environmental Data

Local Air Density	1.2256 kg/m^3
Local Air Temperature	15 deg °C

Table 5.1.5.1 ISO Sea Level Environment Conditions

5.2 Aerodynamic Module Validation

The program output for the Puma SA330 J is compared to flight test data from tests performed in South Africa. The flight tests were performed in August of 1988 and are referenced as flight 135 (translational flight test) and flight 142 (hover flight test) as a clean aircraft flying out of ground effect. The information obtained from these flight tests is performance data only. Thus the validation to date only includes the performance prediction.

5.2.1 Hover Performance

The variation of collective pitch angle at the rotor blade cuff and helicopter all up mass, together with the variation of main rotor torque and helicopter all up mass is presented for performance validation in hover. The pitching axis system used in the computer code considers pitch changes about the center of rotation in the shaft axis system as shown in equation 3.1.1.16. Collective angles measured in the flight test data were measured at the blade cuff thus resolving all collective pitch changes about the cuff requires subtracting 1.2 degrees from the program output. The results are shown in figure 5.2.1.1 and figure 5.2.1.2 (Tables are shown in appendix C).

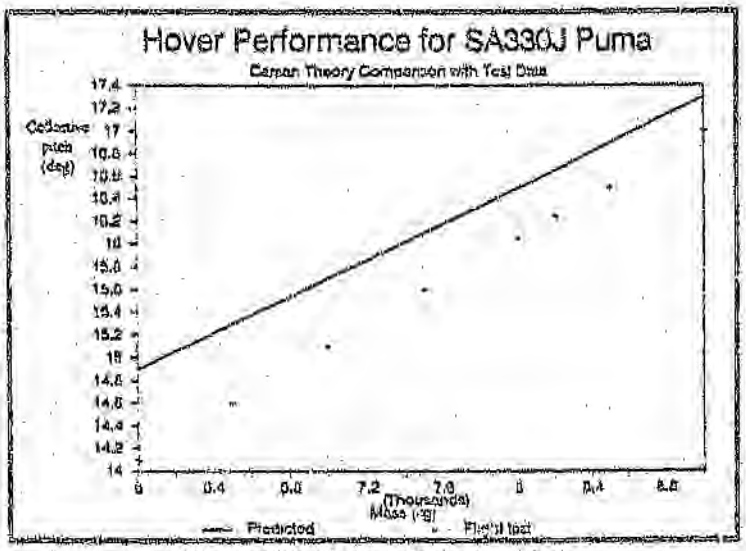

Figure 5.2.1.1 Hover Collective Pitch

The rotor torque prediction in figure 5.2.1.2 falls within the scatter of the flight test data and is thus difficult to calculate an error of prediction. The collective prediction, however, yields errors of between 1.76% (at 9000 kg AUM) and

5.67% (at 6000 kg AUM) representing an over prediction. These errors are attributable to the inflow model, which uses average drag coefficients and a constant lift curve slope for hover inflow convergence.

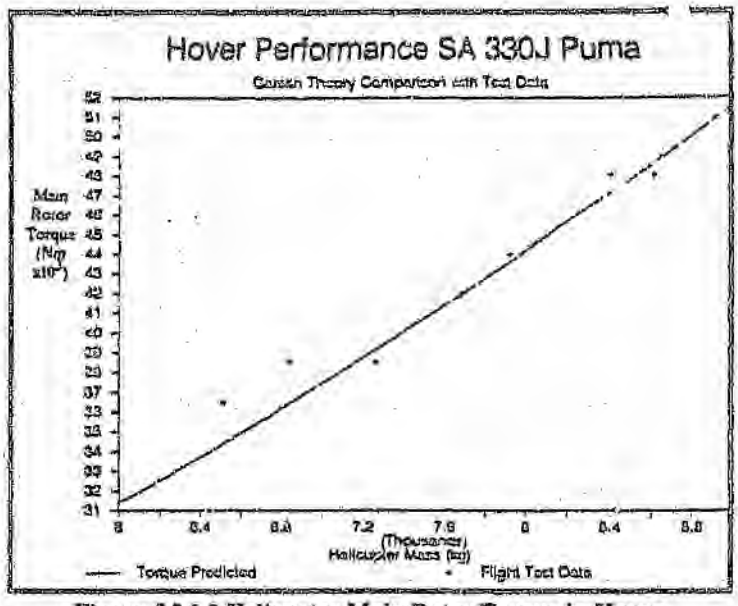

Figure 5.2.1.2 Helicopter Main Rotor Torque in Hover

5.2.2 Translational Flight

The results of the comparison between the predicted performance and the flight test performance are shown in figure 5.2.2.1 and figure 5.2.2.2 (Tables shown in appendix C). The torque prediction in figure 5.2.2.2, as in the case of hover, is difficult to evaluate. The inflow model used is only valid from $\mu = 0.175$ to $\mu = 0.5$, this was the case when trying to evaluate flight conditions below 130 km/h ($\mu = 0.173$) where convergence could not be obtained. The collective angle with forward speed yielded errors of between 7.93% (at 230 km/h) and 13.61% (at 189 km/h)

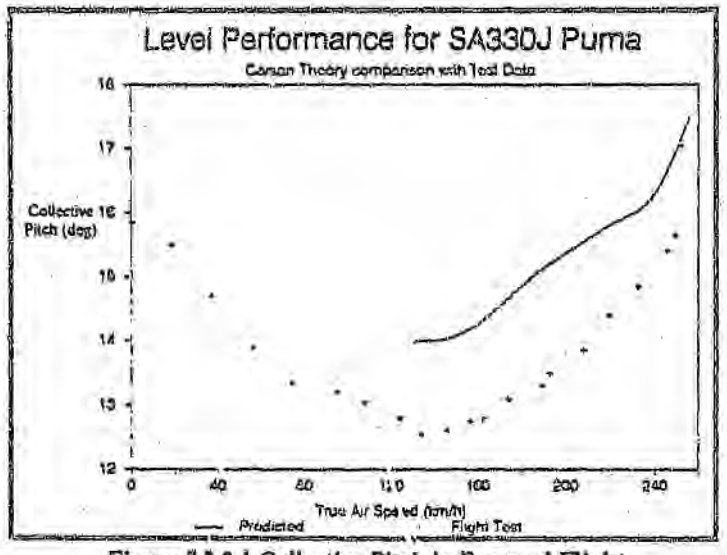

Figure 5.2.2.1 Collective Pitch in Forward Flight

representing an over prediction. These errors are also attributable to the linear inflow model and that the rotor also lags in flight. The lagging could be modelled using the coupled flap-lag module of the aerodynamic code, however, lag damping information was unavailable.

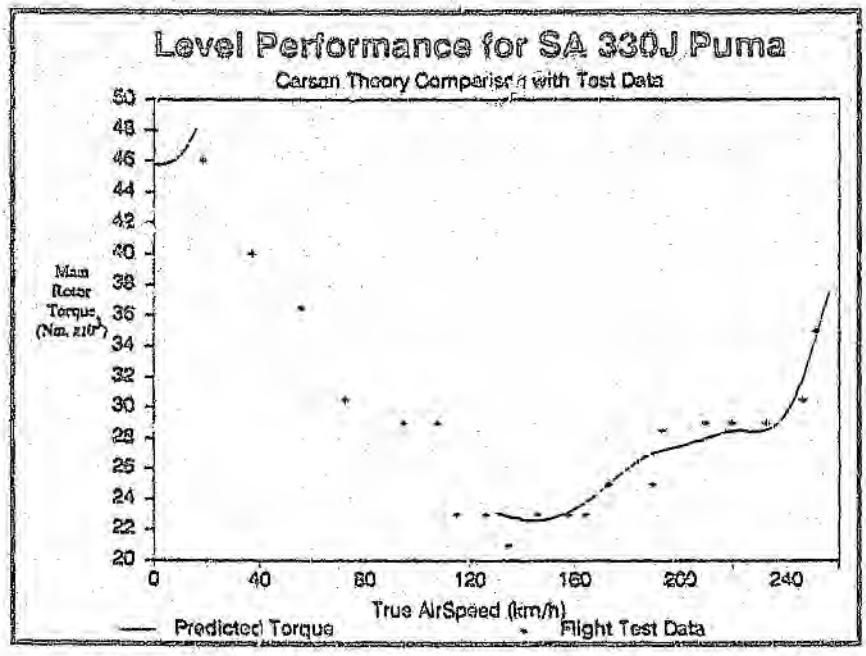

Figure 5.2.2.2 Helicopter Main Rotor Torque for Forward Flight

CONCLUSIONS

A computer code has been developed to analyse single rotor systems for helicopters in both hover and translational flight. The code is suitable for running on IBM PC/AT type computers. The code is general in that teetering, articulated and cantilevered rotor hubs may be considered. Many restrictive assumptions normally associated with analytical blade element theory have been neglected. Reasonable accuracy was obtained in control angle performance calculations, while main rotor torque predictions for the Aerospatiale SA330 J Puma yielded results that fell within the flight test data scatter.

The program operating time was found to be adequate for calculating all performance data normally associated with the design of helicopter rotor systems.

REFERENCES

1 Gessow, Alfred, *Equations and Procedures for Numerically Calculating the Aerodynamic Characteristics of Lifting Rotors*, NACA TN 3747.

2 Gessow, Alfred.,Crim, Almer D., *A Method For Studying the Transient Blade Flapping Behavior of Lifting Rotors at Extreme Operating Conditions*, NACA TN 3366.

3 Mayo, Alton P., *Matrix Method for Obtaining Spanwise Moments and Deflections of Torsionally Rigid Rotor Blades with Arbitrary Loadings*, NACA TN 4304, August 1958.

4 Mayo, Alton P., *Comparison of Measured Flapwise Structural Bending Moments on a Teetering Rotor Blade with Results Calculated from the Measured Pressure Distribution*, NASA MEMO 2-28-59L, March 1959.

5 Weller, William H., Mineck, Raymond E., *An Improved Computational Procudure for Determining Helicopter Rotor Blade Natural Modes*, NASA TM 78670, August 1978.

6 Nikolsky, Alexander A., *Helicopter Analysis*, John Wiley & Sons Inc., New York, 1951.

7 Johnson, Wayne, *Helicopter Theory*, Princeton University Press, 1980.

8 Stepniewski, W.Z., *Rotary - Wing Aerodynamics*, Dover Publications Inc, New York, 1984.

9 Saunders, George H., *Dynamics of Helicopter Flight*, John Wiley & Sons Inc, New York, 1975.

10 Abbott, Ira H., Von Doenhoff, Albert E., *Theory of Wing Sections*, Dover Publications Inc, New York, 1959.

11 Mil' et al, M.L., *Helicopters Calculation and Design*, Mashinostroyeniye Publishing House, Moscow, 1966, NASA TT F-494, September, 1967.

12 Tanner, Watson H., *Charts for Estimating Rotary Wing Performance in Hover and at High Forward Speeds*, NASA CR-114, November 1964.

13 Kawakami, Norimichi, *Dynamics of an Elastic SeeSaw Rotor*, Journal of Aircraft, Vol. 14, No. 3, March 1977.

14 Bailey, F.J., *A Simplified Theoretical Method of Determining the Characteristics of a Lifting Rotor in Forward Flight*, NACA Report No. 716, March 1941.

15 Blankenship, B.L., Harvey, K.W., *A Digital Analysis for Helicopter Performance and Rotor Blade Bending Moments*, Bell Helicopter Company.

16 Wheatly, John B., *An Aerodynamic Analysis of the Autogiro Rotor with a Comparison between Calculated and Experimental Results*, NACA Report No. 487, 1934.

17 Jacobs, Eastman N., Sherman, Albert, *Airfoil Section Characteristics as Affected by Variations of the Reynolds Number*, NACA Report No. 586, 1937.

18 Ludi, LeRoy H., *Flight Investigation of effects of Retreating-Blade Stall on the Bending and Torsional Moments Encountered by a Helicopter Rotor Blade*, NACA TN 4254, May 1958.

19 Heyson, Harry H., *A Note on the Mean Value of Induced Velocity for a Helicopter Rotor*, NASA TN D-240, May 1960.

20 Jewel, Joseph W.,*Charts of the Induced Velocities Near a Lifting Rotor*, NASA MEMO 4-15-59L, May 1959.

21 McCloud III, John L., McCullough, George B., *Wind-Tunnel Tests of a Full-Scale Helicopter Rotor with Symmetrical and with Cambered Blade Sections at Advance Ratios from 0.3 to 0.4*, NACA TN 4367, September 1958.

22 Prouty, R.W., *Helicopter Aerodynamics*, Rotor & Wing International, 1987.

APPENDIX B

Estimation of Section Properties

Blade Properties

Density:		
Glass	2560	kg/m^3
Carbon	1500	kg/m^3
Honeycell	50	kg/m^3
Steel	7600	kg/m^3

Station number	Blade station (mm)	steel (mm^2)	steel (mm^2)	Area carbon (mm^2)	section (mm^2)	Mass (g)
0	0	990	0	0	990	180.58
1	24	990	0	0	990	180.58
2	48	0	0	67.5	67.5	2.43
3	72	0	0	67.5	67.5	2.43
4	96	0	0	67.5	67.5	2.43
5	120	0	0	67.5	67.5	2.43
6	144	0	0	67.5	67.5	58.93
7	168	0	100.89	113.54	763.58	66.33
8	192	0	100.89	113.54	763.58	9.93
9	216	0	100.89	113.54	763.58	9.93
10	240	0	100.89	46.04	763.58	7.48
11	264	0	100.89	46.04	763.58	7.48
12	288	0	100.89	46.04	763.58	7.48
13	312	0	100.89	46.04	763.58	7.48
14	336	0	100.89	46.04	763.58	7.48
15	360	0	100.89	46.04	763.58	7.48
16	384	0	100.89	46.04	763.58	7.48
17	408	0	100.89	46.04	763.58	7.48
18	432	0	100.89	46.04	763.58	7.48
19	456	0	100.89	46.04	763.58	7.48
20	480	0	100.89	46.04	763.58	7.48
21	504	0	100.89	46.04	763.58	7.48
22	528	0	100.89	46.04	763.58	7.48
23	552	0	100.89	46.04	763.58	7.48
24	576	0	100.89	46.04	763.58	7.48
25	600	0	100.89	46.04	763.58	7.48
26	624	0	100.89	46.04	763.58	7.48
27	648	0	100.89	46.04	763.58	7.48
28	672	0	100.89	46.04	763.58	7.48
29	696	0	100.89	46.04	763.58	7.48
30	720	0	100.89	46.04	763.58	7.48
					Total =	672.73

Elo[illegible]	Inertia Moments			Apparent Material Constants		
Station (mm)	Ixx (mm^4)	Iyy (mm^4)	J (mm^4)	Exx (Gpa)	Eyy (Gpa)	Pxy (Gpa)
0	59000	[illegible]	[illegible]	200	200	[illegible]
24	59000	252000	3.1000	200	200	80
48	28.48	5062.5	5090.98	102.95	34.45	4.5
72	28.48	5062.5	5090.98	102.95	34.45	4.5
96	28.48	5062.5	5090.98	102.95	34.45	4.5
120	28.48	5062.5	5090.98	102.95	34.45	4.5
144	28.48	5062.5	5090.98	102.95	34.45	4.5
168	1850	80100	81950	61.78	21.32	5.52
192	1850	80100	81950	61.78	21.32	5.52
216	1850	80100	81950	61.78	21.32	5.52
240	2130	71700	73830	40.21	16.61	8.59
264	2130	71700	73830	40.21	16.61	8.59
288	2590	72000	74590	40.21	16.61	8.59
312	2590	72000	74590	40.21	16.61	8.59
336	2590	72000	74590	40.21	16.61	8.59
360	2590	72000	74590	40.21	16.61	8.59
384	2590	72000	74590	40.21	16.61	8.59
408	2590	72000	74590	40.21	16.61	8.59
432	2590	72000	74590	40.21	16.61	8.59
456	2590	72000	74590	40.21	16.61	8.59
480	2590	72000	74590	40.21	16.61	8.59
504	2590	72000	74590	40.21	16.61	8.59
528	2590	72000	74590	40.21	16.61	8.59
552	2590	72000	74590	40.21	16.61	8.59
576	2590	72000	74590	40.21	16.61	8.59
600	2590	72000	74590	40.21	16.61	8.59
624	2590	72000	74590	40.21	16.61	8.59
648	2590	72000	74590	40.21	16.61	8.59
672	2590	72000	74590	40.21	16.61	8.59
696	2590	72000	74590	40.21	16.61	8.59
720	2590	72000	74590	40.21	16.61	8.59

Blade Stiffness

Station (mm)	EIx (Nm^2)	EIy (Nm^2)	GJ (Nm^2)
0.00	11800.00	50400.00	24820.00
24.00	11800.00	50400.00	24820.00
48.00	2.93	174.40	22.91
72.00	2.93	174.40	22.91
96.00	2.93	174.40	22.91
120.00	2.93	174.40	22.91
144.00	2.93	174.40	22.91
168.00	114.29	1707.73	452.36
192.00	114.29	1707.73	452.36
216.00	114.29	1707.73	452.36
240.00	85.65	1190.94	634.20
264.00	85.65	1190.94	634.20
288.00	104.14	1195.92	640.73
312.00	104.14	1195.92	640.73
336.00	104.14	1195.92	640.73
360.00	104.14	1195.92	640.73
384.00	104.14	1195.92	640.73
408.00	104.14	1195.92	640.73
432.00	104.14	1195.92	640.73
456.00	104.14	1195.92	640.73
480.00	104.14	1195.92	640.73
504.00	104.14	1195.92	640.73
528.00	104.14	1195.92	640.73
552.00	104.14	1195.92	640.73
576.00	104.14	1195.92	640.73
600.00	104.14	1195.92	640.73
624.00	104.14	1195.92	640.73
648.00	104.14	1195.92	640.73
672.00	104.14	1195.92	640.73
696.00	104.14	1195.92	640.73
720.00	104.14	1195.92	640.73

APPENDIX C

Flight Conditions

Hover Hrad

AERODYNAMICS FOR A TEETERING LIFTING ROTOR SYSTEM

FLIGHT INPUT DATA

NUMBER OF ROTOR BLADES =	2
ROTOR BLADE RADIUS =	0.720 m
ROOT CUT OUT RADIUS =	0.000 m
ROTOR BLADE TWIST BETWEEN ROOT AND TIP =	+0.000 deg
ROTOR BLADE CORD =	0.090 m
CYCLIC LATERAL PITCH COEFFICIENT =	+0.000 deg
CYCLIC LONGITUDINAL PITCH COEFFICIENT =	+0.000 deg
ANGULAR ROTOR BLADE SPEED =	2000.00 rpm
HELICOPTER FORWARD SPEED =	0.000 kph
DENSITY OF AIR =	1.20000 kg/m3
HELICOPTER ALL UP WEIGHT =	35.000 kg
ROTOR TORQUE =	6.000 Nm
HELICOPTER PITCHING VELOCITY =	0.000 deg/s
HELICOPTER ROLLING VELOCITY =	0.000 deg/s
ROOT COLLECTIVE PITCH =	10.500 deg
NUMBER OF BLADE ELEMENTS (even number) =	30
AZIMUTH INCREMENT =	20 deg
ROTOR BLADE PRECONE ANGLE =	3.000 deg
MASS MOMENT OF INERTIA ABOUT TEETERING HINGE =	0.095 kg m
ATMOSPHERIC TEMPERATURE =	+15.000 deg C
AEROFOIL LIFT CURVE SLOPE =	6.000 /rad
AEROFOIL AVERAGE DRAG COEFFICIENT =	0.0120

MASS OF ROTOR HUB =	0.3120 kg
BLADE ELEMENT MASS LUMPED AT STATION 0 =	0.0220 kg
BLADE ELEMENT MASS LUMPED AT STATION 1 =	0.0230 kg
BLADE ELEMENT MASS LUMPED AT STATION 2 =	0.0025 kg
BLADE ELEMENT MASS LUMPED AT STATION 3 =	0.0025 kg
BLADE ELEMENT MASS LUMPED AT STATION 4 =	0.0025 kg
BLADE ELEMENT MASS LUMPED AT STATION 5 =	0.0025 kg
BLADE ELEMENT MASS LUMPED AT STATION 6 =	0.0585 kg
BLADE ELEMENT MASS LUMPED AT STATION 7 =	0.0554 kg
BLADE ELEMENT MASS LUMPED AT STATION 8 =	.0094 kg
BLADE ELEMENT MASS LUMPED AT STATION 9 =	0.0094 kg
BLADE ELEMENT MASS LUMPED AT STATION 10 =	0.0076 kg
BLADE ELEMENT MASS LUMPED AT STATION 11 =	0.0076 kg
BLADE ELEMENT MASS LUMPED AT STATION 12 =	0.0076 kg
BLADE ELEMENT MASS LUMPED AT STATION 13 =	0.0076 kg
BLADE ELEMENT MASS LUMPED AT STATION 14 =	0.0076 kg
BLADE ELEMENT MASS LUMPED AT STATION 15 =	0.0076 kg
BLADE ELEMENT MASS LUMPED AT STATION 16 =	0.0076 kg
BLADE ELEMENT MASS LUMPED AT STATION 17 =	0.0076 kg
BLADE ELEMENT MASS LUMPED AT STATION 18 =	0.0076 kg
BLADE ELEMENT MASS LUMPED AT STATION 19 =	0.0076 kg
BLADE ELEMENT MASS LUMPED AT STATION 20 =	0.0076 kg
BLADE ELEMENT MASS LUMPED AT STATION 21 =	0.0076 kg
BLADE ELEMENT MASS LUMPED AT STATION 22 =	0.0076 kg
BLADE ELEMENT MASS LUMPED AT STATION 23 =	0.0076 kg
BLADE ELEMENT MASS LUMPED AT STATION 24 =	0.0076 kg
BLADE ELEMENT MASS LUMPED AT STATION 25 =	0.0076 kg
BLADE ELEMENT MASS LUMPED AT STATION 26 =	0.0076 kg
BLADE ELEMENT MASS LUMPED AT STATION 27 =	0.0076 kg
BLADE ELEMENT MASS LUMPED AT STATION 28 =	0.0076 kg

BLADE ELEME[illegible] MASS LUMPED AT STATION [illegible] = [illegible] kg

BLADE FLAPPING COEFFICIENTS

Fourier series for the Blade Flapping Equation is given as:

$$\beta(\psi) = A_0/2 + A_1\cos(\psi) + B_1\sin(\psi) + A_2\cos(2\psi) + B_2\sin(2\psi) + A_3\cos(3\psi) + B_3\sin(3\psi) \quad \text{deg}$$

Where ψ = AZIMUTH ANGLE (deg)

A_0 = +5.0103 deg
A_1 = −0.0040 deg
B_1 = −0.0005 deg
A_2 = −0.0000 deg
B_2 = −0.0006 deg
A_3 = +0.0000 deg
B_3 = −0.0003 deg

AZIMUTH ANGLE	FLAPPING ANGLE
+0.000 deg	+3.000 deg
+20.000 deg	+3.000 deg
+40.000 deg	+3.001 deg
+60.000 deg	+3.003 deg
+80.000 deg	+3.004 deg
+100.000 deg	+3.006 deg
+120.000 deg	+3.007 deg
+140.000 deg	+3.008 deg
+160.000 deg	+3.009 deg
+180.000 deg	+3.009 deg
+200.000 deg	+3.009 deg
+220.000 deg	+3.008 deg
+240.000 deg	+3.007 deg
+260.000 deg	+3.006 deg
+280.000 deg	+3.005 deg
+300.000 deg	+3.004 deg
+320.000 deg	+3.003 deg
+340.000 deg	+3.003 deg
+360.000 deg	+3.003 deg

HELICOPTER SHAFT ANGLE = +0.00 deg

ROTOR LIFT = +335.199 N

HELICOPTER WEIGHT = 340.350 N

ROTOR TORQUE = -23.323 Nm

ROTOR INDUCED AND PROFILE POWER =
-4.825 kW

(Figures are for the rotor system only)

AERODYNAMICS FOR A TEETERING LIFTING ROTOR SYSTEM

FORCES AND MOMENTS AT ANY STATION

MAXIMUM OUT-OF-PLANE MOMENT ABOUT STATION £12= +4.293 Nm

MAXIMUM IN-PLANE MOMENT ABOUT STATION £12= -5.363 Nm

MAXIMUM IN-PLANE TANGENTIAL SHEAR FORCE ABOUT STATION E12= --.14+ 1

MAXIMUM IN-PLANE RADIAL FORCE ABOUT STATION E12= +3128.150 1

Position of max bend in blade

320 mm . Sta 14.

CF = 2988, 374

-3,963 -4,168

TRANS STATION 12.

AERODYNAMICS FOR A TESTBWING LIFTING ROTOR SYSTEM

FLIGHT INPUT DATA

NUMBER OF ROTOR BLADES =	2
ROTOR BLADE RADIUS =	0.750 m
ROOT CUT OUT RADIUS =	0.075 m
ROTOR BLADE TWIST BETWEEN ROOT AND TIP =	+0.000 deg
ROTOR BLADE CORD =	0.050 m
CYCLIC LATERAL PITCH COEFFICIENT =	+0.734 deg
CYCLIC LONGITUDINAL PITCH COEFFICIENT =	-3.597 deg
ANGULAR ROTOR BLADE SPEED =	2000.00 rpm
HELICOPTER FORWARD SPEED =	100.000 kph
DENSITY OF AIR =	1.20000 kg/m3
HELICOPTER ALL UP WEIGHT =	35.000 kg
ROTOR TORQUE =	0.000 Nm
HELICOPTER PITCHING VELOCITY =	0.000 deg/s
HELICOPTER ROLLING VELOCITY =	0.000 deg/s
ROOT COLLECTIVE PITCH =	8.000 deg
NUMBER OF BLADE ELEMENTS (even number) =	30
AZIMUTH INCREMENT =	20 deg
ROTOR BLADE PRECONE ANGLE =	3.000 deg
MASS MOMENT OF INERTIA ABOUT TEETERING HINGE =	0.095 kg m
ATMOSPHERIC TEMPERATURE =	+15.000 deg C
AEROFOIL LIFT CURVE SLOPE =	6.000 /rad
AEROFOIL AVERAGE DRAG COEFFICIENT =	0.0120

MASS OF ROTOR HUB =	0.3120 kg
BLADE ELEMENT MASS LUMPED AT STATION 0 =	0.0220 kg
BLADE ELEMENT MASS LUMPED AT STATION 1 =	0.0220 kg
BLADE ELEMENT MASS LUMPED AT STATION 2 =	0.0025 kg
BLADE ELEMENT MASS LUMPED AT STATION 3 =	0.0025 kg
BLADE ELEMENT MASS LUMPED AT STATION 4 =	0.0025 kg
BLADE ELEMENT MASS LUMPED AT STATION 5 =	0.0025 kg
BLADE ELEMENT MASS LUMPED AT STATION 6 =	0.0525 kg
BLADE ELEMENT MASS LUMPED AT STATION 7 =	0.0554 kg
BLADE ELEMENT MASS LUMPED AT STATION 8 =	0.0094 kg
BLADE ELEMENT MASS LUMPED AT STATION 9 =	0.0094 kg
BLADE ELEMENT MASS LUMPED AT STATION 10 =	0.0076 kg
BLADE ELEMENT MASS LUMPED AT STATION 11 =	0.0076 kg
BLADE ELEMENT MASS LUMPED AT STATION 12 =	0.0076 kg
BLADE ELEMENT MASS LUMPED AT STATION 13 =	0.0076 kg
BLADE ELEMENT MASS LUMPED AT STATION 14 =	0.0076 kg
BLADE ELEMENT MASS LUMPED AT STATION 15 =	0.0076 kg
BLADE ELEMENT MASS LUMPED AT STATION 16 =	0.0076 kg
BLADE ELEMENT MASS LUMPED AT STATION 17 =	0.0076 kg
BLADE ELEMENT MASS LUMPED AT STATION 18 =	0.0076 kg
BLADE ELEMENT MASS LUMPED AT STATION 19 =	0.0076 kg
BLADE ELEMENT MASS LUMPED AT STATION 20 =	0.0076 kg
BLADE ELEMENT MASS LUMPED AT STATION 21 =	0.0076 kg
BLADE ELEMENT MASS LUMPED AT STATION 22 =	0.0076 kg
BLADE ELEMENT MASS LUMPED AT STATION 23 =	0.0076 kg
BLADE ELEMENT MASS LUMPED AT STATION 24 =	0.0076 kg
BLADE ELEMENT MASS LUMPED AT STATION 25 =	0.0076 kg
BLADE ELEMENT MASS LUMPED AT STATION 26 =	0.0076 kg
BLADE ELEMENT MASS LUMPED AT STATION 27 =	0.0076 kg
BLADE ELEMENT MASS LUMPED AT STATION 28 =	0.0076 kg
BLADE ELEMENT MASS LUMPED AT STATION 29 =	0.0076 kg

AERODYNAMICS FOR A TEETERING LIFTING ROTOR SYSTEM

BLADE FLAPPING COEFFICIENTS

Where θ = AZIMUTH ANGLE (deg)
A0 = +6.1109 deg
A1 = -7.0021 deg
B1 = -1.1744 deg
A2 = -0.3003 deg
B2 = +0.3174 deg
A3 = +0.0026 deg
B3 = +0.0000 deg

AZIMUTH ANGLE	FLAPPING ANGLE
+0.000 deg	-3.963 deg
+20.000 deg	-3.929 deg
+40.000 deg	-3.451 deg
+60.000 deg	-1.440 deg
+80.000 deg	+0.707 deg
+100.000 deg	+3.130 deg
+120.000 deg	+5.537 deg
+140.000 deg	+7.545 deg
+160.000 deg	+9.206 deg
+180.000 deg	+10.035 deg
+200.000 deg	+10.031 deg
+220.000 deg	+9.189 deg
+240.000 deg	+7.601 deg
+260.000 deg	+5.454 deg
+280.000 deg	+3.008 deg
+300.000 deg	+0.564 deg
+320.000 deg	-1.575 deg
+340.000 deg	-3.148 deg
+360.000 deg	-3.966 deg

AERODYNAMICS FOR A TEETERING LIFTING ROTOR SYSTEM

ROTOR PERFORMANCE

THE OVERALL ROTOR PERFORMANCE IS CALCULATED AS:

ROTOR THRUST = +[illegible] N

HELICOPTER SHAFT ANGLE = +11.48 deg

ROTOR LIFT = +[illegible] N

Where θ = AZIMUTH ANGLE (deg)

A0 = +6.1109 deg
A1 = −7.0021 deg
B1 = −1.1744 deg
A2 = −0.0205 deg
B2 = +0.0174 deg
A3 = +0.0025 deg
B3 = +0.0000 deg

AZIMUTH ANGLE	FLAPPING ANGLE
+0.000 deg	−3.963 deg
+20.000 deg	−3.929 deg
+40.000 deg	−3.751 deg
+60.000 deg	−1.440 deg
+80.000 deg	+0.707 deg
+100.000 deg	+3.130 deg
+120.000 deg	+5.537 deg
+140.000 deg	+7.545 deg
+160.000 deg	+9.206 deg
+180.000 deg	+10.035 deg
+200.000 deg	+10.031 deg
+220.000 deg	+9.189 deg
+240.000 deg	+7.601 deg
+260.000 deg	+5.454 deg
+280.000 deg	+3.008 deg
+300.000 deg	+0.564 deg
320.000 deg	−1.575 deg
+340.000 deg	−3.148 deg
+360.000 deg	−3.966 deg

AERODYNAMICS FOR A TEETERING LIFTING ROTOR SYSTEM

ROTOR PERFORMANCE

THE OVERALL ROTOR PERFORMANCE IS CALCULATED AS:

ROTOR THRUST = +[illegible] N

HELICOPTER SHAFT ANGLE = +11.48 deg

ROTOR LIFT = +[illegible] N

ROTOR TORQUE = -1[illegible]

ROTOR INDUCED AND PROFILE POWER =
-2.579 kW

(Figures are for the rotor system only)

AERODYNAMICS FOR A TEETERING LIFTING ROTOR SYSTEM

FORCES AND MOMENTS AT ANY STATION

MAXIMUM OUT-OF-PLANE MOMENT ABOUT STATION £12= +49.290 Nm

MAXIMUM IN-PLANE MOMENT ABOUT STATION £12= -8.442 Nm

MAXIMUM OUT-OF-PLANE SHEAR FORCE ABOUT STATION £12= +108.59[illegible]

MAXIMUM IN-PLANE TANGENTIAL SHEAR FORCE ABOUT STATION £12= -11.[illegible] N

MAXIMUM IN-PLANE RADIAL FORCE ABOUT STATION £12= +3191.381 N

APPENDIX D

Finite Element Method Results

```
NIHRUJOBIGFPRTEDGATHER  13:48:23     6/11/1990
 LINE    1  ** EXECUTIVE
 LINE    2  ANALYSIS=STATIC
 LINE    3  FILE=FLEX
 LINE    4  SAVE=26,27
 LINE    5  #ELTYPE
```

**** PROPRIETARY SOFTWARE PRODUCT OF ****

E N G I N E E R I N G M E C H A N I C S R E S E A R C H

L O R P O R A T I O N

1707 W. BIG BEAVER, TROY, MICHIGAN 48084 U.S.A.

TELEPHONE (313)643-6222 - TELEX 469732

WEST COAST BRANCH OFFICE:

22939 HAWTHORNE BLVD. #206 TORRANCE, CALIFORNIA 90505

TELEPHONE (213)378-8820

***** IBM-PC MS/DOS VERSION 80.7 - RELEASE 083008 *****

STATIC ANALYSIS

SELECTION OF ELEMENT TYPES FROM THE NISA ELEMENT LIBRARY (*ELTYPE DATA GROUP)

NSRL	NKTP	NORDR	NODES/EL	DOF/NODE
1	32	2	8	6

TABLE OF REAL CONSTANTS (TABLE DATA GROUP)

INDEXRC	VALUES OF REAL CONSTANTS							
1	7.500000E-01	7.500000E-01	7.500000E-01	7.500000E-01	7.500000E-01	7.500000E-01	7.500000E-01	7.500000E-01
2	1.250000E-01	1.250000E-01	1.250000E-01	1.250000E-01	1.250000E-01	1.250000E-01	1.250000E-01	1.250000E-01
3	2.400000E+00	2.400000E+00	2.400000E+00	2.400000E+00	2.400000E+00	2.400000E+00	2.400000E+00	2.400000E+00
4	2.400000E+00	2.400000E+00	2.400000E+00	2.400000E+00	2.400000E+00	2.400000E+00	2.400000E+00	2.400000E+00

TABLE OF COMPOSITE ROTATION ANGLES (=LAMANGLE DATA GROUP)

INDEXRA	VALUES OF ROTATION ANGLES							
1	0.000000E-01	0.000000E-01	0.000000E-01	0.000000E-01	0.000000E-01	0.000000E-01	0.000000E-01	0.000000E-01
2	9.000000E+01	9.000000E+01	9.000000E+01	9.000000E+01	9.000000E+01	9.000000E+01	9.000000E+01	9.000000E+01
3	0.000000E-01	0.000000E-01	0.000000E-01	0.000000E-01	0.000000E-01	0.000000E-01	0.000000E-01	0.000000E-01
4	0.000000E-01	0.000000E-01	0.000000E-01	0.000000E-01	0.000000E-01	0.000000E-01	0.000000E-01	0.000000E-01

LAMINATION SEQUENCE DATA (*LAMSEQ DATA GROUP)

```
INDEX--NLAY--- IDRA  /---1---2---3---4---5---6---7---8---9--10--11--12--13--14--15--16--17--18--19--20--21--22--23--24--25--

   1     4       0
          INDEXRC     1   2   2   2
          INDEXRA     1   2   1   2
          MAT  NO     1   1   1   1
   2     8       0
          INDEXRC     1   2   2   2   2   2   2   1
          INDEXRA     1   2   1   2   2   1   2   1
          MATL NO     1   1   1   1   1   1   1   1
   3    10       0
          INDEXRC     3   1   2   2   2   2   2   2   1   3
          INDEXRA     3   1   2   1   2   2   1   2   1   3
          MATL NO     3   1   1   1   1   1   1   1   1   3
   4     1       0
          INDEXRC     4
          INDEXRA     4
          MATL NO     4
```

CONNECTIVITY ECHO SUPPRESSED FOR THIS RUN

MATERIAL PROPERTY TABLE (#MATERIAL DATA GROUP)

MATERIAL INDEX 1

EX	1	0	1.30000000E+05	0.00000000E-01	0.00000000E-01	0.00000000E-01	0.00000000E-01
EY	1	0	7.30000000E+03	0.00000000E-01	0.00000000E-01	0.00000000E-01	0.00000000E-01
EZ	1	0	9.50000000E+03	0.00000000E-01	0.00000000E-01	0.00000000E-01	0.00000000E-01
NUXY	1	0	2.63000000E-01	0.00000000E-01	0.00000000E-01	0.00000000E-01	0.00000000E-01
NUX2	1	0	3.00000000E-01	0.00000000E-01	0.00000000E-01	0.00000000E-01	0.00000000E-01
NUYZ	1	0	3.00000000E-01	0.00000000E-01	0.00000000E-01	0.00000000E-01	0.00000000E-01
GXY	1	0	4.50000000E+03	0.00000000E-01	0.00000000E-01	0.00000000E-01	0.00000000E-01
GYZ	1	0	4.30000000E+03	0.00000000E-01	0.00000000E-01	0.00000000E-01	0.00000000E-01
GXZ	1	0	4.50000000E+03	0.00000000E-01	0.00000000E-01	0.00000000E-01	0.00000000E-01

MATERIAL INDEX 2

EX	2	0	1.30000000E+04	0.00000000E-01	0.00000000E-01	0.00000000E-01	0.00000000E-01
EY	2	0	7.30000000E+03	0.00000000E-01	0.00000000E-01	0.00000000E-01	0.00000000E-01
EZ	2	0	9.50000000E+03	0.00000000E-01	0.00000000E-01	0.00000000E-01	0.00000000E-01
NUXY	2	0	2.63000000E-01	0.00000000E-01	0.00000000E-01	0.00000000E-01	0.00000000E-01
NUX2	2	0	3.00000000E-01	0.00000000E-01	0.00000000E-01	0.00000000E-01	0.00000000E-01
NUYZ	2	0	3.00000000E-01	0.00000000E-01	0.00000000E-01	0.00000000E-01	0.00000000E-01
GXY	2	0	4.50000000E+03	0.00000000E-01	0.00000000E-01	0.00000000E-01	0.00000000E-01
GYZ	2	0	4.30000000E+03	0.00000000E-01	0.00000000E-01	0.00000000E-01	0.00000000E-01
GXZ	2	0	4.50000000E+03	0.00000000E-01	0.00000000E-01	0.00000000E-01	0.00000000E-01

MATERIAL INDEX 3

EX	3	0	5.10000000E+04	0.00000000E-01	0.00000000E-01	0.00000000E-01	0.00000000E-01
EY	3	0	1.30000000E+04	0.00000000E-01	0.00000000E-01	0.00000000E-01	0.00000000E-01
EZ	3	0	1.30000000E+04	0.00000000E-01	0.00000000E-01	0.00000000E-01	0.00000000E-01
NUXY	3	0	3.00000000E-01	0.00000000E-01	0.00000000E-01	0.00000000E-01	0.00000000E-01
NUX2	3	0	3.00000000E-01	0.00000000E-01	0.00000000E-01	0.00000000E-01	0.00000000E-01
NUYZ	3	0	3.00000000E-01	0.00000000E-01	0.00000000E-01	0.00000000E-01	0.00000000E-01
GXY	3	0	6.00000000E+03	0.00000000E-01	0.00000000E-01	0.00000000E-01	0.00000000E-01
GYZ	3	0	6.00000000E+03	0.00000000E-01	0.00000000E-01	0.00000000E-01	0.00000000E-01
GXZ	3	0	6.00000000E+03	0.00000000E-01	0.00000000E-01	0.00000000E-01	0.00000000E-01

MATERIAL INDEX 4

EX	4	0	5.10000000E+04	0.00000000E-01	0.00000000E-01	0.00000000E-01	0.00000000E-01
EY	4	0	1.30000000E+04	0.00000000E-01	0.00000000E-01	0.00000000E-01	0.00000000E-01
EZ	4	0	1.30000000E+04	0.00000000E-01	0.00000000E-01	0.00000000E-01	0.00000000E-01
NUXY	4	0	3.00000000E-01	0.00000000E-01	0.00000000E-01	0.00000000E-01	0.00000000E-01
NUX2	4	0	3.00000000E-01	0.00000000E-01	0.00000000E-01	0.00000000E-01	0.00000000E-01
NUYZ	4	0	3.00000000E-01	0.00000000E-01	0.00000000E-01	0.00000000E-01	0.00000000E-01
GXY	4	0	6.00000000E+03	0.00000000E-01	0.00000000E-01	0.00000000E-01	0.00000000E-01
GYZ	4	0	6.00000000E+03	0.00000000E-01	0.00000000E-01	0.00000000E-01	0.00000000E-01
GXZ	4	0	6.00000000E+03	0.00000000E-01	0.00000000E-01	0.00000000E-01	0.00000000E-01

MATERIAL PROPERTY TABLE (=MATERIAL DATA GROUP)

MATERIAL INDEX 1

EX	1	0	1.30000000E+05	0.00000000E-01	0.00000000E-01	0.00000000E-01	0.00000000E-01
EY	1	0	7.30000000E+03	0.00000000E-01	0.00000000E-01	0.00000000E-01	0.00000000E-01
EZ	1	0	9.50000000E+03	0.00000000E-01	0.00000000E-01	0.00000000E-01	0.00000000E-01
NUXY	1	0	2.63000000E-01	0.00000000E-01	0.00000000E-01	0.00000000E-01	0.00000000E-01
NUXZ	1	0	3.00000000E-01	0.00000000E-01	0.00000000E-01	0.00000000E-01	0.00000000E-01
NUYZ	1	0	3.00000000E-01	0.00000000E-01	0.00000000E-01	0.00000000E-01	0.00000000E-01
GXY	1	0	4.50000000E+03	0.00000000E-01	0.00000000E-01	0.00000000E-01	0.00000000E-01
GYZ	1	0	4.30000000E+03	0.00000000E-01	0.00000000E-01	0.00000000E-01	0.00000000E-01
GXZ	1	0	4.50000000E+03	0.00000000E-01	0.00000000E-01	0.00000000E-01	0.00000000E-01

MATERIAL INDEX 2

EX	2	0	1.30000000E+04	0.00000000E-01	0.00000000E-01	0.00000000E-01	0.00000000E-01
EY	2	0	9.30000000E+03	0.00000000E-01	0.00000000E-01	0.00000000E-01	0.00000000E-01
EZ	2	0	9.50000000E+03	0.00000000E-01	0.00000000E-01	0.00000000E-01	0.00000000E-01
NUXY	2	0	2.63000000E-01	0.00000000E-01	0.00000000E-01	0.00000000E-01	0.00000000E-01
NUXZ	2	0	3.00000000E-01	0.00000000E-01	0.00000000E-01	0.00000000E-01	0.00000000E-01
NUYZ	2	0	3.00000000E-01	0.00000000E-01	0.00000000E-01	0.00000000E-01	0.00000000E-01
GXY	2	0	4.50000000E+03	0.00000000E-01	0.00000000E-01	0.00000000E-01	0.00000000E-01
GYZ	2	0	4.30000000E+03	0.00000000E-01	0.00000000E-01	0.00000000E-01	0.00000000E-01
GXZ	2	0	4.50000000E+03	0.00000000E-01	0.00000000E-01	0.00000000E-01	0.00000000E-01

MATERIAL INDEX 3

EX	3	0	5.10000000E+04	0.00000000E-01	0.00000000E-01	0.00000000E-01	0.00000000E-01
EY	3	0	1.50000000E+04	0.00000000E-01	0.00000000E-01	0.00000000E-01	0.00000000E-01
EZ	3	0	1.50000000E+04	0.00000000E-01	0.00000000E-01	0.00000000E-01	0.00000000E-01
NUXY	3	0	3.00000000E-01	0.00000000E-01	0.00000000E-01	0.00000000E-01	0.00000000E-01
NUXZ	3	0	3.00000000E-01	0.00000000E-01	0.00000000E-01	0.00000000E-01	0.00000000E-01
NUYZ	3	0	3.00000000E-01	0.00000000E-01	0.00000000E-01	0.00000000E-01	0.00000000E-01
GXY	3	0	6.00000000E+03	0.00000000E-01	0.00000000E-01	0.00000000E-01	0.00000000E-01
GYZ	3	0	6.00000000E+03	0.00000000E-01	0.00000000E-01	0.00000000E-01	0.00000000E-01
GXZ	3	0	6.00000000E+03	0.00000000E-01	0.00000000E-01	0.00000000E-01	0.00000000E-01

MATERIAL INDEX 4

EX	4	0	5.10000000E+04	0.00000000E-01	0.00000000E-01	0.00000000E-01	0.00000000E-01
EY	4	0	1.50000000E+04	0.00000000E-01	0.00000000E-01	0.00000000E-01	0.00000000E-01
EZ	4	0	1.50000000E+04	0.00000000E-01	0.00000000E-01	0.00000000E-01	0.00000000E-01
NUXY	4	0	3.00000000E-01	0.00000000E-01	0.00000000E-01	0.00000000E-01	0.00000000E-01
NUXZ	4	0	3.00000000E-01	0.00000000E-01	0.00000000E-01	0.00000000E-01	0.00000000E-01
NUYZ	4	0	3.00000000E-01	0.00000000E-01	0.00000000E-01	0.00000000E-01	0.00000000E-01
GXY	4	0	6.00000000E+03	0.00000000E-01	0.00000000E-01	0.00000000E-01	0.00000000E-01
GYZ	4	0	6.00000000E+03	0.00000000E-01	0.00000000E-01	0.00000000E-01	0.00000000E-01
GXZ	4	0	6.00000000E+03	0.00000000E-01	0.00000000E-01	0.00000000E-01	0.00000000E-01

OUTPUT CONTROL FOR LOAD CASE ID NO. 1

INTERNAL FORCE AND STRAIN ENERGY KEY ...(KEIFR)= 0
REACTION FORCE KEY .....(KRCIN)= 1
STRESS COMPUTATION KEY .....(KSTR)= 3
STRAIN COMPUTATION KEY .....(KSTN)= 0
ELEMENT STRESS/STRAIN OUTPUT OPTIONS ...(LO1)= 0
NODAL STRESSES OUTPUT OPTIONS .....(LO2)= 4
DISPLACEMENT OUTPUT OPTIONS .....(LO7)= 0
STRESS FREE TEMPERATURE .....(TSFRE)= 0.000000E-01

SPECIFIED DISPLACEMENT DATA (ESPDISP DATA GROUP)

NODE NO.	LABEL	DISPLACEMENT VALUE	LAST NODE	INC	LABELS
2300	ROTZ	0.00000E-01	0	0	
2300	ROTY	0.00000E-01	0	0	
2300	ROTX	0.00000E-01	0	0	
2300	UZ	0.00000E-01	0	0	
2300	UY	0.00000E-01	0	0	
2300	UX	0.00000E-01	0	0	
2301	ROTZ	0.00000E-01	0	0	
2301	ROTY	0.00000E-01	0	0	
2301	ROTX	0.00000E-01	0	0	
2301	UZ	0.00000E-01	0	0	
2301	UY	0.00000E-01	0	0	
2301	UX	0.00000E-01	0	0	
2302	ROTZ	0.00000E-01	0	0	
2302	ROTY	0.00000E-01	0	0	
2302	ROTX	0.00000E-01	0	0	
2302	UZ	0.00000E-01	0	0	
2302	UY	0.00000E-01	0	0	
2302	UX	0.00000E-01	0	0	
2303	ROTZ	0.00000E-01	0	0	
2303	ROTY	0.00000E-01	0	0	
2303	ROTX	0.00000E-01	0	0	
2303	UZ	0.0000	0	0	
2303	UY	0.0000	0	0	
2303	UX	0.00000E-01	0	0	
2304	ROTZ	0.00000E-01	0	0	
2304	ROTY	0.00000E-01	0	0	
2304	ROTX	0.00000E-01	0	0	
2304	UZ	0.00000E-01	0	0	
2304	UY	0.00000E-01	0	0	
2304	UX	0.00000E-01	0	0	
2305	ROTZ	0.00000E-01	0	0	
2305	ROTY	0.00000E-01	0	0	
2305	ROTX	0.00000E-01	0	0	
2305	UZ	0.00000E-01	0	0	
2305	UY	0.00000E-01	0	0	
2305	UX	0.00000E-01	0	0	
2306	ROTZ	0.00000E-01	0	0	
2306	ROTY	0.00000E-01	0	0	
2306	ROTX	0.00000E-01	0	0	
2306	UZ	0.00000E-01	0	0	
2306	UY	0.00000E-01	0	0	
2306	UX	0.00000E-01	0	0	
2307	ROTZ	0.00000E-01	0	0	
2307	ROTY	0.00000E-01	0	0	
2307	ROTX	0.00000E-01	0	0	
2307	UZ	0.00000E-01	0	0	
2307	UY	0.00000E-01	0	0	
2307	UX	0.00000E-01	0	0	
2308	ROTZ	0.00000E-01	0	0	
2308	ROTY	0.00000E-01	0	0	
2308	ROTX	0.00000E-01	0	0	
2308	UZ	0.00000E-01	0	0	
2308	UY	0.00000E-01	0	0	
2308	UX	0.00000E-01	0	0	
2309	ROTZ	0.00000E-01	0	0	
2309	ROTY	0.00000E-01	0	0	
2309	ROTX	0.00000E-01	0	0	
2309	UZ	0.00000E-01	0	0	
2309	UY	0.00000E-01	0	0	
2309	UX	0.00000E-01	0	0	
2310	ROTZ	0.00000E-01	0	0	
2310	ROTY	0.00000E-01	0	0	
2310	ROTX	0.00000E-01	0	0	
2310	UZ	0.00000E-01	0	0	

2322	ROTX	0.000000E-01	0	0
2322	UZ	0.000000E-01	0	0
2322	UY	0.000000E-01	0	0
2322	UX	0.000000E-01	0	0
2323	ROTZ	0.000000E-01	0	0
2323	ROTY	0.000000E-01	0	0
2323	ROTX	0.000000E-01	0	0
2323	UZ	0.000000E-01	0	0
2323	UY	0.000000E-01	0	0
2323	UX	0.000000E-01	0	0
2324	ROTZ	0.000000E-01	0	0
2324	ROTY	0.000000E-01	0	0
2324	ROTX	0.000000E-01	0	0
2324	UZ	0.000000E-01	0	0
2324	UY	0.000000E-01	0	0
2324	UX	0.000000E-01	0	0
2325	ROTZ	0.000000E-01	0	0
2325	ROTY	0.000000E-01	0	0
2325	ROTX	0.000000E-01	0	0
2325	UZ	0.000000E-01	0	0
2325	UY	0.000000E-01	0	0
2325	UX	0.000000E-01	0	0
2326	ROTZ	0.000000E-01	0	0
2326	ROTY	0.000000E-01	0	0
2326	ROTX	0.000000E-01	0	0
2326	UZ	0.000000E-01	0	0
2326	UY	0.000000E-01	0	0
2326	UX	0.000000E-01	0	0
2327	ROTZ	0.000000E-01	0	0
2327	ROTY	0.000000E-01	0	0
2327	ROTX	0.000000E-01	0	0
2327	UZ	0.000000E-01	0	0
2327	UY	0.000000E-01	0	0
2327	UX	0.000000E-01	0	0
2328	ROTZ	0.000000E-01	0	0
2328	ROTY	0.000000E-01	0	0
2328	ROTX	0.000000E-01	0	0
2328	UZ	0.000000E-01	0	0
2328	UY	0.000000E-01	0	0
2328	UX	0.000000E-01	0	0
2329	ROTZ	0.000000E-01	0	0
2329	ROTY	0.000000E-01	0	0
2329	ROTX	0.000000E-01	0	0
2329	UZ	0.000000E-01	0	0
2329	UY	0.000000E-01	0	0
2329	UX	0.000000E-01	0	0
2330	ROTZ	0.000000E-01	0	0
2330	ROTY	0.000000E-01	0	0
2330	ROTX	0.000000E-01	0	0
2330	UZ	0.000000E-01	0	0
2330	UY	0.000000E-01	0	0
2330	UX	0.000000E-01	0	0
2331	ROTZ	0.000000E-01	0	0
2331	ROTY	0.000000E-01	0	0
2331	ROTX	0.000000E-01	0	0
2331	UZ	0.000000E-01	0	0
2331	UY	0.000000E-01	0	0
2331	UX	0.000000E-01	0	0
2332	ROTZ	0.000000E-01	0	0
2332	ROTY	0.000000E-01	0	0
2332	ROTX	0.000000E-01	0	0
2332	UZ	0.000000E-01	0	0
2332	UY	0.000000E-01	0	0
2332	UX	0.000000E-01	0	0
2333	ROTZ	0.000000E-01	0	0
2333	ROTY	0.000000E-01	0	0
2333	ROTX	0.000000E-01	0	0
2333	UZ	0.000000E-01	0	0

2334	ROTX	0.00000E-01	0	0
2334	UZ	0.00000E-01	0	0
2334	UY	0.00000E-01	0	0
2334	UX	0.00000E-01	0	0
2335	ROTZ	0.00000E-01	0	0
2335	ROTY	0.00000E-01	0	0
2335	ROTX	0.00000E-01	0	0
2335	UZ	0.00000E-01	0	0
2335	UY	0.00000E-01	0	0
2335	UX	0.00000E-01	0	0
2336	ROTZ	0.00000E-01	0	0
2336	ROTY	0.00000E-01	0	0
2336	ROTX	0.00000E-01	0	0
2336	UZ	0.00000E-01	0	0
2336	UY	0.00000E-01	0	0
2336	UX	0.00000E-01	0	0
2337	ROTZ	0.00000E-01	0	0
2337	ROTY	0.00000E-01	0	0
2337	ROTX	0.00000E-01	0	0
2337	UZ	0.00000E-01	0	0
2337	UY	0.00000E-01	0	0
2337	UX	0.00000E-01	0	0
2338	ROTZ	0.00000E-01	0	0
2338	ROTY	0.00000E-01	0	0
2338	ROTX	0.00000E-01	0	0
2338	UZ	0.00000E-01	0	0
2338	UY	0.00000E-01	0	0
2338	UX	0.00000E-01	0	0
2339	ROTZ	0.00000E-01	0	0
2339	ROTY	0.00000E-01	0	0
2339	ROTX	0.00000E-01	0	0
2339	UZ	0.00000E-01	0	0
2339	UY	0.00000E-01	0	0
2339	UX	0.00000E-01	0	0
2340	ROTZ	0.00000E-01	0	0
2340	ROTY	0.00000E-01	0	0
2340	ROTX	0.00000E-01	0	0
2340	UZ	0.00000E-01	0	0
2340	UY	0.00000E-01	0	0
2340	UX	0.00000E-01	0	0
2341	ROTZ	0.00000E-01	0	0
2341	ROTY	0.00000E-01	0	0
2341	ROTX	0.00000E-01	0	0
2341	UZ	0.00000E-01	0	0
2341	UY	0.00000E-01	0	0
2341	UX	0.00000E-01	0	0
2342	ROTZ	0.00000E-01	0	0
2342	ROTY	0.00000E-01	0	0
2342	ROTX	0.00000E-01	0	0
2342	UZ	0.00000E-01	0	0
2342	UY	0.00000E-01	0	0
2342	UX	0.00000E-01	0	0
2343	ROTZ	0.00000E-01	0	0
2343	ROTY	0.00000E-01	0	0
2343	ROTX	0.00000E-01	0	0
2343	UZ	0.00000E-01	0	0
2343	UY	0.00000E-01	0	0
2343	UX	0.00000E-01	0	0
2344	ROTZ	0.00000E-01	0	0
2344	ROTY	0.00000E-01	0	0
2344	ROTX	0.00000E-01	0	0
2344	UZ	0.00000E-01	0	0
2344	UY	0.00000E-01	0	0
2344	UX	0.00000E-01	0	0
2345	ROTZ	0.00000E-01	0	0
2345	ROTY	0.00000E-01	0	0
2345	ROTX	0.00000E-01	0	0
2345	UZ	0.00000E-01	0	0

2345	ROTX	0.00000E-01	0	0
2346	UZ	0.00000E-01	0	0
2346	UY	0.00000E-01	0	0
2346	UX	0.00000E-01	0	0
2347	ROTZ	0.00000E-01	0	0
2347	ROTY	0.00000E-01	0	0
2347	ROTX	0.00000E-01	0	0
2347	UZ	0.00000E-01	0	0
2347	UY	0.00000E-01	0	0
2347	UX	0.00000E-01	0	0
2348	ROTZ	0.00000E-01	0	0
2348	ROTY	0.00000E-01	0	0
2348	ROTX	0.00000E-01	0	0
2348	UZ	0.00000E-01	0	0
2348	UY	0.00000E-01	0	0
2348	UX	0.00000E-01	0	0
2349	ROTZ	0.00000E-01	0	0
2349	ROTY	0.00000E-01	0	0
2349	ROTX	0.00000E-01	0	0
2349	UZ	0.00000E-01	0	0
2349	UY	0.00000E-01	0	0
2349	UX	0.00000E-01	0	0
2350	ROTZ	0.00000E-01	0	0
2350	ROTY	0.00000E-01	0	0
2350	ROTX	0.00000E-01	0	0
2350	UZ	0.00000E-01	0	0
2350	UY	0.00000E-01	0	0
2350	UX	0.00000E-01	0	0
2351	ROTZ	0.00000E-01	0	0
2351	ROTY	0.00000E-01	0	0
2351	ROTX	0.00000E-01	0	0
2351	UZ	0.00000E-01	0	0
2351	UY	0.00000E-01	0	0
2351	UX	0.00000E-01	0	0
2352	ROTZ	0.00000E-01	0	0
2352	ROTY	0.00000E-01	0	0
2352	ROTX	0.00000E-01	0	0
2352	UZ	0.00000E-01	0	0
2352	UY	0.00000E-01	0	0
2352	UX	0.00000E-01	0	0
2353	ROTZ	0.00000E-01	0	0
2353	ROTY	0.00000E-01	0	0
2353	ROTX	0.00000E-01	0	0
2353	UZ	0.00000E-01	0	0
2353	UY	0.00000E-01	0	0
2353	UX	0.00000E-01	0	0
2354	ROTZ	0.00000E-01	0	0
2354	ROTY	0.00000E-01	0	0
2354	ROTX	0.00000E-01	0	0
2354	UZ	0.00000E-01	0	0
2354	UY	0.00000E-01	0	0
2354	UX	0.00000E-01	0	0
2355	ROTZ	0.00000E-01	0	0
2355	ROTY	0.00000E-01	0	0
2355	ROTX	0.00000E-01	0	0
2355	UZ	0.00000E-01	0	0
2355	UY	0.00000E-01	0	0
2355	UX	0.00000E-01	0	0
2356	ROTZ	0.00000E-01	0	0
2356	ROTY	0.00000E-01	0	0
2356	ROTX	0.00000E-01	0	0
2356	UZ	0.00000E-01	0	0
2356	UY	0.00000E-01	0	0
2356	UX	0.00000E-01	0	0
2357	ROTZ	0.00000E-01	0	0
2357	ROTY	0.00000E-01	0	0
2357	ROTX	0.00000E-01	0	0
2357	UZ	0.00000E-01	0	0

2358	ROTY	0.000000E-01	0	0
2358	ROTX	0.000000E-01	0	0
2358	UZ	0.000000E-01	0	0
2358	UY	0.000000E-01	0	0
2358	UX	0.000000E-01	0	0
2359	ROTZ	0.000000E-01	0	0
2359	ROTY	0.000000E-01	0	0
2359	ROTX	0.000000E-01	0	0
2359	UZ	0.000000E-01	0	0
2359	UY	0.000000E-01	0	0
2359	UX	0.000000E-01	0	0
2360	ROTZ	0.000000E-01	0	0
2360	ROTY	0.000000E-01	0	0
2360	ROTX	0.000000E-01	0	0
2360	UZ	0.000000E-01	0	0
2360	UY	0.000000E-01	0	0
2360	UX	0.000000E-01	0	0
2361	ROTZ	0.000000E-01	0	0
2361	ROTY	0.000000E-01	0	0
2361	ROTX	0.000000E-01	0	0
2361	UZ	0.000000E-01	0	0
2361	UY	0.000000E-01	0	0
2361	UX	0.000000E-01	0	0
2362	ROTZ	0.000000E-01	0	0
2362	ROTY	0.000000E-01	0	0
2362	ROTX	0.000000E-01	0	0
2362	UZ	0.000000E-01	0	0
2362	UY	0.000000E-01	0	0
2362	UX	0.000000E-01	0	0
2363	ROTZ	0.000000E-01	0	0
2363	ROTY	0.000000E-01	0	0
2363	ROTX	0.000000E-01	0	0
2363	UZ	0.000000E-01	0	0
2363	UY	0.000000E-01	0	0
2363	UX	0.000000E-01	0	0
2364	ROTZ	0.000000E-01	0	0
2364	ROTY	0.000000E-01	0	0
2364	ROTX	0.000000E-01	0	0
2364	UZ	0.000000E-01	0	0
2364	UY	0.000000E-01	0	0
2364	UX	0.000000E-01	0	0
2365	ROTZ	0.000000E-01	0	0
2365	ROTY	0.000000E-01	0	0
2365	ROTX	0.000000E-01	0	0
2365	UZ	0.000000E-01	0	0
2365	UY	0.000000E-01	0	0
2365	UX	0.000000E-01	0	0
2366	ROTZ	0.000000E-01	0	0
2366	ROTY	0.000000E-01	0	0
2366	ROTX	0.000000E-01	0	0
2366	UZ	0.000000E-01	0	0
2366	UY	0.000000E-01	0	0
2366	UX	0.000000E-01	0	0
2367	ROTZ	0.000000E-01	0	0
2367	ROTY	0.000000E-01	0	0
2367	ROTX	0.000000E-01	0	0
2367	UZ	0.000000E-01	0	0
2367	UY	0.000000E-01	0	0
2367	UX	0.000000E-01	0	0
2368	ROTZ	0.000000E-01	0	0
2368	ROTY	0.000000E-01	0	0
2368	ROTX	0.000000E-01	0	0
2368	UZ	0.000000E-01	0	0
2368	UY	0.000000E-01	0	0
2368	UX	0.000000E-01	0	0
2369	ROTZ	0.000000E-01	0	0
2369	ROTY	0.000000E-01	0	0
2369	ROTX	0.000000E-01	0	0
2369	UZ	0.000000E-01	0	0

2369	ROTZ	0.00000E-01	0	0
2369	ROTY	0.00000E-01	0	0
2369	ROTX	0.00000E-01	0	0
2369	UZ	0.00000E-01	0	0
2369	UY	0.00000E-01	0	0
2369	UX	0.00000E-01	0	0
2370	ROTZ	0.00000E-01	0	0
2370	ROTY	0.00000E-01	0	0
2370	ROTX	0.00000E-01	0	0
2370	UZ	0.00000E-01	0	0
2370	UY	0.00000E-01	0	0
2370	UX	0.00000E-01	0	0
2371	ROTZ	0.00000E-01	0	0
2371	ROTY	0.00000E-01	0	0
2371	ROTX	0.00000E-01	0	0
2371	UZ	0.00000E-01	0	0
2371	UY	0.00000E-01	0	0
2371	UX	0.00000E-01	0	0
2372	ROTZ	0.00000E-01	0	0
2372	ROTY	0.00000E-01	0	0
2372	ROTX	0.00000E-01	0	0
2372	UZ	0.00000E-01	0	0
2372	UY	0.00000E-01	0	0
2372	UX	0.00000E-01	0	0
2373	ROTZ	0.00000E-01	0	0
2373	ROTY	0.00000E-01	0	0
2373	ROTX	0.00000E-01	0	0
2373	UZ	0.00000E-01	0	0
2373	UY	0.00000E-01	0	0
2373	UX	0.00000E-01	0	0
2374	ROTZ	0.00000E-01	0	0
2374	ROTY	0.00000E-01	0	0
2374	ROTX	0.00000E-01	0	0
2374	UZ	0.00000E-01	0	0
2374	UY	0.00000E-01	0	0
2374	UX	0.00000E-01	0	0
2375	ROTZ	0.00000E-01	0	0
2375	ROTY	0.00000E-01	0	0
2375	ROTX	0.00000E-01	0	0
2375	UZ	0.00000E-01	0	0
2375	UY	0.00000E-01	0	0
2375	UX	0.00000E-01	0	0
2376	ROTZ	0.00000E-01	0	0
2376	ROTY	0.00000E-01	0	0
2376	ROTX	0.00000E-01	0	0
2376	UZ	0.00000E-01	0	0
2376	UY	0.00000E-01	0	0
2376	UX	0.00000E-01	0	0
2377	ROTZ	0.00000E-01	0	0
2377	ROTY	0.00000E-01	0	0
2377	ROTX	0.00000E-01	0	0
2377	UZ	0.00000E-01	0	0
2377	UY	0.00000E-01	0	0
2377	UX	0.00000E-01	0	0
2378	ROTZ	0.00000E-01	0	0
2378	ROTY	0.00000E-01	0	0
2378	ROTX	0.00000E-01	0	0
2378	UZ	0.00000E-01	0	0
2378	UY	0.00000E-01	0	0
2378	UX	0.00000E-01	0	0
2379	ROTZ	0.00000E-01	0	0
2379	ROTY	0.00000E-01	0	0
2379	ROTX	0.00000E-01	0	0
2379	UZ	0.00000E-01	0	0
2379	UY	0.00000E-01	0	0
2379	UX	0.00000E-01	0	0
2380	ROTZ	0.00000E-01	0	0
2380	ROTY	0.00000E-01	0	0
2380	ROTX	0.00000E-01	0	0
2380	UZ	0.00000E-01	0	0
2380	UY	0.00000E-01	0	0
2380	UX	0.00000E-01	0	0
2381	ROTZ	0.00000E-01	0	0
2381	ROTY	0.00000E-01	0	0
2381	ROTX	0.00000E-01	0	0
2381	UZ	0.00000E-01	0	0

2382	ROTY	0.000000E-01	0	0
2382	ROTX	0.000000E-01	0	0
2382	UZ	0.000000E-01	0	0
2382	UY	0.000000E-01	0	0
2382	UX	0.000000E-01	0	0
2383	ROTZ	0.000000E-01	0	0
2383	ROTY	0.000000E-01	0	0
2383	ROTX	0.000000E-01	0	0
2383	UZ	0.000000E-01	0	0
2383	UY	0.000000E-01	0	0
2383	UX	0.000000E-01	0	0
2384	ROTZ	0.000000E-01	0	0
2384	ROTY	0.000000E-01	0	0
2384	ROTX	0.000000E-01	0	0
2384	UZ	0.000000E-01	0	0
2384	UY	0.000000E-01	0	0
2384	UX	0.000000E-01	0	0
2385	ROTZ	0.000000E-01	0	0
2385	ROTY	0.000000E-01	0	0
2385	ROTX	0.000000E-01	0	0
2385	UZ	0.000000E-01	0	0
2385	UY	0.000000E-01	0	0
2385	UX	0.000000E-01	0	0
2386	ROTZ	0.000000E-01	0	0
2386	ROTY	0.000000E-01	0	0
2386	ROTX	0.000000E-01	0	0
2386	UZ	0.000000E-01	0	0
2386	UY	0.000000E-01	0	0
2386	UX	0.000000E-01	0	0
2387	ROTZ	0.000000E-01	0	0
2387	ROTY	0.000000E-01	0	0
2387	ROTX	0.000000E-01	0	0
2387	UZ	0.000000E-01	0	0
2387	UY	0.000000E-01	0	0
2387	UX	0.000000E-01	0	0
2388	ROTZ	0.000000E-01	0	0
2388	ROTY	0.000000E-01	0	0
2388	ROTX	0.000000E-01	0	0
2388	UZ	0.000000E-01	0	0
2388	UY	0.000000E-01	0	0
2388	UX	0.000000E-01	0	0
2389	ROTZ	0.000000E-01	0	0
2389	ROTY	0.000000E-01	0	0
2389	ROTX	0.000000E-01	0	0
2389	UZ	0.000000E-01	0	0
2389	UY	0.000000E-01	0	0
2389	UX	0.000000E-01	0	0
2401	ROTZ	0.000000E-01	0	0
2401	ROTY	0.000000E-01	0	0
2401	ROTX	0.000000E-01	0	0
2401	UZ	0.000000E-01	0	0
2401	UY	0.000000E-01	0	0
2401	UX	0.000000E-01	0	0
2402	ROTZ	0.000000E-01	0	0
2402	ROTY	0.000000E-01	0	0
2402	ROTX	0.000000E-01	0	0
2402	UZ	0.000000E-01	0	0
2402	UY	0.000000E-01	0	0
2402	UX	0.000000E-01	0	0
2403	ROTZ	0.000000E-01	0	0
2403	ROTY	0.000000E-01	0	0
2403	ROTX	0.000000E-01	0	0
2403	UZ	0.000000E-01	0	0
2403	UY	0.000000E-01	0	0
2403	UX	0.000000E-01	0	0
2404	ROTZ	0.000000E-01	0	0
2404	ROTY	0.000000E-01	0	0
2404	ROTX	0.000000E-01	0	0
2404	UZ	0.000000E-01	0	0

2405	ROTX	0.000000E-01	0	0
2405	UZ	0.000000E-01	0	0
2405	UY	0.000000E-01	0	0
2405	UX	0.000000E-01	0	0
2406	ROTZ	0.000000E-01	0	0
2406	ROTY	0.000000E-01	0	0
2406	ROTX	0.000000E-01	0	0
2406	UZ	0.000000E-01	0	0
2406	UY	0.000000E-01	0	0
2406	UX	0.000000E-01	0	0
2407	ROTZ	0.000000E-01	0	0
2407	ROTY	0.000000E-01	0	0
2407	ROTX	0.000000E-01	0	0
2407	UZ	0.000000E-01	0	0
2407	UY	0.000000E-01	0	0
2407	UX	0.000000E-01	0	0
2408	ROTZ	0.000000E-01	0	0
2408	ROTY	0.000000E-01	0	0
2408	ROTX	0.000000E-01	0	0
2408	UZ	0.000000E-01	0	0
2408	UY	0.000000E-01	0	0
2408	UX	0.000000E-01	0	0
2409	ROTZ	0.000000E-01	0	0
2409	ROTY	0.000000E-01	0	0
2409	ROTX	0.000000E-01	0	0
2409	UZ	0.000000E-01	0	0
2409	UY	0.000000E-01	0	0
2409	UX	0.000000E-01	0	0
2410	ROTZ	0.000000E-01	0	0
2410	ROTY	0.000000E-01	0	0
2410	ROTX	0.000000E-01	0	0
2410	UZ	0.000000E-01	0	0
2410	UY	0.000000E-01	0	0
2410	UX	0.000000E-01	0	0
2411	ROTZ	0.000000E-01	0	0
2411	ROTY	0.000000E-01	0	0
2411	ROTX	0.000000E-01	0	0
2411	UZ	0.000000E-01	0	0
2411	UY	0.000000E-01	0	0
2411	UX	0.000000E-01	0	0
2412	ROTZ	0.000000E-01	0	0
2412	ROTY	0.000000E-01	0	0
2412	ROTX	0.000000E-01	0	0
2412	UZ	0.000000E-01	0	0
2412	UY	0.000000E-01	0	0
2412	UX	0.000000E-01	0	0
2413	ROTZ	0.000000E-01	0	0
2413	ROTY	0.000000E-01	0	0
2413	ROTX	0.000000E-01	0	0
2413	UZ	0.000000E-01	0	0
2413	UY	0.000000E-01	0	0
2413	UX	0.000000E-01	0	0
2414	ROTZ	0.000000E-01	0	0
2414	ROTY	0.000000E-01	0	0
2414	ROTX	0.000000E-01	0	0
2414	UZ	0.000000E-01	0	0
2414	UY	0.000000E-01	0	0
2414	UX	0.000000E-01	0	0
2415	ROTZ	0.000000E-01	0	0
2415	ROTY	0.000000E-01	0	0
2415	ROTX	0.000000E-01	0	0
2415	UZ	0.000000E-01	0	0
2415	UY	0.000000E-01	0	0
2415	UX	0.000000E-01	0	0
2416	ROTZ	0.000000E-01	0	0
2416	ROTY	0.000000E-01	0	0
2416	ROTX	0.000000E-01	0	0
2416	UZ	0.000000E-01	0	0

2417	ROTY	0.000000E-01	0	0
2417	ROTX	0.000000E-01	0	0
2417	UZ	0.000000E-01	0	0
2417	UY	0.000000E-01	0	0
2417	UX	0.000000E-01	0	0
2418	ROTZ	0.000000E-01	0	0
2418	ROTY	0.000000E-01	0	0
2418	ROTX	0.000000E-01	0	0
2418	UZ	0.000000E-01	0	0
2418	UY	0.000000E-01	0	0
2418	UX	0.000000E-01	0	0
2419	ROTZ	0.000000E-01	0	0
2419	ROTY	0.000000E-01	0	0
2419	ROTX	0.000000E-01	0	0
2419	UZ	0.000000E-01	0	0
2419	UY	0.000000E-01	0	0
2419	UX	0.000000E-01	0	0
2420	ROTZ	0.000000E-01	0	0
2420	ROTY	0.000000E-01	0	0
2420	ROTX	0.000000E-01	0	0
2420	UZ	0.000000E-01	0	0
2420	UY	0.000000E-01	0	0
2420	UX	0.000000E-01	0	0
2421	ROTZ	0.000000E-01	0	0
2421	ROTY	0.000000E-01	0	0
2421	ROTX	0.000000E-01	0	0
2421	UZ	0.000000E-01	0	0
2421	UY	0.000000E-01	0	0
2421	UX	0.000000E-01	0	0
2422	ROTZ	0.000000E-01	0	0
2422	ROTY	0.000000E-01	0	0
2422	ROTX	0.000000E-01	0	0
2422	UZ	0.000000E-01	0	0
2422	UY	0.000000E-01	0	0
2422	UX	0.000000E-01	0	0
2423	ROTZ	0.000000E-01	0	0
2423	ROTY	0.000000E-01	0	0
2423	ROTX	0.000000E-01	0	0
2423	UZ	0.000000E-01	0	0
2423	UY	0.000000E-01	0	0
2423	UX	0.000000E-01	0	0
2424	ROTZ	0.000000E-01	0	0
2424	ROTY	0.000000E-01	0	0
2424	ROTX	0.000000E-01	0	0
2424	UZ	0.000000E-01	0	0
2424	UY	0.000000E-01	0	0
2424	UX	0.000000E-01	0	0
2425	ROTZ	0.000000E-01	0	0
2425	ROTY	0.000000E-01	0	0
2425	RL	0.000000E-01	0	0
2425	UZ	0.000000E-01	0	0
2425	UY	0.000000E-01	0	0
2425	UX	0.000000E-01	0	0
2426	ROTZ	0.000000E-01	0	0
2426	ROTY	0.000000E-01	0	0
2426	ROTX	0.000000E-01	0	0
2426	UZ	0.000000E-01	0	0
2426	UY	0.000000E-01	0	0
2426	UX	0.000000E-01	0	0
2427	ROTZ	0.000000E-01	0	0
2427	ROTY	0.000000E-01	0	0
2427	ROTX	0.000000E-01	0	0
2427	UZ	0.000000E-01	0	0
2427	UY	0.000000E-01	0	0
2427	UX	0.000000E-01	0	0
2428	ROTZ	0.000000E-01	0	0
2428	ROTY	0.000000E-01	0	0
2428	ROTX	0.000000E-01	0	0
2428	UZ	0.000000E-01	0	0

2429	ROTZ	0.00000E-01	0	0
2429	ROTY	0.00000E-01	0	0
2429	ROTX	0.00000E-01	0	0
2429	UZ	0.00000E-01	0	0
2429	UY	0.00000E-01	0	0
2429	UX	0.00000E-01	0	0
2430	ROTZ	0.00000E-01	0	0
2430	ROTY	0.00000E-01	0	0
2430	ROTX	0.00000E-01	0	0
2430	UZ	0.00000E-01	0	0
2430	UY	0.00000E-01	0	0
2430	UX	0.00000E-01	0	0
2431	ROTZ	0.00000E-01	0	0
2431	ROTY	0.00000E-01	0	0
2431	ROTX	0.00000E-01	0	0
2431	UZ	0.00000E-01	0	0
2431	UY	0.00000E-01	0	0
2431	UX	0.00000E-01	0	0
2432	ROTZ	0.00000E-01	0	0
2432	ROTY	0.00000E-01	0	0
2432	ROTX	0.00000E-01	0	0
2432	UZ	0.00000E-01	0	0
2432	UY	0.00000E-01	0	0
2432	UX	0.00000E-01	0	0
2433	ROTZ	0.00000E-01	0	0
2433	ROTY	0.00000E-01	0	0
2433	ROTX	0.00000E-01	0	0
2433	UZ	0.00000E-01	0	0
2433	UY	0.00000E-01	0	0
2433	UX	0.00000E-01	0	0
2434	ROTZ	0.00000E-01	0	0
2434	ROTY	0.00000E-01	0	0
2434	ROTX	0.00000E-01	0	0
2434	UZ	0.00000E-01	0	0
2434	UY	0.00000E-01	0	0
2434	UX	0.00000E-01	0	0
2435	ROTZ	0.00000E-01	0	0
2435	ROTY	0.00000E-01	0	0
2435	ROTX	0.00000E-01	0	0
2435	UZ	0.00000E-01	0	0
2435	UY	0.00000E-01	0	0
2435	UX	0.00000E-01	0	0
2436	ROTZ	0.00000E-01	0	0
2436	ROTY	0.00000E-01	0	0
2436	ROTX	0.00000E-01	0	0
2436	UZ	0.00000E-01	0	0
2436	UY	0.00000E-01	0	0
2436	UX	0.00000E-01	0	0
2437	ROTZ	0.00000E-01	0	0
2437	ROTY	0.00000E-01	0	0
2437	ROTX	0.00000E-01	0	0
2437	UZ	0.00000E-01	0	0
2437	UY	0.00000E-01	0	0
2437	UX	0.00000E-01	0	0
2438	ROTZ	0.00000E-01	0	0
2438	ROTY	0.00000E-01	0	0
2438	ROTX	0.00000E-01	0	0
2438	UZ	0.00000E-01	0	0
2438	UY	0.00000E-01	0	0
2438	UX	0.00000E-01	0	0
2439	ROTZ	0.00000E-01	0	0
2439	ROTY	0.00000E-01	0	0
2439	ROTX	0.00000E-01	0	0
2439	UZ	0.00000E-01	0	0
2439	UY	0.00000E-01	0	0
2439	UX	0.00000E-01	0	0
2440	ROTZ	0.00000E-01	0	0
2440	ROTY	0.00000E-01	0	0

2441	ROTY	0.000000E-01	0	0
2441	ROTX	0.000000E-01	0	0
2441	UZ	0.000000E-01	0	0
2441	UY	0.000000E-01	0	0
2441	UX	0.000000E-01	0	0
2442	ROTZ	0.000000E-01	0	0
2442	ROTY	0.000000E-01	0	0
2442	ROTX	0.000000E-01	0	0
2442	UZ	0.000000E-01	0	0
2442	UY	0.000000E-01	0	0
2442	UX	0.000000E-01	0	0
2443	ROTZ	0.000000E-01	0	0
2443	ROTY	0.000000E-01	0	0
2443	ROTX	0.000000E-01	0	0
2443	UZ	0.000000E-01	0	0
2443	UY	0.000000E-01	0	0
2443	UX	0.000000E-01	0	0
2444	ROTZ	0.000000E-01	0	0
2444	ROTY	0.000000E-01	0	0
2444	ROTX	0.000000E-01	0	0
2444	UZ	0.000000E-01	0	0
2444	UY	0.000000E-01	0	0
2444	UX	0.000000E-01	0	0
2445	ROTZ	0.000000E-01	0	0
2445	ROTY	0.000000E-01	0	0
2445	ROTX	0.000000E-01	0	0
2445	UZ	0.000000E-01	0	0
2445	UY	0.000000E-01	0	0
2445	UX	0.000000E-01	0	0
2446	ROTZ	0.000000E-01	0	0
2446	ROTY	0.000000E-01	0	0
2446	ROTX	0.000000E-01	0	0
2446	UZ	0.000000E-01	0	0
2446	UY	0.000000E-01	0	0
2446	UX	0.000000E-01	0	0
2447	ROTZ	0.000000E-01	0	0
2447	ROTY	0.000000E-01	0	0
2447	ROTX	0.000000E-01	0	0
2447	UZ	0.000000E-01	0	0
2447	UY	0.000000E-01	0	0
2447	UX	0.000000E-01	0	0
2448	ROTZ	0.000000E-01	0	0
2448	ROTY	0.000000E-01	0	0
2448	ROTX	0.000000E-01	0	0
2448	UZ	0.000000E-01	0	0
2448	UY	0.000000E-01	0	0
2448	UX	0.000000E-01	0	0
2449	ROTZ	0.000000E-01	0	0
2449	ROTY	0.000000E-01	0	0
2449	ROTX	0.000000E-01	0	0
2449	UZ	0.000000E-01	0	0
2449	UY	0.000000E-01	0	0
2449	UX	0.000000E-01	0	0
2450	ROTZ	0.000000E-01	0	0
2450	ROTY	0.000000E-01	0	0
2450	ROTX	0.000000E-01	0	0
2450	UZ	0.000000E-01	0	0
2450	UY	0.000000E-01	0	0
2450	UX	0.000000E-01	0	0
2451	ROTZ	0.000000E-01	0	0
2451	ROTY	0.000000E-01	0	0
2451	ROTX	0.000000E-01	0	0
2451	UZ	0.000000E-01	0	0
2451	UY	0.000000E-01	0	0
2451	UX	0.000000E-01	0	0
2452	ROTZ	0.000000E-01	0	0
2452	ROTY	0.000000E-01	0	0
2452	ROTX	0.000000E-01	0	0
2452	UZ	0.000000E-01	0	0

2453	ROTZ	0.00000E-01	0	0
2453	ROTY	0.00000E-01	0	0
2453	ROTX	0.00000E-01	0	0
2453	UZ	0.00000E-01	0	0
2453	UY	0.00000E-01	0	0
2453	UX	0.00000E-01	0	0
2454	ROTZ	0.00000E-01	0	0
2454	ROTY	0.00000E-01	0	0
2454	ROTX	0.00000E-01	0	0
2454	UZ	0.00000E-01	0	0
2454	UY	0.00000E-01	0	0
2454	UX	0.00000E-01	0	0
2455	ROTZ	0.00000E-01	0	0
2455	ROTY	0.00000E-01	0	0
2455	ROTX	0.00000E-01	0	0
2455	UZ	0.00000E-01	0	0
2455	UY	0.00000E-01	0	0
2455	UX	0.00000E-01	0	0
2456	ROTZ	0.00000E-01	0	0
2456	ROTY	0.00000E-01	0	0
2456	ROTX	0.00000E-01	0	0
2456	UZ	0.00000E-01	0	0
2456	UY	0.00000E-01	0	0
2456	UX	0.00000E-01	0	0
2457	ROTZ	0.00000E-01	0	0
2457	ROTY	0.00000E-01	0	0
2457	ROTX	0.00000E-01	0	0
2457	UZ	0.00000E-01	0	0
2457	UY	0.00000E-01	0	0
2457	UX	0.00000E-01	0	0

CONCENTRATED NODAL FORCE AND MOMENT DATA (EQFORCE DATA GROUP)

NODE NO.	LABEL	FORCE VALUE	LASTNOD	INC	LFN
3125	MZ	1.40000E+00	3125	1	1
3125	MY	2.70000E+00	3125	1	1
3125	MX	0.00000E-01	3125	1	1
3125	FZ	0.00000E-01	3125	1	1
3125	FY	-2.70000E+00	3125	1	1
3125	FX	4.13000E+02	3125	1	1
3126	MZ	1.40000E+00	3126	1	1
3126	MY	2.70000E+00	3126	1	1
3126	MX	0.00000E-01	3126	1	1
3126	FZ	0.00000E-01	3126	1	1
3126	FY	-2.70000E+00	3126	1	1
3126	FX	4.13000E+02	3126	1	1
3127	MZ	1.40000E+00	3127	1	1
3127	MY	2.70000E+00	3127	1	1
3127	MX	0.00000E-01	3127	1	1
3127	FZ	0.00000E-01	3127	1	1
3127	FY	-2.70000E+00	3127	1	1
3127	FX	4.13000E+02	3127	1	1
3128	MZ	1.40000E+00	3128	1	1
3128	MY	2.70000E+00	3128	1	1
3128	MX	0.00000E-01	3128	1	1
3128	FZ	0.00000E-01	3128	1	1
3128	FY	-2.70000E+00	3128	1	1
3128	FX	4.13000E+02	3128	1	1
3129	MZ	1.40000E+00	3129	1	1
3129	MY	2.70000E+00	3129	1	1
3129	MX	0.00000E-01	3129	1	1
3129	FZ	0.00000E-01	3129	1	1
3129	FY	-2.70000E+00	3129	1	1
3127	FX	4.13000E+02	3129	1	1
3130	MZ	1.40000E+00	3130	1	1
3130	MY	2.70000E+00	3130	1	1
3130	MX	0.00000E-01	3130	1	1
3130	FZ	0.00000E-01	3130	1	1
3130	FY	-2.70000E+00	3130	1	1
3130	FX	4.13000E+02	3130	1	1
3131	MZ	1.40000E+00	3131	1	1
3131	MY	2.70000E+00	3131	1	1
3131	MX	0.00000E-01	3131	1	1
3131	FZ	0.00000E-01	3131	1	1
3131	FY	-2.70000E+00	3131	1	1
3131	FX	4.13000E+02	3131	1	1
3132	MZ	1.40000E+00	3132	1	1
3132	MY	2.70000E+00	3132	1	1
3132	MX	0.00000E-01	3132	1	1
3132	FZ	0.00000E-01	3132	1	1
3132	FY	-2.70000E+00	3132	1	1
3132	FX	4.13000E+02	3132	1	1
3133	MZ	1.40000E+00	3133	1	1
3133	MY	2.70000E+00	3133	1	1
3133	MX	0.00000E-01	3133	1	1
3133	FZ	0.00000E-01	3133	1	1
3133	FY	-2.70000E+00	3133	1	1
3133	FX	4.13000E+02	3133	1	1
3134	MZ	1.40000E+00	3134	1	1
3134	MY	2.70000E+00	3134	1	1
3134	MX	0.00000E-01	3134	1	1
3134	FZ	0.00000E-01	3134	1	1
3134	FY	-2.70000E+00	3134	1	1
3134	FX	4.13000E+02	3134	1	1
3135	MZ	1.40000E+00	3135	1	1
3135	MY	2.70000E+00	3135	1	1
3135	MX	0.00000E-01	3135	1	1
3135	FZ	0.00000E-01	3135	1	1

3221	MZ	1.40000E+00	3221	1	1
3221	MY	2.70000E+00	3221	1	1
3221	MX	0.00000E-01	3221	1	1
3221	FZ	0.00000E-01	3221	1	1
3221	FY	-2.70000E+00	3221	1	1
3221	FX	4.45000E+02	3221	1	1
3222	MZ	1.40000E+00	3222	1	1
3222	MY	2.70000E+00	3222	1	1
3222	MX	0.00000E-01	3222	1	1
3222	FZ	0.00000E-01	3222	1	1
3222	FY	-2.70000E+00	3222	1	1
3222	FX	4.45000E+02	3222	1	1
3223	MZ	1.40000E+00	3223	1	1
3223	MY	2.70000E+00	3223	1	1
3223	MX	0.00000E-01	3223	1	1
3223	FZ	0.00000E-01	3223	1	1
3223	FY	-2.70000E+00	3223	1	1
3223	FX	4.45000E+02	3223	1	1
3224	MZ	1.40000E+00	3224	1	1
3224	MY	2.70000E+00	3224	1	1
3224	MX	0.00000E-01	3224	1	1
3224	FZ	0.00000E-01	3224	1	1
3224	FY	-2.70000E+00	3224	1	1
3224	FX	4.45000E+02	3224	1	1
3225	MZ	1.40000E+00	3225	1	1
3225	MY	2.70000E+00	3225	1	1
3225	MX	0.00000E-01	3225	1	1
3225	FZ	0.00000E-01	3225	1	1
3225	FY	-2.70000E+00	3225	1	1
3225	FX	4.45000E+02	3225	1	1
3226	MZ	1.40000E+00	3226	1	1
3226	MY	2.70000E+00	3226	1	1
3226	MX	0.00000E-01	3226	1	1
3226	FZ	0.00000E-01	3226	1	1
3226	FY	-2.70000E+00	3226	1	1
3226	FX	4.45000E+02	3226	1	1
3227	MZ	1.40000E+00	3227	1	1
3227	MY	2.70000E+00	3227	1	1
3227	MX	0.00000E-01	3227	1	1
3227	FZ	0.00000E-01	3227	1	1
3227	FY	-2.70000E+00	3227	1	1
3227	FX	4.45000E+02	3227	1	1
3228	MZ	1.40000E+00	3228	1	1
3228	MY	2.70000E+00	3228	1	1
3228	MX	0.00000E-01	3228	1	1
3228	FZ	0.00000E-01	3228	1	1
3228	FY	-2.70000E+00	3228	1	1
3228	FX	4.45000E+02	3228	1	1
3229	MZ	1.40000E+00	3229	1	1
3229	MY	2.70000E+00	3229	1	1
3229	MX	0.00000E-01	3229	1	1
3229	FZ	0.00000E-01	3229	1	1
3229	FY	-2.70000E+00	3229	1	1
3229	FX	4.45000E+02	3229	1	1
3230	MZ	1.40000E+00	3230	1	1
3230	MY	2.70000E+00	3230	1	1
3230	MX	0.00000E-01	3230	1	1
3230	FZ	0.00000E-01	3230	1	1
3230	FY	-2.70000E+00	3230	1	1
3230	FX	4.45000E+02	3230	1	1
3231	MZ	1.40000E+00	3231	1	1
3231	MY	2.70000E+00	3231	1	1
3231	MX	0.00000E-01	3231	1	1
3231	FZ	0.00000E-01	3231	1	1
3231	FY	-2.70000E+00	3231	1	1
3231	FX	4.45000E+02	3231	1	1

```
      PROCESS NODAL COORDINATES DATA

      PROCESS #2 (ELEMENT CONNECTIVITY) DATA



      TOTAL NUMBER OF ELEMENTS ..............:  270
      TOTAL NUMBER OF NODES  ................:  918
      TOTAL NUMBER OF ACTIVE NODES ..........:  918
      LARGEST NODE NUMBER    ................:  3231



      MINIMUM X-COORD =  -0.33045E+01   MAXIMUM X-COORD =   0.28500E+03
      MINIMUM Y-COORD =   0.00000E+00   MAXIMUM Y-COORD =   0.30000E+02
      MINIMUM Z-COORD =  -0.87000E+01   MAXIMUM Z-COORD =   0.87000E+01

      PROCESS #03 (COMPOSITE LAMINATION SEQUENCE) DATA


WAVE FRONT STATUS BEFORE MINIMIZATION
-------------------------------------

   MAXIMUM WAVE FRONT ..........:  162
   RMS WAVE FRONT ..............:  131
   AVERAGE WAVE FRONT ..........:  127
   TOTAL NO. OF DOF IN MODEL ...:  5508
WAVE FRONT STATUS AFTER MINIMIZATION (ITERATION NO. 1 )
-------------------------------------
   MAXIMUM WAVE FRONT ..........:  174
   RMS WAVE FRONT ..............:  125
   AVERAGE WAVE FRONT ..........:  117
   TOTAL NO. OF DOF IN MODEL ...:  5508
WAVE FRONT STATUS AFTER MINIMIZATION (ITERATION NO. 2 )
-------------------------------------
   MAXIMUM WAVE FRONT ..........:  174
   RMS WAVE FRONT ..............:  123
   AVERAGE WAVE FRONT ..........:  117
   TOTAL NO. OF DOF IN MODEL ...:  5508
WAVE FRONT STATUS AFTER MINIMIZATION (ITERATION NO. 4 )
-------------------------------------
   MAXIMUM WAVE FRONT ..........:  162
   RMS WAVE FRONT ..............:  124
   AVERAGE WAVE FRONT ..........:  120
   TOTAL NO. OF DOF IN MODEL ...:  5508
WAVE FRONT STATUS AFTER MINIMIZATION (ITERATION NO. 3 )
-------------------------------------
   MAXIMUM WAVE FRONT ..........:  162
   RMS WAVE FRONT ..............:  134
   AVERAGE WAVE FRONT ..........:  130
   TOTAL NO. OF DOF IN MODEL ...:  5508



***** WAVE FRONT MINIMIZATION WAS SUCCESSFUL, ITERATION NO. 1 IS SELECTED
 WAVE FRONT PARAMETERS ARE-
 MAXIMUM WAVE FRONT :  174
 RMS WAVE FRONT     :  123
 AVERAGE WAVE FRONT :  117
```

```
TOTAL NUMBER OF VALID DOFS IN MODEL .............=  5500
TOTAL NUMBER OF UNCONSTRAINED DOFS ..............=  4692
TOTAL NUMBER OF CONSTRAINED DOFS ................=   816
TOTAL NUMBER OF SLAVES IN MPC EQS ...............=     0
```

*** WAVE FRONT SOLUTION PARAMETERS ***

MAXIMUM WAVEFRONT (MAXPA)	=	174
R.M.S. WAVEFRONT	=	102
AVERAGE WAVEFRONT	=	71
LARGEST ELEMENT MATRIX RANK USED (LVMAX)	=	48
TOTAL NUMBER OF DEGREES OF FREEDOM	=	4872
ESTIMATED NUMBER OF RECORDS ON FILE 30	=	115

***** REACTION FORCES AND MOMENTS AT NODES *****

LOAD CASE ID NO. 1

NODE	FX	FY	FZ	MX	MY	MZ
2300	0.000000E-01	0.000[illegible]E-01	0.000000E-01	0.000000E-01	0.000000E-01	0.000000E-01
2301	0.000000E-01	0.000000E-01	0.000000E-01	0.000000E-01	0.000000E-01	0.000000E-01
2302	0.000000E-01	0.000000E-01	0.000000E-01	0.000000E-01	0.000000E-01	0.000000E-01
2303	0.000000E-01	0.000000E-01	0.000000E-01	0.000000E-01	0.000000E-01	0.000000E-01
2304	0.000000E-01	0.000000E-01	0.000000E-01	0.000000E-01	0.000000E-01	0.000000E-01
2305	0.000000E-01	0.000000E-01	0.000000E-01	0.000000E-01	0.000000E-01	0.000000E-01
2306	0.000000E-01	0.000000E-01	0.000000E-01	0.000000E-01	0.000000E-01	0.000000E-01
2307	0.000000E-01	0.000000E-01	0.000000E-01	0.000000E-01	0.000000E-01	0.000000E-01
2308	0.000000E-01	0.000000E-01	0.000000E-01	0.000000E-01	0.000000E-01	0.000000E-01
2309	0.000000E-01	0.000000E-01	0.000000E-01	0.000000E-01	0.000000E-01	0.000000E-01
2310	0.000000E-01	0.000000E-01	0.000000E-01	0.000000E-01	0.000000E-01	0.000000E-01
2322	0.000000E-01	0.000000E-01	0.000000E-01	0.000000E-01	0.000000E-01	0.000000E-01
2323	0.000000E-01	0.000000E-01	0.000000E-01	0.000000E-01	0.000000E-01	0.000000E-01
2324	0.000000E-01	0.000000E-01	0.000000E-01	0.000000E-01	0.000000E-01	0.000000E-01
2325	0.000000E-01	0.000000E-01	0.000000E-01	0.000000E-01	0.000000E-01	0.000000E-01
2326	0.000000E-01	0.000000E-01	0.000000E-01	0.000000E-01	0.000000E-01	0.000000E-01
2327	0.000000E-01	0.000000E-01	0.000000E-01	0.000000E-01	0.000000E-01	0.000000E-01
2328	0.000000E-01	0.000000E-01	0.000000E-01	0.000000E-01	0.000000E-01	0.000000E-01
2329	0.000000E-01	0.000000E-01	0.000000E-01	0.000000E-01	0.000000E-01	0.000000E-01
2330	0.000000E-01	0.000000E-01	0.000000E-01	0.000000E-01	0.000000E-01	0.000000E-01
2331	0.000000E-01	0.000000E-01	0.000000E-01	0.000000E-01	0.000000E-01	0.000000E-01
2332	0.000000E-01	0.000000E-01	0.000000E-01	0.000000E-01	0.000000E-01	0.000000E-01
2333	0.000000E-01	0.000000E-01	0.000000E-01	0.000000E-01	0.000000E-01	0.000000E-01
2334	0.000000E-01	0.000000E-01	0.000000E-01	0.000000E-01	0.000000E-01	0.000000E-01
2335	0.000000E-01	0.000000E-01	0.000000E-01	0.000000E-01	0.000000E-01	0.000000E-01
2336	0.000000E-01	0.000000E-01	0.000000E-01	0.000000E-01	0.000000E-01	0.000000E-01
2337	0.000000E-01	0.000000E-01	0.000000E-01	0.000000E-01	0.000000E-01	0.000000E-01
2338	0.000000E-01	0.000000E-01	0.000000E-01	0.000000E-01	0.000000E-01	0.000000E-01
2339	0.000000E-01	0.000000E-01	0.000000E-01	0.000000E-01	0.000000E-01	0.000000E-01
2340	0.000000E-01	0.000000E-01	0.000000E-01	0.000000E-01	0.000000E-01	0.000000E-01
2341	0.000000E-01	0.000000E-01	0.000000E-01	0.000000E-01	0.000000E-01	0.000000E-01
2342	0.000000E-01	0.000000E-01	0.000000E-01	0.000000E-01	0.000000E-01	0.000000E-01
2343	0.000000E-01	0.000000E-01	0.000000E-01	0.000000E-01	0.000000E-01	0.000000E-01
2344	0.000000E-01	0.000000E-01	0.000000E-01	0.000000E-01	0.000000E-01	0.000000E-01
2345	0.000000E-01	0.000000E-01	0.000000E-01	0.000000E-01	0.000000E-01	0.000000E-01
2346	0.000000E-01	0.000000E-01	0.000000E-01	0.000000E-01	0.000000E-01	0.000000E-01
2347	0.000000E-01	0.000000E-01	0.000000E-01	0.000000E-01	0.000000E-01	0.000000E-01
2348	0.000000E-01	0.000000E-01	0.000000E-01	0.000000E-01	0.000000E-01	0.000000E-01
2349	0.000000E-01	0.000000E-01	0.000000E-01	0.000000E-01	0.000000E-01	0.000000E-01
2350	0.000000E-01	0.000000E-01	0.000000E-01	0.000000E-01	0.000000E-01	0.000000E-01
2351	0.000000E-01	0.000000E-01	0.000000E-01	0.000000E-01	0.000000E-01	0.000000E-01
2352	0.000000E-01	0.000000E-01	0.000000E-01	0.000000E-01	0.000000E-01	0.000000E-01
2353	0.000000E-01	0.000000E-01	0.000000E-01	0.000000E-01	0.000000E-01	0.000000E-01
2354	0.000000E-01	0.000000E-01	0.000000E-01	0.000000E-01	0.000000E-01	0.000000E-01
2355	0.000000E-01	0.000000E-01	0.000000E-01	0.000000E-01	0.000000E-01	0.000000E-01
2356	0.000000E-01	0.000000E-01	0.000000E-01	0.000000E-01	0.000000E-01	0.000000E-01
2357	0.000000E-01	0.000000E-01	0.000000E-01	0.000000E-01	0.000000E-01	0.000000E-01
2358	0.000000E-01	0.000000E-01	0.000000E-01	0.000000E-01	0.000000E-01	0.000000E-01
2359	0.000000E-01	0.000000E-01	0.000000E-01	0.000000E-01	0.000000E-01	0.000000E-01
2360	0.000000E-01	0.000000E-01	0.000000E-01	0.000000E-01	0.000000E-01	0.000000E-01
2361	0.000000E-01	0.000000E-01	0.000000E-01	0.000000E-01	0.000000E-01	0.000000E-01
2362	0.000000E-01	0.000000E-01	0.000000E-01	0.000000E-01	0.000000E-01	0.000000E-01
2363	0.000000E-01	0.000000E-01	0.000000E-01	0.000000E-01	0.000000E-01	0.000000E-01
2364	0.000000E-01	0.000000E-01	0.000000E-01	0.000000E-01	0.000000E-01	0.000000E-01
2365	0.000000E-01	0.000000E-01	0.000000E-01	0.000000E-01	0.000000E-01	0.000000E-01
2366	0.000000E-01	0.000000E-01	0.000000E-01	0.000000E-01	0.000000E-01	0.000000E-01
2367	0.000000E-01	0.000000E-01	0.000000E-01	0.000000E-01	0.000000E-01	0.000000E-01
2368	0.000000E-01	0.000000E-01	0.000000E-01	0.000000E-01	0.000000E-01	0.000000E-01
2369	0.000000E-01	0.000000E-01	0.000000E-01	0.000000E-01	0.000000E-01	0.000000E-01
2370	0.000000E-01	0.000000E-01	0.000000E-01	0.000000E-01	0.000000E-01	0.000000E-01
2371	0.000000E-01	0.000000E-01	0.000000E-01	0.000000E-01	0.000000E-01	0.000000E-01

2374	0.000000E-01	0.000000E-01	0.000000E-01	0.000000E-01	0.000000E-01	0.000000E-01
2375	0.000000E-01	0.000000E-01	0.000000E-01	0.000000E-01	0.000000E-01	0.000000E-01
2376	0.000000E-01	0.000000E-01	0.000000E-01	0.000000E-01	0.000000E-01	0.000000E-01
2377	0.000000E-01	0.000000E-01	0.000000E-01	0.000000E-01	0.000000E-01	0.000000E-01
2378	0.000000E-01	0.000000E-01	0.000000E-01	0.000000E-01	0.000000E-01	0.000000E-01
2379	-2.23857E+02	-1.28752E+01	-2.01113E-01	3.14119E-01	-1.82411E+00	0.000000E-01
2380	-9.68901E+02	-4.02988E+00	1.54648E-02	-1.73220E-01	-7.49715E+00	0.000000E-01
2381	-5.41087E+02	-3.38710E+00	1.40147E-02	2.16760E-01	-1.02783E+00	0.000000E-01
2382	-1.14176E+03	5.02251E-01	6.21511E-02	-8.62386E-02	-8.14339E+00	0.000000E-01
2383	-6.11314E+02	7.36786E-01	8.88420E-02	5.55056E-02	-1.10534E+00	0.000000E-01
2384	-1.30191E+03	4.64245E+00	5.72903E-02	7.76697E-06	-8.20859E+00	0.000000E-01
2385	-6.90018E+02	7.85001E+00	8.09425E-02	-6.34867E-02	-1.10333E+00	0.000000E-01
2386	-1.46255E+03	8.76888E+00	8.21472E-02	8.42437E-02	-8.14330E+00	0.000000E-01
2387	-7.71173E+02	2.40308E+01	1.40111E-02	-2.78765E-01	-1.02781E+00	0.000000E-01
2388	-1.65754E+03	8.84764E+00	1.54674E-02	1.76281E-01	-7.49705E+00	0.000000E-01
2389	-1.49764E+02	2.91038E+01	-2.01113E-01	-3.14439E-01	-1.82405E+00	0.000000E-01
2401	0.000000E-01	0.000000E-01	0.000000E-01	0.000000E-01	0.000000E-01	0.000000E-01
2402	0.000000E-01	0.000000E-01	0.000000E-01	0.000000E-01	0.000000E-01	0.000000E-01
2403	0.000000E-01	0.000000E-01	0.000000E-01	0.000000E-01	0.000000E-01	0.000000E-01
2404	0.000000E-01	0.000000E-01	0.000000E-01	0.000000E-01	0.000000E-01	0.000000E-01
2405	0.000000E-01	0.000000E-01	0.000000E-01	0.000000E-01	0.000000E-01	0.000000E-01
2406	0.000000E-01	0.000000E-01	0.000000E-01	0.000000E-01	0.000000E-01	0.000000E-01
2407	0.000000E-01	0.000000E-01	0.000000E-01	0.000000E-01	0.000000E-01	0.000000E-01
2408	0.000000E-01	0.000000E-01	0.000000E-01	0.000000E-01	0.000000E-01	0.000000E-01
2409	0.000000E-01	0.000000E-01	0.000000E-01	0.000000E-01	0.000000E-01	0.000000E-01
2410	0.000000E-01	0.000000E-01	0.000000E-01	0.000000E-01	0.000000E-01	0.000000E-01
2411	0.000000E-01	0.000000E-01	0.000000E-01	0.000000E-01	0.000000E-01	0.000000E-01
2412	0.000000E-01	0.000000E-01	0.000000E-01	0.000000E-01	0.000000E-01	0.000000E-01
2413	0.000000E-01	0.000000E-01	0.000000E-01	0.000000E-01	0.000000E-01	0.000000E-01
2414	0.000000E-01	0.000000E-01	0.000000E-01	0.000000E-01	0.000000E-01	0.000000E-01
2415	0.000000E-01	0.000000E-01	0.000000E-01	0.000000E-01	0.000000E-01	0.000000E-01
2416	0.000000E-01	0.000000E-01	0.000000E-01	0.000000E-01	0.000000E-01	0.000000E-01
2417	0.000000E-01	0.000000E-01	0.000000E-01	0.000000E-01	0.000000E-01	0.000000E-01
2418	0.000000E-01	0.000000E-01	0.000000E-01	0.000000E-01	0.000000E-01	0.000000E-01
2419	0.000000E-01	0.000000E-01	0.000000E-01	0.000000E-01	0.000000E-01	0.000000E-01
2420	0.000000E-01	0.000000E-01	0.000000E-01	0.000000E-01	0.000000E-01	0.000000E-01
2421	0.000000E-01	0.000000E-01	0.000000E-01	0.000000E-01	0.000000E-01	0.000000E-01
2422	0.000000E-01	0.000000E-01	0.000000E-01	0.000000E-01	0.000000E-01	0.000000E-01
2423	0.000000E-01	0.000000E-01	0.000000E-01	0.000000E-01	0.000000E-01	0.000000E-01
2424	0.000000E-01	0.000000E-01	0.000000E-01	0.000000E-01	0.000000E-01	0.000000E-01
2425	0.000000E-01	0.000000E-01	0.000000E-01	0.000000E-01	0.000000E-01	0.000000E-01
2426	0.000000E-01	0.000000E-01	0.000000E-01	0.000000E-01	0.000000E-01	0.000000E-01
2427	0.000000E-01	0.000000E-01	0.000000E-01	0.000000E-01	0.000000E-01	0.000000E-01
2428	0.000000E-01	0.000000E-01	0.000000E-01	0.000000E-01	0.000000E-01	0.000000E-01
2429	0.000000E-01	0.000000E-01	0.000000E-01	0.000000E-01	0.000000E-01	0.000000E-01
2430	0.000000E-01	0.000000E-01	0.000000E-01	0.000000E-01	0.000000E-01	0.000000E-01
2431	0.000000E-01	0.000000E-01	0.000000E-01	0.000000E-01	0.000000E-01	0.000000E-01
2432	0.000000E-01	0.000000E-01	0.000000E-01	0.000000E-01	0.000000E-01	0.000000E-01
2433	0.000000E-01	0.000000E-01	0.000000E-01	0.000000E-01	0.000000E-01	0.000000E-01
2434	0.000000E-01	0.000000E-01	0.000000E-01	0.000000E-01	0.000000E-01	0.000000E-01
2435	0.000000E-01	0.000000E-01	0.000000E-01	0.000000E-01	0.000000E-01	0.000000E-01
2436	0.000000E-01	0.000000E-01	0.000000E-01	0.000000E-01	0.000000E-01	0.000000E-01
2437	0.000000E-01	0.000000E-01	0.000000E-01	0.000000E-01	0.000000E-01	0.000000E-01
2438	0.000000E-01	0.000000E-01	0.000000E-01	0.000000E-01	0.000000E-01	0.000000E-01
2439	0.000000E-01	0.000000E-01	0.000000E-01	0.000000E-01	0.000000E-01	0.000000E-01
2440	0.000000E-01	0.000000E-01	0.000000E-01	0.000000E-01	0.000000E-01	0.000000E-01
2441	0.000000E-01	0.000000E-01	0.000000E-01	0.000000E-01	0.000000E-01	0.000000E-01
2442	0.000000E-01	0.000000E-01	0.000000E-01	0.000000E-01	0.000000E-01	0.000000E-01
2443	0.000000E-01	0.000000E-01	0.000000E-01	0.000000E-01	0.000000E-01	0.000000E-01
2444	0.000000E-01	0.000000E-01	0.000000E-01	0.000000E-01	0.000000E-01	0.000000E-01
2445	0.000000E-01	0.000000E-01	0.000000E-01	0.000000E-01	0.000000E-01	0.000000E-01
2446	0.000000E-01	0.000000E-01	0.000000E-01	0.000000E-01	0.000000E-01	0.000000E-01
2447	0.000000E-01	0.000000E-01	0.000000E-01	0.000000E-01	0.000000E-01	0.000000E-01
2448	0.000000E-01	0.000000E-01	0.000000E-01	0.000000E-01	0.000000E-01	0.000000E-01
2449	0.000000E-01	0.000000E-01	0.000000E-01	0.000000E-01	0.000000E-01	0.000000E-01
2450	0.000000E-01	0.000000E-01	0.000000E-01	0.000000E-01	0.000000E-01	0.000000E-01
2451	0.000000E-01	0.000000E-01	0.000000E-01	0.000000E-01	0.000000E-01	0.000000E-01
2452	0.000000E-01	0.000000E-01	0.000000E-01	0.000000E-01	0.000000E-01	0.000000E-01
2453	0.000000E-01	0.000000E-01	0.000000E-01	0.000000E-01	0.000000E-01	0.000000E-01
2454	0.000000E-01	0.000000E-01	0.000000E-01	0.000000E-01	0.000000E-01	0.000000E-01

SUMMATION OF REACTION FORCES IN GLOBAL DIRECTIONS

FX	FY	FZ
-9.790000E+03	5.940000E+01	1.886494E-08

****** DISPLACEMENT SOLUTION ******

LOAD CASE ID NO. 1

NODE	UX	UY	UZ	ROTX	ROTY	ROTZ
2215	0.000000E-01	0.000000E-01	0.000000E-01	0.000000E-01	0.000000E-01	0.000000E-01
2216	0.000000E-01	0.000000E-01	0.000000E-01	0.000000E-01	0.000000E-01	0.000000E-01
2217	0.000000E-01	0.000000E-01	0.000000E-01	0.000000E-01	0.000000E-01	0.000000E-01
2218	0.000000E-01	0.000000E-01	0.000000E-01	0.000000E-01	0.000000E-01	0.000000E-01
2219	0.000000E-01	0.000000E-01	0.000000E-01	0.000000E-01	0.000000E-01	0.000000E-01
2220	0.000000E-01	0.000000E-01	0.000000E-01	0.000000E-01	0.000000E-01	0.000000E-01
2221	0.000000E-01	0.000000E-01	0.000000E-01	0.000000E-01	0.000000E-01	0.000000E-01
2222	0.000000E-01	0.000000E-01	0.000000E-01	0.000000E-01	0.000000E-01	0.000000E-01
2223	0.000000E-01	0.000000E-01	0.000000E-01	0.000000E-01	0.000000E-01	0.000000E-01
2224	0.000000E-01	0.000000E-01	0.000000E-01	0.000000E-01	0.000000E-01	0.000000E-01
2225	0.000000E-01	0.000000E-01	0.000000E-01	0.000000E-01	0.000000E-01	0.000000E-01
2226	0.000000E-01	0.000000E-01	0.000000E-01	0.000000E-01	0.000000E-01	0.000000E-01
2227	0.000000E-01	0.000000E-01	0.000000E-01	0.000000E-01	0.000000E-01	0.000000E-01
2228	0.000000E-01	0.000000E-01	0.000000E-01	0.000000E-01	0.000000E-01	0.000000E-01
2229	0.000000E-01	0.000000E-01	0.000000E-01	0.000000E-01	0.000000E-01	0.000000E-01
2230	0.000000E-01	0.000000E-01	0.000000E-01	0.000000E-01	0.000000E-01	0.000000E-01
2231	0.000000E-01	0.000000E-01	0.000000E-01	0.000000E-01	0.000000E-01	0.000000E-01
2232	0.000000E-01	0.000000E-01	0.000000E-01	0.000000E-01	0.000000E-01	0.000000E-01
2233	0.000000E-01	0.000000E-01	0.000000E-01	0.000000E-01	0.000000E-01	0.000000E-01
2234	0.000000E-01	0.000000E-01	0.000000E-01	0.000000E-01	0.000000E-01	0.000000E-01
2235	0.000000E-01	0.000000E-01	0.000000E-01	0.000000E-01	0.000000E-01	0.000000E-01
2236	0.000000E-01	0.000000E-01	0.000000E-01	0.000000E-01	0.000000E-01	0.000000E-01
2237	0.000000E-01	0.000000E-01	0.000000E-01	0.000000E-01	0.000000E-01	0.000000E-01
2238	0.000000E-01	0.000000E-01	0.000000E-01	0.000000E-01	0.000000E-01	0.000000E-01
2239	0.000000E-01	0.000000E-01	0.000000E-01	0.000000E-01	0.000000E-01	0.000000E-01
2240	0.000000E-01	0.000000E-01	0.000000E-01	0.000000E-01	0.000000E-01	0.000000E-01
2241	0.000000E-01	0.000000E-01	0.000000E-01	0.000000E-01	0.000000E-01	0.000000E-01
2242	0.000000E-01	0.000000E-01	0.000000E-01	0.000000E-01	0.000000E-01	0.000000E-01
2243	0.000000E-01	0.000000E-01	0.000000E-01	0.000000E-01	0.000000E-01	0.000000E-01
2244	0.000000E-01	0.000000E-01	0.000000E-01	0.000000E-01	0.000000E-01	0.000000E-01
2245	0.000000E-01	0.000000E-01	0.000000E-01	0.000000E-01	0.000000E-01	0.000000E-01
2246	0.000000E-01	0.000000E-01	0.000000E-01	0.000000E-01	0.000000E-01	0.000000E-01
2247	0.000000E-01	0.000000E-01	0.000000E-01	0.000000E-01	0.000000E-01	0.000000E-01
2248	0.000000E-01	0.000000E-01	0.000000E-01	0.000000E-01	0.000000E-01	0.000000E-01
2249	0.000000E-01	0.000000E-01	0.000000E-01	0.000000E-01	0.000000E-01	0.000000E-01
2250	0.000000E-01	0.000000E-01	0.000000E-01	0.000000E-01	0.000000E-01	0.000000E-01
2251	0.000000E-01	0.000000E-01	0.000000E-01	0.000000E-01	0.000000E-01	0.000000E-01
2252	0.000000E-01	0.000000E-01	0.000000E-01	0.000000E-01	0.000000E-01	0.000000E-01
2253	0.000000E-01	0.000000E-01	0.000000E-01	0.000000E-01	0.000000E-01	0.000000E-01
2254	0.000000E-01	0.000000E-01	0.000000E-01	0.000000E-01	0.000000E-01	0.000000E-01
2255	0.000000E-01	0.000000E-01	0.000000E-01	0.000000E-01	0.000000E-01	0.000000E-01
2256	0.000000E-01	0.000000E-01	0.000000E-01	0.000000E-01	0.000000E-01	0.000000E-01
2257	0.000000E-01	0.000000E-01	0.000000E-01	0.000000E-01	0.000000E-01	0.000000E-01
2258	0.000000E-01	0.000000E-01	0.000000E-01	0.000000E-01	0.000000E-01	0.000000E-01
2259	0.000000E-01	0.000000E-01	0.000000E-01	0.000000E-01	0.000000E-01	0.000000E-01
2260	0.000000E-01	0.000000E-01	0.000000E-01	0.000000E-01	0.000000E-01	0.000000E-01
2261	0.000000E-01	0.000000E-01	0.000000E-01	0.000000E-01	0.000000E-01	0.000000E-01
2262	0.000000E-01	0.000000E-01	0.000000E-01	0.000000E-01	0.000000E-01	0.000000E-01
2263	0.000000E-01	0.000000E-01	0.000000E-01	0.000000E-01	0.000000E-01	0.000000E-01
2264	0.000000E-01	0.000000E-01	0.000000E-01	0.000000E-01	0.000000E-01	0.000000E-01
2265	0.000000E-01	0.000000E-01	0.000000E-01	0.000000E-01	0.000000E-01	0.000000E-01
2266	0.000000E-01	0.000000E-01	0.000000E-01	0.000000E-01	0.000000E-01	0.000000E-01
2267	0.000000E-01	0.000000E-01	0.000000E-01	0.000000E-01	0.000000E-01	0.000000E-01
2268	0.000000E-01	0.000000E-01	0.000000E-01	0.000000E-01	0.000000E-01	0.000000E-01
2269	0.000000E-01	0.000000E-01	0.000000E-01	0.000000E-01	0.000000E-01	0.000000E-01
2270	0.000000E-01	0.000000E-01	0.000000E-01	0.000000E-01	0.000000E-01	0.000000E-01
2271	0.000000E-01	0.000000E-01	0.000000E-01	0.000000E-01	0.000000E-01	0.000000E-01
2272	0.000000E-01	0.000000E-01	0.000000E-01	0.000000E-01	0.000000E-01	0.000000E-01
2273	0.000000E-01	0.000000E-01	0.000000E-01	0.000000E-01	0.000000E-01	0.000000E-01

2279	0.000000E-01	0.000000E-01	0.000000E-01	0.000000E-01	0.000000E-01	0.000000E-01
2280	0.000000E-01	0.000000E-01	0.000000E-01	0.000000E-01	0.000000E-01	0.000000E-01
2281	0.000000E-01	0.000000E-01	0.000000E-01	0.000000E-01	0.000000E-01	0.000000E-01
2282	0.000000E-01	0.000000E-01	0.000000E-01	0.000000E-01	0.000000E-01	0.000000E-01
2283	0.000000E-01	0.000000E-01	0.000000E-01	0.000000E-01	0.000000E-01	0.000000E-01
2284	0.000000E-01	0.000000E-01	0.000000E-01	0.000000E-01	0.000000E-01	0.000000E-01
2285	0.000000E-01	0.000000E-01	0.000000E-01	0.000000E-01	0.000000E-01	0.000000E-01
2286	0.000000E-01	0.000000E-01	0.000000E-01	0.000000E-01	0.000000E-01	0.000000E-01
2287	0.000000E-01	0.000000E-01	0.000000E-01	0.000000E-01	0.000000E-01	0.000000E-01
2288	0.000000E-01	0.000000E-01	0.000000E-01	0.000000E-01	0.000000E-01	0.000000E-01
2289	0.000000E-01	0.000000E-01	0.000000E-01	0.000000E-01	0.000000E-01	0.000000E-01
2290	0.000000E-01	0.000000E-01	0.000000E-01	0.000000E-01	0.000000E-01	0.000000E-01
2291	0.000000E-01	0.000000E-01	0.000000E-01	0.000000E-01	0.000000E-01	0.000000E-01
2292	0.000000E-01	0.000000E-01	0.000000E-01	0.000000E-01	0.000000E-01	0.000000E-01
2293	0.000000E-01	0.000000E-01	0.000000E-01	0.000000E-01	0.000000E-01	0.000000E-01
2294	0.000000E-01	0.000000E-01	0.000000E-01	0.000000E-01	0.000000E-01	0.000000E-01
2295	0.000000E-01	0.000000E-01	0.000000E-01	0.000000E-01	0.000000E-01	0.000000E-01
2296	0.000000E-01	0.000000E-01	0.000000E-01	0.000000E-01	0.000000E-01	0.000000E-01
2297	0.000000E-01	0.000000E-01	0.000000E-01	0.000000E-01	0.000000E-01	0.000000E-01
2298	0.000000E-01	0.000000E-01	0.000000E-01	0.000000E-01	0.000000E-01	0.000000E-01
2299	0.000000E-01	0.000000E-01	0.000000E-01	0.000000E-01	0.000000E-01	0.000000E-01
2300	0.000000E-01	0.000000E-01	0.000000E-01	0.000000E-01	0.000000E-01	0.000000E-01
2301	0.000000E-01	0.000000E-01	0.000000E-01	0.000000E-01	0.000000E-01	0.000000E-01
2302	0.000000E-01	0.000000E-01	0.000000E-01	0.000000E-01	0.000000E-01	0.000000E-01
2303	0.000000E-01	0.000000E-01	0.000000E-01	0.000000E-01	0.000000E-01	0.000000E-01
2304	0.000000E-01	0.000000E-01	0.000000E-01	0.000000E-01	0.000000E-01	0.000000E-01
2305	0.000000E-01	0.000000E-01	0.000000E-01	0.000000E-01	0.000000E-01	0.000000E-01
2306	0.000000E-01	0.000000E-01	0.000000E-01	0.000000E-01	0.000000E-01	0.000000E-01
2307	0.000000E-01	0.000000E-01	0.000000E-01	0.000000E-01	0.000000E-01	0.000000E-01
2308	0.000000E-01	0.000000E-01	0.000000E-01	0.000000E-01	0.000000E-01	0.000000E-01
2309	0.000000E-01	0.000000E-01	0.000000E-01	0.000000E-01	0.000000E-01	0.000000E-01
2310	0.000000E-01	0.000000E-01	0.000000E-01	0.000000E-01	0.000000E-01	0.000000E-01
2322	0.000000E-01	0.000000E-01	0.000000E-01	0.000000E-01	0.000000E-01	0.000000E-01
2323	0.000000E-01	0.000000E-01	0.000000E-01	0.000000E-01	0.000000E-01	0.000000E-01
2324	0.000000E-01	0.000000E-01	0.000000E-01	0.000000E-01	0.000000E-01	0.000000E-01
2325	0.000000E-01	0.000000E-01	0.000000E-01	0.000000E-01	0.000000E-01	0.000000E-01
2326	0.000000E-01	0.000000E-01	0.000000E-01	0.000000E-01	0.000000E-01	0.000000E-01
2327	0.000000E-01	0.000000E-01	0.000000E-01	0.000000E-01	0.000000E-01	0.000000E-01
2328	0.000000E-01	0.000000E-01	0.000000E-01	0.000000E-01	0.000000E-01	0.000000E-01
2329	0.000000E-01	0.000000E-01	0.000000E-01	0.000000E-01	0.000000E-01	0.000000E-01
2330	0.000000E-01	0.000000E-01	0.000000E-01	0.000000E-01	0.000000E-01	0.000000E-01
2331	0.000000E-01	0.000000E-01	0.000000E-01	0.000000E-01	0.000000E-01	0.000000E-01
2332	0.000000E-01	0.000000E-01	0.000000E-01	0.000000E-01	0.000000E-01	0.000000E-01
2333	0.000000E-01	0.000000E-01	0.000000E-01	0.000000E-01	0.000000E-01	0.000000E-01
2334	0.000000E-01	0.000000E-01	0.000000E-01	0.000000E-01	0.000000E-01	0.000000E-01
2335	0.000000E-01	0.000000E-01	0.000000E-01	0.000000E-01	0.000000E-01	0.000000E-01
2336	0.000000E-01	0.000000E-01	0.000000E-01	0.000000E-01	0.000000E-01	0.000000E-01
2337	0.000000E-01	0.000000E-01	0.000000E-01	0.000000E-01	0.000000E-01	0.000000E-01
2338	0.000000E-01	0.000000E-01	0.000000E-01	0.000000E-01	0.000000E-01	0.000000E-01
2339	0.000000E-01	0.000000E-01	0.000000E-01	0.000000E-01	0.000000E-01	0.000000E-01
2340	0.000000E-01	0.000000E-01	0.000000E-01	0.000000E-01	0.000000E-01	0.000000E-01
2341	0.000000E-01	0.000000E-01	0.000000E-01	0.000000E-01	0.000000E-01	0.000000E-01
2342	0.000000E-01	0.000000E-01	0.000000E-01	0.000000E-01	0.000000E-01	0.000000E-01
2343	0.000000E-01	0.000000E-01	0.000000E-01	0.000000E-01	0.000000E-01	0.000000E-01
2344	0.000000E-01	0.000000E-01	0.000000E-01	0.000000E-01	0.000000E-01	0.000000E-01
2345	0.000000E-01	0.000000E-01	0.000000E-01	0.000000E-01	0.000000E-01	0.000000E-01
2346	0.000000E-01	0.000000E-01	0.000000E-01	0.000000E-01	0.000000E-01	0.000000E-01
2347	0.000000E-01	0.000000E-01	0.000000E-01	0.000000E-01	0.000000E-01	0.000000E-01
2348	0.000000E-01	0.000000E-01	0.000000E-01	0.000000E-01	0.000000E-01	0.000000E-01
2349	0.000000E-01	0.000000E-01	0.000000E-01	0.000000E-01	0.000000E-01	0.000000E-01
2350	0.000000E-01	0.000000E-01	0.000000E-01	0.000000E-01	0.000000E-01	0.000000E-01
2351	0.000000E-01	0.000000E-01	0.000000E-01	0.000000E-01	0.000000E-01	0.000000E-01
2352	0.000000E-01	0.000000E-01	0.000000E-01	0.000000E-01	0.000000E-01	0.000000E-01
2353	0.000000E-01	0.000000E-01	0.000000E-01	0.000000E-01	0.000000E-01	0.000000E-01
2354	0.000000E-01	0.000000E-01	0.000000E-01	0.000000E-01	0.000000E-01	0.000000E-01
2355	0.000000E-01	0.000000E-01	0.000000E-01	0.000000E-01	0.000000E-01	0.000000E-01
2356	0.000000E-01	0.000000E-01	0.000000E-01	0.000000E-01	0.000000E-01	0.000000E-01
2357	0.000000E-01	0.000000E-01	0.000000E-01	0.000000E-01	0.000000E-01	0.000000E-01
2358	0.000000E-01	0.000000E-01	0.000000E-01	0.000000E-01	0.000000E-01	0.000000E-01

2361	0.000000E-01	0.000000E-01	0.000000E-01	0.000000E-01	0.000000E-01	0.000000E-01
2362	0.000000E-01	0.000000E-01	0.000000E-01	0.000000E-01	0.000000E-01	0.000000E-01
2363	0.000000E-01	0.000000E-01	0.000000E-01	0.000000E-01	0.000000E-01	0.000000E-01
2364	0.000000E-01	0.000000E-01	0.000000E-01	0.000000E-01	0.000000E-01	0.000000E-01
2365	0.000000E-01	0.000000E-01	0.000000E-01	0.000000E-01	0.000000E-01	0.000000E-01
2366	0.000000E-01	0.000000E-01	0.000000E-01	0.000000E-01	0.000000E-01	0.000000E-01
2367	0.000000E-01	0.000000E-01	0.000000E-01	0.000000E-01	0.000000E-01	0.000000E-01
2368	0.000000E-01	0.000000E-01	0.000000E-01	0.000000E-01	0.000000E-01	0.000000E-01
2369	0.000000E-01	0.000000E-01	0.000000E-01	0.000000E-01	0.000000E-01	0.000000E-01
2370	0.000000E-01	0.000000E-01	0.000000E-01	0.000000E-01	0.000000E-01	0.000000E-01
2371	0.000000E-01	0.000000E-01	0.000000E-01	0.000000E-01	0.000000E-01	0.000000E-01
2372	0.000000E-01	0.000000E-01	0.000000E-01	0.000000E-01	0.000000E-01	0.000000E-01
2373	0.000000E-01	0.000000E-01	0.000000E-01	0.000000E-01	0.000000E-01	0.000000E-01
2374	0.000000E-01	0.000000E-01	0.000000E-01	0.000000E-01	0.000000E-01	0.000000E-01
2375	0.000000E-01	0.000000E-01	0.000000E-01	0.000000E-01	0.000000E-01	0.000000E-01
2376	0.000000E-01	0.000000E-01	0.000000E-01	0.000000E-01	0.000000E-01	0.000000E-01
2377	0.000000E-01	0.000000E-01	0.000000E-01	0.000000E-01	0.000000E-01	0.000000E-01
2378	0.000000E-01	0.000000E-01	0.000000E-01	0.000000E-01	0.000000E-01	0.000000E-01
2379	0.000000E-01	0.000000E-01	0.000000E-01	0.000000E-01	0.000000E-01	0.000000E-01
2380	0.000000E-01	0.000000E-01	0.000000E-01	0.000000E-01	0.000000E-01	0.000000E-01
2381	0.000000E-01	0.000000E-01	0.000000E-01	0.000000E-01	0.000000E-01	0.000000E-01
2382	0.000000E-01	0.000000E-01	0.000000E-01	0.000000E-01	0.000000E-01	0.000000E-01
2383	0.000000E-01	0.000000E-01	0.000000E-01	0.000000E-01	0.000000E-01	0.000000E-01
2384	0.000000E-01	0.000000E-01	0.000000E-01	0.000000E-01	0.000000E-01	0.000000E-01
2385	0.000000E-01	0.000000E-01	0.000000E-01	0.000000E-01	0.000000E-01	0.000000E-01
2386	0.000000E-01	0.000000E-01	0.000000E-01	0.000000E-01	0.000000E-01	0.000000E-01
2387	0.000000E-01	0.000000E-01	0.000000E-01	0.000000E-01	0.000000E-01	0.000000E-01
2388	0.000000E-01	0.000000E-01	0.000000E-01	0.000000E-01	0.000000E-01	0.000000E-01
2389	0.000000E-01	0.000000E-01	0.000000E-01	0.000000E-01	0.000000E-01	0.000000E-01
2401	0.000000E-01	0.000000E-01	0.000000E-01	0.000000E-01	0.000000E-01	0.000000E-01
2402	0.000000E-01	0.000000E-01	0.000000E-01	0.000000E-01	0.000000E-01	0.000000E-01
2403	0.000000E-01	0.000000E-01	0.000000E-01	0.000000E-01	0.000000E-01	0.000000E-01
2404	0.000000E-01	0.000000E-01	0.000000E-01	0.000000E-01	0.000000E-01	0.000000E-01
2405	0.000000E-01	0.000000E-01	0.000000E-01	0.000000E-01	0.000000E-01	0.000000E-01
2406	0.000000E-01	0.000000E-01	0.000000E-01	0.000000E-01	0.000000E-01	0.000000E-01
2407	0.000000E-01	0.000000E-01	0.000000E-01	0.000000E-01	0.000000E-01	0.000000E-01
2408	0.000000E-01	0.000000E-01	0.000000E-01	0.000000E-01	0.000000E-01	0.000000E-01
2409	0.000000E-01	0.000000E-01	0.000000E-01	0.000000E-01	0.000000E-01	0.000000E-01
2410	0.000000E-01	0.000000E-01	0.000000E-01	0.000000E-01	0.000000E-01	0.000000E-01
2411	0.000000E-01	0.000000E-01	0.000000E-01	0.000000E-01	0.000000E-01	0.000000E-01
2412	0.000000E-01	0.000000E-01	0.000000E-01	0.000000E-01	0.000000E-01	0.000000E-01
2413	0.000000E-01	0.000000E-01	0.000000E-01	0.000000E-01	0.000000E-01	0.000000E-01
2414	0.000000E-01	0.000000E-01	0.000000E-01	0.000000E-01	0.000000E-01	0.000000E-01
2415	0.000000E-01	0.000000E-01	0.000000E-01	0.000000E-01	0.000000E-01	0.000000E-01
2416	0.000000E-01	0.000000E-01	0.000000E-01	0.000000E-01	0.000000E-01	0.000000E-01
2417	0.000000E-01	0.000000E-01	0.000000E-01	0.000000E-01	0.000000E-01	0.000000E-01
2418	0.000000E-01	0.000000E-01	0.000000E-01	0.000000E-01	0.000000E-01	0.000000E-01
2419	0.000000E-01	0.000000E-01	0.000000E-01	0.000000E-01	0.000000E-01	0.000000E-01
2420	0.000000E-01	0.000000E-01	0.000000E-01	0.000000E-01	0.000000E-01	0.000000E-01
2421	0.000000E-01	0.000000E-01	0.000000E-01	0.000000E-01	0.000000E-01	0.000000E-01
2422	0.000000E-01	0.000000E-01	0.000000E-01	0.000000E-01	0.000000E-01	0.000000E-01
2423	0.000000E-01	0.000000E-01	0.000000E-01	0.000000E-01	0.000000E-01	0.000000E-01
2424	0.000000E-01	0.000000E-01	0.000000E-01	0.000000E-01	0.000000E-01	0.000000E-01
2425	0.000000E-01	0.000000E-01	0.000000E-01	0.000000E-01	0.000000E-01	0.000000E-01
2426	0.000000E-01	0.000000E-01	0.000000E-01	0.000000E-01	0.000000E-01	0.000000E-01
2427	0.000000E-01	0.000000E-01	0.000000E-01	0.000000E-01	0.000000E-01	0.000000E-01
2428	0.000000E-01	0.000000E-01	0.000000E-01	0.000000E-01	0.000000E-01	0.000000E-01
2429	0.000000E-01	0.000000E-01	0.000000E-01	0.000000E-01	0.000000E-01	0.000000E-01
2430	0.000000E-01	0.000000E-01	0.000000E-01	0.000000E-01	0.000000E-01	0.000000E-01
2431	0.000000E-01	0.000000E-01	0.000000E-01	0.000000E-01	0.000000E-01	0.000000E-01
2432	0.000000E-01	0.000000E-01	0.000000E-01	0.000000E-01	0.000000E-01	0.000000E-01
2433	0.000000E-01	0.000000E-01	0.000000E-01	0.000000E-01	0.000000E-01	0.000000E-01
2434	0.000000E-01	0.000000E-01	0.000000E-01	0.000000E-01	0.000000E-01	0.000000E-01
2435	0.000000E-01	0.000000E-01	0.000000E-01	0.000000E-01	0.000000E-01	0.000000E-01
2436	0.000000E-01	0.000000E-01	0.000000E-01	0.000000E-01	0.000000E-01	0.000000E-01
2437	0.000000E-01	0.000000E-01	0.000000E-01	0.000000E-01	0.000000E-01	0.000000E-01
2438	0.000000E-01	0.000000E-01	0.000000E-01	0.000000E-01	0.000000E-01	0.000000E-01
2439	0.000000E-01	0.000000E-01	0.000000E-01	0.000000E-01	0.000000E-01	0.000000E-01

2444	[illegible]	[illegible]	[illegible]	[illegible]	[illegible]	[illegible]
2445	0.00000E-01	0.00000E-01	0.00000E-01	0.00000E-01	0.00000E-01	0.00000E-01
2446	0.00000E-01	0.00000E-01	0.00000E-01	0.00000E-01	0.00000E-01	0.00000E-01
2447	0.00000E-01	0.00000E-01	0.00000E-01	0.00000E-01	0.00000E-01	0.00000E-01
2448	0.00000E-01	0.00000E-01	0.00000E-01	0.00000E-01	0.00000E-01	0.00000E-01
2449	0.00000E-01	0.00000E-01	0.00000E-01	0.00000E-01	0.00000E-01	0.00000E-01
2450	0.00000E-01	0.00000E-01	0.00000E-01	0.00000E-01	0.00000E-01	0.00000E-01
2451	0.00000E-01	0.00000E-01	0.00000E-01	0.00000E-01	0.00000E-01	0.00000E-01
2452	0.00000E-01	0.00000E-01	0.00000E-01	0.00000E-01	0.00000E-01	0.00000E-01
2453	0.00000E-01	0.00000E-01	0.00000E-01	0.00000E-01	0.00000E-01	0.00000E-01
2454	0.00000E-01	0.00000E-01	0.00000E-01	0.00000E-01	0.00000E-01	0.00000E-01
2455	0.00000E-01	0.00000E-01	0.00000E-01	0.00000E-01	0.00000E-01	0.00000E-01
2456	0.00000E-01	0.00000E-01	0.00000E-01	0.00000E-01	0.00000E-01	0.00000E-01
2457	0.00000E-01	0.00000E-01	0.00000E-01	0.00000E-01	0.00000E-01	0.00000E-01
2458	-1.87524E-02	-2.76055E-03	-9.10143E-04	2.79266E-05	5.46118E-04	0.00000E-01
2459	-1.85077E-02	-1.74180E-03	-7.71679E-04	1.06600E-05	5.68949E-04	0.00000E-01
2460	-1.47684E-02	-1.34684E-03	-1.02081E-03	2.58532E-06	5.78897E-04	0.00000E-01
2461	-1.30668E-02	-9.46400E-04	-1.02081E-03	-2.53437E-06	5.78897E-04	0.00000E-01
2462	-1.13221E-02	-5.21456E-04	-9.97688E-04	-1.06589E-05	5.68954E-04	0.00000E-01
2463	-9.63753E-03	-3.90752E-03	-9.10211E-04	-2.79266E-05	5.46128E-04	0.00000E-01
2464	-8.72541E-02	-4.93547E-03	-3.80351E-03	-3.42202E-05	1.12505E-03	0.00000E-01
2465	-8.19442E-02	-4.66200E-03	-3.70675E-03	-2.60834E-05	1.12693E-03	0.00000E-01
2466	-8.30931E-02	-8.42890E-03	-3.97414E-03	-1.96274E-05	1.13863E-03	0.00000E-01
2467	-8.12759E-02	-8.09537E-03	-8.01923E-03	-1.20456E-05	1.14053E-03	0.00000E-01
2468	-2.95564E-02	-3.79235E-03	-8.04417E-03	-5.84793E-06	1.14560E-03	0.00000E-01
2469	-2.78580E-02	-3.49802E-03	-8.03175E-03	-1.84037E-09	1.14629E-03	0.00000E-01
2470	-2.61664E-02	-3.22247E-03	-8.04418E-03	-5.84420E-06	1.14561E-03	0.00000E-01
2471	-2.44538E-02	-2.96394E-03	-8.01925E-03	-1.20418E-05	1.14054E-03	0.00000E-01
2472	-2.26823E-02	-2.71938E-03	-3.97418E-03	-1.96230E-05	1.13564E-03	0.00000E-01
2473	-2.08345E-02	-2.54832E-03	-3.90679E-03	-2.60788E-05	1.12974E-03	0.00000E-01
2474	-1.86422E-02	-2.39488E-03	-3.80357E-03	-3.42235E-05	1.12506E-03	0.00000E-01
2475	-1.63311E-02	-8.55033E-03	-8.73857E-03	-4.58560E-05	1.07916E-03	0.00000E-01
2476	-1.95866E-02	-7.76954E-03	-8.94360E-03	-2.52033E-05	1.70525E-03	0.00000E-01
2477	-1.43450E-02	-7.14473E-03	-8.04157E-03	-8.19561E-06	1.71053E-03	0.00000E-01
2478	-1.92709E-02	-6.57582E-03	-8.04159E-03	-8.18772E-06	1.71056E-03	0.00000E-01
2479	-1.40416E-02	-6.07354E-03	-8.94367E-03	-2.51952E-05	1.70526E-03	0.00000E-01
2480	-1.82169E-02	-5.60910E-03	-8.73870E-03	-4.58473E-05	1.69918E-03	0.00000E-01
2481	-1.76189E-02	-1.20338E-02	-1.56861E-02	1.42253E-05	2.27188E-03	0.00000E-01
2482	-1.97781E-02	-1.25105E-02	-1.58106E-02	3.60401E-05	2.27293E-03	0.00000E-01
2483	-1.80854E-02	-1.22013E-02	-1.59084E-02	2.77176E-05	2.27176E-03	0.00000E-01
2484	-1.65541E-02	-1.18573E-02	-1.59775E-02	1.84510E-05	2.27615E-03	0.00000E-01
2485	-1.91273E-02	-1.15278E-02	-1.60180E-02	9.06076E-06	2.27697E-03	0.00000E-01
2486	-1.57549E-02	-1.12296E-02	-1.60325E-02	6.46897E-09	2.27741E-03	0.00000E-01
2487	-1.23814E-02	-1.09471E-02	-1.60180E-02	-9.04770E-06	2.27698E-03	0.00000E-01
2488	-1.89709E-02	-1.06756E-02	-1.59775E-02	-1.84379E-05	2.27616E-03	0.00000E-01
2489	-1.54682E-02	-1.04221E-02	-1.59085E-02	-2.77043E-05	2.27478E-03	0.00000E-01
2490	-1.18008E-02	-1.02155E-02	-1.58108E-02	-3.69268E-05	2.27294E-03	0.00000E-01
2491	-1.78274E-02	-1.00283E-02	-1.56863E-02	-4.42120E-05	2.27170E-03	0.00000E-01
2492	-1.19467E-02	-1.82813E-02	-2.46372E-02	4.84730E-05	2.84348E-03	0.00000E-01
2493	-1.25332E-02	-1.75579E-02	-2.48666E-02	3.85825E-05	2.84432E-03	0.00000E-01
2494	-1.39080E-02	-1.69037E-02	-2.49817E-02	9.59453E-06	2.84504E-03	0.00000E-01
2495	-1.53003E-02	-1.63227E-02	-2.49817E-02	-9.57573E-06	2.84507E-03	0.00000E-01
2496	-1.68971E-02	-1.58167E-02	-2.48667E-02	-2.85439E-05	2.84433E-03	0.00000E-01
2497	-1.75213E-02	-1.53629E-02	-2.46375E-02	-4.84542E-05	2.84331E-03	0.00000E-01
2498	-1.10065E-01	-2.45978E-02	-3.58868E-02	4.72154E-05	3.41354E-03	0.00000E-01
2499	-1.04372E-01	-2.42805E-02	-3.57172E-02	3.81597E-05	3.41374E-03	0.00000E-01
2500	-9.89715E-02	-2.39218E-02	-3.58185E-02	2.91674E-05	3.41398E-03	0.00000E-01
2501	-9.37626E-02	-2.33806E-02	-3.58910E-02	1.93013E-05	3.41391E-03	0.00000E-01
2502	-8.86800E-02	-2.32571E-02	-3.59346E-02	9.61480E-06	3.41403E-03	0.00000E-01
2503	-8.35305E-02	-2.29612E-02	-3.59491E-02	1.22525E-08	3.41392E-03	0.00000E-01
2504	-7.86235E-02	-2.28622E-02	-3.59347E-02	-9.59530E-06	3.41404E-03	0.00000E-01
2505	-7.35430E-02	-2.24130E-02	-3.58912E-02	-1.93379E-05	3.41372E-03	0.00000E-01
2506	-6.83560E-02	-2.21600E-02	-3.58187E-02	-2.91428E-05	3.41349E-03	0.00000E-01
2507	-6.27881E-02	-2.17412E-02	-3.57173E-02	-3.81307E-05	3.41376E-03	0.00000E-01
2508	-5.72887E-02	-2.17391E-02	-3.55871E-02	-4.71904E-05	3.41357E-03	0.00000E-01
2509	-1.28116E-01	-3.17310E-02	-4.05[illegible]8E-02	4.36012E-05	3.98535E-03	0.00000E-01
2510	-1.15370E-01	-3.12248E-02	-4.07635E-02	2.88612E-05	3.98528E-03	0.00000E-01
2511	-1.03139E-01	-3.08852E-02	-4.08776E-02	9.70417E-06	3.98529E-03	0.00000E-01
2512	-9.17601E-02	-3.00044E-02	-4.08797E-02	-9.67349E-06	3.98529E-03	0.00000E-01
2513	-7.99167E-02	-2.94754E-02	-4.07630E-02	-2.[illegible]505E-05	3.98533E-03	0.00000E-01
[illegible]	[illegible]	[illegible]	[illegible]	[illegible]	[illegible]	[illegible]

2538	1.387779E-01	-3.982414E-02	-6.360026E-02	3.840306E-05	4.552782E-03	0.000006-01
2539	1.317326E-01	-3.781316E-02	-6.370166E-02	2.911296E-05	4.552726E-03	0.000006-01
2540	1.248976E-01	-3.917716E-02	-6.377406E-02	1.936966E-05	4.552716E-03	0.000006-01
2541	1.181896E-01	-3.883756E-02	-6.381746E-02	9.612406E-06	4.552716E-03	0.000006-01
2542	1.115456E-01	-3.856226E-02	-6.383206E-02	1.548146E-08	4.552686E-03	0.000006-01
2543	1.049966E-01	-3.828316E-02	-6.381756E-02	-9.573446E-06	4.552666E-03	0.000006-01
2544	9.820206E-02	-3.801546E-02	-6.377426E-02	-1.935266E-05	4.552726E-03	0.000006-01
2545	9.137136E-02	-3.776446E-02	-6.370176E-02	-2.907806E-05	4.552746E-03	0.000006-01
2546	8.453626E-02	-3.753796E-02	-6.360076E-02	-3.836606E-05	4.552786E-03	0.000006-01
2547	7.701346E-02	-3.732836E-02	-6.347076E-02	-4.766516E-05	4.552736E-03	0.000006-01
2548	1.640646E-01	-4.943086E-02	-8.040126E-02	4.853986E-05	5.122166E-03	0.000006-01
2549	1.480376E-01	-4.871306E-02	-8.063236E-02	2.684516E-05	5.122116E-03	0.000006-01
2550	1.329286E-01	-4.807506E-02	-8.074836E-02	9.683076E-06	5.122096E-03	0.000006-01
2551	1.180576E-01	-4.747406E-02	-8.074846E-02	-9.657476E-06	5.122106E-03	0.000006-01
2552	1.029306E-01	-4.687236E-02	-8.063296E-02	-2.880196E-05	5.122136E-03	0.000006-01
2553	8.697086E-02	-4.653176E-02	-8.040196E-02	-4.829636E-05	5.122176E-03	0.000006-01
2554	1.819036E-01	-5.955586E-02	-9.952526E-02	4.789746E-05	5.691546E-03	0.000006-01
2555	1.729936E-01	-5.919836E-02	-9.945536E-02	3.846496E-05	5.691586E-03	0.000006-01
2556	1.643646E-01	-5.885706E-02	-9.955646E-02	2.903686E-05	5.691566E-03	0.000006-01
2557	1.557126E-01	-5.852446E-02	-9.962876E-02	1.932206E-05	5.691546E-03	0.000006-01
2558	1.476376E-01	-5.820756E-02	-9.967216E-02	9.608656E-06	5.691536E-03	0.000006-01
2559	1.394396E-01	-5.791226E-02	-9.968666E-02	2.490006E-09	5.691526E-03	0.000006-01
2560	1.312226E-01	-5.763246E-02	-9.967236E-02	-9.558856E-06	5.691546E-03	0.000006-01
2561	1.229406E-01	-5.736316E-02	-9.962906E-02	-1.927226E-05	5.691536E-03	0.000006-01
2562	1.147246E-01	-5.711456E-02	-9.955646E-02	-2.898706E-05	5.691576E-03	0.000006-01
2563	1.058976E-01	-5.688576E-02	-9.945546E-02	-3.841316E-05	5.691376E-03	0.000006-01
2564	9.649016E-02	-5.666966E-02	-9.932606E-02	-4.784766E-05	5.691576E-03	0.000006-01
2565	1.997136E-01	-7.060476E-02	-1.202426E-01	1.925216E-05	6.260966E-03	0.000006-01
2566	1.806256E-01	-6.987546E-02	-1.204736E-01	2.885506E-05	6.260956E-03	0.000006-01
2567	1.623746E-01	-6.923386E-02	-1.205896E-01	9.675296E-06	6.260966E-03	0.000006-01
2568	1.443976E-01	-6.867576E-02	-1.205896E-01	-9.612986E-06	6.260976E-03	0.000006-01
2569	1.261526E-01	-6.816156E-02	-1.204716E-01	-2.877876E-05	6.260776E-03	0.000006-01
2570	1.070706E-01	-6.770856E-02	-1.202436E-01	-4.814946E-05	6.260996E-03	0.000006-01
2571	2.174626E-01	-8.253756E-02	-1.441526E-01	1.930326E-05	6.830376E-03	0.000006-01
2572	2.070176E-01	-8.218006E-02	-1.432826E-01	3.850916E-05	6.830376E-03	0.000006-01
2573	1.968526E-01	-8.183816E-02	-1.433836E-01	2.877356E-05	6.830396E-03	0.000006-01
2574	1.868966E-01	-8.150016E-02	-1.434556E-01	1.930676E-05	6.830386E-03	0.000006-01
2575	1.770776E-01	-8.117376E-02	-1.434976E-01	9.617206E-06	6.830376E-03	0.000006-01
2576	1.673316E-01	-8.086756E-02	-1.435136E-01	3.139216E-08	6.830386E-03	0.000006-01
2577	1.575836E-01	-8.061706E-02	-1.434976E-01	-9.339506E-06	6.830386E-03	0.000006-01
2578	1.477696E-01	-8.035006E-02	-1.434566E-01	-1.924396E-05	6.830376E-03	0.000006-01
2579	1.378166E-01	-8.007806E-02	-1.433046E-01	-2.893286E-05	6.830396E-03	0.000006-01
2580	1.276546E-01	-7.986546E-02	-1.432836E-01	-3.843736E-05	6.830396E-03	0.000006-01
2581	1.172106E-01	-7.964776E-02	-1.431536E-01	-4.794046E-05	6.830396E-03	0.000006-01
2582	2.351526E-01	-9.535986E-02	-1.680126E-01	4.821816E-05	7.399796E-03	0.000006-01
2583	2.130436E-01	-9.465526E-02	-1.682866E-01	2.887216E-05	7.399796E-03	0.000006-01
2584	1.917736E-01	-9.401606E-02	-1.684026E-01	9.677806E-06	7.399796E-03	0.000006-01
2585	1.707816E-01	-9.343636E-02	-1.684026E-01	-9.608496E-06	7.399806E-03	0.000006-01
2586	1.495166E-01	-9.292006E-02	-1.682676E-01	-2.880286E-05	7.399806E-03	0.000006-01
2587	1.274076E-01	-9.246396E-02	-1.680366E-01	-4.814886E-05	7.399816E-03	0.000006-01
2588	2.527826E-01	-1.090416E-01	-1.949506E-01	4.805766E-05	7.969206E-03	0.000006-01
2589	2.408506E-01	-1.086836E-01	-1.950806E-01	3.851776E-05	7.969206E-03	0.000006-01
2590	2.291996E-01	-1.083436E-01	-1.951826E-01	2.898226E-05	7.969216E-03	0.000006-01
2591	2.177376E-01	-1.080186E-01	-1.952546E-01	1.930526E-05	7.969216E-03	0.000006-01
2592	2.064556E-01	-1.077036E-01	-1.952976E-01	9.628216E-06	7.969216E-03	0.000006-01
2593	1.952226E-01	-1.074066E-01	-1.953126E-01	3.791166E-08	7.969216E-03	0.000006-01
2594	1.839906E-01	-1.071256E-01	-1.952986E-01	-9.562386E-06	7.969226E-03	0.000006-01
2595	1.726906E-01	-1.068536E-01	-1.952546E-01	-1.922136E-05	7.969226E-03	0.000006-01
2596	1.612506E-01	-1.066066E-01	-1.951826E-01	-2.890646E-05	7.969226E-03	0.000006-01
2597	1.496016E-01	-1.063706E-01	-1.950816E-01	-3.841396E-05	7.969236E-03	0.000006-01
2598	1.376696E-01	-1.061506E-01	-1.949526E-01	-4.792186E-05	7.969236E-03	0.000006-01
2599	2.703546E-01	-1.238506E-01	-2.238596E-01	4.821346E-05	8.538626E-03	0.000006-01
2600	2.465206E-01	-1.229826E-01	-2.240706E-01	2.888476E-05	8.538626E-03	0.000006-01
2601	2.211256E-01	-1.222146E-01	-2.241866E-01	9.682776E-06	8.538636E-03	0.000006-01
2602	1.972116E-01	-1.216656E-01	-2.241866E-01	-9.600426E-06	8.538636E-03	0.000006-01
2603	1.736206E-01	-1.211466E-01	-2.240716E-01	-2.880246E-05	8.538616E-03	0.000006-01
2604	1.479886E-01	-1.206876E-01	-2.238406E-01	-4.813116E-05	8.538656E-03	0.000006-01
2605	2.878666E-01	-1.387366E-01	-2.347216E-01	4.806756E-05	9.108046E-03	0.000006-01

2610	[illegible]	[illegible]	[illegible]	[illegible]	[illegible]	[illegible]
2611	2.10443E-01	-1.37045E-01	-2.53068E-01	-9.54735E-06	9.10805E-03	0.00000E-01
2612	1.97704E-01	-1.36778E-01	-2.53025E-01	-1.92217E-05	9.10805E-03	0.00000E-01
2613	1.84926E-01	-1.36525E-01	-2.52933E-01	-2.88758E-05	9.10806E-03	0.00000E-01
2614	1.71737E-01	-1.36287E-01	-2.52852E-01	-3.84381E-05	9.10806E-03	0.00000E-01
2615	1.58367E-01	-1.36044E-01	-2.52722E-01	-4.79306E-05	9.10806E-03	0.00000E-01
2616	3.05318E-01	-1.35154E-01	-2.87595E-01	4.82254E-05	9.67765E-03	0.00000E-01
2617	2.77458E-01	-1.34463E-01	-2.87827E-01	2.88893E-05	9.67746E-03	0.00000E-01
2618	2.50431E-01	-1.33828E-01	-2.87967E-01	9.68918E-06	9.67746E-03	0.00000E-01
2617	2.23686E-01	-1.33230E-01	-2.87913E-01	-9.57579E-06	9.67747E-03	0.00000E-01
2620	1.96667E-01	-1.32729E-01	-2.87528E-01	-2.87439E-05	9.67748E-03	0.00000E-01
2621	1.69806E-01	-1.32266E-01	-2.87577E-01	-1.81305E-05	9.67749E-03	0.00000E-01
2622	3.22711E-01	-1.72172E-01	-3.22663E-01	4.80406E-05	1.02469E-02	0.00000E-01
2623	3.07930E-01	-1.71817E-01	-3.22593E-01	3.83217E-05	1.02469E-02	0.00000E-01
2624	2.93469E-01	-1.71480E-01	-3.22694E-01	2.90017E-05	1.02469E-02	0.00000E-01
2625	2.79170E-01	-1.71155E-01	-3.22767E-01	1.93220E-05	1.02469E-02	0.00000E-01
2626	2.65066E-01	-1.70845E-01	-3.22810E-01	9.64185E-06	1.02469E-02	0.00000E-01
2627	2.51003E-01	-1.70548E-01	-3.22825E-01	5.07583E-08	1.02469E-02	0.00000E-01
2628	2.36942E-01	-1.70266E-01	-3.22810E-01	-9.53993E-06	1.02469E-02	0.00000E-01
2629	2.22812E-01	-1.69998E-01	-3.22787E-01	-1.92201E-05	1.02469E-02	0.00000E-01
2630	2.08543E-01	-1.69744E-01	-3.22693E-01	-2.88998E-05	1.02469E-02	0.00000E-01
2631	1.94065E-01	-1.69503E-01	-3.22596E-01	-3.84193E-05	1.02469E-02	0.00000E-01
2632	1.79304E-01	-1.69279E-01	-3.22464E-01	-4.79387E-05	1.02469E-02	0.00000E-01
2633	3.40043E-01	-1.89983E-01	-3.59523E-01	4.82647E-05	1.08163E-02	0.00000E-01
2634	3.09448E-01	-1.89293E-01	-3.59555E-01	2.88846E-05	1.08163E-02	0.00000E-01
2635	2.79689E-01	-1.88650E-01	-3.59671E-01	9.64773E-06	1.08163E-02	0.00000E-01
2636	2.50208E-01	-1.88080E-01	-3.59671E-01	-9.58932E-06	1.08163E-02	0.00000E-01
2637	2.20455E-01	-1.87557E-01	-3.59556E-01	-2.87812E-05	1.08163E-02	0.00000E-01
2638	1.89862E-01	-1.87059E-01	-3.59325E-01	-3.81562E-05	1.08163E-02	0.00000E-01
2639	3.37320E-01	-2.08570E-01	-3.98177E-01	4.79528E-05	1.13857E-02	0.00000E-01
2640	3.12126E-01	-2.08227E-01	-3.98307E-01	3.84994E-05	1.13857E-02	0.00000E-01
2641	2.88392E-01	-2.07887E-01	-3.98408E-01	2.90376E-05	1.13857E-02	0.00000E-01
2642	3.09777E-01	-2.07566E-01	-3.98481E-01	1.93433E-05	1.13857E-02	0.00000E-01
2643	2.94301E-01	-2.07258E-01	-3.98524E-01	9.64018E-06	1.13857E-02	0.00000E-01
2644	2.78893E-01	-2.06960E-01	-3.98539E-01	5.74528E-08	1.13857E-02	0.00000E-01
2645	2.63487E-01	-2.06677E-01	-3.98524E-01	-9.53320E-06	1.13857E-02	0.00000E-01
2646	2.48013E-01	-2.06407E-01	-3.98481E-01	-1.92265E-05	1.13857E-02	0.00000E-01
2647	2.32403E-01	-2.06154E-01	-3.98409E-01	-2.87247E-05	1.13857E-02	0.00000E-01
2648	2.16583E-01	-2.05912E-01	-3.98308E-01	-3.83845E-05	1.13857E-02	0.00000E-01
2649	2.00479E-01	-2.05684E-01	-3.98179E-01	-4.78479E-05	1.13857E-02	0.00000E-01
2650	3.74535E-01	-2.27941E-01	-4.39023E-01	4.83493E-05	1.19531E-02	0.00000E-01
2651	3.41300E-01	-2.27236E-01	-4.39283E-01	2.88760E-05	1.19531E-02	0.00000E-01
2652	3.08900E-01	-2.26625E-01	-4.39371E-01	9.71287E-06	1.19532E-02	0.00000E-01
2653	2.78778E-01	-2.26015E-01	-4.39371E-01	-9.59153E-06	1.19532E-02	0.00000E-01
2654	2.44385E-01	-2.25520E-01	-4.39286E-01	-2.87747E-05	1.19531E-02	0.00000E-01
2655	2.11157E-01	-2.25049E-01	-4.39025E-01	-4.82280E-05	1.19531E-02	0.00000E-01
2656	3.41690E-01	-2.48063E-01	-4.81862E-01	4.77730E-05	1.25245E-02	0.00000E-01
2657	3.74291E-01	-2.47713E-01	-4.81993E-01	3.84447E-05	1.25245E-02	0.00000E-01
2658	3.57174E-01	-2.47376E-01	-4.82094E-01	2.90979E-05	1.25245E-02	0.00000E-01
2659	3.40263E-01	-2.47053E-01	-4.82167E-01	1.93835E-05	1.25245E-02	0.00000E-01
2660	3.23469E-01	-2.46746E-01	-4.82210E-01	9.66261E-06	1.25246E-02	0.00000E-01
2661	3.06792E-01	-2.46430E-01	-4.82225E-01	5.38784E-08	1.25246E-02	0.00000E-01
2662	2.90076E-01	-2.46167E-01	-4.82211E-01	-9.53486E-06	1.25246E-02	0.00000E-01
2663	2.73307E-01	-2.45879E-01	-4.82167E-01	-1.92578E-05	1.25246E-02	0.00000E-01
2664	2.56403E-01	-2.45643E-01	-4.82095E-01	-2.89702E-05	1.25246E-02	0.00000E-01
2665	2.37892E-01	-2.45379E-01	-4.81994E-01	-3.81170E-05	1.25246E-02	0.00000E-01
2666	2.21896E-01	-2.45167E-01	-4.81864E-01	-4.76452E-05	1.25246E-02	0.00000E-01
2667	4.00788E-01	-2.69922E-01	-5.26673E-01	4.85033E-05	1.30937E-02	0.00000E-01
2668	3.70013E-01	-2.69741E-01	-5.26976E-01	2.89451E-05	1.30940E-02	0.00000E-01
2669	3.53[illegible]E-01	-2.67619E-01	-5.27043E-01	9.74262E-06	1.30940E-02	0.00000E-01
2670	3.03388E-01	-2.67032E-01	-5.27043E-01	-9.60857E-06	1.30940E-02	0.00000E-01
2671	2.69436E-01	-2.66503E-01	-5.26978E-01	-2.88110E-05	1.30940E-02	0.00000E-01
2672	2.32694E-01	-2.66032E-01	-5.26807E-01	-4.68492E-05	1.30939E-02	0.00000E-01
2673	4.23821E-01	-2.98513E-01	-5.73520E-01	4.73799E-05	1.36636E-02	0.00000E-01
2674	4.07177E-01	-2.98166E-01	-5.73650E-01	3.82236E-05	1.36635E-02	0.00000E-01
2675	3.88817E-01	-2.97829E-01	-5.73752E-01	2.91241E-05	1.36633E-02	0.00000E-01
2676	3.70658E-01	-2.97509E-01	-5.73824E-01	1.93956E-05	1.36633E-02	0.00000E-01
2677	3.52662E-01	-2.97202E-01	-5.73868E-01	9.67642E-06	1.36633E-02	0.00000E-01
2678	3.34669E-01	-2.96905E-01	-5.73883E-01	7.91261E-08	1.36634E-02	0.00000E-01
2679	3.16709E-01	-2.96623E-01	-5.73869E-01	-9.53616E-06	1.36633E-02	0.00000E-01
[illegible]	[illegible]	[illegible]	[illegible]	[illegible]	[illegible]	[illegible]

2681	2.803452E-01	-2.880172E-01	-5.737352E-01	-2.878192E-05	1.388888E-02	0.000000E-01
2682	2.821946E-01	-2.870511E-01	-5.736526E-01	-3.806834E-05	1.386835E-02	0.000000E-01
2683	2.135335E-01	-2.876168E-01	-5.735226E-01	-4.723468E-05	1.386637E-02	0.000000E-01
2684	2.427746E-01	-3.128126E-01	-6.225360E-01	4.855849E-05	1.423335E-02	0.000000E-01
2685	2.045853E-01	-3.121376E-01	-6.225706E-01	2.975022E-05	1.423329E-02	0.000000E-01
2686	3.671876E-01	-3.115066E-01	-6.226066E-01	9.680788E-06	1.423324E-02	0.000000E-01
2687	3.300416E-01	-3.109286E-01	-6.226066E-01	-7.884576E-06	1.423324E-02	0.000000E-01
2688	2.926856E-01	-3.103496E-01	-6.225726E-01	-2.868040E-05	1.423296E-02	0.000000E-01
2689	2.544806E-01	-3.097236E-01	-6.225426E-01	-4.841286E-05	1.423336E-02	0.000000E-01
2690	2.597026E-01	-3.358216E-01	-6.731576E-01	4.443726E-05	1.480486E-02	0.000000E-01
2691	1.998736E-01	-3.334716E-01	-6.732636E-01	3.650546E-05	1.480386E-02	0.000000E-01
2692	1.208206E-01	-3.351536E-01	-6.733876E-01	2.795316E-05	1.480246E-02	0.000000E-01
2693	1.007676E-01	-3.348156E-01	-6.734526E-01	1.868236E-05	1.480146E-02	0.000000E-01
2694	3.817816E-01	-3.345106E-01	-6.734946E-01	9.253006E-06	1.480086E-02	0.000000E-01
2695	3.623556E-01	-3.342136E-01	-6.733076E-01	7.375816E-06	1.480046E-02	0.000000E-01
2696	3.433836E-01	-3.339316E-01	-6.734946E-01	-9.101136E-06	1.480086E-02	0.000000E-01
2697	3.241566E-01	-3.336636E-01	-6.734536E-01	-1.850036E-05	1.480146E-02	0.000000E-01
2698	3.048216E-01	-3.334086E-01	-6.733846E-01	-2.780156E-05	1.480246E-02	0.000000E-01
2699	2.852916E-01	-3.331546E-01	-6.732856E-01	-3.683396E-05	1.480386E-02	0.000000E-01
2700	2.654726E-01	-3.329136E-01	-6.731596E-01	-4.478556E-05	1.480486E-02	0.000000E-01
2701	4.755626E-01	-3.594956E-01	-7.259756E-01	4.677916E-05	1.537656E-02	0.000000E-01
2702	4.560296E-01	-3.588286E-01	-7.261876E-01	2.632956E-05	1.537196E-02	0.000000E-01
2703	4.362666E-01	-3.581936E-01	-7.262906E-01	8.661986E-06	1.536796E-02	0.000000E-01
2704	3.567326E-01	-3.576176E-01	-7.262916E-01	-8.505016E-06	1.536796E-02	0.000000E-01
2705	3.170006E-01	-3.570886E-01	-7.261896E-01	-2.617286E-05	1.537196E-02	0.000000E-01
2706	2.765236E-01	-3.566136E-01	-7.259786E-01	-4.642286E-05	1.537656E-02	0.000000E-01
2707	4.953316E-01	-3.938766E-01	-7.808016E-01	3.688876E-05	1.594996E-02	0.000000E-01
2708	4.723676E-01	-3.835246E-01	-7.809126E-01	2.853416E-05	1.594826E-02	0.000000E-01
2709	4.517096E-01	-3.831786E-01	-7.809876E-01	2.151216E-05	1.594156E-02	0.000000E-01
2710	4.311946E-01	-3.828626E-01	-7.810396E-01	1.360156E-05	1.593776E-02	0.000000E-01
2711	4.107936E-01	-3.825376E-01	-7.810496E-01	6.733906E-06	1.593376E-02	0.000000E-01
2712	3.906396E-01	-3.822596E-01	-7.810796E-01	8.089646E-08	1.593336E-02	0.000000E-01
2713	3.700876E-01	-3.819766E-01	-7.810676E-01	-6.572546E-06	1.593376E-02	0.000000E-01
2714	3.497006E-01	-3.817036E-01	-7.810406E-01	-1.344046E-05	1.593776E-02	0.000000E-01
2715	3.292076E-01	-3.814436E-01	-7.809796E-01	-2.133126E-05	1.594156E-02	0.000000E-01
2716	3.086966E-01	-3.811796E-01	-7.808916E-01	-2.837346E-05	1.594826E-02	0.000000E-01
2717	2.876506E-01	-3.809246E-01	-7.808046E-01	-3.672346E-05	1.594996E-02	0.000000E-01
2718	5.160286E-01	-4.088736E-01	-8.376606E-01	3.310886E-05	1.652696E-02	0.000000E-01
2719	4.673436E-01	-4.082076E-01	-8.377606E-01	1.523186E-05	1.650886E-02	0.000000E-01
2720	4.253126E-01	-4.075386E-01	-8.378266E-01	4.396666E-06	1.650096E-02	0.000000E-01
2721	3.834336E-01	-4.068586E-01	-8.378276E-01	-4.232506E-06	1.650096E-02	0.000000E-01
2722	3.414686E-01	-4.064216E-01	-8.377626E-01	-1.306776E-05	1.650886E-02	0.000000E-01
2723	2.989286E-01	-4.059616E-01	-8.376626E-01	-2.294536E-05	1.652686E-02	0.000000E-01
2724	5.266026E-01	-4.346986E-01	-8.965086E-01	8.031546E-06	1.709006E-02	0.000000E-01
2725	5.046986E-01	-4.343156E-01	-8.965346E-01	6.400046E-06	1.707966E-02	0.000000E-01
2726	4.829696E-01	-4.339476E-01	-8.965566E-01	4.702746E-06	1.707796E-02	0.000000E-01
2727	4.613606E-01	-4.335926E-01	-8.965716E-01	3.223156E-06	1.707706E-02	0.000000E-01
2728	4.398266E-01	-4.332616E-01	-8.965816E-01	1.704666E-06	1.707656E-02	0.000000E-01
2729	4.183286E-01	-4.329026E-01	-8.965846E-01	8.281616E-08	1.707636E-02	0.000000E-01
2730	3.968326E-01	-4.325646E-01	-8.965826E-01	-1.539026E-06	1.707656E-02	0.000000E-01
2731	3.753076E-01	-4.322296E-01	-8.965726E-01	-3.057496E-06	1.707706E-02	0.000000E-01
2732	3.537296E-01	-4.319066E-01	-8.965576E-01	-4.537056E-06	1.707796E-02	0.000000E-01
2733	3.320446E-01	-4.315916E-01	-8.965386E-01	-6.234316E-06	1.707966E-02	0.000000E-01
2734	3.102866E-01	-4.312906E-01	-8.965106E-01	-7.865096E-06	1.708806E-02	0.000000E-01
2746	3.188716E-01	-4.279666E-01	-9.819716E-01	-6.486696E-06	1.710166E-02	0.000000E-01
2747	3.630546E-01	-4.684776E-01	-9.820046E-01	-4.340086E-06	1.710086E-02	0.000000E-01
2748	4.069866E-01	-4.691396E-01	-9.820226E-01	-1.414796E-06	1.709976E-02	0.000000E-01
2749	4.508136E-01	-4.698596E-01	-9.820216E-01	1.580176E-06	1.709996E-02	0.000000E-01
2750	4.947816E-01	-4.706536E-01	-9.820026E-01	4.368506E-06	1.710086E-02	0.000000E-01
2751	5.390696E-01	-4.715116E-01	-9.819656E-01	6.652196E-06	1.710166E-02	0.000000E-01
2752	5.274876E-01	-5.051166E-01	-1.067546E+00	-5.963346E-06	1.712376E-02	0.000000E-01
2753	5.499986E-01	-5.054256E-01	-1.067556E+00	-4.702406E-06	1.712376E-02	0.000000E-01
2754	5.723196E-01	-5.057476E-01	-1.067576E+00	-3.380706E-06	1.712356E-02	0.000000E-01
2755	5.946186E-01	-5.060776E-01	-1.067576E+00	-2.292396E-06	1.712356E-02	0.000000E-01
2756	1.171256E-01	-5.064226E-01	-1.067586E+00	-1.152646E-06	1.712316E-02	0.000000E-01
2757	8.394716E-01	-5.067826E-01	-1.067586E+00	8.270656E-08	1.712316E-02	0.000000E-01
2758	4.617926E-01	-5.071586E-01	-1.067586E+00	1.318086E-06	1.712316E-02	0.000000E-01
2759	4.844196E-01	-5.075366E-01	-1.067576E+00	2.457826E-06	1.712356E-02	0.000000E-01
2760	5.065346E-01	-5.079286E-01	-1.067566E+00	3.846156E-06	1.712356E-02	0.000000E-01
2761	5.290056E-01	-5.083306E-01	-1.067556E+00	4.867856E-06	1.712376E-02	0.000000E-01
2762	5.513156E-01	-5.087436E-01	-1.067536E+00	6.128806E-06	1.712376E-02	0.000000E-01
2763	5.734116E-01	-5.091776E-01	-1.067506E+00	7.698196E-06	1.712436E-02	0.000000E-01

2765	4.27344E-01	-5.44329E-01	-1.15325E+00	-1.07839E-06	1.71460E-02	0.00000E-01
2766	4.72747E-01	-5.45054E-01	-1.15325E+00	1.24372E-06	1.71460E-02	0.00000E-01
2767	5.18242E-01	-5.45839E-01	-1.15324E+00	3.65605E-06	1.71461E-02	0.00000E-01
2768	5.63962E-01	-5.46667E-01	-1.15321E+00	5.77450E-06	1.71463E-02	0.00000E-01
2769	3.44902E-01	-5.81540E-01	-1.23900E+00	-5.71733E-06	1.71688E-02	0.00000E-01
2770	3.88137E-01	-5.81856E-01	-1.23901E+00	-4.48421E-06	1.71688E-02	0.00000E-01
2771	3.91335E-01	-5.82185E-01	-1.23903E+00	-3.25803E-06	1.71688E-02	0.00000E-01
2772	4.14459E-01	-5.82514E-01	-1.23905E+00	-2.17410E-06	1.71688E-02	0.00000E-01
2773	4.37845E-01	-5.82855E-01	-1.23904E+00	-1.09662E-06	1.71688E-02	0.00000E-01
2774	4.60614E-01	-5.83217E-01	-1.23904E+00	8.26234E-08	1.71688E-02	0.00000E-01
2775	4.83604E-01	-5.83591E-01	-1.23904E+00	1.26186E-06	1.71688E-02	0.00000E-01
2776	5.06773E-01	-5.83968E-01	-1.23903E+00	2.33935E-06	1.71688E-02	0.00000E-01
2777	5.29912E-01	-5.84358E-01	-1.23902E+00	3.42529E-06	1.71688E-02	0.00000E-01
2778	5.53097E-01	-5.84769E-01	-1.23901E+00	4.44946E-06	1.71688E-02	0.00000E-01
2779	5.76356E-01	-5.85194E-01	-1.23900E+00	5.88258E-06	1.71688E-02	0.00000E-01
2780	3.33709E-01	-6.20677E-01	-1.32490E+00	-5.54128E-06	1.71915E-02	0.00000E-01
2781	4.00845E-01	-6.21300E-01	-1.32493E+00	-3.36125E-06	1.71915E-02	0.00000E-01
2782	4.47760E-01	-6.21986E-01	-1.32494E+00	-1.03396E-06	1.71915E-02	0.00000E-01
2783	4.94608E-01	-6.22710E-01	-1.32494E+00	1.19410E-06	1.71915E-02	0.00000E-01
2784	5.41537E-01	-6.23492E-01	-1.32493E+00	3.52640E-06	1.71915E-02	0.00000E-01
2785	5.88684E-01	-6.24306E-01	-1.32490E+00	5.70643E-06	1.71915E-02	0.00000E-01
2786	5.82583E-01	-6.60350E-01	-1.41071E+00	-3.67805E-06	1.72142E-02	0.00000E-01
2787	3.88521E-01	-6.60677E-01	-1.41093E+00	-4.45767E-06	1.72142E-02	0.00000E-01
2788	4.10378E-01	-6.61017E-01	-1.41094E+00	-3.22911E-06	1.72142E-02	0.00000E-01
2789	4.34208E-01	-6.61344E-01	-1.41095E+00	-2.16426E-06	1.72142E-02	0.00000E-01
2790	4.57987E-01	-6.61684E-01	-1.41095E+00	-1.09538E-06	1.72142E-02	0.00000E-01
2791	4.81750E-01	-6.62045E-01	-1.41096E+00	8.25204E-08	1.72142E-02	0.00000E-01
2792	5.05514E-01	-6.62418E-01	-1.41095E+00	1.28840E-06	1.72142E-02	0.00000E-01
2793	5.29301E-01	-6.62791E-01	-1.41095E+00	2.32930E-06	1.72142E-02	0.00000E-01
2794	5.53127E-01	-6.63174E-01	-1.41094E+00	3.39415E-06	1.72142E-02	0.00000E-01
2795	5.77001E-01	-6.63597E-01	-1.41093E+00	4.62271E-06	1.72142E-02	0.00000E-01
2796	6.00752E-01	-6.64030E-01	-1.41071E+00	5.84309E-06	1.72142E-02	0.00000E-01
2797	3.71508E-01	-7.00632E-01	-1.49704E+00	-5.54971E-06	1.72368E-02	0.00000E-01
2798	4.19977E-01	-7.01253E-01	-1.49707E+00	-3.39179E-06	1.72369E-02	0.00000E-01
2799	4.662[illegible]-01	-7.01947E-01	-1.49708E+00	-1.03725E-06	1.72369E-02	0.00000E-01
2800	5.1340[illegible]-01	-7.02671E-01	-1.49708E+00	1.20217E-06	1.72367E-02	0.00000E-01
2801	5.64670E-01	-7.03455E-01	-1.49707E+00	3.55672E-06	1.72369E-02	0.00000E-01
2802	6.13130E-01	-7.04247E-01	-1.49704E+00	5.71464E-06	1.72368E-02	0.00000E-01
2803	3.80501E-01	-7.41369E-01	-1.58328E+00	-5.86297E-06	1.72595E-02	0.00000E-01
2804	4.05110E-01	-7.41719E-01	-1.58330E+00	-4.55267E-06	1.72595E-02	0.00000E-01
2805	4.29600E-01	-7.42078E-01	-1.58331E+00	-3.25256E-06	1.72595E-02	0.00000E-01
2806	4.54060E-01	-7.42404E-01	-1.58332E+00	-2.18339E-06	1.72596E-02	0.00000E-01
2807	4.78475E-01	-7.42730E-01	-1.58332E+00	-1.12473E-06	1.72596E-02	0.00000E-01
2808	5.02874E-01	-7.43096E-01	-1.58332E+00	8.24073E-08	1.72597E-02	0.00000E-01
2809	5.27284E-01	-7.43465E-01	-1.58332E+00	1.28955E-06	1.72596E-02	0.00000E-01
2810	5.51717E-01	-7.43829E-01	-1.58332E+00	2.34820E-06	1.72596E-02	0.00000E-01
2811	5.76181E-01	-7.44206E-01	-1.58331E+00	3.41734E-06	1.72595E-02	0.00000E-01
2812	6.00718E-01	-7.44643E-01	-1.58330E+00	4.71748E-06	1.72593E-02	0.00000E-01
2813	6.25287E-01	-7.45104E-01	-1.58328E+00	6.02775E-06	1.72595E-02	0.00000E-01
2814	3.89622E-01	-7.82742E-01	-1.66964E+00	-5.70074E-06	1.72819E-02	0.00000E-01
2815	4.39281E-01	-7.83340E-01	-1.66966E+00	-3.64788E-06	1.72822E-02	0.00000E-01
2816	4.88733E-01	-7.84043E-01	-1.66968E+00	-1.12766E-06	1.72825E-02	0.00000E-01
2817	5.38144E-01	-7.84776E-01	-1.66968E+00	1.29235E-06	1.72825E-02	0.00000E-01
2818	5.87663E-01	-7.85561E-01	-1.66966E+00	3.81256E-06	1.72822E-02	0.00000E-01
2819	6.37119E-01	-7.86309E-01	-1.66963E+00	5.86542E-06	1.72819E-02	0.00000E-01
2820	3.98804E-01	-8.24338E-01	-1.75810E+00	-6.4767/E-06	1.73042E-02	0.00000E-01
2821	4.23850E-01	-8.24782E-01	-1.75812E+00	-5.06893E-06	1.73044E-02	0.00000E-01
2822	4.49017E-01	-8.25145E-01	-1.75813E+00	-3.53338E-06	1.7304/E-02	0.00000E-01
2823	4.74010E-01	-8.25495E-01	-1.75814E+00	-2.45564E-06	1.73052E-02	0.00000E-01
2824	4. 0777E-01	-8.25831E-01	-1.75813E+00	-1.27031E-06	1.73056E-02	0.00000E-01
2825	5. 5005E-01	-8.26195E-01	-1.75815E+00	8.22850E-08	1.73056E-02	0.00000E-01
2826	5.48785E-01	-8.26560E-01	-1.75815E+00	1.43188E-06	1.73056E-02	0.00000E-01
2827	5.74018E-01	-8.26952E-01	-1.75814E+00	2.62020E-06	1.73052E-02	0.00000E-01
2828	5.99126E-01	-8.27335E-01	-1.75813E+00	3.69792E-06	1.73047E-02	0.00000E-01
2829	6.24198E-01	-8.27842E-01	-1.75812E+00	5.23143E-06	1.73044E-02	0.00000E-01
2830	6.49488E-01	-8.28347E-01	-1.75810E+00	6.64124E-06	1.73042E-02	0.00000E-01
2831	4.07956E-01	-8.66654E-01	-1.84267E+00	-7.56317E-06	1.73260E-02	0.00000E-01
2832	4.58833E-01	-8.67257E-01	-1.84271E+00	-5.32970E-06	1.73278E-02	0.00000E-01
2833	5.09321E-01	-8.68056E-01	-1.84274E+00	-1.84650E-06	1.73293E-02	0.00000E-01
2834	5.59845E-01	-8.68915E-01	-1.84273E+00	2.00503E-06	1.73293E-02	0.00000E-01
[illegible]	[illegible]	[illegible]	[illegible]	[illegible]	[illegible]	[illegible]

2836	6.814931E-01	-9.787782E-01	-1.912817E+00	-1.127302E-05	1.734[illegible]E-02	-[illegible]
2837	6.168249E-01	-9.080538E-01	-1.929346+00	-1.145066E-05	1.73464E-02	-1.068226E-01
2838	6.429276-01	-9.086446-01	-1.92738E+00	-9.056766-06	1.73449E-02	-8.11536E-02
2839	6.68849[illegible]-01	-9.09248E-01	-1.92941E+00	-8.47574E-06	1.73508E-02	-3.43017E-02
2840	1.741736-01	-9.09868E-01	-1.92943E+00	-6.39427E-06	1.73527E-02	-1.44891E-02
2841	5.14759E-01	-9.10506E-01	-1.92944E+00	-2.24201E-06	1.73538E-02	-1.36819E-02
2842	5.41517E-01	-9.11188E-01	-1.92945E+00	2.20756E-08	1.73542E-02	-8.79048E-03
2843	5.70803E-01	-9.11886E-01	-1.92944E+00	2.40620E-06	1.73538E-02	-3.94831E-03
2844	5.96302E-01	-9.12540E-01	-1.92943E+00	4.55845E-06	1.73527E-02	-8.16301E-03
2845	6.21801E-01	-9.13248E-01	-1.92941E+00	6.63491E-06	1.73508E-02	1.66856E-02
2846	6.47565E-01	-9.13979E-01	-1.92938E+00	9.22077E-06	1.73467E-02	3.36391E-02
2847	6.73037E-01	-9.14727E-01	-1.92933E+00	1.16144E-05	1.73464E-02	9.03098E-02
2857	5.348[illegible]E-01	-9.49372E-01	-2.63382E+00	-3.35784E-02	2.91112E-01	-1.49750E-03
2860	6.63512E-01	-9.51883E-01	-2.77994E+00	-1.38548E-02	3.18914E-01	-1.85721E-03
2861	6.80637E-01	-9.53407E-01	-2.81450E+00	-4.27742E-03	3.25689E-01	-5.73442E-04
2862	7.12765E-01	-9.55674E-01	-2.81650E+00	1.25016E-03	3.26420E-01	1.68594E-04
2863	7.60910E-01	-9.57916E-01	-2.78612E+00	1.08042E-02	3.17148E-01	1.44777E-03
2864	7.97521E-01	-9.60612E-01	-2.66633E+00	3.06188E-02	2.94667E-01	4.10291E-03
2865	8.42641E-01	-9.93643E-01	-4.80246E+00	-5.37232E-02	5.77295E-01	-7.19891E-03
2866	8.87462E-01	-9.94603E-01	-4.93817E+00	-3.93013E-02	5.75844E-01	-5.26637E-03
2867	9.26079E-01	-9.95574E-01	-5.02679E+00	-2.87496E-02	5.80434E-01	-3.58445E-03
2868	9.60078E-01	-9.96713E-01	-5.08856E+00	-1.72309E-02	5.84392E-01	-2.30894E-03
2869	9.72154E-01	-9.97860E-01	-5.12389E+00	-9.23414E-03	5.88557E-01	-1.23737E-03
2870	1.020516+00	-9.99028E-01	-5.13709E+00	-2.31494E-03	5.89585E-01	-3.10202E-04
2871	1.06821E+00	-1.00023E+00	-5.13075E+00	4.59551E-03	5.89478E-01	6.15799E-04
2872	1.06[illegible]E+00	-1.00145E+00	-5.10233E+00	1.25734E-02	5.86697E-01	1.68480E-03
2873	1.08885E+00	-1.00272E+00	-5.04754E+00	2.20697E-02	5.83379E-01	2.95734E-03
2874	1.10434E+00	-1.00385E+00	-4.96548E+00	3.46232E-02	5.80490E-01	4.63951E-03
2875	1.11408E+00	-1.00502E+00	-4.83721E+00	4.90811E-02	5.82578E-01	6.57688E-03
2876	1.33167E+00	-1.03857E+00	-8.30203E+00	-5.40378E-02	8.18511E-01	-7.24106E-03
2877	1.41714E+00	-1.04081E+00	-8.54709E+00	-3.09722E-02	8.20258E-01	-4.15028E-03
2878	1.48944E+00	-1.04308E+00	-8.66765E+00	-1.21717E-02	8.22378E-01	-1.63101E-03
2879	1.54533E+00	-1.04546E+00	-8.68063E+00	5.14275E-03	8.23673E-01	7.27529E-04
2880	1.58659E+00	-1.04791E+00	-8.58610E+00	2.42162E-02	8.24060E-01	3.24497E-03
2881	1.61228E+00	-1.05056E+00	-8.36712E+00	4.73140E-02	8.24486E-01	6.34008E-03
2882	1.97447E+00	-1.08467E+00	-1.[illegible]E+01	-5.07921E-02	1.02925E+00	-6.80614E-03
2883	2.02004E+00	-1.08871E+00	-1.30774E+01	-4.10449E-02	1.02881E+00	-5.50002E-03
2884	2.06180E+00	-1.09278E+00	-1.31829E+01	-3.14792E-02	1.02637E+00	-4.21821E-03
2885	2.09965E+00	-1.09792E+00	-1.32595E+01	-2.22631E-02	1.02702E+00	-2.98526E-03
2886	2.13367E+00	-1.08910E+00	-1.33080E+01	-1.31577E-02	1.02732E+00	-1.76313E-03
2887	2.16440E+00	-1.09027E+00	-1.33320E+01	-4.48526E-03	1.02812E+00	-6.01025E-04
2888	2.19138E+00	-1.09147E+00	-1.33277E+01	4.18558E-03	1.02872E+00	5.60848E-04
2889	2.21512E+00	-1.09272E+00	-1.32990E+01	1.32887E-02	1.02986E+00	1.78069E-03
2890	2.23513E+00	-1.09399E+00	-1.32421E+01	2.25031E-02	1.03042E+00	3.01541E-03
2891	2.25137E+00	-1.09521E+00	-1.31564E+01	3.20399E-02	1.03452E+00	4.29590E-03
2892	2.26400E+00	-1.09645E+00	-1.30436E+01	4.18041E-02	1.03559E+00	5.60175E-03
2893	2.27747E+00	-1.13137E+00	-1.83589E+01	-4.58854E-02	1.20629E+00	-6.09504E-03
2894	2.28287E+00	-1.13359E+00	-1.87762E+01	-2.94455E-02	1.20275E+00	-3.94570E-03
2895	2.29051E+00	-1.13587E+00	-1.88980E+01	-1.36013E-02	1.20141E+00	-1.82257E-03
2896	2.29669E+00	-1.13824E+00	-1.89248E+01	2.20626E-03	1.20282E+00	2.95639E-04
2897	3.01161E+00	-1.14069E+00	-1.88564E+01	1.80419E-02	1.20689E+00	2.41762E-03
2898	3.04600E+00	-1.14326E+00	-1.86926E+01	3.40927E-02	1.21281E+00	4.56842E-03
2899	3.62852E+00	-1.17894E+00	-2.49780E+01	-4.01343E-02	1.35105E+00	-5.37779E-03
2900	3.67129E+00	-1.17993E+00	-2.50839E+01	-3.33053E-02	1.34972E+00	-4.46291E-03
2901	3.71123E+00	-1.18104E+00	-2.51694E+01	-2.65581E-02	1.34662E+00	-3.55877E-03
2902	3.74843E+00	-1.18218E+00	-2.52311E+01	-1.99574E-02	1.34563E+00	-2.67429E-03
2903	3.78296E+00	-1.18334E+00	-2.52813E+01	-1.33784E-02	1.34470E+00	-1.79271E-03
2904	3.81490E+00	-1.18451E+00	-2.53080E+01	-6.85358E-03	1.34530E+00	-9.18560E-04
2905	3.84424E+00	-1.18570E+00	-2.53152E+01	-3.28686E-04	1.34831E+00	-4.40439E-05
2906	3.87103E+00	-1.18691E+00	-2.53028E+01	6.29906E-03	1.34803E+00	8.38710E-04
2907	3.89525E+00	-1.18813E+00	-2.52709E+01	1.28088E-02	1.35077E+00	1.72139E-03
2908	3.91687E+00	-1.18940E+00	-2.52193E+01	1.96032E-02	1.35538E+00	2.62687E-03
2909	3.93589E+00	-1.19067E+00	-2.51472E+01	2.64180E-02	1.35783E+00	3.54001E-03
2910	4.09993E+00	-1.22695E+00	-3.20406E+01	-3.30646E-02	1.46324E+00	-4.43079E-03
2911	4.67335E+00	-1.22918E+00	-3.22020E+01	-2.30657E-02	1.45859E+00	-3.04081E-03
2912	4.74633E+00	-1.23146E+00	-3.23032E+01	-1.31025E-02	1.45575E+00	-1.75574E-03
2913	4.80931E+00	-1.23380E+00	-3.23441E+01	-3.10179E-03	1.45813E+00	-4.15665E-04
2914	4.86446E+00	-1.23623E+00	-3.23247E+01	6.86456E-03	1.46265E+00	9.19865E-04
2915	4.91174E+00	-1.23877E+00	-3.22449E+01	1.68764E-02	1.46964E+00	2.26144E-03
2916	5.62798E+00	-1.27564E+00	-3.95838E+01	-2.70025E-02	1.54810E+00	-3.61854E-03
2917	5.66676E+00	-1.27878E+00	-3.96594E+01	-2.35727E-02	1.54201E+00	-3.15814E-03
2918	5.[illegible]E+00	-1.28[illegible]E+00	-3.97[illegible]E+01	-2.00943E-02	1.53877E+00	-2.69778E-03

2920	5.774066E+00	-1.280108E+00	-3.980588E+01	-1.281776E-02	1.537688E+00	-1.717575E-03
2921	5.810702E+00	-1.281346E+00	-3.983508E+01	-9.149196E-03	1.535756E+00	-1.225996E-03
2922	5.838665E+00	-1.282526E+00	-3.985355E+01	-5.475523E-03	1.535639E+00	-7.336816E-04
2923	5.868953E+00	-1.283708E+00	-3.986126E+01	-1.799726E-03	1.534063E+00	-2.398236E-04
2924	5.897908E+00	-1.284926E+00	-3.985846E+01	1.847656E-03	1.534260E+00	2.475896E-04
2925	5.925356E+00	-1.286176E+00	-3.984516E+01	5.300736E-03	1.536746E+00	7.103256E-04
2926	5.951822E+00	-1.287476E+00	-3.982196E+01	8.690906E-03	1.540908E+00	1.164508E-03
2927	6.703196E+00	-1.324966E+00	-4.044516E+01	-2.017716E-02	1.591176E+00	-2.703736E-03
2928	6.775776E+00	-1.327186E+00	-4.058006E+01	-1.666726E-02	1.587366E+00	-2.232736E-03
2929	6.844926E+00	-1.329476E+00	-4.071016E+01	-1.284616E-02	1.585866E+00	-1.721186E-03
2930	6.911006E+00	-1.331776E+00	-4.083516E+01	-8.138086E-03	1.587026E+00	-1.090506E-03
2931	6.974156E+00	-1.334176E+00	-4.095206E+01	-3.976846E-03	1.590706E+00	-5.328766E-04
2932	7.034486E+00	-1.336696E+00	-4.106056E+01	-4.631946E-04	1.596536E+00	-6.206866E-05
2933	7.090226E+00	-1.339326E+00	-4.116066E+01	-1.351336E-02	1.607476E+00	-2.305206E-02
2934	7.835006E+00	-1.375176E+00	-4.250766E+01	-1.309706E-02	1.606426E+00	-2.200626E-02
2935	7.867586E+00	-1.376436E+00	-4.264866E+01	-1.283706E-02	1.604506E+00	-2.028716E-02
2936	7.900396E+00	-1.377706E+00	-4.278676E+01	-1.187716E-02	1.603846E+00	-1.960276E-02
2937	7.933796E+00	-1.379006E+00	-4.292196E+01	-1.100486E-02	1.603376E+00	-1.899216E-02
2938	7.971746E+00	-1.380406E+00	-4.305316E+01	-1.001126E-02	1.603596E+00	-1.848176E-02
2939	8.005276E+00	-1.381806E+00	-4.318106E+01	-9.007916E-03	1.604136E+00	-1.809236E-02
2940	8.038606E+00	-1.383136E+00	-4.330476E+01	-8.119636E-03	1.605466E+00	-1.782776E-02
2941	8.071756E+00	-1.384506E+00	-4.342586E+01	-7.429286E-03	1.606[illegible]+00	-1.760306E-02
2942	8.104756E+00	-1.385866E+00	-4.354356E+01	-6.856476E-03	1.607766E+00	-1.854176E-02
2943	8.137746E+00	-1.387246E+00	-4.365046E+01	-6.673796E-03	1.611316E+00	-1.853286E-02
2944	5.114756E-01	-9.493746E-01	-1.377566E+00	3.348366E-02	-2.558816E-01	-4.486816E-03
2945	5.180076E-01	-9.515376E-01	-1.253816E+00	1.381586E-02	-2.776426E-01	-1.835136E-03
2946	6.386176E-01	-9.536076E-01	-1.219406E+00	4.266866E-03	-2.903476E-01	-5.717606E-04
2947	6.895106E-01	-9.558736E-01	-1.217406E+00	-1.249226E-03	-2.911366E-01	1.688686E-04
2948	7.374686E-01	-9.579136E-01	-1.247636E+00	-1.075986E-02	-2.810756E-01	1.441816E-03
2949	7.743236E-01	-9.596096E-01	-1.367046E+00	-3.032376E-02	-2.879366E-01	1.070196E-03
2950	7.954536E-01	-9.938466E-01	2.915676E-01	5.360656E-02	-3.414666E-01	-7.183146E-03
2951	8.402276E-01	-9.946046E-01	7.268866E-01	5.921236E-02	-3.400136E-01	-8.254456E-03
2952	8.788166E-01	-9.955746E-01	8.152616E-01	2.668446E-02	-3.445916E-01	-3.575716E-03
2953	9.133756E-01	-9.967136E-01	8.768606E-01	1.710776E-02	-3.483416E-01	-2.303446E-03
2954	9.448606E-01	-9.978606E-01	9.121096E-01	9.214186E-03	-3.524996E-01	-1.234706E-03
2955	9.732116E-01	-9.990286E-01	9.252766E-01	2.815106E-03	-3.557236E-01	-3.102246E-04
2956	9.986946E-01	-1.000226E+00	9.189696E-01	-4.575206E-03	-3.534206E-01	6.130776E-04
2957	1.021826E+00	-1.001456E+00	8.908576E-01	-1.253216E-02	-3.508476E-01	1.679306E-03
2958	1.041296E+00	-1.002726E+00	8.360206E-01	-2.200426E-02	-3.478566E-01	2.948566E-03
2959	1.057106E+00	-1.003856E+00	7.546976E-01	-3.453396E-02	-3.446606E-01	4.627586E-03
2960	1.066896E+00	-1.005026E+00	6.262636E-01	-4.896316E-02	-3.465496E-01	6.561066E-03
2961	1.260476E+00	-1.038576E+00	3.910506E+00	3.389486E-02	-7.820996E-01	-7.221906E-03
2962	1.347676E+00	-1.040816E+00	4.154916E+00	3.089196E-02	-7.830376E-01	-4.139516E-03
2963	1.417936E+00	-1.043086E+00	4.275166E+00	1.214566E-02	-7.857506E-01	-1.527516E-03
2964	1.473826E+00	-1.045466E+00	4.288146E+00	-5.416326E-03	-7.872466E-01	7.257876E-04
2965	1.515526E+00	-1.047916E+00	4.193736E+00	-2.413556E-02	-7.876396E-01	3.234166E-03
2966	1.540896E+00	-1.050566E+00	3.975596E+00	-4.717076E-02	-7.880746E-01	6.320076E-03
2967	1.578506E+00	-1.084866E+00	8.369856E+00	5.065326E-02	-9.722606E-01	-6.787536E-03
2968	1.624016E+00	-1.085716E+00	8.502016E+00	4.693326E-02	-9.918126E-01	-5.485046E-03
2969	1.765746E+00	-1.086786E+00	8.607186E+00	3.137486E-02	-9.893726E-01	-4.206916E-03
2970	2.003566E+00	-1.088926E+00	8.683596E+00	2.220716E-02	-9.900216E-01	-2.975756E-03
2971	2.037366E+00	-1.089106E+00	8.731936E+00	1.313016E-02	-9.903476E-01	-1.759446E-03
2972	2.068296E+00	-1.090276E+00	8.755866E+00	4.485426E-03	-9.911176E-01	-6.010476E-04
2973	2.093276E+00	-1.091476E+00	8.751696E+00	-4.157696E-03	-9.917206E-01	5.371306E-04
2974	2.119036E+00	-1.092726E+00	8.723676E+00	-1.323246E-02	-9.926586E-01	1.773146E-03
2975	2.139076E+00	-1.093996E+00	8.686416E+00	-2.241046E-02	-9.934206E-01	3.004066E-03
2976	2.155346E+00	-1.095276E+00	8.581006E+00	-3.194686E-02	-9.975236E-01	4.280886E-03
2977	2.168036E+00	-1.096546E+00	8.448576E+00	-4.166486E-02	-9.985796E-01	5.583096E-03
2978	2.426516E+00	-1.131376E+00	1.379756E+01	4.533616E-02	-1.160716E+00	-6.075036E-03
2979	2.711826E+00	-1.133596E+00	1.401406E+01	2.735726E-02	-1.165176E+00	-3.733866E-03
2980	2.784086E+00	-1.135086E+00	1.413356E+01	1.357196E-02	-1.163046E+00	-1.818646E-03
2981	2.843606E+00	-1.138246E+00	1.416236E+01	-2.176616E-03	-1.165246E+00	2.916456E-04
2982	2.890566E+00	-1.140696E+00	1.409436E+01	-1.795336E-02	-1.169326E+00	2.405746E-03
2983	2.922506E+00	-1.143266E+00	1.393126E+01	-3.394516E-02	-1.175246E+00	4.548376E-03
2984	3.462206E+00	-1.178846E+00	2.002736E+01	3.998856E-02	-1.512906E+00	-5.356396E-03
2985	3.529916E+00	-1.179736E+00	2.013286E+01	3.318806E-02	-1.511576E+00	-4.447196E-03
2986	3.564816E+00	-1.181046E+00	2.021796E+01	2.668746E-02	-1.508466E+00	-3.544906E-03
2987	3.601936E+00	-1.182186E+00	2.028346E+01	1.989846E-02	-1.507476E+00	-2.666396E-03
2988	3.636506E+00	-1.183336E+00	2.032956E+01	1.334916E-02	-1.506756E+00	-1.788786E-03
3000	3.668436E+00	-1.184506E+00	2.035816E+01	6.853746E-03	-1.507156E+00	-9.184016E-04

3002	[illegible]	[illegible]	[illegible]	[illegible]	[illegible]	[illegible]
3003	3.748835E+00	[illegible]	2.03194E+01	-1.27768E-02	-1.31262E+00	1.71247E-03
3004	3.77059E+00	-1.18940E+00	2.02681E+01	-1.94858E-02	-1.31743E+00	2.61110E-03
3005	3.79[illegible]	-1.19061E+00	2.01964E+01	-2.62714E-02	-1.31940E+00	3.52037E-03
3006	4.42383E+00	-1.22694E+00	2.68776E+01	3.29155E-02	-1.42451E+00	-4.41057E-03
3007	4.56317E+00	-1.22918E+00	2.70583E+01	2.29747E-02	-1.41986E+00	-3.07888E-03
3008	4.57412E+00	-1.23146E+00	2.71572E+01	1.30730E-02	-1.41801E+00	-1.75178E-03
3009	4.63709E+00	-1.23380E+00	2.72001E+01	3.13186E-03	-1.41439E+00	-4.19669E-04
3010	4.69229E+00	-1.23627E+00	2.71810E+01	-6.77530E-03	-1.42392E+00	9.07890E-04
3011	4.73956E+00	-1.23877E+00	2.71019E+01	-1.67260E-02	-1.43091E+00	2.24126E-03
3012	5.42975E+00	-1.27364E+00	3.42455E+01	2.585622E-02	-1.30379E+00	-3.59973E-03
3013	5.46848E+00	-1.27678E+00	3.43104E+01	2.34554E-02	-1.50270E+00	-3.14303E-03
3014	5.50585E+00	-1.27972E+00	3.43765E+01	2.000666E-02	-1.49746E+00	-2.68089E-03
3015	5.54137E+00	-1.28905E+00	3.44287E+01	1.64218E-02	-1.49862E+00	-2.20052E-03
3016	5.57570E+00	-1.29010E+00	3.44868E+01	1.27807E-02	-1.49777E+00	-1.71368E-03
3017	5.60865E+00	-1.28134E+00	3.44958E+01	9.14935E-03	-1.49825E+00	-1.22601E-03
3018	5.64029E+00	-1.28252E+00	3.45144E+01	5.50452E-03	-1.49906E+00	-7.37617E-04
3019	5.67039E+00	-1.28370E+00	3.45222E+01	1.84865E-03	-1.50132E+00	-2.47719E-04
3020	5.67959E+00	-1.28492E+00	3.45176E+01	-1.75904E-03	-1.50529E+00	2.35711E-04
3021	5.72727E+00	-1.28617E+00	3.45068E+01	-5.18338E-03	-1.50813E+00	6.94573E-04
3022	5.75360E+00	-1.28747E+00	3.44838E+01	-8.54424E-03	-1.50977E+00	1.14493E-03
3023	6.47841E+00	-1.32493E+00	4.19090E+01	2.00301E-02	-1.55130E+00	-2.68404E-03
3024	6.53091E+00	-1.32718E+00	4.20152E+01	1.65755E-02	-1.54748E+00	-2.22112E-03
3025	6.62004E+00	-1.32947E+00	4.20935E+01	1.25175E-02	-1.54597E+00	-1.67734E-03
3026	6.66612E+00	-1.33177E+00	4.21479E+01	8.16704E-03	-1.54713E+00	-1.09438E-03
3027	6.74930E+00	-1.33419E+00	4.21752E+01	4.06380E-03	-1.55089E+00	-5.44549E-04
3028	6.80963E+00	-1.33669E+00	4.21784E+01	6.10470E-04	-1.55664E+00	-8.18030E-05
3029	7.54849E+00	-1.37394E+00	4.97206E+01	1.31599E-02	-1.56701E+00	-2.31120E-02
3030	7.58325E+00	-1.37519E+00	4.97702E+01	1.2979E-02	-1.56578E+00	-2.20303E-02
3031	7.61781E+00	-1.37644E+00	4.98110E+01	1.24735E-02	-1.56404E+00	-2.02744E-02
3032	7.65212E+00	-1.37771E+00	4.98488E+01	1.18203E-02	-1.56338E+00	-1.80138E-02
3033	7.68617E+00	-1.37901E+00	4.98839E+01	1.09762E-02	-1.56290E+00	-1.59923E-02
3034	7.71995E+00	-1.38040E+00	4.99131E+01	1.00114E-02	-1.56312E+00	-8.48317E-03
3035	7.75360E+00	-1.38180E+00	4.99430E+01	9.03885E-03	-1.56369E+00	-4.92290E-03
3036	7.78682E+00	-1.38314E+00	4.99670E+01	8.17878E-03	-1.56477E+00	-7.92274E-04
3037	7.81988E+00	-1.38448E+00	4.99881E+01	7.51514E-03	-1.56636E+00	3.74755E-03
3038	7.85300E+00	-1.38586E+00	5.00062E+01	6.97613E-03	-1.56729E+00	4.87823E-03
3039	7.88602E+00	-1.38722E+00	5.00235E+01	6.82769E-03	-1.57085E+00	5.24333E-03
3051	7.82254E+00	-1.43181E+00	-6.35057E+01	-1.21619E-02	1.60688E+00	1.82681E-17
3052	7.89147E+00	-1.43376E+00	-6.35731E+01	-1.19083E-02	1.60579E+00	-1.79463E-17
3053	7.96003E+00	-1.43607E+00	-6.36433E+01	-1.08772E-02	1.60512E+00	-9.90703E-18
3054	8.02788E+00	-1.43838E+00	-6.37053E+01	-9.63445E-03	1.60551F+00	1.48392E-17
3055	8.09520E+00	-1.44081E+00	-6.37608E+01	-8.56680E-03	1.60698E+00	8.21607E-17
3056	8.16269E+00	-1.44326E+00	-6.38133E+01	-8.41279E-03	1.60871E+00	-3.20371E-17
3057	7.84167E+00	-1.48087E+00	-7.15385E+01	-1.10007E-02	1.60683E+00	-8.52673E-18
3058	7.87897E+00	-1.48982E+00	-7.15725E+01	-1.09543E-02	1.60670E+00	2.33427E-17
3059	7.91351E+00	-1.49107E+00	-7.16064E+01	-1.09663E-02	1.60641E+00	-7.16378E-18
3060	7.94786E+00	-1.49217E+00	-7.16394E+01	-1.08332E-02	1.60631E+00	1.09665E-17
3061	7.98218E+00	-1.49327E+00	-7.16722E+01	-1.07636E-02	1.60622E+00	1.71383E-19
3062	8.01637E+00	-1.49447E+00	-7.17081E+01	-1.06292E-02	1.60627E+00	3.67544E-19
3063	8.05050E+00	-1.49559E+00	-7.17353E+01	-1.04703E-02	1.60641E+00	5.53790E-18
3064	8.08453E+00	-1.49681E+00	-7.17661E+01	-1.04213E-02	1.60671E+00	-1.40092E-17
3065	8.11863E+00	-1.49797E+00	-7.17983E+01	-1.03866E-02	1.60702E+00	1.29024E-17
3066	8.15268E+00	-1.49930E+00	-7.18278E+01	-1.02741E-02	1.60750F+00	-3.23843E-17
3067	8.18712E+00	-1.50066E+00	-7.18580E+01	-1.02223E-02	1.60773E+00	1.30032E-17
3068	7.86632E+00	-1.54631E+00	-7.95739E+01	-1.10715E-02	1.60797E+00	-6.73665E-18
3069	7.93532E+00	-1.54853E+00	-7.96376E+01	-1.10009E-02	1.60687E+00	-9.81887E-18
3070	8.00445E+00	-1.55094E+00	-7.97047E+01	-1.07683E-02	1.60680E+00	-3.46571E-18
3071	8.07518E+00	-1.55323E+00	-7.97688E+01	-1.05168E-02	1.60689E+00	4.70713E-18
3072	8.14188E+00	-1.55572E+00	-7.98316E+01	-1.02855E-02	1.60714E+00	1.28494F-17
3073	8.21087E+00	-1.55810E+00	-7.98938E+01	-1.02238E-02	1.60753E+00	5.20428E-18
3074	7.88811E+00	-1.60386E+00	-8.76097E+01	-1.07732E-02	1.60726E+00	1.81274E-18
3075	7.92316E+00	-1.60635E+00	-8.76424E+01	-1.07315E-02	1.60727E+00	-1.27881E-18
3076	7.95764E+00	-1.60871E+00	-8.76741E+01	-1.07209E-02	1.60728E+00	1.36237E-18
3077	7.99252E+00	-1.61076E+00	-8.77076E+01	-1.07468E-02	1.60725E+00	-1.23201E-18
3078	8.02786E+00	-1.61280E+00	-8.77399E+01	-1.07699E-02	1.60723E+00	1.80632E-18
3079	8.06136E+00	-1.61001E+00	-8.77722E+01	-1.07572E-02	1.60725E+00	1.38901E-18
3080	8.09588E+00	-1.61122E+00	-8.78043E+01	-1.07434E-02	1.60728E+00	1.37849E-18
3081	8.13053E+00	-1.61229E+00	-8.78362E+01	-1.07698E-02	1.60735E+00	2.48584E-18
3082	8.16507E+00	-1.61337E+00	-8.78681E+01	-1.07993E-02	1.60742E+00	1.86143E-18
3083	8.19796E+00	-1.61481E+00	-8.78998E+01	-1.07589E-02	1.60746E+00	2.59546E-18
3084	8.23[illegible]	-1.61[illegible]	-8.79[illegible]	-1.07594E-02	1.60[illegible]	1.2[illegible]E-18

3086	7.98008E+00	-1.86469E+00	-9.57121E+01	-1.08704E-02	1.60757E+00	-6.18552E-18
3087	8.04923E+00	-1.86711E+00	-9.57770E+01	-1.07767E-02	1.60737E+00	-2.51603E-18
3088	8.11862E+00	-1.86932E+00	-9.58415E+01	-1.07052E-02	1.60760E+00	2.66022E-19
3089	8.18842E+00	-1.87181E+00	-9.59057E+01	-1.06026E-02	1.60783E+00	4.37049E-18
3090	8.25846E+00	-1.87390E+00	-9.59696E+01	-1.05282E-02	1.60773E+00	4.60131E-18
3091	7.93343E+00	-1.72018E+00	-1.03388E+02	-1.09060E-02	1.60787E+00	2.42225E-18
3092	7.96742E+00	-1.72187E+00	-1.03718E+02	-1.07838E-02	1.60788E+00	-1.72473E-18
3093	8.00275E+00	-1.72361E+00	-1.03751E+02	-1.07614E-02	1.60790E+00	2.02883E-18
3094	8.03880E+00	-1.72540E+00	-1.03783E+02	-1.07752E-02	1.60789E+00	-8.50748E-19
3095	8.07532E+00	-1.72733E+00	-1.03816E+02	-1.07882E-02	1.60787E+00	1.77992E-18
3096	8.10578E+00	-1.72865E+00	-1.03848E+02	-1.07797E-02	1.60789E+00	1.33346E-18
3097	8.14114E+00	-1.72777E+00	-1.03880E+02	-1.07709E-02	1.60790E+00	1.07103E-18
3098	8.17610E+00	-1.72873E+00	-1.03912E+02	-1.07872E-02	1.60791E+00	3.25668E-18
3099	8.21184E+00	-1.72773E+00	-1.03943E+02	-1.08040E-02	1.60793E+00	8.07305E-19
3100	8.24641E+00	-1.73153E+00	-1.03977E+02	-1.07749E-02	1.60792E+00	4.62697E-18
3101	8.28256E+00	-1.73328E+00	-1.04007E+02	-1.07474E-02	1.60791E+00	1.74154E-19
3102	7.95479E+00	-1.77978E+00	-1.11726E+02	-1.08604E-02	1.60818E+00	-5.47628E-18
3103	8.02436E+00	-1.78172E+00	-1.11791E+02	-1.08422E-02	1.60817E+00	-3.50076E-18
3104	8.09324E+00	-1.78417E+00	-1.11858E+02	-1.07868E-02	1.60817E+00	-2.14527E-18
3105	8.16306E+00	-1.78637E+00	-1.11926E+02	-1.07486E-02	1.60818E+00	-1.08967E-18
3106	8.23401E+00	-1.78885E+00	-1.11985E+02	-1.06873E-02	1.60818E+00	5.34372E-19
3107	8.30486E+00	-1.79085E+00	-1.12049E+02	-1.06696E-02	1.60821E+00	1.85793E-18
3108	7.97735E+00	-1.83713E+00	-1.19768E+02	-1.08397E-02	1.60845E+00	2.08189E-18
3109	8.01516E+00	-1.83979E+00	-1.19800E+02	-1.08152E-02	1.60848E+00	-7.84850E-19
3110	8.04632E+00	-1.84215E+00	-1.19833E+02	-1.07887E-02	1.60846E+00	1.97604E-18
3111	8.08112E+00	-1.84486E+00	-1.19865E+02	-1.07918E-02	1.60846E+00	2.01286E-19
3112	8.11424E+00	-1.84751E+00	-1.19897E+02	-1.07950E-02	1.60846E+00	1.60633E-18
3113	8.14774E+00	-1.84401E+00	-1.19930E+02	-1.07917E-02	1.60848E+00	1.13404E-18
3114	8.18419E+00	-1.84452E+00	-1.19962E+02	-1.07683E-02	1.60846E+00	1.27184E-18
3115	8.22107E+00	-1.84517E+00	-1.19994E+02	-1.07741E-02	1.60848E+00	1.71356E-18
3116	8.25638E+00	-1.84589E+00	-1.20026E+02	-1.07798E-02	1.60846E+00	9.04179E-19
3117	8.27574E+00	-1.84833E+00	-1.20059E+02	-1.07493E-02	1.60848E+00	3.11080E-18
3118	8.32810E+00	-1.85107E+00	-1.20091E+02	-1.07209E-02	1.60848E+00	5.60460E-19
3119	8.01058E+00	-1.90037E+00	-1.27811E+02	-1.08502E-02	1.60870E+00	-3.77578E-18
3120	8.07077E+00	-1.90990E+00	-1.27876E+02	-1.08337E-02	1.60878E+00	-3.47079E-18
3121	8.13623E+00	-1.90173E+00	-1.27940E+02	-1.07880E-02	1.60877E+00	-2.38211E-18
3122	8.20426E+00	-1.90405E+00	-1.28003E+02	-1.07576E-02	1.60877E+00	-1.71221E-18
3123	8.23103E+00	-1.90588E+00	-1.28070E+02	-1.07073E-02	1.60879E+00	-7.66229E-19
3124	8.36184E+00	-1.90535E+00	-1.28134E+02	-1.06969E-02	1.60879E+00	1.61982E-18
3125	8.03147E+00	-1.94180E+00	-1.35855E+02	-1.08320E-02	1.60918E+00	1.11351E-02
3126	8.06137E+00	-1.94753E+00	-1.35888E+02	-1.08158E-02	1.60904E+00	1.11351E-02
3127	8.09225E+00	-1.95302E+00	-1.35920E+02	-1.07853E-02	1.60907E+00	5.56757E-03
3128	8.12091E+00	-1.95893E+00	-1.35953E+02	-1.07890E-02	1.60901E+00	1.11351E-02
3127	8.15218E+00	-1.95899E+00	-1.35985E+02	-1.07725E-02	1.60907E+00	5.56757E-03
3130	8.18970E+00	-1.96170E+00	-1.36017E+02	-1.07810E-02	1.60901E+00	1.11351E-02
3131	8.22922E+00	-1.96444E+00	-1.36050E+02	-1.07674E-02	1.60907E+00	5.56757E-03
3132	8.26103E+00	-1.96757E+00	-1.36082E+02	-1.07745E-02	1.60901E+00	1.11351E-02
3133	8.30259E+00	-1.97058E+00	-1.36114E+02	-1.07795E-02	1.60907E+00	5.56757E-03
3134	8.34214E+00	-1.97625E+00	-1.36146E+02	-1.07458E-02	1.60903E+00	1.11351E-02
3135	8.40304E+00	-1.98216E+00	-1.36178E+02	-1.07066E-02	1.60917E+00	1.11351E-02
3147	7.57079E+00	-1.43161E+00	5.75630E+01	1.20174E-02	-1.56584E+00	2.47981E-17
3148	7.63971E+00	-1.43376E+00	5.76337E+01	1.18200E-02	-1.56475E+00	-1.37618E-17
3149	7.70825E+00	-1.43609E+00	5.77015E+01	1.08503E-02	-1.56408E+00	-5.08582E-18
3150	7.77610E+00	-1.43838E+00	5.77635E+01	9.66361E-03	-1.56447E+00	1.08C72E-17
3151	7.84343E+00	-1.44081E+00	5.78194E+01	8.05544E-03	-1.56592E+00	3.41534E-17
3152	7.91075E+00	-1.44327E+00	5.78725E+01	8.55763E-03	-1.56768E+00	-3.04075E-17
3153	7.59285E+00	-1.48857E+00	6.53913E+01	1.00420E-02	-1.56522E+00	-1.16974E-17
3154	7.62720E+00	-1.48782E+00	6.54248E+01	1.08307E-02	-1.56507E+00	2.36740E-17
3155	7.66174E+00	-1.49107E+00	6.54583E+01	1.07776E-02	-1.56483E+00	-9.21743E-18
3156	7.69609E+00	-1.49217E+00	6.54911E+01	1.07741E-02	-1.56470E+00	1.10238E-17
3157	7.73041E+00	-1.49327E+00	6.55238E+01	1.07339E-02	-1.56460E+00	-1.84259E-18
3158	7.76459E+00	-1.49447E+00	6.55556E+01	1.06293E-02	-1.56465E+00	3.83026E-17
3159	7.79872E+00	-1.49568E+00	6.55871E+01	1.05205E-02	-1.56480E+00	3.42620E-18
3160	7.83276E+00	-1.49801E+00	6.56178E+01	1.04007E-02	-1.56510E+00	-1.40516E-17
3161	7.86686E+00	-1.49797E+00	6.56483E+01	1.04756E-02	-1.56540E+00	1.09172E-17
3162	7.90092E+00	-1.49930E+00	6.56779E+01	1.03980E-02	-1.56587E+00	-5.25699E-17
3163	7.93536E+00	-1.50066E+00	6.57077E+01	1.03914E-02	-1.56612E+00	1.50078E-17
3164	7.61456E+00	-1.54631E+00	7.32171E+01	1.09287E-02	-1.56407E+00	7.95387E-20
3165	7.66375E+00	-1.54853E+00	7.32821E+01	1.09183E-02	-1.56469E+00	-5.78117E-18
3166	7.72686E+00	-1.55093E+00	7.33469E+01	1.07383E-02	-1.56462E+00	3.45994E-19

3086	7.98008E+00	-1.66469E+00	-9.57121E+01	-1.08704E-02	1.60757E+00	-6.18552E-18
3087	8.04723E+00	-1.66711E+00	-9.57770E+01	-1.07767E-02	1.60757E+00	-2.51603E-18
3088	8.11862E+00	-1.66932E+00	-9.58415E+01	-1.07052E-02	1.60760E+00	2.66822E-19
3089	8.18812E+00	-1.67181E+00	-9.59057E+01	-1.06026E-02	1.60763E+00	1.39049E-18
3090	8.25846E+00	-1.67390E+00	-9.59696E+01	-1.05782E-02	1.60773E+00	8.60131E-18
3091	7.93345E+00	-1.72018E+00	-1.03636E+02	-1.08060E-02	1.60787E+00	2.42225E-18
3092	7.98742E+00	-1.72187E+00	-1.03718E+02	-1.07838E-02	1.60788E+00	-1.72473E-18
3093	8.00278E+00	-1.72381E+00	-1.03751E+02	-1.07814E-02	1.60790E+00	2.02868E-18
3094	8.03890E+00	-1.72580E+00	-1.03783E+02	-1.07752E-02	1.60789E+00	-8.50748E-19
3095	8.07152E+00	-1.72835E+00	-1.03816E+02	-1.07882E-02	1.60789E+00	1.77272E-18
3096	8.10508E+00	-1.73068E+00	-1.03848E+02	-1.07797E-02	1.60789E+00	1.33344E-19
3097	8.14114E+00	-1.73277E+00	-1.03880E+02	-1.07709E-02	1.60790E+00	1.07108E-18
3098	8.17610E+00	-1.73873E+00	-1.03912E+02	-1.07872E-02	1.60791E+00	3.93668E-18
3099	8.21184E+00	-1.73972E+00	-1.03945E+02	-1.08040E-02	1.60793E+00	8.07303E-19
3100	8.24681E+00	-1.73153E+00	-1.03977E+02	-1.07745E-02	1.60792E+00	4.42497E-18
3101	8.28256E+00	-1.73328E+00	-1.04009E+02	-1.07474E-02	1.60791E+00	1.74154E-19
3102	7.95479E+00	-1.77978E+00	-1.11726E+02	-1.08654E-02	1.60818E+00	-5.47428E-18
3103	8.02436E+00	-1.78172E+00	-1.11791E+02	-1.08422E-02	1.60817E+00	-3.50076E-18
3104	8.09324E+00	-1.78417E+00	-1.11856E+02	-1.07888E-02	1.60817E+00	-2.14527E-18
3105	8.16308E+00	-1.78637E+00	-1.11920E+02	-1.07466E-02	1.60818E+00	-1.08967E-18
3106	8.23401E+00	-1.78885E+00	-1.11982E+02	-1.06873E-02	1.60818E+00	5.34372E-19
3107	8.30486E+00	-1.79085E+00	-1.12049E+02	-1.06596E-02	1.60821E+00	1.85993E-18
3108	7.97739E+00	-1.83713E+00	-1.19768E+02	-1.06377E-02	1.60845E+00	2.08189E-18
3109	8.01540E+00	-1.83979E+00	-1.19800E+02	-1.08132E-02	1.60848E+00	-7.84850E-19
3110	8.04632E+00	-1.84215E+00	-1.19833E+02	-1.07887E-02	1.60846E+00	97804E-18
3111	8.08112E+00	-1.84286E+00	-1.19865E+02	-1.07919E-02	1.60848E+00	2.01286E-19
3112	8.11424E+00	-1.84351E+00	-1.19897E+02	-1.07950E-02	1.60848E+00	1.60633E-18
3113	8.14771E+00	-1.84401E+00	-1.19930E+02	-1.07817E-02	1.60849E+00	1.13[illegible]E-18
3114	8.18019E+00	-1.84452E+00	-1.19962E+02	-1.07683E-02	1.60848E+00	1.27[illegible]E-18
3115	8.22107E+00	-1.84517E+00	-1.19994E+02	-1.07741E-02	1.60848E+00	1.91556E-18
3116	8.25638E+00	-1.84569E+00	-1.20026E+02	-1.07798E-02	1.60848E+00	9.04170E-19
3117	8.29374E+00	-1.84833E+00	-1.20059E+02	-1.07493E-02	1.60848E+00	3.11080E-18
3118	8.32810E+00	-1.85107E+00	-1.20091E+02	-1.07209E-02	1.60848E+00	5.60460E-19
3119	8.01056E+00	-1.90037E+00	-1.27911E+02	-1.08502E-02	1.60878E+00	-5.97598E-18
3120	8.07677E+00	-1.89990E+00	-1.27976E+02	-1.08337E-02	1.60878E+00	-3.47879E-18
3121	8.14623E+00	-1.90173E+00	-1.28040E+02	-1.07830E-02	1.60877E+00	-2.38211E-18
3122	8.20696E+00	-1.90405E+00	-1.28005E+02	-1.07576E-02	1.60877E+00	-1.71221E-18
3123	8.28103E+00	-1.90388E+00	-1.28070E+02	-1.07075E-02	1.60878E+00	-7.36229E-19
3124	8.36184E+00	-1.90535E+00	-1.28134E+02	-1.06965E-02	1.60879E+00	1.61982E-18
3125	8.03147E+00	-1.94180E+00	-1.35835E+02	-1.08520E-02	1.60918E+00	1.11331E-02
3126	8.06137E+00	-1.94753E+00	-1.35888E+02	-1.08138E-02	1.60904E+00	1.11351E-02
3127	8.09223E+00	-1.95302E+00	-1.35942E+02	-1.07853E-02	1.60910E+00	5.56757E-03
3128	8.12091E+00	-1.95593E+00	-1.35953E+02	-1.07890E-02	1.60901E+00	1.11351E-02
3129	8.15918E+00	-1.95878E+00	-1.35985E+02	-1.07725E-02	1.60907E+00	5.56757E-03
3130	8.18970E+00	-1.96170E+00	-1.36017E+02	-1.07810E-02	1.60901E+00	1.11351E-02
3131	8.22922E+00	-1.96444E+00	-1.36050E+02	-1.07674E-02	1.60907E+00	5.5675/E-03
3132	8.26103E+00	-1.96757E+00	-1.36082E+02	-1.07745E-02	1.60901E+00	1.11351E-02
3133	8.30259E+00	-1.97058E+00	-1.36114E+02	-1.07796E-02	1.60907E+00	5.56757E-03
3134	8.34214E+00	-1.97625E+00	-1.36146E+02	-1.07456E-02	1.60903E+00	1.11351E-02
3135	8.40304E+00	-1.98216E+00	-1.36178E+02	-1.07064E-02	1.60917E+00	1.11351E-02
3147	7.57079E+00	-1.[illegible]1E+00	5.76630E+01	1.20174E-02	-1.56584E+00	2.47951E-17
3148	7.63971E+00	-1.43378E+00	5.76337E+01	1.18200E-02	-1.56475E+00	-1.37618E-17
3149	7.70825E+00	-1.43609E+00	5.77015E+01	1.08503E-02	-1.56408E+00	-8.88562E-18
3150	7.77810E+00	-1.43830E+00	5.77835E+01	9.66361E-03	-1.56447E+00	1.08377E-17
3151	7.84343E+00	-1.44061E+00	5.78194E+01	8.65544E-03	-1.56592E+00	3.61935E-17
3152	7.91075E+00	-1.44327E+00	5.78723E+01	8.55753E-03	-1.56738E+00	-3.04075E-17
3153	7.59285E+00	-1.48857E+00	6.53713E+01	1.00470E-02	-1.56522E+00	-1.16978E-17
3154	7.62720E+00	-1.48982E+00	6.54249E+01	1.08304E-02	-1.56507E+00	2.34740E-17
3155	7.66174E+00	-1.49107E+00	6.54283E+01	1.07778E-02	-1.56483E+00	-9.21743E-18
3156	7.67607E+00	-1.49217E+00	6.54711E+01	1.07741E-02	-1.56470E+00	1.10238E-17
3157	7.73041E+00	-1.49327E+00	6.55238E+01	1.07339E-02	-1.56460E+00	-1.86269E-18
3158	7.76459E+00	-1.49447E+00	6.55556E+01	1.08279E-02	-1.56466E+00	3.83026E-19
3159	7.79872E+00	-1.49648E+00	6.55871E+01	1.05203E-02	-1.56480E+00	3.42620E-18
3160	7.83276E+00	-1.49801E+00	6.56178E+01	1.04807E-02	-1.56510E+00	-1.40516E-17
3161	7.86886E+00	-1.49797E+00	6.56483E+01	1.04756E-02	-1.56540E+00	1.09172E-17
3162	7.90092E+00	-1.49930E+00	6.56779E+01	1.03980E-02	-1.56587E+00	-5.23697E-17
3163	7.93535E+00	-1.50068E+00	6.57077E+01	1.03814E-02	-1.56612E+00	1.50078E-17
3164	7.81458E+00	-1.54831E+00	7.32171E+01	.092878-02	-1.56489E+00	7.95387E-20
3165	7.88375E+00	-1.54953E+00	7.32821E+01	1.09183E-02	-1.56469E+00	-5.78117E-18
3166	7.75288E+00	-1.55093E+00	7.33469E+01	1.07385E-02	-1.56462E+00	5.45994E-19

3168	[illegible]	-1.[illegible]	[illegible]	[illegible]	[illegible]	[illegible]
3169	7.95912E+00	-1.95810E+00	7.35370E+01	1.03700E-02	-1.56535E+00	4.63393E-18
3170	7.83634E+00	-1.80396E+00	8.10406E+01	1.06079E-02	-1.56450E+00	-1.38145E-18
3171	7.87139E+00	-1.80536E+00	8.10729E+01	1.06732E-02	-1.56452E+00	-9.95791E-19
3172	7.70887E+00	-1.80671E+00	8.11032E+01	1.06304E-02	-1.56452E+00	-7.47502E-19
3173	7.74055E+00	-1.80776E+00	8.11325E+01	1.06866E-02	-1.56456E+00	-1.20545E-18
3174	7.77477E+00	-1.80830E+00	8.11877E+01	1.07377E-02	-1.56448E+00	-2.30410E-19
3175	7.80959E+00	-1.81001E+00	8.12019E+01	1.07574E-02	-1.56450E+00	1.49527E-18
3176	7.84407E+00	-1.81122E+00	8.12340E+01	1.07738E-02	-1.56453E+00	-6.28045E-19
3177	7.87876E+00	-1.81228E+00	8.12661E+01	1.08504E-02	-1.56460E+00	2.41638E-18
3178	7.91330E+00	-1.81337E+00	8.12982E+01	1.08701E-02	-1.56457E+00	-4.78974E-20
3179	7.94819E+00	-1.81481E+00	8.13302E+01	1.08843E-02	-1.56471E+00	2.24527E-18
3180	7.98270E+00	-1.81628E+00	8.13622E+01	1.08915E-02	-1.56471E+00	5.31210E-19
3181	8.01803E+00	-1.81770E+00	8.13927E+01	1.07631E-02	-1.56478E+00	-4.09687E-19
3182	7.72831E+00	-1.66468E+00	8.97270E+01	1.07787E-02	-1.56429E+00	-1.70812E-18
3183	7.75746E+00	-1.66711E+00	8.97915E+01	1.07460E-02	-1.56428E+00	1.58093E-18
3184	7.78685E+00	-1.66932E+00	8.98560E+01	1.07562E-02	-1.56426E+00	1.33485E-18
3185	7.81665E+00	-1.67181E+00	8.99205E+01	1.06944E-02	-1.56430E+00	8.14156E-18
3186	8.00687E+00	-1.67389E+00	8.91852E+01	1.07214E-02	-1.56409E+00	3.68775E-18
3187	7.68168E+00	-1.72018E+00	9.66833E+01	1.06249E-02	-1.56398E+00	-6.85702E-19
3188	7.71565E+00	-1.72183E+00	9.67533E+01	1.06464E-02	-1.56398E+00	-7.90295E-19
3189	7.75099E+00	-1.72361E+00	9.67478E+01	1.06665E-02	-1.56399E+00	-3.67441E-20
3190	7.78503E+00	-1.72438E+00	9.67798E+01	1.07123E-02	-1.56399E+00	-1.03317E-18
3191	7.81974E+00	-1.72553E+00	9.68121E+01	1.07577E-02	-1.56398E+00	-1.89758E-19
3192	7.85421E+00	-1.72685E+00	9.68446E+01	1.07799E-02	-1.56399E+00	1.32283E-18
3193	7.88937E+00	-1.72777E+00	9.68767E+01	1.08017E-02	-1.56399E+00	-9.43350E-19
3194	7.92453E+00	-1.72875E+00	9.69090E+01	1.08504E-02	-1.56401E+00	3.25585E-18
3195	7.96007E+00	-1.72972E+00	9.69414E+01	1.08992E-02	-1.56402E+00	-1.15621E-18
3196	7.99464E+00	-1.73153E+00	9.69738E+01	1.09128E-02	-1.56403E+00	5.49441E-18
3197	8.03079E+00	-1.73328E+00	9.70063E+01	1.09[illegible]	-1.56401E+00	-4.93784E-19
3198	7.70302E+00	-1.77777E+00	1.01505E+02	[illegible]	[illegible]+00	2.17587E-18
3199	7.73259E+00	-1.78172E+00	1.01867E+02	1.0[illegible]	[illegible]0	3.79839E-19
3200	7.81147E+00	-1.78417E+00	1.01631E+02	1.075[illegible]	[illegible]	1.70489E-18
3201	7.81179E+00	-1.78636E+00	1.01696E+02	1.077[illegible]	[illegible]	2.87130E-18
3202	7.78224E+00	-1.78803E+00	1.01761E+02	1.07794E-02	[illegible]	[illegible]35037E-18
3203	8.05309E+00	-1.79085E+00	1.01826E+02	1.08091E-0[illegible]	[illegible]	[illegible]8561E-18
3204	7.72538E+00	-1.83713E+00	1.12320E+02	1.07472E-02	-[illegible]	[illegible]36376-18
3205	7.76363E+00	-1.83979E+00	1.12352E+02	1.06680E-02	-1.56341E+00	8.55419E-19
3206	7.77433E+00	-1.84213E+00	1.12385E+02	1.06915E-02	-1.56344E+00	-5.42911E-19
3207	7.82955E+00	-1.84286E+00	1.12417E+02	1.07266E-02	-1.56342E+00	-9.70171E-20
3208	7.86247E+00	-1.84550E+00	1.12449E+02	1.07615E-02	-1.56343E+00	-3.78663E-19
3209	7.89817E+00	-1.84401E+00	1.12481E+02	1.07818E-02	-1.56342E+00	1.17328E-18
3210	7.93292E+00	-1.84452E+00	1.12514E+02	1.08023E-02	-1.56343E+00	-7.87159E-19
3211	7.96930E+00	-1.84517E+00	1.12546E+02	1.08398E-02	-1.56343E+00	2.23211E-18
3212	8.00461E+00	-1.84589E+00	1.12579E+02	1.08773E-02	-1.56345E+00	-7.21914E-19
3213	8.04397E+00	-1.84832E+00	1.12611E+02	1.08968E-02	-1.56341E+00	1.73964E-18
3214	8.07853E+00	-1.85106E+00	1.12644E+02	1.09137E-02	-1.56343E+00	1.33986E-19
3215	7.75879E+00	-1.90037E+00	1.20137E+02	1.07271E-02	-1.56311E+00	5.70292E-18
3216	7.81900E+00	-1.89990E+00	1.20201E+02	1.07479E-02	-1.56311E+00	2.91478E-18
3217	7.88648E+00	-1.90173E+00	1.20266E+02	1.07613E-02	-1.56313E+00	2.19416E-18
3218	7.95449E+00	-1.90405E+00	1.20330E+02	1.07947E-02	-1.56313E+00	1.85445E-18
3219	8.02927E+00	-1.90588E+00	1.20395E+02	1.07957E-02	-1.56311E+00	1.52851E-18
3220	8.11003E+00	-1.90533E+00	1.20460E+02	1.08204E-02	-1.56311E+00	-1.38307E-19
3221	7.79970E+00	-1.94180E+00	1.27451E+02	1.06645E-02	-1.56260E+00	1.11351E-02
3222	7.80786E+00	-1.94753E+00	1.27784E+02	1.07006E-02	-1.56283E+00	1.11351E-02
3223	7.84048E+00	-1.95302E+00	1.28016E+02	1.07775E-02	-1.56284E+00	5.56757E-03
3224	7.86214E+00	-1.95573E+00	1.28048E+02	1.07492E-02	-1.56291E+00	1.11351E-02
3225	7.90741E+00	-1.95858E+00	1.28081E+02	1.07707E-02	-1.56285E+00	5.56757E-03
3226	7.93175E+00	-1.96170E+00	1.28113E+02	1.07812E-02	-1.56271E+00	1.11351E-02
3227	7.97745E+00	-1.96443E+00	1.28146E+02	1.07915E-02	-1.56285E+00	5.56757E-03
3228	8.00726E+00	-1.96756E+00	1.28178E+02	1.08146E-02	-1.56291E+00	1.11351E-02
3229	8.04082E+00	-1.97058E+00	1.28210E+02	1.08379E-02	-1.56284E+00	5.56757E-03
3230	8.07037E+00	-1.97823E+00	1.28243E+02	1.08511E-02	-1.56283E+00	1.11351E-02
3231	8.15127E+00	-1.98216E+00	1.28275E+02	1.08845E-02	-1.56263E+00	1.11351E-02

LARGEST MAGNITUDES OF DISPLACEMENT VECTOR =

	8.40304E+00	-1.98216E+00	-1.36178E+02	-5.40378E-02	1.61131E+00	-1.06822E-01
AT NODE	3135	3133	3135	2876	2943	2937

O V E R A L L T I M E L O G I N S E C O N D S

INPUT (READ,GENERATE)	47.270
DATA SORTING AND CHECKING	17.970
REORDERING OF ELEMENTS	25.760
FORM ELEMENT MATRICES	1020.970
FORM GLOBAL LOAD VECTOR	3.490
MATRIX TRANSFORMATION DUE TO RPC	0.000
PRE-FRONT	10.620
SOLUTION OF SYSTEM EQUATIONS	1711.740
INTERNAL FORCES AND REACTIONS	49.100
STRESS CALCULATION	511.410
LOAD COMBINATION	0.000
TOTAL CPU	3400.330

NISA JOB FINISHED AT - 16:45:24 6/14/1990

TOTAL ELAPSED TIME IS = 5420.000

APPENDIX E

Aerodynamic Data for NACA 63_2-015 Series Aerofoil

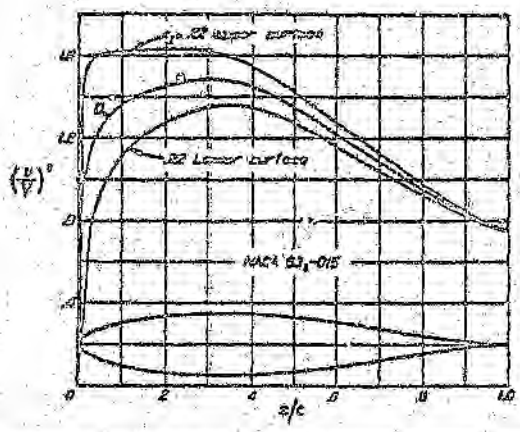

z (per cent c)	y (per cent c)	$(v/V)^2$	s/V	$\Delta s_c/V$
0	0	0	0	1.918
0.5	1.204	0.600	0.775	1.513
0.75	1.462	0.822	0.907	1.379
1.25	1.878	0.936	0.969	1.182
2.5	2.610	1.105	1.051	0.903
5.0	3.648	1.244	1.115	0.674
7.5	4.427	1.315	1.147	0.557
10	5.055	1.360	1.166	0.484
15	6.011	1.415	1.190	0.393
20	6.693	1.448	1.203	0.330
25	7.155	1.467	1.211	0.286
30	7.421	1.481	1.217	0.251
35	7.500	1.475	1.214	0.222
40	7.393	1.446	1.202	0.196
45	7.099	1.401	1.184	0.174
50	6.665	1.345	1.160	0.153
55	6.108	1.281	1.132	0.135
60	5.453	1.220	1.105	0.118
65	4.721	1.155	1.075	0.102
70	3.934	1.085	1.042	0.088
75	3.119	1.019	1.009	0.076
80	2.310	0.953	0.976	0.063
85	1.541	0.894	0.946	0.051
90	0.852	0.838	0.916	0.039
95	0.300	0.789	0.888	0.028
100	0	0.750	0.866	0
L.E. radius: 1.584 per cent c				

NACA 63$_1$-015 Basic Thickness Form

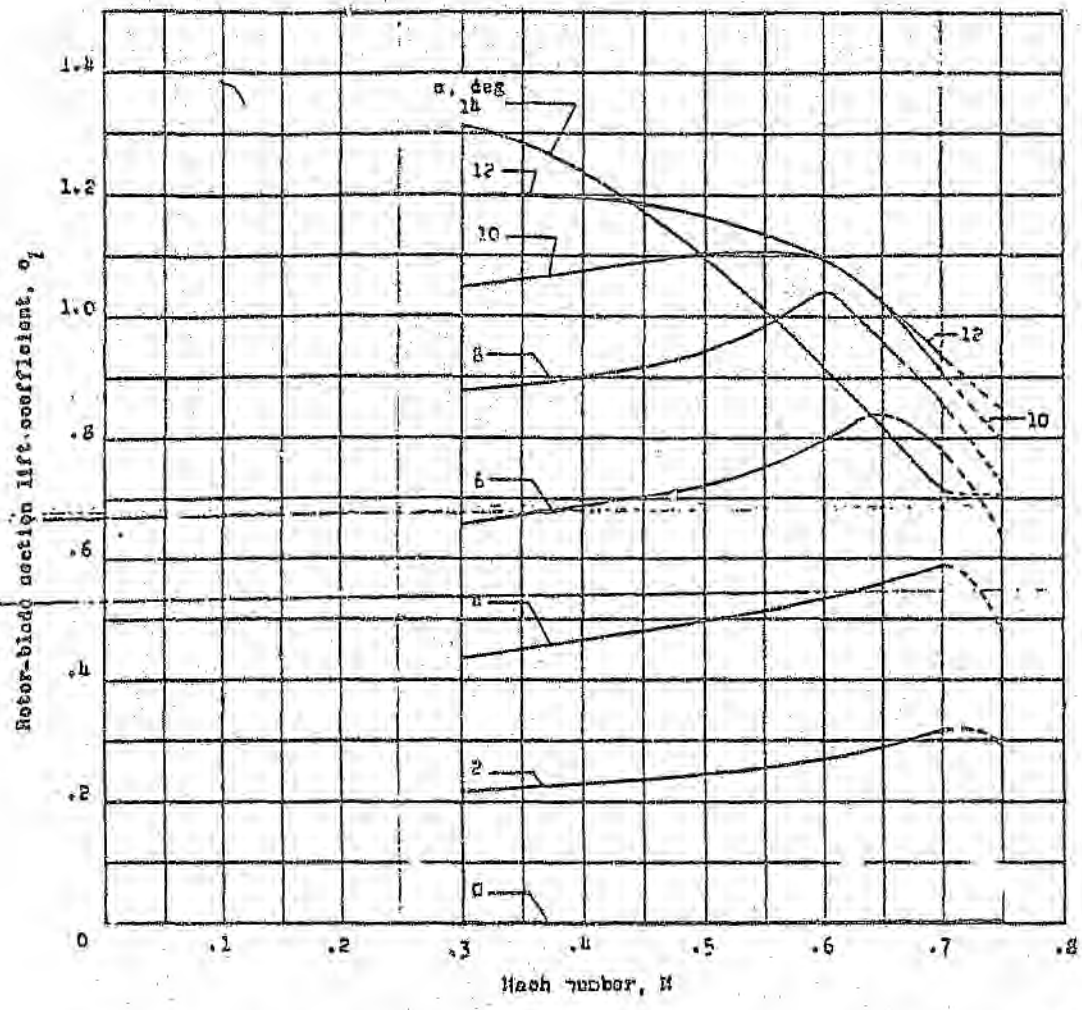

Figure 11.- Synthesized rotor-blade section lift coefficient plotted against Mach number for NACA 63_2-015 airfoil.

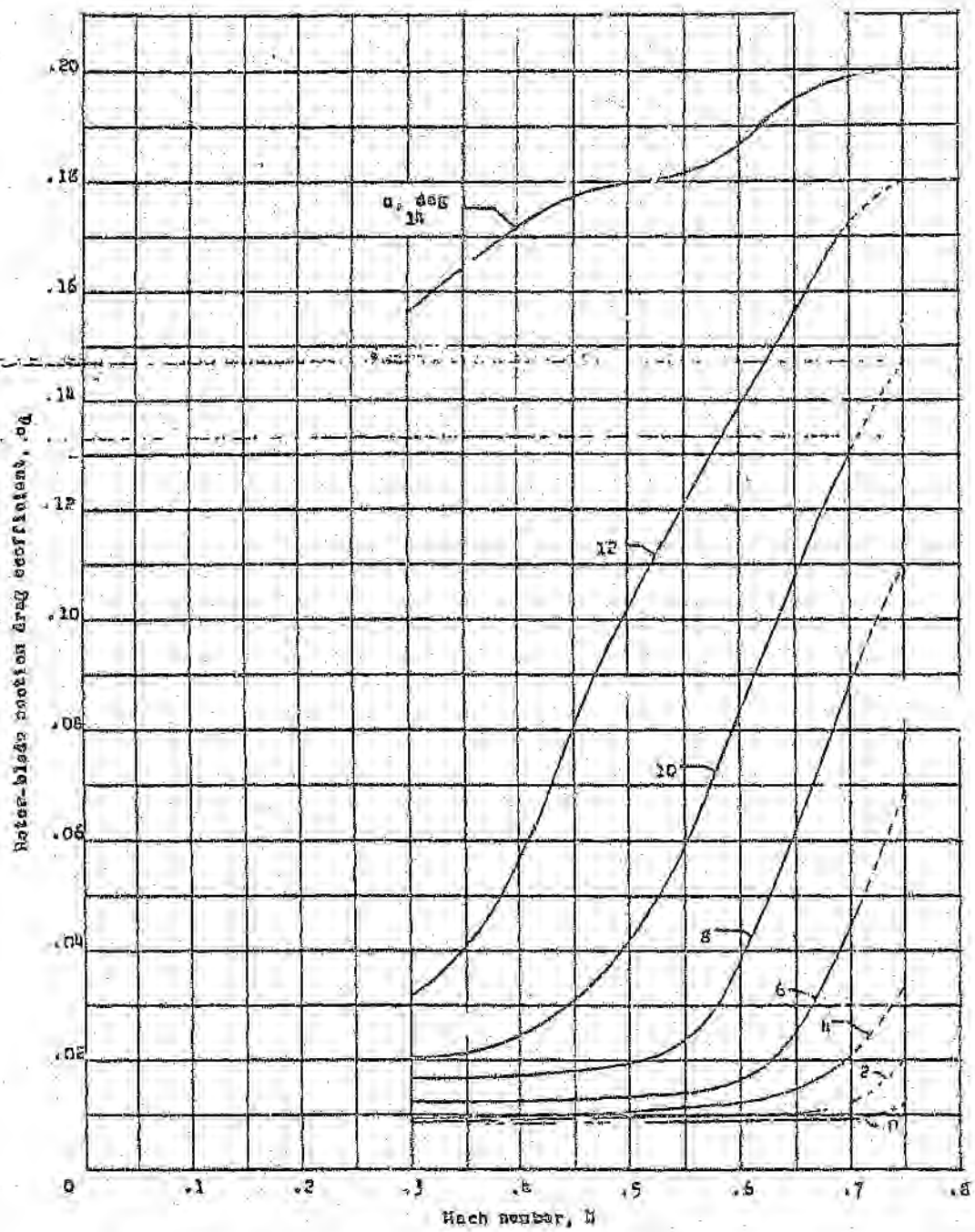

Figure 10.- Synthesized rotor-blade section drag coefficient plotted against Mach number for NACA 63_2-015 airfoil.

APPENDIX F

Computer Codes

```
program sectproperties;
{ this program calculates the section properties of any aerofoil }

{$M 32000,0,32000}
{$E+}
USES crt,dos,sectview,inp;

{CONST
     filename='a632-015.dat';}
VAR
   filename : STRING;

PROCEDURE getfile;
          CONST
               direc = 'dirfile.txt';
          VAR
             filebuf,chk : STRING;
             file1       : TEXT;
             i,pgc,pgl,j : BYTE;
             fl1         : BOOLEAN;
          BEGIN
               EXEC('c:\command.com','/C dir *.*>dirfile.txt');
               ASSIGN(file1,direc);
               RESET(file1);
               clrscr;
               gotoxy(1,1);
               FOR i:=1 TO 6 DO
                   readln(file1,fi'     ');
               pgc:=1;
               pgl:=1;
               fl1:=false;
               WHILE not EOF(file1) DO
                     BEGIN
                          readln(file1,filebuf);
                          filebuf:=COPY(filebuf,1,12);
                          INSERT('.',filebuf,10);
                          chk:=COPY(filebuf,1,7);
                          IF chk='DIRFILE' THEN
                             fl1:=true;
                          IF chk='        ' THEN
                             fl1:=true;
                          IF not fl1 THEN
                             BEGIN
                                  fl1:=false;
                                  IF pgc<65 THEN
                                     BEGIN
                                          gotoxy(pgc,pgl);
                                          writeln(filebuf);
                                          inc(pgc,20);
                                     END
                                  ELSE
                                     BEGIN
                                          inc(pgl,1);
                                          pgc:=1;
                                          gotoxy(pgc,pgl);
```

```
                                        writeln(filebuf);
                                    END;
                                END;
                        END;
                writeln;
                writeln('Enter Filename ?');
                j:=wherey;
                gotoxy(17,j-1);
                readln(filename);
                EXEC('c:\command.com','/C del dirfile.txt');
        END;{getfile}

PROCEDURE readdata;
        VAR
           file1 : TEXT;
        BEGIN
                ASSIGN(file1,filename);
                RESET(file1);
                count:=1;
                WHILE not EOF(file1) DO
                        BEGIN
                                readln(file1,x[count],y[count]);
                                inc(count,1);
                        END;
                CLOSE(file1);
                dec(count,1);
                clrscr;
                gotoxy(1,1);
                write('Enter skin thickness ?');
                readln(t[1,1]);
                write('Enter first thickening ?');
                readln(t[2,1]);
                IF t[2,1]<>0 THEN
                   BEGIN
                        write('Enter first thickening start pos ?');
                        readln(t[2,2]);
                        write('Enter first thickening end pos ?');
                        readln(t[2,3]);
                   END
                ELSE
                    BEGIN
                         t[2,2]:=0;
                         t[2,3]:=0;
                    END;
                write('Enter second thickening ?');
                readln(t[3,1]);
                IF t[3,1]<>0 THEN
                   BEGIN
                        write('Enter second thickening start pos ?');
                        readln(t[3,2]);
                        write('Enter second thickening end pos ?');
                        readln(t[3,3]);
                   END
                ELSE
                    BEGIN
```

```
                    t[3,2]:=0;
                    t[3,3]:=0;
                END;
            write('Enter third thickening ?');
            readln(t[4,1]);
            IF t[4,1]<>0 THEN
               BEGIN
                    write('Enter third thickening start pos ?');
                    readln(t[4,2]);
                    write('Enter third thickening end pos ?');
                    readln(t[4,3])
               END
            ELSE
                BEGIN
                    t[4,2]:=0;
                    t[4,3]:=0;
                END;
        END;{readdata}

PROCEDURE additionalarea;
        VAR
        i   : INTEGER;
        ans : CHAR;
        BEGIN
            add:=false;
            write('Additional information (Y/N) ?');
            readln(ans);
            ans:=upcase(ans);
            IF ans='Y' THEN
               BEGIN
                    add:=true;
                    write('Enter start X ?');
                    readln(sx1);
                    write('Enter end X ?');
                    readln(sx2);
                    write('Enter bottom Y pos ?');
                    readln(sy1);
                    write('Enter thickness ?');
                    readln(sy2);
               END;
        END;

PROCEDURE totalarea;
        VAR
           i  : INTEGER;
        BEGIN
            area:=0;
            FOR i:=1 TO count-1 DO
                BEGIN
                    IF (x[i]>=t[2,2]) and (x[i]<=t[2,3]) THEN
                       th:=t[1,1]+t[2,1]
                    ELSE
                        IF (x[i]>=t[3,2]) and (x[i]<=t[3,3]) THEN
                           th:=t[1,1]+t[3,1]
                        ELSE
```

```
                                        IF (x[i]>=t[4,2]) and (x[i]<=t[4,3]) THE
N
                                           th:=t[1,1]+t[4,1]
                                        ELSE
                                           th:=t[1,1];
                                     area:=area+SQRT(SQR(x[i+1]-x[i])+SQR(y[i+1]-y[i]
))*th
                                END;
                             IF add THEN
                                     area:=area+((sx2-sx1)*sy2);
                             area:=area*2;
                          END;

               PROCEDURE centroid;
                          VAR
                             i      : INTEGER;
                          BEGIN
                               xb:=0;
                               yb:=0;
                               FOR i:=1 TO count-1 DO
                                   BEGIN
                                        IF (x[i]>=t[2,2]) and (x[i]<=t[2,3]) THEN
                                           th:=t[1,1]+t[2,1]
                                        ELSE
                                            IF (x[i]>=t[3,2]) and (x[i]<=t[3,3]) THEN
                                               th:=t[1,1]+t[3,1]
                                            ELSE
                                                IF (x[i]>=t[4,2]) and (x[i]<=t[4,3]) THE
N
                                                   th:=t[1,1]+t[4,1]
                                                ELSE
                                                   th:=t[1,1];
                                        theta:=ARCTAN((y[i+1]-y[i])/(x[i+1]-x[i]));
                                        xb:=xb+ SQRT(SQR(x[i+1]-x[i])+SQR(y[i+1]-y[i]))*
th*(x[i+1]+x[i])/2);
                                        yb:=yb+(SQRT(SQR(x[i+1]-x[i])+SQR(y[i+1]-y[i]))*
th*((y[i+1]+y[i])/2-th/2/COS(theta)));
                                   END;
                               IF add THEN
                                  BEGIN
                                       xb:=xb+(sx2-sx1)*sy2*(sx2+sx1)/2;
                                       yb:=yb+(sx2-sx1)*sy2*(sy1+sy2/2);
                                  END;
                               FOR i:=1 TO count-1 DO
                                   BEGIN
                                        IF (x[i]>=t[2,2]) and (x[i]<=t[2,3]) THEN
                                           th:=t[1,1]+t[2,1]
                                        ELSE
                                            IF (x[i]>=t[3,2]) and (x[i]<=t[3,3]) THEN
                                               th:=t[1,1]+t[3,1]
                                            ELSE
                                                IF (x[i]>=t[4,2]) and (x[i]<=t[4,3]) THE
N
                                                   th:=t[1,1]+t[4,1]
                                                ELSE
                                                   th:=t[1,1];
                                        theta:=ARCTAN((-y[i+1]+y[i])/(x[i+1]-x[i]));
                                        xb:=xb+(SQRT(SQR(x[i+1]-x[i])+SQR(y[i+1]-y[i]))*
th*(x[i+1]+x[i])/2);
                                        yb:=yb+(SQRT(SQR(x[i+1]-x[i])+SQR(y[i+1]-y[i]))*
th*((-y[i+1]-y[i])/2+th/2/COS(theta)));
                                   END;
```

```
                    BEGIN
                        xb:=xb+(sx2-sx1)*sy2*(sx2+sx1)/2;
                        yb:=yb+(sx2-sx1)*sy2*(-sy1-sy2/2);
                    END;
                xb:=xb/area;
                yb:=yb/area;
            END;

    PROCEDURE sectionmoments;
            VAR
               i  : INTEGER;
            BEGIN
                ix:=0;
                iy:=0;
                ixy:=0;
                FOR i:=1 TO count-1 DO
                    BEGIN
                        IF (x[i]>=t[2,2]) and (x[i]<=t[2,3]) THEN
                           th:=t[1,1]+t[2,1]
                        ELSE
                            IF (x[i]>=t[3,2]) and (x[i]<=t[3,3]) THEN
                               th:=t[1,1]+t[3,1]
                            ELSE
                                IF (x[i]>=t[4,2]) and (x[i]<=t[4,3]) THE
N
                                   th:=t[1,1]+t[4,1]
                                ELSE
                                   th:=t[1,1];
                        theta:=ARCTAN((y[i+1]-y[i])/(x[i+1]-x[i]));
    ix:=ix+(SQRT(SQR(x[i+1]-x[i])+SQR(y[i+1]-y[i]))*th*SQR((y[i+1]+y[i])/2-t
h/2/COS(theta)));
    iy:=iy+(SQRT(SQR(x[i+1]-x[i])+SQR(y[i+1]-y[i]))*th*SQR((x[i+1]+x[i])/2))
;
    ixy:=ixy+(SQRT(SQR(x[i+1]-x[i])+SQR(y[i+1]-y[i]))*th*(x[i+1]+x[i])/2*((y
[i+1]+y[i])/2-th/2/COS(theta)));
                    END;
                IF add THEN
                   BEGIN
                        iy:=iy+(sx2-sx1)*sy2*SQR((sx2+sx1)/2);
                        ix:=ix+(sx2-sx1)*sy2*SQR((sy1+sy2/2));
                        ixy:=ixy+(sx2-sx1)*sy2*(sx2+sx1)/2*(sy1+sy2/2);
                   END;
                FOR i:=1 TO count-1 DO
                    BEGIN
                        IF (x[i]>=t[2,2]) and (x[i]<=t[2,3]) THEN
                           th:=t[1,1]+t[2,1]
                        ELSE
                            IF (x[i]>=t[3,2]) and (x[i]<=t[3,3]) THEN
                               th:=t[1,1]+t[3,1]
                            ELSE
                                IF (x[i]>=t[4,2]) and (x[i]<=t[4,3]) THE
N
                                   th:=t[1,1]+t[4,1]
                                ELSE
                                   th:=t[1,1];
                        theta:=ARCTAN((-y[i+1]+y[i])/(x[i+1]-x[i]));
    ix:=ix+(SQRT(SQR(x[i+1]-x[i])+SQR(y[i+1]-y[i]))*th*SQR((-y[i+1]-y[i])/2+
th/2/COS(theta)));
    iy:=iy+(SQRT(SQR(x[i+1]-x[i])+SQR(y[i+1]-y[i]))*th*SQR((x[i+1]+x[i])/2))
;
    ixy:=ixy+(SQRT(SQR(x[i+1]-x[i])+SQR(y[i+1]-y[i]))*th*(x[i+1]+x[i])/2*((-
y[i+1]-y[i])/2+th/2/COS(theta)));
```

```
                    IF add THEN
                       BEGIN
                            iy:=iy+(sx2-sx1)*sy2*SQR((sx2+sx1)/2);
                            ix:=ix+(sx2-sx1)*sy2*SQR((-sy1-sy2/2));
                            ixy:=ixy+(sx2-sx1)*sy2*(sx2+sx1)/2*(-sy1-sy2/2);
                       END;
               END;

     PROCEDURE centroidmoments;
               BEGIN
                    ixb:=ix+area*SQR(yb);
                    iyb:=iy+area*SQR(xb);
                    ixyb:=ixy+area*xb*yb;
               END;

     PROCEDURE principlemoments;
               BEGIN
                    phi:=ARCTAN(2*ixy/(iy-ix))/2;
                    ixp:=ixb*SQR(COS(phi))+iyb*SQR(SIN(phi))-2*ixy*SIN(phi)*C
OS(phi);
                    iyp:=ixb*SQR(SIN(phi))+iyb*SQR(COS(phi))+2*ixy*SIN(phi)*C
OS(phi);
               END;
     BEGIN
          getfile;
          readdata;
          additionalarea;
          totalarea;
          centroid;
          sectionmoments;
          centroidmoments;
          principlemoments;
          clrscr;
          view;
     (*
          gotoxy(1,1);
          writeln('area =',area:9:2);
          writeln('xb =',xb:9:2);
          writeln('yb =',yb:9:2);
          writeln('ix =',ix:9);
          writeln('iy =',iy:9);
          writeln('ixy =',ixy:9);
          writeln('ixb =',ixb:9);
          writeln('iyb =',iyb:9);
          writeln('ixyb =',ixyb:9);
          writeln('phi =',phi*180/pi:9:2);
          writeln('ixp =',ixp:9);
          writeln('iyp =',iyp:9);
     *)
     END.
```

```
UNIT sectview;

INTERFACE

USES graph,scrdrv,inp;

PROCEDURE view;

IMPLEMENTATION
            VAR
               maxx,maxy,pos          : INTEGER;
               maxth                  : REAL;

PROCEDURE axes;
          VAR
             b1,b2,b3   : INTEGER;
          BEGIN
               setlinestyle(0,0,3);
               rectangle(0,0,maxx,maxy);
               setlinestyle(0,0,1);
               b1:=trunc(maxx-0.95*maxx);
               b2:=trunc(maxx-0.05*maxx);
               b3:=trunc(maxy/pos);
               line(b1,b3,b2,b3);
               b1:=trunc(maxy/pos-0.3*maxy);
               b2:=trunc(maxy/pos+0.3*maxy);
               b3:=trunc(maxx-0.9*maxx);
               line(b3,b1,b3,b2);
               settextstyle(0,0,0);
               b1:=trunc(maxx-0.15*maxx);
               b2:=trunc(maxy/pos+0.02*maxy);
               outtextxy(b1,b2,'x - axis');
               settextstyle(0,1,0);
               b1:=trunc(maxx-0.92*maxx);
               b2:=trunc(maxy/pos-0.3*maxy);
               outtextxy(b1,b2,'y - axis');
          END;

PROCEDURE getmaxth;
          VAR
             i      : INTEGER;
             buf    : REAL;
          BEGIN
               maxth:=0;
               FOR i:=1 TO count-1 DO
                   BEGIN
                        IF (y[i+1]>=y[i]) THEN
                           buf:=y[i+1];
                        IF buf>=maxth THEN
                           maxth:=buf;
                   END;
          END;

FUNCTION scalex(xcord : REAL):INTEGER;
```

```
            VAR
               cm : REAL;
               scx : INTEGER;
            BEGIN
                 cm:=x[count];
                 scx:=trunc((maxx-0.2*maxx)/x[count]*xcord+(maxx-0.9*maxx))
;
                 scalex:=scx;
            END;

FUNCTIO ' scaley(ycord : REAL):INTEGER;
            VAR
               cm : REAL;
               scy : INTEGER;
            BE IN
                 cm:=x[count];
                 scy:=trunc((maxx-0.2*maxx)/x[count]*ycord+maxy/pos);
                 scaley:=scy;
            END;

FUNCTION confx(num : REAL;
                 form1,form2,pos : INTEGER;
                 main : STRING) : STRING;
            VAR
               temp : STRING;
            BEGIN
                 STR(num:form1:form2,temp);
                 INSERT(temp,main,pos);
                 confx:=main;
            END;

FUNCTION conex(num : REAL;
                 form1,pos : INTEGER;
                 main : STRING) : STRING;
            VAR
               temp : STRING;
            BEGIN
                 STR(num:form1,temp);
                 INSERT(temp,main,pos);
                 conex:=main;
            END;

PROCEDURE addarea;
            VAR
               xa1,xa2,ya1,ya2 : INTEGER;
            BEGIN
                 xa1:=scalex(sx1);
                 xa2:=scalex(sx2);
                 ya1:=scaley(sy1);
                 ya2:=scaley(sy1+sy2);
                 moveto(xa1,ya1);
                 lineto(xa1,ya2);
                 lineto(xa2,ya2);
                 lineto(xa2,ya1);
                 lineto(xa1,ya1);
                 ya1:=scaley(-sy1);
```

```
            ya2:=scaley(-sy1-sy2);
            moveto(xa1,ya1);
            lineto(xa1,ya2);
            lineto(xa2,ya2);
            lineto(xa2,ya1);
            lineto(xa1,ya1);
        END;

PROCEDURE vwcentroid;
        VAR
           xc,yc,rad,b1,b2 : INTEGER;
        BEGIN
            setfillstyle(0,0);
            xc:=scalex(xb);
            yc:=scaley(yb);
            rad:=trunc(0.015*maxx);
            pieslice(xc,yc,0,90,rad);
            pieslice(xc,yc,180,270,rad);
            setfillstyle(1,15);
            pieslice(xc,yc,90,180,rad);
            pieslice(xc,yc,270,360,rad);
            setlinestyle(2,0,1);
            b1:=trunc(maxx-0.90*maxx);
            b2:=trunc(maxx-0.10*maxx);
            line(b1,yc,b2,yc);
            b1:=trunc(maxy/pos-0.3*maxy);
            b2:=trunc(maxy/pos+0.3*maxy);
            line(xc,b1,xc,b2);
            setlinestyle(0,0,1);
        END;

PROCEDURE results;
        VAR
           xt1,yt1,xt2,yt2 : INTEGER;
           ct : STRING;
        BEGIN
            settextstyle(0,0,0);
            xt1:=trunc(maxx-0.90*maxx);
            yt1:=trunc(0.7*maxy);
            xt2:=trunc(maxx-0.10*maxx);
            yt2:=trunc(0.9*maxy);
            rectangle(xt1,yt1,xt2,yt2);
            ct:='Centroid =(,)';
            ct:=confx(xb,6,2,12,ct);
            ct:=confx(yb,6,2,19,ct);
            xt1:=trunc(maxx-0.85*maxx);
            yt1:=trunc(0.72*maxy);
            outtextxy(xt1,yt1,ct);
            yt1:=trunc(0.75*maxy);
            ct:='Area      =';
            ct:=confx(area,6,2,11,ct);
            outtextxy(xt1,yt1,ct);
            yt1:=trunc(0.78*maxy);
            ct:='Ix    =';
            ct:=conex(ix,9,6,ct);
```

```
            outtextxy(xt1,yt1,ct);
            yt1:=trunc(0.81*maxy);
            ct:='Iy  =';
            ct:=conex(iy,9,6,ct);
            outtextxy(xt1,yt1,ct);
            yt1:=trunc(0.84*maxy);
            ct:='Ixy =';
            ct:=conex(ixy,9,6,ct);
            outtextxy(xt1,yt1,ct);
            xt1:=trunc(maxx-0.60*maxx);
            yt1:=trunc(0.78*maxy);
            ct:='Ixb =';
            ct:=conex(ixb,9,6,ct);
            outtextxy(xt1,yt1,ct);
            yt1:=trunc(0.81*maxy);
            ct:='Iyb =';
            ct:=conex(iyb,9,6,ct);
            outtextxy(xt1,yt1,ct);
            yt1:=trunc(0.84*maxy);
            ct:='Ixyb=';
            ct:=conex(ixyb,9,6,ct);
            outtextxy(xt1,yt1,ct);
            xt1:=trunc(maxx-0.35*maxx);
            yt1:=trunc(0.78*maxy);
            ct:='Phi =';
            ct:=conex(phi,9,6,ct);
            outtextxy(xt1,yt1,ct);
            yt1:=trunc(0.81*maxy);
            ct:='Ixp =';
            ct:=conex(ixp,9,6,ct);
            outtextxy(xt1,yt1,ct);
            yt1:=trunc(0.84*maxy);
            ct:='Iyp =';
            ct:=conex(iyp,9,6,ct);
            outtextxy(xt1,yt1,ct);

        END;

PROCEDURE view;{main unit procedure}
        VAR
           k,
           x1,y1,x2,y2 : INTEGER;

        BEGIN
            graphinitialize;
            maxx:=getmaxx;
            maxy:=getmaxy;
            getmaxth;
            pos:=3;
            axes;
            x1:=scalex(x[1]);
            y1:=scaley(y[1]);
            moveto(x1,y1);
            FOR k:=2 TO count DO
                BEGIN
```

```
                    x1:=scalex(x[k]);
                    y1:=scaley(y[k]);
                    lineto(x1,y1);
                END;
            FOR k:=count DOWNTO 1 DO
                BEGIN
                    x1:=scalex(x[k]);
                    y1:=scaley(-y[k]);
                    lineto(x1,y1);
                END;
            IF add THEN
               addarea;
            vwcentroid;
            results;
            readln;
            CloseGraph;
        END;
END.
```

APPENDIX G

Dynamic Analysis Results

CASE 1 FLEX DYNAMICS

SEGMNT LNTH	EI BEAM	EI CHORD	WT/IN	TWIST (INBD)	C.F. (INBD)	IBB	ICC	BJ	SHEAR OFFSET BEAM	SHEAR OFFSET CHORD	C.G. OFFSET BEAM	C.G. OFFSET CHORD
IN	— LB-IN**2 —		LB/IN	DEG	LB/RPM**2	IN-LB-SEC**2/IN		LB-IN**2	IN	IN	IN	IN
1 .94	.4112E+07	.3023E+07	.0513	.00	.2955E-03	.0000E+00	.1034E-03				.000	.000
2 .94	.4112E+07	.3023E+07	.0513	.00	.2856E-03	.0000E+00	.1034E-03				.000	.000
3 .94	.4112E+07	.6063E+05	.0058	.00	.2839E-03	.0000E+00	.1025E-07				.000	.000
4 .94	.1021E+04	.6063E+05	.0058	.00	.2835E-03	.0000E+00	.1025E-07				.000	.000
5 .94	.1021E+04	.6063E+05	.0058	.00	.2830E-03	.0000E+00	.1025E-07				.000	.000
6 .94	.1021E+04	.6063E+05	.1366	.00	.2824E-03	.0000E+00	.1025E-07				.000	.000
7 .94	.1021E+04	.5952E+06	.1523	.00	.2635E-03	.0000E+00	.8318E-06				.000	.000
8 .94	.1021E+04	.5952E+06	.0218	.00	.2397E-03	.0000E+00	.8318E-06				.000	.000
9 .94	.3982E+05	.5952E+06	.0218	.00	.2346E-03	.0000E+00	.8318E-06				.000	.000
10 .94	.3983E+05	.4150E+06	.0178	.00	.2299E-03	.0000E+00	.9577E-06				.000	.000
11 .94	.3983E+05	.4150E+06	.0178	.00	.2257E-03	.0000E+00	.9577E-06				.000	.000
12 .94	.2997E+05	.4150E+06	.0178	.00	.2210E-03	.0000E+00	.1165E-05				.000	.000
13 .94	.2997E+05	.4150E+06	.0178	.00	.2159E-03	.0000E+00	.1165E-05				.000	.000
14 .94	.3624E+05	.4150E+06	.0178	.00	.2103E-03	.0000E+00	.1165E-05				.000	.000
15 .94	.3624E+05	.4150E+06	.0178	.00	.2043E-03	.0000E+00	.1165E-05				.000	.000
16 .94	.3624E+05	.4150E+06	.0178	.00	.1979E-03	.0000E+00	.1165E-05				.000	.000
17 .94	.3624E+05	.4150E+06	.0178	.00	.1910E-03	.0000E+00	.1165E-05				.000	.000
18 .94	.3624E+05	.4150E+06	.0178	.00	.1836E-03	.0000E+00	.1165E-05				.000	.000
19 .94	.3624E+05	.4150E+06	.0178	.00	.1758E-03	.0000E+00	.1165E-05				.000	.000
20 .94	.3624E+05	.4150E+06	.0178	.00	.1676E-03	.0000E+00	.1165E-05				.000	.000
21 .94	.3624E+05	.4150E+06	.0178	.00	.1589E-03	.0000E+00	.1165E-05				.000	.000
22 .94	.3624E+05	.4150E+06	.0178	.00	.1498E-03	.0000E+00	.1165E-05				.000	.000
23 .94	.3624E+05	.4150E+06	.0178	.00	.1402E-03	.0000E+00	.1165E-05				.000	.000
24 .94	.3624E+05	.4150E+06	.0178	.00	.1302E-03	.0000E+00	.1165E-05				.000	.000
25 .94	.3624E+05	.4150E+06	.0178	.00	.1198E-03	.0000E+00	.1165E-05				.000	.000
26 .94	.3624E+05	.4150E+06	.0178	.00	.1088E-03	.0000E+00	.1165E-05				.000	.000
27 .94	.3624E+05	.4150E+06	.0178	.00	.9749E-04	.0000E+00	.1165E-05				.000	.000
28 .94	.3624E+05	.4150E+06	.0178	.00	.8570E-04	.0000E+00	.1165E-05				.000	.000
29 .94	.3624E+05	.4150E+06	.0178	.00	.7346E-04	.0000E+00	.1165E-05				.000	.000
30 .94	.3624E+05	.4150E+06	.0178	.00	.6077E-04	.0000E+00	.1165E-05				.000	.000
TIP			.0595	.00							.000	.000

2, BLADES RADIUS 28.20 IN BLADE WEIGHT .84 LB
2 HUB SEGMENTS BLADE FLAP INERTIA .04 SLUG-FT**2

FLAP HNG OFST .00 IN FLAP SPRING .000E+00 IN-LB/RAD HUB C.P. INERTIA .000 LB-SEC**2/IN HUB C.P. STIFF .223E+02 LB/IN
LAG HNG OFST .00 IN LAG SPRING .000E+00 IN-LB/RAD HUB I.P. INERTIA .000 LB-SEC**2/IN HUB I.P. STIFF .501E+04 LB/IN
PITCH HORN OFST 1.97 IN CNTRL STIFF .649E+06 IN-LB/RAD
MAST TORSION SPR .130E+05 IN-LB/RAD

CASE 1 FLEX DYNAMICS

8.00 DEGREES ROOT COLLECTIVE 500.0 ROTOR SPEED, RPM
COLLECTIVE MODE OF BLADE AT 552.85 CPM
OR 1.106 PER REV

BLADE STA IN	DEFLECTIONS IN VERT	DEFLECTIONS IN HORIZ	MOMENTS IN-LB BEAM	MOMENTS IN-LB CHORD	SHEAR FORCES LB BEAM	SHEAR FORCES LB CHORD	TWIST DEG	TORQUE IN-LB
1 .00	.139	.000	20.	8.	3.	1.		
2 .94	.139	.001	17.	7.	3.	1.		
3 1.88	.139	.001	15.	4.	3.	0.		
4 2.82	.139	.002	13.	4.	3.	0.		
5 3.76	.144	.003	10.	4.	3.	0.		
6 4.70	.159	.005	8.	4.	3.	0.		
7 5.64	.178	.009	7.	4.	3.	0.		
8 6.58	.205	.014	6.	3.	3.	0.		
9 7.52	.236	.019	5.	3.	3.	0.		
10 8.46	.271	.026	5.	2.	2.	0.		

11	9.40	.304	.030	3.	3.	2.	0.
12	10.34	.338	.035	4.	3.	2.	0.
13	11.28	.373	.041	4.	2.	2.	0.
14	12.22	.407	.047	4.	2.	2.	0.
15	13.16	.441	.052	3.	2.	2.	0.
16	14.10	.476	.058	3.	2.	2.	0.
17	15.04	.511	.064	3.	2.	2.	0.
18	15.98	.545	.069	2.	2.	2.	0.
19	16.92	.580	.075	2.	1.	2.	0.
20	17.86	.615	.081	2.	1.	2.	0.
21	18.80	.650	.086	2.	1.	2.	0.
22	19.74	.685	.092	1.	1.	2.	0.
23	20.68	.720	.098	1.	1.	2.	0.
24	21.62	.755	.104	1.	1.	1.	0.
25	22.56	.790	.109	1.	1.	1.	0.
26	23.50	.825	.115	1.	0.	1.	0.
27	24.44	.860	.121	0.	0.	1.	0.
28	25.38	.895	.126	0.	0.	1.	0.
29	26.32	.930	.132	0.	0.	1.	0.
30	27.26	.965	.138	0.	0.	1.	0.
31	28.20	1.000	.144	0.	0.	1.	0.

GENERALIZED INERTIA (IN-LBF-SEC**2) VERT .00059 HORIZ .00001 TWIST .00000
BOUNDARY CONDITION CHECK .30560E-07 .50117E-08 .11777E-06 .81934E-06

CASE 1 FLEX DYNAMICS

8.00 DEGREES ROOT COLLECTIVE 500.0 ROTOR SPEED, RPM
COLLECTIVE MODE OF BLADE AT 1219.97 CPM
OR 2.440 PER REV

BLADE STA IN	DEFLECTIONS IN		MOMENTS IN-LB		SHEAR FORCES LB.		TWIST DEG	TORQUE IN-LB
	VERT	HORIZ	BEAM	CHORD	BEAM	CHORD		
1 .00	-.292	.000	-50.	268.	-6.	16.		
2 .94	-.292	.018	-44.	255.	-6.	16.		
3 1.88	-.292	.037	-5.	244.	-3.	17.		
4 2.82	-.292	.057	-2.	230.	-3.	16.		
5 3.76	-.293	.081	1.	216.	-3.	16.		
6 4.70	-.294	.107	4.	203.	-3.	16.		
7 5.64	-.293	.137	6.	190.	-2.	16.		
8 6.58	-.287	.170	7.	178.	-0.	15.		
9 7.52	-.275	.203	7.	167.	0.	14.		
10 8.46	-.260	.237	8.	156.	1.	14.		
11 9.40	-.245	.271	8.	145.	1.	13.		
12 10.34	-.230	.306	8.	134.	1.	13.		
13 11.28	-.214	.341	8.	124.	1.	13.		
14 12.27	-.199	.376	8.	114.	1.	13.		
15 13.16	-.183	.411	8.	104.	1.	12.		
16 14.10	-.167	.447	8.	94.	1.	12.		
17 15.04	-.151	.483	8.	85.	1.	12.		
18 15.98	-.135	.519	7.	76.	2.	11.		
19 16.92	-.119	.556	7.	67.	2.	11.		
20 17.86	-.102	.592	6.	59.	2.	10.		
21 18.80	-.085	.629	6.	51.	2.	10.		
22 19.74	-.069	.666	5.	44.	2.	9.		
23 20.68	-.052	.703	4.	37.	2.	9.		
24 21.62	-.035	.740	4.	31.	1.	8.		
25 22.56	-.018	.777	3.	25.	1.	8.		
26 23.50	-.000	.814	2.	19.	1.	7.		
27 24.44	.017	.851	2.	14.	1.	6.		
28 25.38	.034	.888	1.	10.	1.	6.		
29 26.32	.051	.925	1.	6.	1.	5.		
30 27.26	.068	.963	0.	3.	1.	4.		
31 28.20	.086	1.000	0.	0.	1.	3.		

GENERALIZED INERTIA (IN-LBF-SEC**2) VERT .00011 HORIZ .00056 TWIST .00000
BOUNDARY CONDITION CHECK .[illegible]

15	13.16	.980	.219	-858.	-249.	62.	-13.
16	14.10	1.000	.211	-897.	-238.	42.	-15.
17	15.04	.999	.200	-917.	-221.	22.	-16.
18	15.98	.975	.186	-920.	-205.	2.	-17.
19	16.92	.929	.167	-905.	-185.	-18.	-18.
20	17.86	.862	.146	-874.	-171.	-36.	-19.
21	18.80	.774	.121	-827.	-153.	-54.	-20.
22	19.74	.666	.093	-766.	-135.	-69.	-20.
23	20.68	.539	.062	-693.	-116.	-82.	-20.
24	21.62	.396	.028	-610.	-98.	-92.	-20.
25	22.56	.239	-.007	-520.	-81.	-101.	-19.
26	23.50	.066	-.045	-426.	-64.	-104.	-18.
27	24.44	-.113	-.085	-330.	-48.	-107.	-17.
28	25.38	-.301	-.125	-235.	-34.	-104.	-16.
29	26.32	-.496	-.167	-147.	-21.	-98.	-14.
30	27.26	-.694	-.208	-67.	-9.	-88.	-12.
31	28.20	-.893	-.251	-0.	0.	-74.	-10.

GENERALIZED INERTIA (IN-LBF-SEC**2) VERT .00094 HORIZ .00005 TWIST .00000
BOUNDARY CONDITION CHECK .34373E-05 .72707E-06 .40545E-05 .14444E-04

CASE 1 FLEX. DYNAMICS

0.00 DEGREES ROOT COLLECTIVE 500.0 ROTOR SPEED, RPM
COLLECTIVE MODE OF BLADE AT 10836.56 CPM
OR 21.673 PER REV

BLADE STA IN	DEFLECTIONS IN		MOMENTS IN-LB		SHEAR FORCES LB		TWIST DEG	TORQUE IN-LB
	VERT	HORIZ	BEAM	CHORD	BEAM	CHORD		
1 .00	.909	.000	-1468.	-1338.	-17.	-732.		
2 .94	.908	-.092	-1384.	-650.	-90.	-732.		
3 1.88	.909	-.184	-1146.	193.	-333.	-678.		
4 2.82	.907	-.278	-761.	805	-411.	-650.		
5 3.76	.637	-.388	-379.	1407.	-427.	-643.		
6 4.70	.041	-.528	-10.	1996.	-438.	-634.		
7 5.64	-.564	-.640	364.	2480.	-430.	-516.		
8 6.58	-.894	-.695	490.	2728.	-137.	-264.		
9 7.52	-.840	-.692	373.	2832.	131.	-110.		
10 8.46	-.608	-.659	203.	2898.	194.	-71.		
11 9.40	-.372	-.621	-8.	2932.	237.	-36.		
12 10.34	-.137	-.576	-243.	2937.	263.	-4.		
13 11.28	.090	-.526	-489.	2913.	275.	26.		
14 12.22	.302	-.472	-736.	2861.	274.	56.		
15 13.16	.494	-.415	-972.	2783.	261.	85.		
16 14.10	.662	-.355	-1187.	2680.	237.	111.		
17 15.04	.800	-.294	-1371.	2554.	203.	136.		
18 15.98	.905	-.232	-1518.	2407.	161.	158.		
19 16.92	.972	-.170	-1622.	2242.	113.	178.		
20 17.86	1.000	-.108	-1678.	2061.	61.	195.		
21 18.80	.987	-.048	-1685.	1867.	7.	209.		
22 19.74	.933	.010	-1642.	1663.	-47.	219.		
23 20.68	.839	.066	-1553.	1453.	-98.	226.		
24 21.62	.707	.120	-1420.	1240.	-145.	229.		
25 22.56	.540	.172	-1250.	1028.	-185.	227.		
26 23.50	.344	.222	-1052.	821.	-216.	222.		
27 24.44	.122	.270	-834.	622.	-237.	213.		
28 25.38	-.121	.316	-607.	437.	-246.	199.		
29 26.32	-.378	.362	-384.	269.	-241.	180.		
30 27.26	-.645	.406	-178.	122.	-223.	157.		
31 28.20	-.916	.450	-1.	0.	-191.	130.		

GENERALIZED INERTIA (IN-LBF-SEC**2 VERT .00109 HORIZ .00048 TWIST .00000
BOUNDARY CONDITION CHECK -.72168E-05 .11930E-05 .11240E-04 -.22859E-04

CASE 1 FLEX DYNAMICS

CASE 1 FLEX DYNAMICS

8.00 DEGREES ROOT COLLECTIVE 500.0 ROTOR SPEED, RPM
COLLECTIVE MODE OF BLADE AT 140 CPM
OR 2.899 PER REV

BLADE STA IN	DEFLECTIONS IN VERT	HORIZ	MOMENTS IN-LB BEAM	CHORD	SHEAR FORCES LB BEAM	CHORD	TWIST DEG	TORQUE IN-LB
1 .00	.993	.000	35.	259.	21.	16.		
2 .94	.993	.018	17.	245.	20.	16.		
3 1.88	.992	.035	33.	229.	19.	13.		
4 2.82	.992	.055	16.	216.	18.	13.		
5 3.76	.990	.079	1.	207.	17.	13.		
6 4.70	1.000	.104	-15.	197.	17.	13.		
7 5.64	.992	.132	-27.	186.	13.	13.		
8 6.58	.962	.158	-33.	176.	5.	13.		
9 7.52	.904	.180	-36.	165.	0.	13.		
10 8.46	.831	.201	-39.	155.	-1.	13.		
11 9.40	.757	.221	-41.	145.	-2.	13.		
12 10.34	.682	.242	-42.	135.	-3.	13.		
13 11.28	.606	.263	-43.	125.	-4.	12.		
14 12.22	.529	.284	-43.	115.	-4.	12.		
15 13.16	.451	305	-42.	105.	-5.	12.		
16 14.10	.371	.326	-41.	96.	-5.	12.		
17 15.04	.291	.347	-39.	87.	-6.	11.		
18 15.98	.209	.368	-37.	78.	-6.	11.		
19 16.92	.127	.390	-35.	69.	-7.	11.		
20 17.86	.044	.411	-32.	61.	-7.	10.		
21 18.80	-.041	.432	-29.	53.	-7.	10.		
22 19.74	-.125	.454	-26.	46.	-7.	9.		
23 20.68	-.211	.475	-23.	38.	-7.	9.		
24 21.62	-.297	.496	-19.	32.	-6.	8.		
25 22.56	-.383	.518	-16.	26.	-6.	8.		
26 23.50	-.470	.539	-13.	20.	-6.	7.		
27 24.44	-.557	.560	-10.	15.	-6.	6.		
28 25.38	-.644	.582	-7.	10.	-5.	6.		
29 26.32	-.732	.603	-4.	6.	-5.	5.		
30 27.26	-.820	.625	-2.	3.	-4.	4.		
31 28.20	-.907	.646	0.	0.	-3.	3.		

GENERALIZED INERTIA (IN-LBF-SEC**2) VERT .00142 HORIZ .00026 TWIST .00000
BOUNDARY CONDITION CHECK -.34025E-04 .82846E-05 .23554E-03 -.33085E-03

CASE 1 FLEX DYNAMICS

8.00 DEGREES ROOT COLLECTIVE 500.0 ROTOR SPEED, RPM
COLLECTIVE MODE OF BLADE AT 6459.87 CPM
OR 12.918 PER REV

BLADE STA IN	DEFLECTIONS IN VERT	HORIZ	MOMENTS IN-LB BEAM	CHORD	SHEAR FORCES LB BEAM	CHORD	TWIST DEG	IN-LB
1 .00	-.924	.000	505.	81.	-7.	66.		
2 .94	-.924	.006	487.	19.	19.	66.		
3 1.88	-.924	.011	409.	-101.	80.	55.		
4 2.82	-.924	.016	306.	-148.	109.	51.		
5 3.76	-.809	.035	206.	-195.	115.	50.		
6 4.70	-.517	.075	113.	-241.	121.	49.		
7 5.64	-.134	.125	-13	-277.	160.	37.		
8 6.58	.233	.171	-163.	-290.	179.	14.		
9 7.52	.464	.197	-296.	-292.	154.	1.		
10 8.46	.584	.207	-423.	-290.	142.	-2.		
11 9.40	.695	.215	-538.	-286.	129.	-5.		
12 10.34	.795	.221	-641.	-280.	115.	-7.		

15	13.16	.980	.219	-858.	-249.	62.	-13.
16	14.10	1.000	.211	-897.	-236.	42.	-15.
17	15.04	.999	.200	-917.	-221.	22.	-16.
18	15.98	.975	.186	-920.	-205.	2.	-17.
19	16.92	.929	.167	-905.	-185.	-18.	-18.
20	17.86	.862	.146	-874.	-171.	-36.	-19.
21	18.80	.774	.121	-827.	-153.	-54.	-20.
22	19.74	.666	.093	-766.	-135.	-69.	-20.
23	20.68	.539	.062	-693.	-116.	-82.	-20.
24	21.62	.396	.028	-610.	-98.	-91.	-20.
25	22.56	.239	-.007	-520.	-81.	-101.	-19.
26	23.50	.068	-.045	-426.	-64.	-106.	-18.
27	24.44	-.113	-.085	-330.	-48.	-107.	-17.
28	25.38	-.301	-.125	-235.	-34.	-104.	-16.
29	26.32	-.496	-.167	-147.	-21.	-98.	-14.
30	27.26	-.694	-.208	-67.	-9.	-88.	-12.
31	28.20	-.893	-.251	-0.	0.	-74.	-10.

GENERALIZED INERTIA (IN-LBF-SEC**2) VERT .00094 HORIZ .00005 TWIST .00000
BOUNDARY CONDITION CHECK .34373E-05 .72707E-06 .40545E-05 .14444E-04

CASE 1 FLEX. DYNAMICS

8.00 DEGREES ROOT COLLECTIVE 500.0 ROTOR SPEED, RPM
COLLECTIVE MODE OF BLADE AT 10836.56 CPM
OR 21.673 PER REV

BLADE STA IN	DEFLECTIONS IN		MOMENTS IN-LB		SHEAR FORCES LB		TWIST DEG	TORQUE IN-LB
	VERT	HORIZ	BEAM	CHORD	BEAM	CHORD		
1 .00	.909	.000	-1468.	-1338.	-17.	-732.		
2 .94	.908	-.092	-1394.	-650.	-90.	-732.		
3 1.88	.908	-.184	-1146.	193.	-333.	-678.		
4 2.82	.907	-.273	-761.	805.	-411.	-650.		
5 3.76	.637	-.388	-379.	1407.	-427.	-643.		
6 4.70	.041	-.528	-10.	1996.	-438.	-634.		
7 5.64	-.564	-.640	364.	2480.	-430.	-516.		
8 6.58	-.894	-.695	490.	2728.	-137.	-264.		
9 7.52	-.840	-.692	373.	2832.	131.	-110.		
10 8.46	-.608	-.659	203.	2898.	194.	-71.		
11 9.40	-.372	-.621	-8.	2932.	237.	-36.		
12 10.34	-.137	-.576	-243.	2937.	263.	-4.		
13 11.28	.090	-.526	-489.	2913.	275.	26.		
14 12.22	.302	-.472	-736.	2861.	271.	56.		
15 13.16	.494	-.415	-972.	2783.	261.	85.		
16 14.10	.662	-.355	-1187.	2680.	237.	111.		
17 15.04	.800	-.294	-1371.	2554.	203.	136.		
18 15.98	.905	-.232	-1518.	2407.	161.	158.		
19 16.92	.972	-.170	-1622.	2242.	113.	178.		
20 17.86	1.000	-.108	-1678.	2061.	61.	195.		
21 18.80	.987	-.048	-1685.	1867.	7.	209.		
22 19.74	.933	.010	-1642.	1663.	-47.	219.		
23 20.68	.839	.066	-1553.	1453.	-98.	226.		
24 21.62	.707	.120	-1420.	1240.	-145.	229.		
25 22.56	.540	.172	-1250.	1028.	-185.	227.		
26 23.50	.344	.222	-1052.	821.	-216.	222.		
27 24.44	.122	.270	-834.	622.	-237.	213.		
28 25.38	-.121	.316	-607.	437.	-246.	199.		
29 26.32	-.378	.362	-394.	269.	-241.	180.		
30 27.26	-.645	.406	-178.	122.	-223.	157.		
31 28.20	-.916	.450	-1.	0.	-191.	130.		

GENERALIZED INERTIA (IN-LBF-SEC**2) VERT .00109 HORIZ .00049 TWIST .00000
BOUNDARY CONDITION CHECK -.72168E-05 .11930E-05 .11240E-04 -.22859E-04

8.00 DEGREES ROOT COLLECTIVE 500.0 ROTOR SPEED, RPM

COLLECTIVE MODE OF BLADE AT 12e.7.51 CPM

OR 25.215 PER REV

BLADE STA IN	DEFLECTIONS IN VERT	DEFLECTIONS IN HORIZ	MOMENTS IN-LB BEAM	MOMENTS IN-LB CHORD	SHEAR FORCES LB BEAM	SHEAR FORCES LB CHORD	TWIST DEG	TORQUE IN-LB
1 .00	-.823	.000	1114.	-2649.	27.	-1396.		
2 .94	-.822	-.183	1065.	-1352.	116.	-1375.		
3 1.88	-.821	-.366	713.	-155.	104.	-1394.		
4 2.82	-.821	-.547	515.	1123.	206.	-1354.		
5 3.76	-.634	-.686	311.	2374.	230.	-1343.		
6 4.70	-.189	-.753	107.	3614.	248.	-1328.		
7 5.64	.325	-.759	-186.	4855.	336.	-1111.		
8 6.58	.683	-.750	-378.	5239.	204.	-622.		
9 7.52	.743	-.776	-374.	5532.	-7.	-312.		
10 8.46	.638	-.817	-319.	5748.	-65.	-231.		
11 9.40	.525	-.848	-222.	5894.	-109.	-156.		
12 10.34	.404	-.868	-48.	5975.	-139.	-87.		
13 11.28	.280	-.875	47.	5993.	-160.	-18.		
14 12.22	.156	-.870	202.	5947.	-172.	50.		
15 13.16	.035	-.851	361.	5839.	-174.	117.		
16 14.10	-.079	-.819	514.	5671.	-168.	181.		
17 15.04	-.182	-.773	654.	5447.	-153.	241.		
18 15.98	-.271	-.713	774.	5171.	-132.	297.		
19 16.92	-.344	-.640	870.	4847.	-104.	347.		
20 17.86	-.396	-.554	936.	4483.	-72.	391.		
21 18.80	-.428	-.455	969.	4083.	-36.	429.		
22 19.74	-.437	-.345	969.	3656.	0.	458.		
23 20.68	-.425	-.223	936.	3209.	37.	479.		
24 21.62	-.390	-.092	871.	2750.	71.	491.		
25 22.56	-.336	.049	778.	2289.	101.	494.		
26 23.50	-.264	.196	663.	1834.	125.	487.		
27 24.44	-.176	.350	531.	1393.	143.	470.		
28 25.38	-.076	.509	390.	982.	152.	442.		
29 26.32	.033	.671	248.	605.	153.	403.		
30 27.26	.148	.835	115.	275.	143.	353.		
31 28.20	.266	1.000	0.	1.	123.	292.		

GENERALIZED INERTIA (IN-LBF-SEC**2) VERT .00049 HORIZ .00103 TWIST .00000

BOUNDARY CONDITION CHECK .63318E-04 .88531E-04 .50355E-03 .13385E-03

CASE 1 FLEX DYNAMICS

8.00 DEGREES ROOT COLLECTIVE 500.0 ROTOR SPEED, RPM

CYCLIC MODE OF BLADE AT 499.85 CPM

OR 1.000 PER REV

BLADE STA IN	DEFLECTIONS IN VERT	DEFLECTIONS IN HORIZ	MOMENTS IN-LB BEAM	MOMENTS IN-LB CHORD	SHEAR FORCES LB BEAM	SHEAR FORCES LB CHORD	TWIST DEG	TORQUE IN-LB
1 .00	.000	.000	0.	0.	3.	0.		
2 .94	.033	.000	0.	0.	3.	0.		
3 1.88	.067	.000	0.	0.	3.	-0.		
4 2.82	.100	.000	0.	0.	2.	-0.		
5 3.76	.133	.000	0.	0.	2.	-0.		
6 4.70	.167	.000	0.	0.	2.	-0.		
7 5.64	.200	.001	0.	0.	2.	-0.		
8 6.58	.233	.001	0.	0.	2.	-0.		
9 7.52	.267	.001	0.	0.	2.	-0.		
10 8.46	.300	.001	0.	0.	2.	-0.		
11 9.40	.333	.001	0.	0.	2.	-0.		
12 10.34	.367	.001	0.	0.	2.	-0.		
13 11.28	.400	.001	0.	0.	2.	-0.		
14 12.22	.433	.001	0.	0.	2.	-0.		
15 13.16	.467	.001	0.	0.	2.	-0.		
16 14.10	.500	.001	0.	0.	2.	-0.		

17	15.04	.533	.002	0.	0.	2.	-0.
18	15.98	.567	.002	0.	0.	2.	-0.
19	16.92	.600	.002	0.	0.	2.	-0.
20	17.86	.633	.002	0.	0.	2.	-0.
21	18.80	.667	.002	0.	0.	1.	-0.
22	19.74	.700	.002	0.	0.	1.	-0.
23	20.68	.733	.002	0.	0.	1.	-0.
24	21.62	.767	.002	0.	0.	1.	-0.
25	22.56	.800	.002	0.	0.	1.	-0.
26	23.50	.833	.002	0.	0.	1.	-0.
27	24.44	.867	.003	0.	0.	1.	-0.
28	25.38	.900	.003	0.	0.	1.	-0.
29	26.32	.933	.003	0.	0.	1.	0.
30	27.26	.967	.003	0.	0.	1.	0.
31	28.20	1.000	.003	0.	0.	0.	0.

GENERALIZED INERTIA (IN-LBF-SEC**2) VERT .00061 HORIZ .00000 TWIST .00000
BOUNDARY CONDITION CHECK .32667E-05 .98319E-08 .27085E-06 .92669E-04

CASE 1 FLEX DYNAMICS

8.00 DEGREES ROOT COLLECTIVE 500.0 ROTOR SPEED, RPM
CYCLIC MODE OF BLADE AT 1347.67 CPM
OR 2.695 PER REV

BLADE STA IN	DEFLECTIONS IN VERT	DEFLECTIONS IN HORIZ	MOMENTS IN-LB BEAM	MOMENTS IN-LB CHORD	SHEAR FORCES LB BEAM	SHEAR FORCES LB CHORD	TWIST DEG	TORQUE IN-LB
1 .00	.000	.003	0.	307.	-9.	16.		
2 .94	-.115	.003	0.	292.	-9.	16.		
3 1.88	-.230	.003	39.	278.	-6.	17.		
4 2.82	-.345	.006	37.	258.	-6.	17.		
5 3.76	-.446	.014	35.	244.	-6.	17.		
6 4.70	-.517	.029	36.	229.	-6.	17.		
7 5.64	-.558	.053	38.	215.	-4.	17.		
8 6.58	-.567	.082	34.	202.	-0.	16.		
9 7.52	-.545	.116	37.	190.	2.	15.		
10 8.46	-.506	.153	38.	177.	2.	15.		
11 9.40	-.467	.191	37.	165.	3.	15.		
12 10.34	-.427	.228	37.	153.	3.	15.		
13 11.28	-.386	.266	36.	141.	4.	14.		
14 12.22	-.344	.305	35.	130.	4.	14.		
15 13.16	-.301	.344	33.	119.	4.	14.		
16 14.10	-.257	.384	31.	108.	4.	13.		
17 15.04	-.213	.423	30.	97.	5.	13.		
18 15.98	-.168	.463	28.	87.	5.	12.		
19 16.92	-.122	.504	25.	77.	5.	12.		
20 17.86	-.075	.544	23.	68.	5.	12.		
21 18.80	-.029	.585	21.	59.	5.	11.		
22 19.74	.019	.626	18.	51.	5.	10.		
23 20.68	.066	.667	16.	43.	5.	10.		
24 21.62	.115	.709	13.	35.	4.	9.		
25 22.56	.163	.750	11.	28.	4.	8.		
26 23.50	.212	.792	9	22.	4.	8.		
27 24.44	.261	.833	7.	16.	4.	7.		
28 25.38	.310	.875	5.	11.	3.			
29 26.32	.359	.917	3.	7.	3.	5.		
30 27.26	.408	.958	1.	3.	3.	5.		
31 28.20	.457	1.000	0.	0.	2.	4.		

GENERALIZED INERTIA (IN-LBF-SEC**2) VERT .00036 HORIZ .00051 TWIST .00000
BOUNDARY CONDITION CHECK -.38881E-07 -.31252E-07 -.70389E-06 -.32180E-06

CASE 1 FLEX DYNAMICS

8.00 DEGREES ROOT COLLECTIVE 500.0 ROTOR SPEED, RPM

BLADE STA IN	DEFLECTIONS IN VERT	HORIZ	MOMENTS IN-LB BEAM	CHORD	SHEAR FORCES LB BEAM	CHORD	TWIST DEG	TORQUE IN-LB
1 .00	.000	.011	0.	1089.	44.	57.		
2 .94	.129	.012	-32.	1036.	44.	57.		
3 1.88	.259	.012	73.	982.	50.	50.		
4 2.82	.387	.020	38.	934.	49.	50.		
5 3.76	.525	.042	2.	887.	48.	50.		
6 4.70	.663	.078	-33.	841.	48.	50.		
7 5.64	.773	.122	-62.	795.	40.	51.		
8 6.58	.831	.165	-79.	750.	22.	50.		
9 7.52	.823	.201	-82.	706.	10.	49.		
10 8.46	.777	.232	-97.	662.	7.	49.		
11 9.40	.729	.263	-103.	618.	4.	49.		
12 10.34	.679	.296	-106.	575.	2.	48.		
13 11.28	.626	.330	-110.	533.	-0.	47.		
14 12.22	.569	.364	-111.	491.	-2.	47.		
15 13.16	.509	.399	-110.	450.	-4.	46.		
16 14.10	.447	.435	-108.	410.	-6.	45.		
17 15.04	.382	.471	-104.	371.	-7.	44.		
18 15.98	.314	.507	-99.	333.	-8.	43.		
19 16.92	.243	.544	-93.	297.	-9.	41.		
20 17.86	.171	.582	-86.	262.	-10.	40.		
21 18.80	.096	.619	-79.	228.	-11.	39.		
22 19.74	.019	.657	-70.	196.	-12.	36.		
23 20.68	-.059	.694	-62.	165.	-12.	34.		
24 21.62	-.139	.732	-53.	137.	-12.	32.		
25 22.56	-.221	.770	-44.	110.	-12.	30.		
26 23.50	-.303	.809	-35.	86.	-12.	27.		
27 24.44	-.387	.847	-27.	64.	-11.	25.		
28 25.38	-.471	.885	-19.	44.	-10.	22.		
29 26.32	-.555	.923	-12.	27.	-9.	19.		
30 27.26	-.640	.962	-5.	12.	-8.	16.		
31 28.20	-.725	1.000	0.	0.	-7.	13.		

GENERALIZED INERTIA (IN-LBF-SEC**2) VERT .00077 HORIZ .00055 TWIST .00000
BOUNDARY CONDITION CHECK -.16243E-06 .73265E-07 .17975E-05 -.13028E-05

CASE 1 FLEX DYNAMICS

8.00 DEGREES ROOT COLLECTIVE 500.0 ROTOR SPEED, RPM
CYCLIC MODE OF BLADE AT 7865.91 CPM
OR 15.732 PER REV

BLADE STA IN	DEFLECTIONS IN VERT	HORIZ	MOMENTS IN-LB BEAM	CHORD	SHEAR FORCES LB BEAM	CHORD	TWIST DEG	TORQUE IN-LB
1 .00	.000	.008	0.	-244.	-81.	40.		
2 .94	-.167	.008	65.	-281.	-81.	40.		
3 1.88	-.334	.008	72.	-331.	-61.	48.		
4 2.82	-.501	.005	103.	-374.	-45.	46.		
5 3.76	-.619	.004	133.	-415.	-41.	45.		
6 4.70	-.624	.012	166.	-455.	-35.	44.		
7 5.64	-.516	.033	139.	-486.	38.	32.		
8 6.58	-.245	.064	6.	-493.	154.	8.		
9 7.52	-.036	.094	-162.	-488.	190.	-6.		
10 8.46	.146	.117	-331.	-478.	191.	-10.		
11 9.40	.321	.139	-496.	-466.	186.	-13.		
12 10.34	.485	.156	-652.	-452.	176.	-16.		
13 11.28	.632	.171	-796.	-435.	161.	-19.		
14 12.22	.756	.182	-923.	-416.	142.	-21.		
15 13.16	.856	.188	-1030.	-395.	119.	-23.		
16 14.10	.931	.190	-1113.	-372.	94.	-25.		
17 15.04	.980	.188	-1174.	-347.	66.	-27.		
18 15.98	1.000	.181	-1208.	-321.	37.	-28.		
19 16.92	.991	.169	-1215.	-294.	7.	-29.		

20	17.86	.954	.153	-1196.	-266.	-29.	-30.
21	18.80	.887	.132	-1150.	-238.	-51.	-31.
22	19.74	.793	.106	-1081.	-209.	-77.	-31.
23	20.68	.673	.076	-991.	-180.	-101.	-31.
24	21.62	.530	.043	-882.	-152.	-120.	-30.
25	22.56	.365	.006	-760.	-125.	-136.	-29.
26	23.50	.181	-.033	-627.	-99.	-147.	-28.
27	24.44	-.017	-.075	-489.	-75.	-152.	-26.
28	25.38	-.227	-.119	-351.	-52.	-151.	-24.
29	26.32	-.446	-.164	-220.	-32.	-144.	-22.
30	27.26	-.669	-.209	-101.	-14.	-130.	-19.
31	28.20	-.895	-.256	-0.	0.	-110.	-15.

GENERALIZED INERTIA (IN-LBF-SEC**2) VERT .00076 HORIZ .00003 TWIST .00000
BOUNDARY CONDITION CHECK -.58508E-07 -.11874E-07 -.61991E-07 -.21722E-06

CASE 1 FLEX DYNAMICS

8.00 DEGREES ROOT COLLECTIVE 500.0 ROTOR SPEED, RPM
CYCLIC MODE OF BLADE AT 14083.92 CPM
OR 28.169 PER REV

BLADE STA IN	DEFLECTIONS IN		MOMENTS IN-LB		SHEAR FORCES LB		TWIST DEG	TORQUE IN-LB
	VERT	HORIZ	BEAM	CHORD	BEAM	CHORD		
1 .00	.000	.437	0.	7486.	-231.	2159.		
2 .94	-.273	.438	201.	5514.	-231.	2098.		
3 1.88	-.546	.440	840.	3570.	120.	1982.		
4 2.82	-.821	.445	644.	1779.	192.	1905.		
5 3.76	-.858	.550	440.	12.	215.	1887.		
6 4.70	-.522	.687	240.	-1737.	239.	1866.		
7 5.64	-.003	.825	-111.	-3222.	390.	1582.		
8 6.58	.422	.927	-409.	-4122.	312.	957.		
9 7.52	.528	.978	-470.	-4648.	60.	561.		
10 8.46	.437	.994	-459.	-5077.	-16.	457.		
11 9.40	.338	1.000	-393.	-5415.	-76.	360.		
12 10.34	.231	.993	-285.	-5670.	-120.	272.		
13 11.28	.120	.974	-145.	-5841.	-155.	182.		
14 12.22	.006	.941	18.	-5930.	-179.	93.		
15 13.16	-.106	.897	192.	-5936.	-192.	5.		
16 14.10	-.212	.840	369.	-5863.	-193.	-79.		
17 15.04	-.307	.772	539.	-5715.	-185.	-160.		
18 15.98	-.387	.694	691.	-5495.	-166.	-236.		
19 16.92	-.449	.607	820.	-5210.	-139.	-306.		
20 17.86	-.490	.512	917.	-4866.	-106.	-369.		
21 18.80	-.507	.409	979.	-4472.	-67.	-423.		
22 19.74	-.500	.301	1002.	-4036.	-25.	-467.		
23 20.68	-.467	.187	986.	-3568.	18.	-502.		
24 21.62	-.410	.069	932.	-307	59.	-525.		
25 22.56	-.329	-.052	843.	-2575.	96.	-537.		
26 23.50	-.227	-.176	726.	-2073.	127.	-537.		
27 24.44	-.108	-.302	586.	-1593.	151.	-523.		
28 25.38	.027	-.429	433.	-1118.	165.	-496.		
29 26.32	.172	-.557	277.	-691.	168.	-456.		
30 27.26	.324	-.686	129.	-314.	159.	-402.		
31 28.20	.479	-.814	1.	-1.	138.	-334.		

GENERALIZED INERTIA (IN-LBF-SEC**2) VERT .00031 HORIZ .00114 TWIST .00000
BOUNDARY CONDITION CHECK -.13356E-05 .10225E-05 .60727E-05 -.35712E-05

CASE 1 FLEX DYNAMICS

8.00 DEGREES ROOT COLLECTIVE 500.0 ROTOR SPEED, RPM
SCISSORS MODE OF BLADE AT 611.99 CPM
OR 1.224 PER REV

		VERT	HORIZ	BEAM	CHORD	BEAM	CHORD
1	.00	.000	.000	21.	10.	3.	1.
2	.94	.000	.000	18.	9.	3.	1.
3	1.88	.000	.000	17.	8.	3.	0.
4	2.82	.000	.000	14.	6.	3.	0.
5	3.76	.005	.001	11.	5.	3.	0.
6	4.70	.020	.003	9.	5.	3.	0.
7	5.64	.043	.007	8.	5.	3.	0.
8	6.58	.074	.011	7.	4.	3.	0.
9	7.52	.110	.017	7.	4.	3.	0.
10	8.46	.149	.023	6.	4.	3.	0.
11	9.40	.189	.029	6.	4.	3.	0.
12	10.34	.229	.034	6.	3.	3.	0.
13	11.28	.268	.040	5.	3.	3.	0.
14	12.22	.308	.046	5.	3.	3.	0.
15	13.16	.349	.052	5.	3.	3.	0.
16	14.10	.389	.058	4.	2.	3.	0.
17	15.04	.429	.064	4.	2.	3.	0.
18	15.98	.470	.071	3.	2.	2.	0.
19	16.92	.510	.077	3.	2.	2.	0.
20	17.86	.551	.083	3.	2.	2.	0.
21	18.80	.591	.089	2.	1.	2.	0.
22	19.74	.632	.095	2.	1.	2.	0.
23	20.68	.673	.101	2.	1.	2.	0.
24	21.62	.714	.107	1.	1.	2.	0.
25	22.56	.754	.113	1.	1.	2.	0.
26	23.50	.795	.120	1.	0.	2.	0.
27	24.44	.836	.126	1.	0.	1.	0.
28	25.38	.877	.132	0.	0.	1.	0.
29	26.32	.918	.139	0.	0.	1.	0.
30	27.26	.959	.144	0.	0.	1.	0.
31	28.20	1.000	.150	0.	0.	1.	0.

GENERALIZED INERTIA (IN-LBF-SEC**2) VERT .00051 HORIZ .00001 TWIST .00000

BOUNDARY CONDITION CHECK .21478E-08 .32326E-09 .74122E-08 .49313E-07

CASE 1 FLEX DYNAMICS

8.00 DEGREES ROOT COLLECTIVE 500.0 ROTOR SPEED, RPM

SCISSORS MODE OF BLADE AT 1993.92 CPM

OR 3.988 PER REV

BLADE STA IN	DEFLECTIONS IN VERT	DEFLECTIONS IN HORIZ	MOMENTS IN-LB BEAM	MOMENTS IN-LB CHORD	SHEAR FORCES LB BEAM	SHEAR FORCES LB CHORD	TWIST DEG	TORQUE IN-LB
1 .00	.000	.000	-93.	676.	-5.	34.		
2 .94	.000	.000	-91.	644.	-5.	34.		
3 1.88	.000	.000	-0.	618.	0.	34.		
4 2.82	-.001	.005	-0.	586.	0.	34.		
5 3.76	-.003	.018	-0.	555.	0.	34.		
6 4.70	-.006	.040	0.	524.	0.	34.		
7 5.64	-.010	.068	0.	494.	0.	34.		
8 6.58	-.015	.101	0.	465.	0.	33.		
9 7.52	-.020	.134	0.	437.	0.	32.		
10 8.46	-.025	.168	0.	409.	0.	32.		
11 9.40	-.030	.203	0.	381.	0.	31.		
12 10.34	-.036	.239	0.	354.	0.	31.		
13 11.28	-.041	.275	0.	328.	0.	30.		
14 12.22	-.047	.312	0.	302.	0.	30.		
15 13.16	-.052	.350	0.	276.	0.	29.		
16 14.10	-.058	.388	0.	251.	0.	29.		
17 15.04	-.064	.427	0.	227.	0.	28.		
18 15.98	-.070	.466	0.	204.	0.	27.		
19 16.92	-.076	.506	0.	181.	0.	26.		
20 17.86	-.082	.546	0.	159.	0.	25.		
21 18.80	-.088	.586	0.	139.	0.	24.		

23	20.68	-.100	.688	0.	100.	0.	21.
24	21.62	-.107	.709	0.	83.	0.	20.
25	22.56	-.113	.750	0.	67.	0.	19.
26	23.50	-.119	.792	0.	52.	0.	17.
27	24.44	-.125	.833	0.	38.	0.	15.
28	25.38	-.132	.875	0.	26.	0.	14.
29	26.32	-.136	.917	0.	16.	0.	12.
30	27.26	-.144	.958	0.	7.	0.	10.
31	28.20	-.150	1.000	0.	0.	0.	8.

GENERALIZED INERTIA (IN-LBF-SEC**2) VERT .00001 HORIZ .00051 TWIST .00000
BOUNDARY CONDITION CHECK -.10241E-07 .68107E-07 .15333E-05 -.23058E-06

1 PAGE 15 MYKLESTAD ANALYSIS NASA TM 78670 0/ 0/ 0

CASE 1 FLEX DYNAMICS

8.00 DEGREES ROOT COLLECTIVE 500.0 ROTOR SPEED, RPM
SCISSORS MODE OF BLADE AT 4292.42 CPM
OR 8.565 PER REV

BLADE STA IN	DEFLECTIONS IN		MOMENTS IN-LB		SHEAR FORCES LB		TWIST DEG	TORQUE IN-LB
	VERT	HORIZ	BEAM	CHORD	BEAM	CHORD		
1 .00	.000	.000	773.	109.	162.	23.		
2 .94	.000	.000	620.	88.	162.	23.		
3 1.88	.000	.000	473.	0.	164.	0.		
4 2.82	.001	.000	319.	0.	164.	0.		
5 3.76	.115	.016	173.	-0.	164.	0.		
6 4.70	.377	.053	38.	-1.	163.	0.		
7 5.64	.673	.095	-84.	-1.	150.	0.		
8 6.58	.903	.127	-167.	-1.	102.	0.		
9 7.52	.996	.140	-221.	-1.	33.	0.		
10 8.46	1.000	.141	-271.	-1.	53.	0.		
11 9.40	.998	.140	-311.	-1.	43.	0.		
12 10.34	.989	.139	-343.	-1.	34.	0.		
13 11.28	.972	.137	-368.	-1.	25.	0.		
14 12.22	.944	.133	-386.	-1.	17.	0.		
15 13.16	.905	.127	-396.	-1.	9.	0.		
16 14.10	.857	.121	-399.	-1.	1.	0.		
17 15.04	.800	.112	-395.	-1.	-7.	0.		
18 15.98	.732	.103	-385.	-1.	-14.	0.		
19 16.92	.656	.092	-369.	-1.	-20.	0.		
20 17.86	.571	.080	-348.	-1.	-26.	0.		
21 18.80	.477	.067	-323.	-1.	-31.	0.		
22 19.74	.376	.053	-294.	-1.	-35.	0.		
23 20.68	.267	.037	-261.	-1.	-39.	-0.		
24 21.62	.153	.021	-227.	-1.	-41.	-0.		
25 22.56	.032	.004	-191.	-1.	-42.	-0.		
26 23.50	-.093	-.013	-154.	-0.	-43.	-0.		
27 24.44	-.221	-.031	-118.	-0.	-42.	-0.		
28 25.38	-.353	-.050	-84.	-0.	-40.	0.		
29 26.32	-.486	-.069	-52.	-0.	-37.	0.		
30 27.26	-.621	-.088	-24.	0.	-32.	0.		
31 28.20	-.756	-.107	0.	0.	-27.	0.		

GENERALIZED INERTIA (IN-LBF-SEC**2) VERT .00093 HORIZ .00002 TWIST .00000
BOUNDARY CONDITION CHECK -.20374E-05 -.28689E-06 -.15035E-05 -.10694E-04

1 PAGE 16 MYKLESTAD ANALYSIS NASA TM 78670 0/ 0/ 0

CASE 1 FLEX DYNAMICS

8.00 DEGREES ROOT COLLECTIVE 500.0 ROTOR SPEED, RPM
SCISSORS MODE OF BLADE AT 9485.95 CPM
OR 18.972 PER REV

BLADE STA IN	DEFLECTIONS IN		MOMENTS IN-LB		SHEAR FORCES LB		TWIST DEG	TORQUE IN-LB
	VERT	HORIZ	BEAM	CHORD	BEAM	CHORD		

1	.00	.000	.000	-1022.	-143.	-303.	-43.
2	.94	-.000	.000	-1022.	-143.	-303.	-43.
3	1.88	-.000	-.000	-744.	0.	-306.	-0.
4	2.82	-.001	-.000	-456.	0.	-306.	-0.
5	3.76	-.155	-.022	-180.	1.	-306.	-0.
6	4.70	-.464	-.065	84.	1.	-304.	-0.
7	5.64	-.710	-.100	252.	1.	-224.	-0.
8	6.58	-.747	-.105	260.	1.	25.	0.
9	7.52	-.583	-.082	97.	1.	183.	0.
10	8.46	-.355	-.050	-91.	1.	214.	0.
11	9.40	-.128	-.018	-296.	1.	231.	0.
12	10.34	.091	.013	-506.	0.	236.	0.
13	11.28	.298	.042	-713.	0.	232.	0.
14	12.22	.484	.068	-910.	0.	219.	0.
15	13.16	.646	.091	-1089.	0.	198.	0.
16	14.10	.782	.110	-1243.	0.	171.	0.
17	15.04	.887	.125	-1367.	0.	137.	0.
18	15.98	.960	.135	-1457.	-0.	99.	0.
19	16.92	.998	.140	-1509.	-0.	58.	0.
20	17.86	1.000	.141	-1523.	-0.	15.	0.
21	18.80	.965	.136	-1498.	-0.	-28.	0.
22	19.74	.894	.126	-1434.	-0.	-70.	0.
23	20.68	.789	.111	-1336.	-0.	-108.	0.
24	21.62	.651	.092	-1207.	-0.	-142.	0.
25	22.56	.485	.068	-1051.	-0.	-170.	0.
26	23.50	.293	.041	-876.	-0.	-191.	0.
27	24.44	.080	.011	-689.	-0.	-204.	0.
28	25.38	-.150	-.021	-499.	-0.	-207.	0.
29	26.32	-.392	-.055	-314.	0.	-201.	0.
30	27.26	-.641	-.090	-145.	0.	-184.	0.
31	28.20	-.894	-.125	-0.	0.	-156.	0.

GENERALIZED INERTIA (IN-LBF-SEC**2) VERT .00083 HORIZ .00002 TWIST .00000

BOUNDARY CONDITION CHECK .35942E-05 .50504E-06 .16729E-05 .11913E-04

CASE 1 FLEX DYNAMICS

8.00 DEGREES ROOT COLLECTIVE 700.0 ROTOR SPEED, RPM

COLLECTIVE MODE OF BLADE AT 676.02 CPM

OR .966 PER REV

BLADE STA IN	DEFLECTIONS IN		MOMENTS IN-LB		SHEAR FORCES LB		TWIST DEG	TORQUE IN-LB
	VERT	HORIZ	BEAM	CHORD	BEAM	CHORD		
1 .00	.245	.000	28.	11.	5.	1.		
2 .94	.245	.001	23.	10.	5.	1.		
3 1.88	.245	.002	19.	7.	5.	0.		
4 2.82	.245	.002	14.	6.	5.	0.		
5 3.76	.251	.004	10.	6.	5.	0.		

APPENDIX H

Sample Data from Flight Tests

Translational Flight Test Data

Windtunnel Speed 12
Collective Setting 18.6
Rotor Speed 800

Azimuth x 10	Flap	Torque	L1	L2	Thrust
0	2922	2559	1657	1376	1516.5
1	2923	2558	1660	1376	1518
2	2918	2560	1670	1375	1522.5
3	2918	2565	1680	1392	1536
4	2912	2573	1700	1416	1558
5	2912	2579	1703	1437	1570
6	2907	2586	1717	1462	1589.5
7	2907	2596	1729	1470	1599.5
8	2907	2598	1728	1480	1604
9	2907	2594	1727	1481	1604
10	2908	2581	1719	1476	1597.5
11	2898	2575	1712	1473	1592.5
12	2908	2565	1699	1461	1580
13	2908	2558	1690	1455	1572.5
14	2912	2549	1685	1442	1563.5
15	2912	2544	1676	1434	1555
16	2913	2543	1675	1422	1548.5
17	2918	2546	1669	1415	1542
18	2922	2554	1675	1406	1540.5
19	2922	2558	1679	1392	1535.5
20	2927	2573	1685	1394	1539.5
21	2940	2574	1695	1397	1546
22	2934	2573	1709	1405	1557
23	2933	2570	1718	1414	1566
24	2936	2563	1725	1420	1572.5
25	2933	2549	1735	1426	1580.5
26	2937	2543	1736	1423	1579.5
27	2938	2546	1734	1424	1579
28	2933	2541	1723	1417	1570
29	2935	2552	1711	1413	1562
30	2932	2568	1695	1413	1554
31	2933	2575	1678	1405	1541.5
32	2935	2581	1665	1403	1534
33	2932	2580	1655	1396	1525.5
34	2929	2576	1650	1392	1521
35	2923	2570	1650	1391	1520.5
36	2926	2563	1651	1383	1517
37	2922	2558	1659	1382	1520.5
38	2917	2551	1662	1389	1525.5
39	2911	2553	1680	1406	1543
40	2909	2559	1691	1423	1557
41	2907	2570	1703	1446	1574.5
42	2910	2575	1712	1463	1587.5
43	2906	2582	1715	1473	1594
44	2907	2583	1721	1481	1601
45	2908	2580	1722	1477	1599.5
46	2952	2579	1714	1475	1594.5
47	2910	2570	1703	1465	1584
48	2909	2571	1696	1456	1576
49	2908	2559	1690	1449	1569.5

50	2910	2545	1680	1437	1558.5
51	2911	2545	1678	1428	1553
52	2918	2537	1671	1420	1545.5
53	2919	2548	1677	1411	1544
54	2921	2543	1679	1403	1541
55	2926	2554	1682	1397	1539.5
56	2929	2568	1697	1397	1547
57	2933	2567	1701	1403	1552
58	2935	2584	1715	1418	1566.5
59	2936	2581	1723	142[illegible]	1572
60	2935	2578	1734	143[illegible]	1582
61	2936	2574	1738	1434	1586
62	2940	2569	1736	1429	1582.5
63	2937	2568	1736	1429	1582.5
64	2938	2570	1726	1423	1574.5
65	2935	2577	1713	1420	1566.5
66	2935	2577	1695	1411	1553
67	2933	2586	1673	1406	1539.5
68	2932	2590	1658	1402	1530
69	2928	2586	1651	1395	1523
70	2928	2589	1648	1389	1518.5
71	2964	2578	1648	1383	1515.5
72	2921	2572	1651	1379	1515
73	2918	2571	1659	1379	1519
74	2916	2573	1669	1395	1532
75	2915	2582	1688	1418	1553
76	2912	2579	1702	1441	1571.5
77	2907	2589	1718	1466	1592
78	2908	2582	1725	1477	1601
79	2907	2591	1730	1488	1609
80	2905	2586	1735	1489	1612
81	2907	2570	1727	1484	1605.5
82	2905	2566	1717	1477	1597
83	2907	2561	1707	1473	1590
84	2909	2558	1696	1460	1578
85	2908	2545	1683	1450	1566.5
86	2911	2546	1675	1440	1557.5
87	2910	2534	1671	1429	1550
88	2916	2544	1669	1415	1542
89	2918	2540	1671	1409	1540
90	2923	2542	1673	1398	1535.5
91	2925	2552	1680	1392	1536
92	2928	2555	1687	1393	1540
93	2931	2558	1699	1402	1550.5
94	2931	2565	1714	1412	1563
95	2934	2550	1726	1419	1572.5
96	2934	2546	1733	1428	1580.5
97	2934	2530	1736	1427	1581.5
98	2957	2536	1740	1426	1583
99	2936	2541	1737	1423	1580
100	2932	2549	1721	1417	1569
101	2935	2561	1707	1415	1561
102	2934	2569	1685	1407	1546
103	2933	2577	1670	1404	1537
104	2954	2574	1655	1397	1526
105	2929	2574	1649	1398	1523.5
106	2926	2571	1645	1388	1516.5
107	2925	2557	1643	1383	1513

108	2922	2550	1651	1381	1516
109	2920	2551	1653	1383	1518
110	2915	2549	1669	1405	1537
111	2913	2557	1687	1423	1555
112	2908	2568	1696	1448	1572
113	2906	2579	1709	1467	1588
114	2906	2589	1719	1479	1599
115	2907	2595	1721	1489	1605
116	2906	2596	1725	1487	1606
117	2907	2596	1717	1486	1601.5
118	2907	2596	1712	1475	1593.5
119	2906	2584	1700	1469	1584.5
120	2908	2580	1695	1456	1575.5
121	2911	2561	1685	1441	1563
122	2910	2555	1683	1435	1559
123	2916	2548	1679	1421	1550
124	2918	2549	1680	1413	1546.5
125	2921	2553	1684	1402	1543
126	2922	2563	1685	1396	1540.5
127	2922	2572	1693	1391	1542
128	2928	2580	1703	1391	1547
129	2933	2582	1713	1404	1558.5
130	2935	2578	1721	1413	1567
131	2937	2580	1729	1426	1577.5
132	2935	2563	1736	1435	1585.5
133	2936	2559	1737	1436	1586.5
134	2936	2553	1737	1437	1587
135	2937	2550	1730	1432	1581
136	2937	2561	1721	1432	1576.5
137	2935	2561	1703	1423	1563
138	2935	2568	1689	1417	1553
139	2933	2566	1676	1413	1544.5
140	2931	2573	1665	1402	1533.5
141	2928	2567	1661	1398	1529.5
142	2925	2566	1655	1391	1523
143	2925	2550	1657	1387	1522
144	2921	2549	1663	1383	1523
145	2918	2554	1670	1385	1527.5
146	2915	2550	1688	1400	1544
147	2912	2551	1704	1423	1563.5
148	2911	2563	1718	1448	1583
149	2906	2567	1727	1464	1595.5
150	2905	2570	1738	1482	1610
151	2903	2572	1742	1487	1614.5
152	2905	2564	1735	1481	1608
153	2907	2570	1732	1480	1606
154	2907	2555	1722	1469	1595.5
155	2908	2549	1708	1464	1586
156	2908	2547	1692	1451	1571.5
157	2911	2544	1677	1440	1558.5
158	2911	2543	1666	1431	1548.5
159	2915	2540	1657	1419	1538
160	2918	2536	1658	1412	1535
161	2921	2536	1652	1401	1526.5
162	2923	2544	1667	1394	1530.5
163	2944	2541	1673	1391	1532
164	2929	2559	1684	1397	1540.5
165	2931	2562	1701	1407	1554

166	2936	2555	1717	1417	1547
167	2934	2557	1730	1422	1576
168	2940	2550	1739	1425	1582
169	2938	2542	1746	1426	1586
170	2936	2548	1747	1425	1586
171	2937	2553	1731	1420	1575.5
172	2935	2558	1717	1416	1566.5
173	2939	2567	1698	1409	1553.5
174	2933	2575	1683	1407	1545
175	2932	2575	1663	1401	1532
176	2929	2574	1655	1399	1527
177	2915	2570	1647	1395	1521
178	2930	2567	1645	1389	1517
179	2921	2558	1649	1388	1518.5

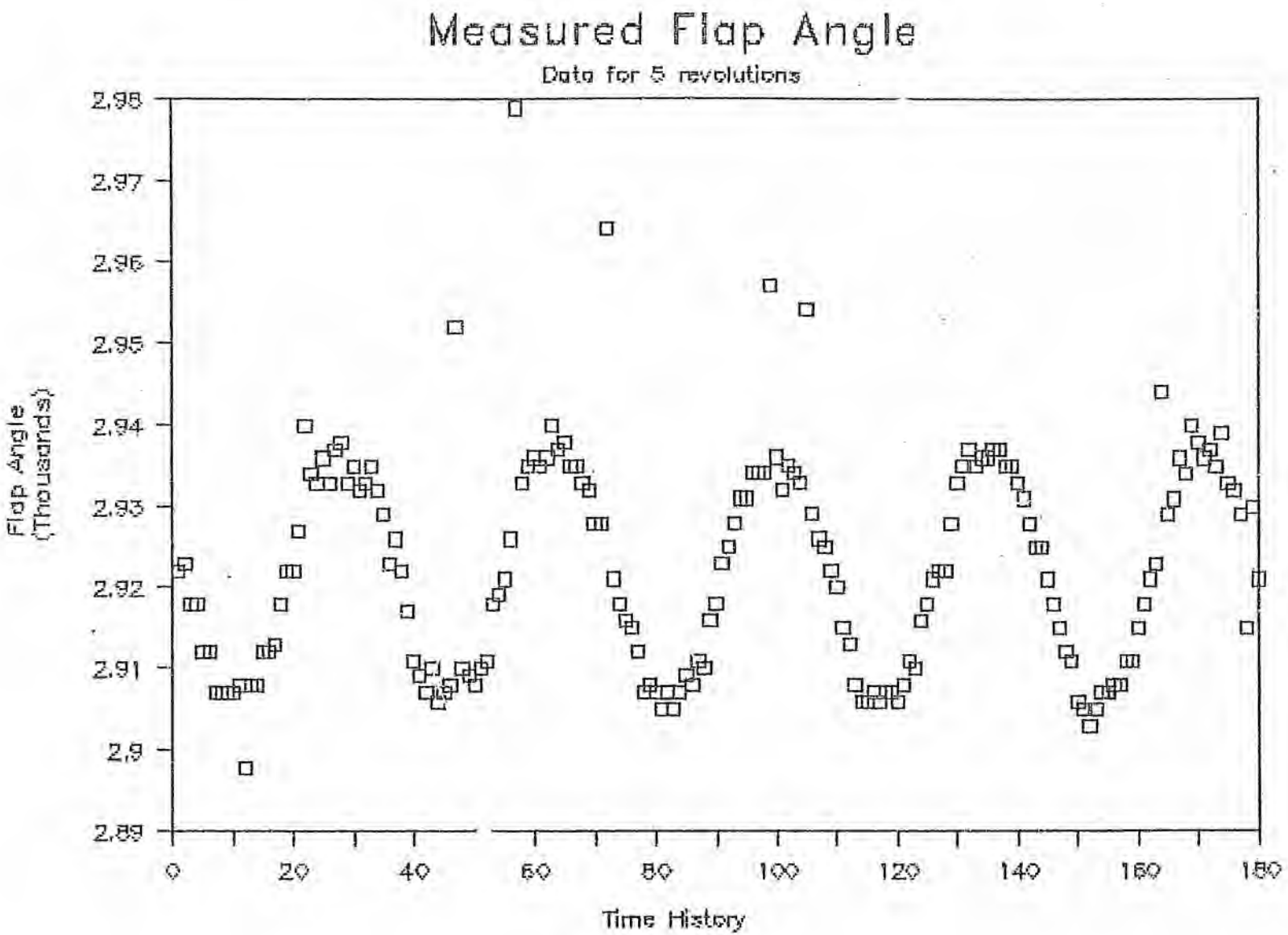
Measured Flap Angle
Data for 5 revolutions
Flap Angle (Thousands)
2.98
2.97
2.96
2.95
2.94
2.93
2.92
2.91
2.9
2.89
0
20
40
60
80
100
120
140
160
180
Time History

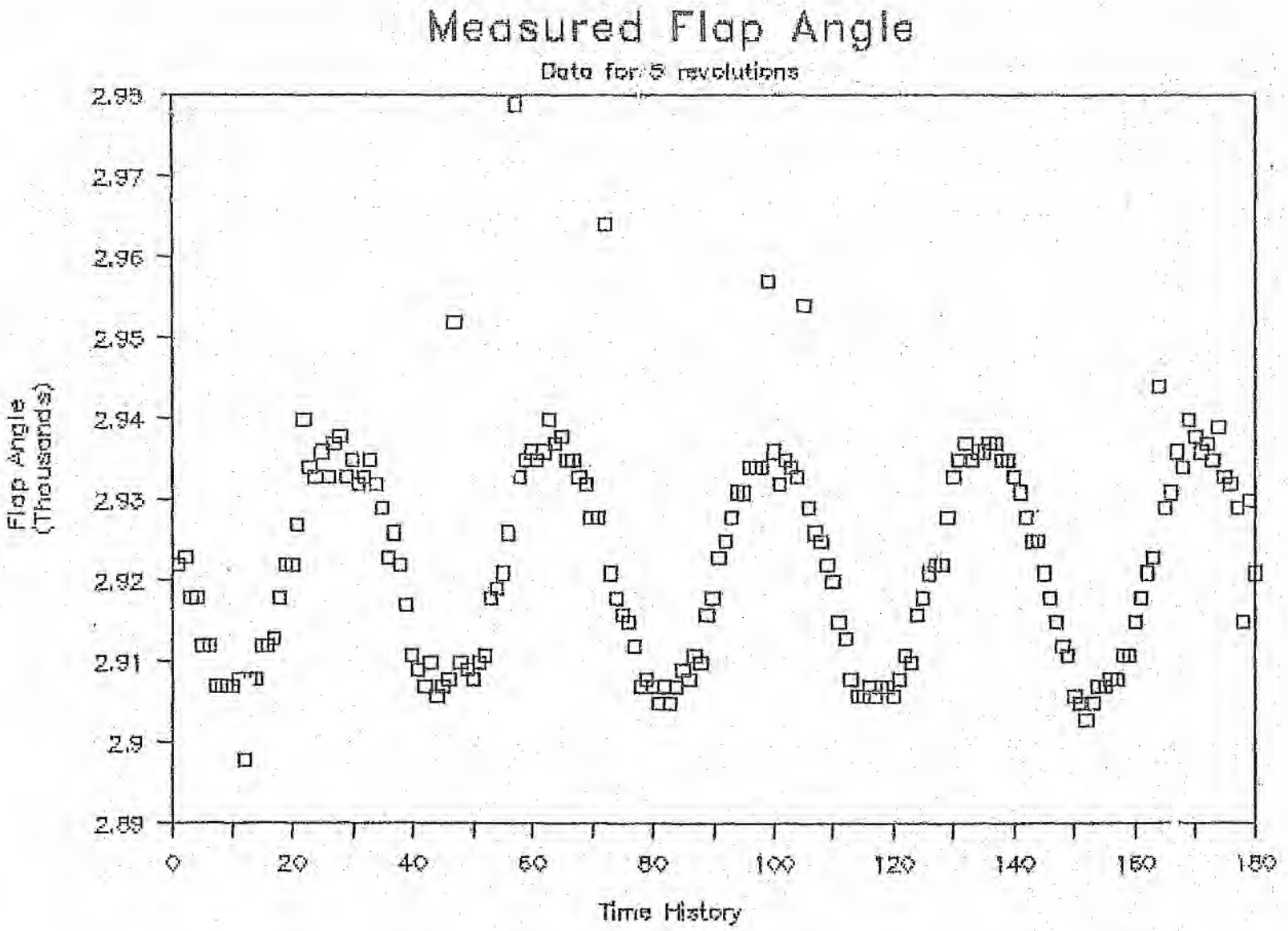
Measured Flap Angle
Data for 5 revolutions
Flap Angle (Thousands)
2.98
2.97
2.96
2.95
2.94
2.93
2.92
2.91
2.9
2.89
0
20
40
60
80
100
120
140
160
180
Time History

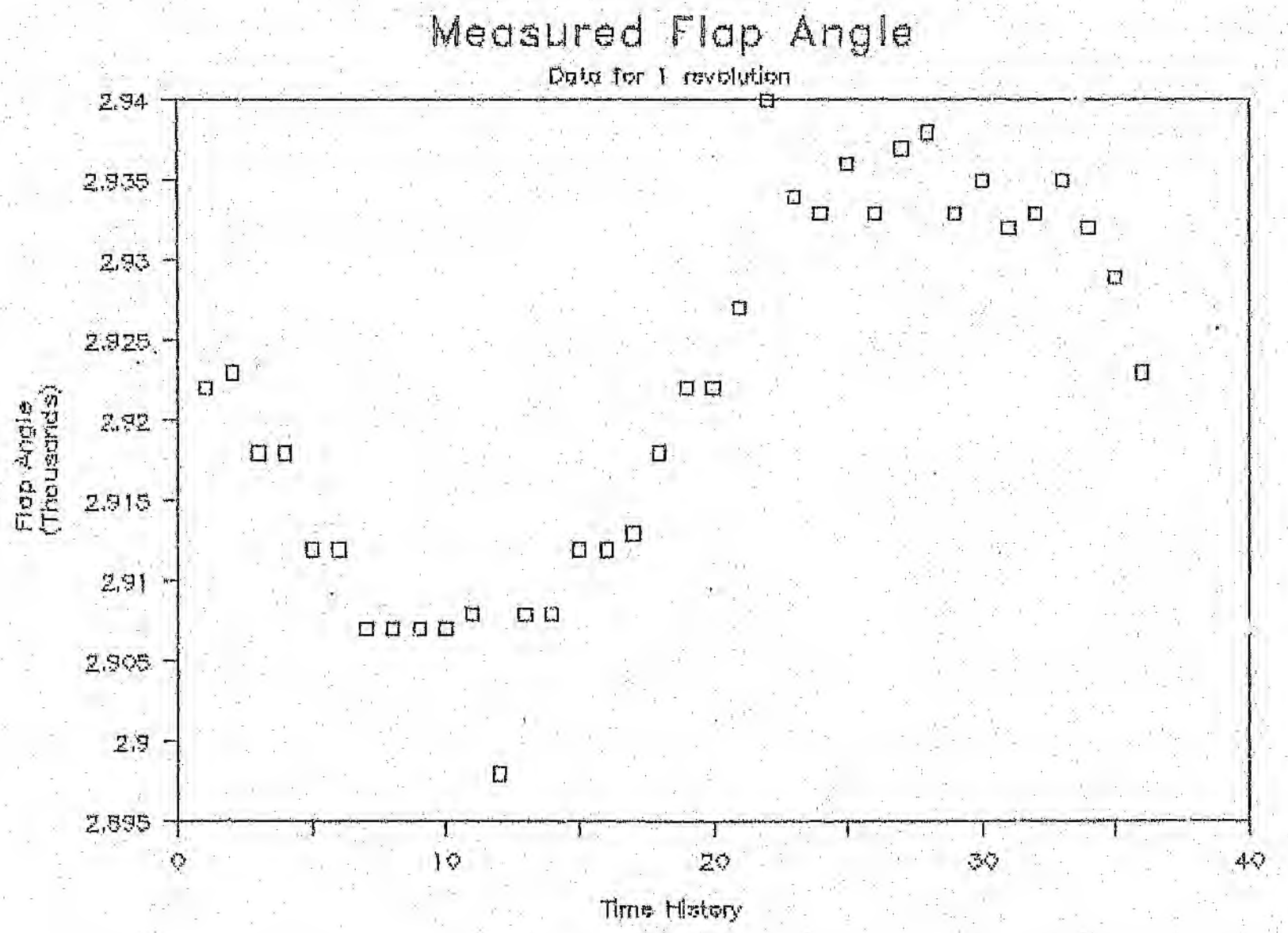
Measured Flap Angle
Data for 1 revolution
Flap Angle (Thousandths)
2.94
2.935
2.93
2.925
2.92
2.915
2.91
2.905
2.9
2.895
0
10
20
30
40
Time History

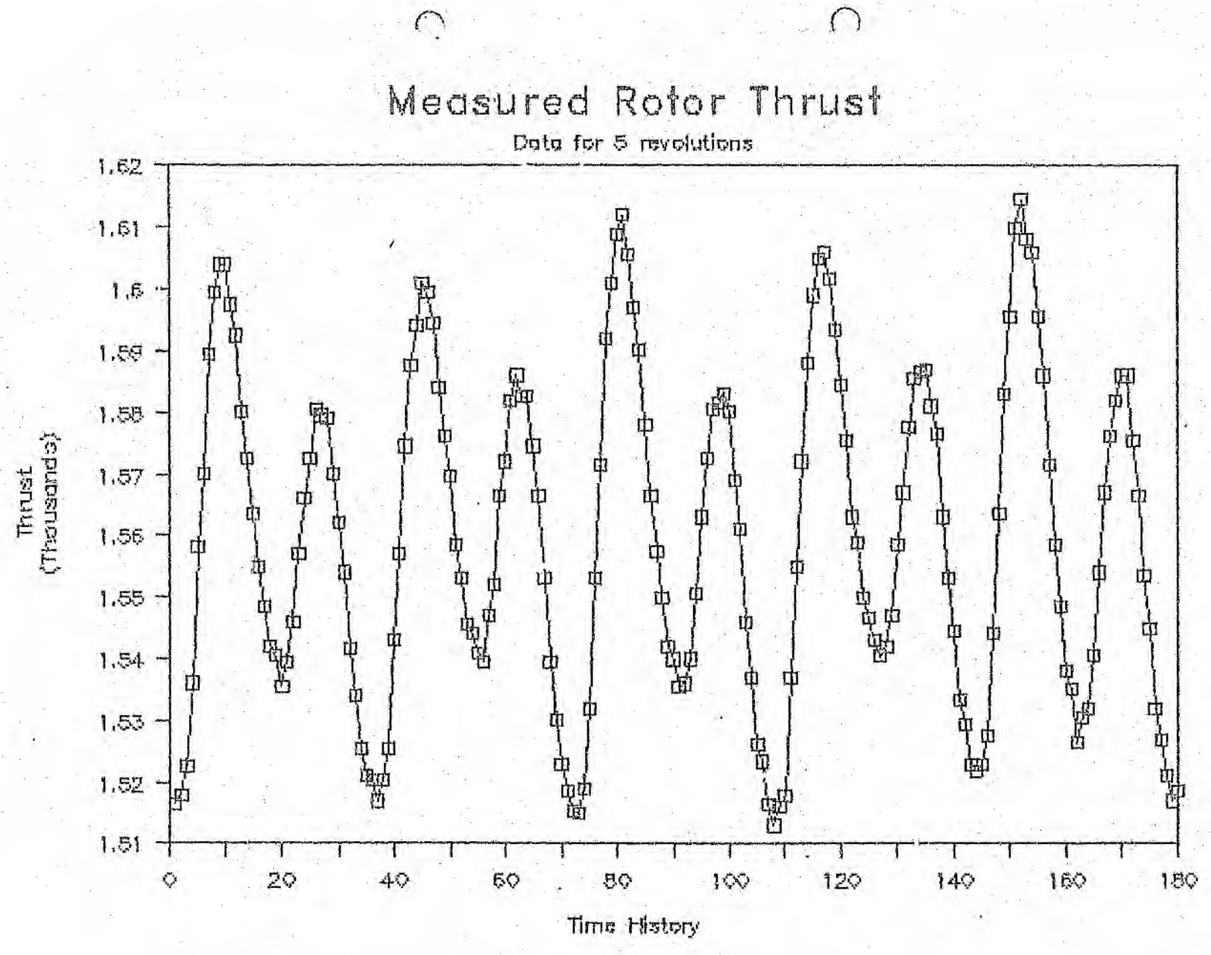
Measured Rotor Thrust
Data for 5 revolutions
Thrust (Thousands)
1.62
1.61
1.6
1.59
1.58
1.57
1.56
1.55
1.54
1.53
1.52
1.51
0
20
40
60
80
100
120
140
160
180
Time History

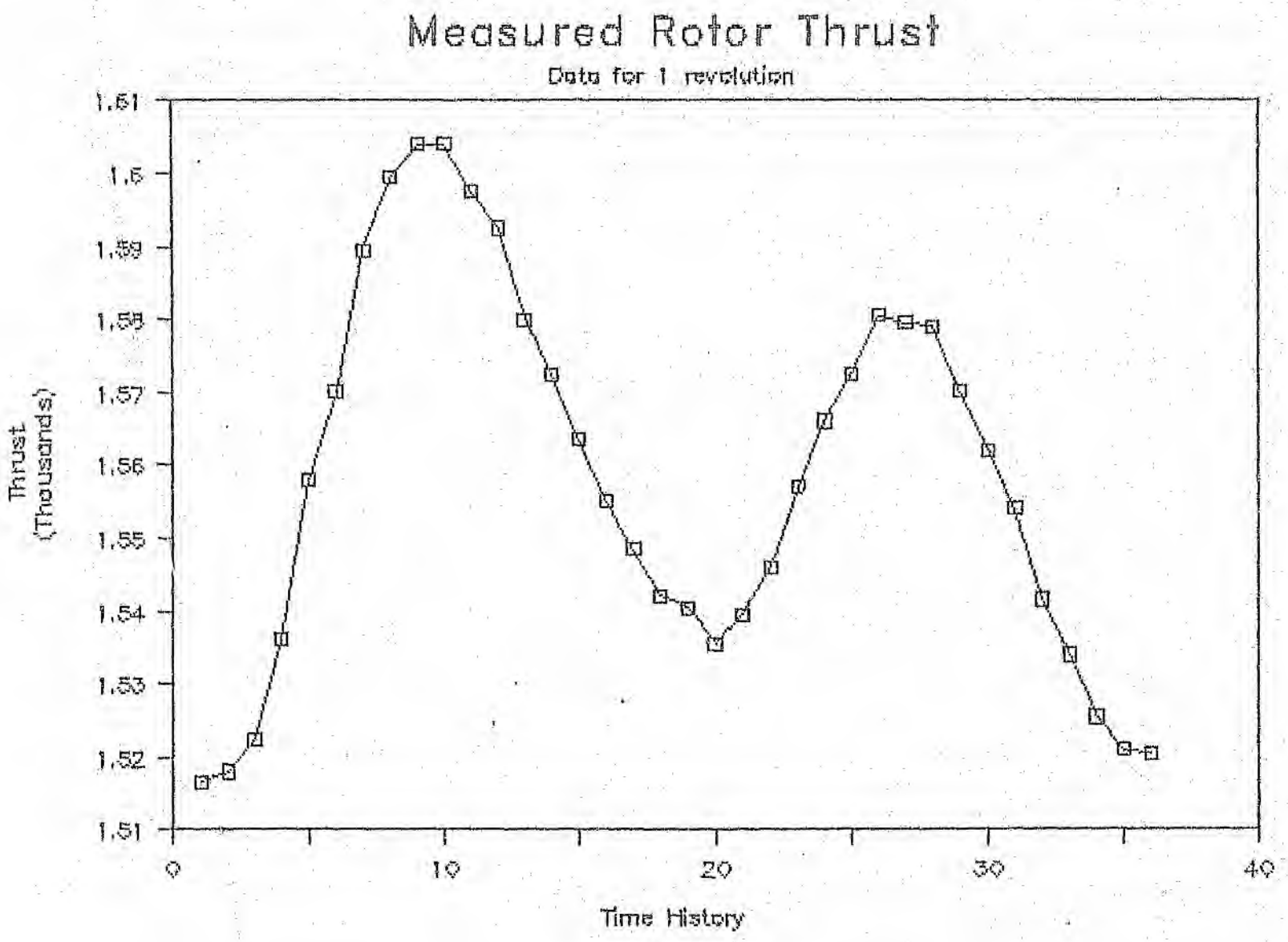
Measured Rotor Thrust
Data for 1 revolution
Thrust
(Thousands)
1.61
1.6
1.59
1.58
1.57
1.56
1.55
1.54
1.53
1.52
1.51
0
10
20
30
40
Time History

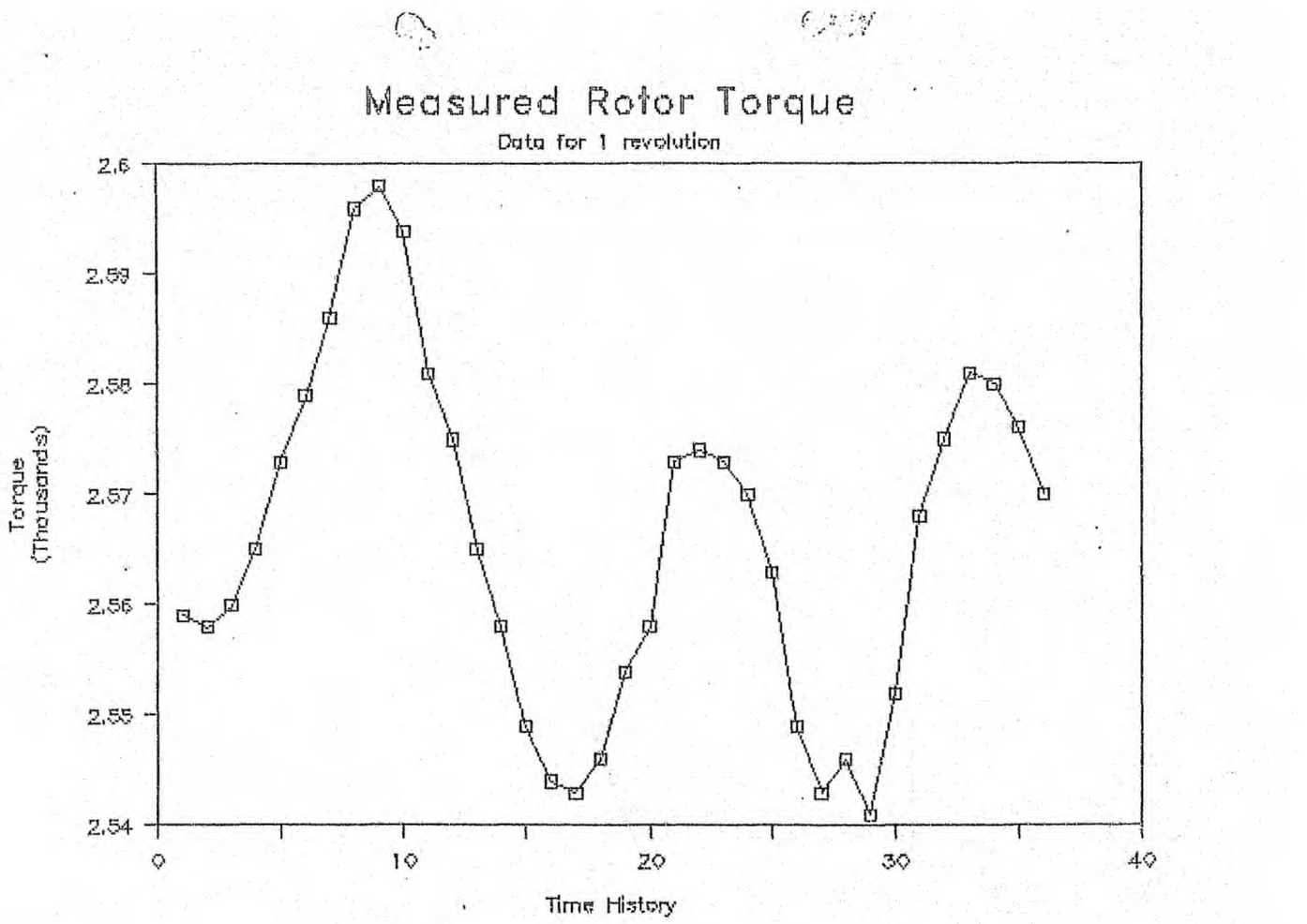
Measured Rotor Torque
Data for 1 revolution
2.6
2.59
2.58
2.57
2.56
2.55
2.54
Torque
(Thousands)
0
10
20
30
40
Time History

APPENDIX I

Calibration Equipment

Revolution Counter

Make	Ono Sokki
Type	MT-346
Range	15 - 20 000 rev/min
Accuracy	15 - 14 999 rev/min ± 1 $rev/_{min}$
Serial No.	34602649

Angle Measurement

Make	Hilger & Watts Ltd. Clinometer
Range	0 - 180 degrees
Accuracy	± 1 *minute*
Serial No.	126692

Distance Measurement

Make	Mitutoyo Vernier
Range	0.01 - 150 mm
Accuracy	± 0.01 *mm*
Serial No.	6003037

Mass Measurement

Make	unknown
Model	GC32/50
Range	0 - 3 000 g
Accuracy	± 0.01 *g*
Serial No.	783649

Author: Cohen Gary M.
Name of thesis: A Design Study Of A Scale Model Bearingless Helicopter Rotor System Using Composite Materials.

PUBLISHER:
University of the Witwatersrand, Johannesburg
©2015

LEGALNOTICES:

Copyright Notice: All materials on the University of the Witwatersrand, Johannesburg Library website are protected by South African copyright law and may not be distributed, transmitted, displayed or otherwise published in any format, without the prior written permission of the copyright owner.

Disclaimer and Terms of Use: Provided that you maintain all copyright and other notices contained therein, you may download material (one machine readable copy and one print copy per page)for your personal and/or educational non-commercial use only.

The University of the Witwatersrand, Johannesburg, is not responsible for any errors or omissions and excludes any and all liability for any errors in or omissions from the information on the Library website.